RICE UNIVERSITY

Kinetic and Stoichiometric Modeling of the Metabolism of *Escherichia coli* for the Synthesis of Biofuels and Chemicals

By

Angela Cintolesi Makuc

A THESIS SUBMITED
IN PARTIAL FULFILLMENT OF THE
REQUIREMENT FOR THE DEGREE

Doctor of Philosophy

Approved, Thesis Committee:

Ramon Gonzalez,
Associate Professor in Chemical and Biomolecular Engineering
Associate Professor in Bioengineering

Deepak Nagrath,
Assistant Professor in Chemical and Biomolecular Engineering

Luay Nakhleh,
Associate Professor in Computer Science
Associate Professor in Ecology and Evolutionary Biology
Associate Professor in Biochemistry and Cell Biology

Houston, Texas
April 2013

ABSTRACT

Kinetic and Stoichiometric Modeling of the Metabolism of *Escherichia coli* for the Synthesis of Biofuels and Chemicals.

by

Angela Cintolesi

This thesis presents the mathematical modeling of two new *Escherichia coli* platforms with economical potential for the production of biofuels and chemicals, namely glycerol fermentation and the reversal of the β-oxidation cycle. With the increase in traditional fuel prices, alternative renewable energy sources are needed, and the efficient production of biofuels becomes imperative. So far studies have focused on using glucose as feedstock for the production of ethanol and other fuels, but a recent increase in glycerol availability and its consequent decrease in price make it an attractive feedstock. Furthermore, the reversed β-oxidation cycle is a highly efficient mechanism for the synthesis of long-chain products. These two platforms have been reported experimentally in *E. coli* but their mathematical modeling is presented for the first time here.

Because mathematical models have proved to be useful in the optimization of microbial metabolism, two complementary models were used in this study: kinetic and stoichiometric. Kinetic models can identify the control structure within a specific pathway, but they require highly detailed information, making them applicable to small sets of reactions. In contrast, stoichiometric models require only mass balance information, making them suitable for genome-scale modeling to study the effect of adding or removing reactions for the optimization of the synthesis of desired products.

To study glycerol fermentation, a kinetic model was implemented, allowing prediction of the limiting enzymes of this process: glycerol dehydrogenase and di-hydroxyacetone kinase. This prediction was experimentally validated by increasing their enzymatic activities, resulting in a two-fold increase in the rate of ethanol production. Additionally, a stoichiometric genome-scale model (GEM) was modified to represent the fermentative metabolism of glycerol, identifying key metabolic pathways for glycerol fermentation (including a new glycerol dissimilation pathway). The GEM was used to identify genetic modifications that would increase the synthesis of desired products, such as succinate and butanol.

Finally, glucose metabolism using the reversal β-oxidation cycle was modeled using a GEM to simulate the synthesis of a variety of medium and long chain products (including advanced biofuels). The model was used to design strategies that can lead to increase the productivity of target products.

Acknowledgement

This thesis represents the result of four and a half years of work that would not have been possible if it was not for wonderful people that God has put on my path.

First, I would like to thank my mom for her love, encouragement and support. I hope I will always live up to her vision: "hijos, el limite son las estrellas" ("children, the stars are the limit").

I would like to thank my brothers and sisters, for their love and example.

I would like to thank my advisor Dr. Ramon Gonzalez, for careful and patient advice and feedback throughout the years. This thesis would not have been possible without him.

I would like to thank my thesis committee members, Dr. Luay Nakhleh and Dr. Deepak Nagrath, for their encouragement, feedback and support.

I would like to thank my former professors from Rice and from Chile, who have believed in me and have encouraged me to be my very best.

I would like to thank an enormous number of friends, who throughout the years have believed in me and supported my work.

Last but not least, I want to express my gratitude to my Heavenly Father, for being the inspiration in my life, the one who has encouraged me the most to go to higher skies. The greatest scientist and the source of all good.

Table of Contents

1 Introduction

1.1 Motivation and justification

The current petrochemical industry controls most of the production of transportation energy and other petrochemicals; however, this platform has several issues that make it necessary to look for alternative sources. The main issues are related to the instability of petroleum prices, the uncertainty of its availability in the future, and its negative impact in the environment. Although there are renewable sources to produce biofuels and biochemicals, which are environmentally friendlier, the price of using these alternative sources is not yet competitive with the traditional petrochemical industry. Therefore, there is an imperative necessity to continue exploring renewable sources to produce fuels and chemicals, as well as to optimize these processes.

In this thesis, two new platforms for the production of renewable biofuels and chemicals in *E. coli* are studied using mathematical models: glycerol fermentation and the reversal of the β-oxidation cycle. Glycerol can be consumed for *E. coli* in order to produce biofuels and biochemicals, and its use is promising when compared to other traditional carbon and energy sources for *E. coli* (glucose, for instance). The reversal of the β-oxidation cycle is highly efficient in the synthesis of long chain products, such as advanced biofuels. A full study to increase the understanding of glycerol fermentation and the use of the reversal β-oxidation cycle in *E. coli*, as well as to optimize and expand these mechanisms, requires mathematical modeling of the metabolism, a task that has not been fully explored yet and which is the focus of this thesis.

1.1.1 The problem of fuels and chemical production

Our current society relies on the petrochemical industry for the production of transportation energy (fuels) and chemicals. Petrochemical products are those chemicals produced from petroleum, also called crude oil and natural gas. Crude oil and natural gas are a mixture of hydrocarbons, among them alkanes, cycloalkanes, and aromatic hydrocarbons. Petroleum is extracted and processed to obtain two main kinds of products: fuels and chemicals. Crude oil is extracted from the earth, and it is processed to separate the different components that originate valuable products. Petroleum products can be classified into two main groups: fuels and other derivatives (chemicals). Among the fuels are ethane, diesel fuel, fuel oils, gasoline, jet fuel, and kerosene. Some petroleum derivatives are alkenes, lubricants, wax, sulfuric acid, tar, asphalt, petroleum coke, paraffin wax, and aromatic petrochemicals. While petroleum derived fuels represent about the 94% of the source for total transportation energy (Reijnders & Huijbregts, 2009), derivative chemicals are used in the production of plastic, cosmetic, agrochemicals, adhesives, etc. But all this reliance on the petrochemical industry has achieved (and it will continue to achieve) unstable and even dangerous levels for society and the environment.

The first concern is related to economic issues. Petroleum prices have been subject to enormous variation in past and present years. Few countries in the world produce petroleum, and these countries often have unstable political systems (Soetaert & Vandamme, 2009). The crisis in the 1970s, triggered by political issues in the Middle East, caused an enormous increase in the price of oil (Figure 1). In more recent years, the price of petroleum has continued to suffer huge increases and fluctuations. Before

September 2003, the price of crude oil was about $25/barrel (real price), and since then it has increased to over $100/barrel in 2011 (BP's Statistical Review of World's Energy Full Report 2012. Website: http://www.bp.com/statisticalreview. Figure 1 shows historical prices. Projections for the future are discouraging as, regardless of political issues, crude oil is a limited resource expected to run out in the near future.

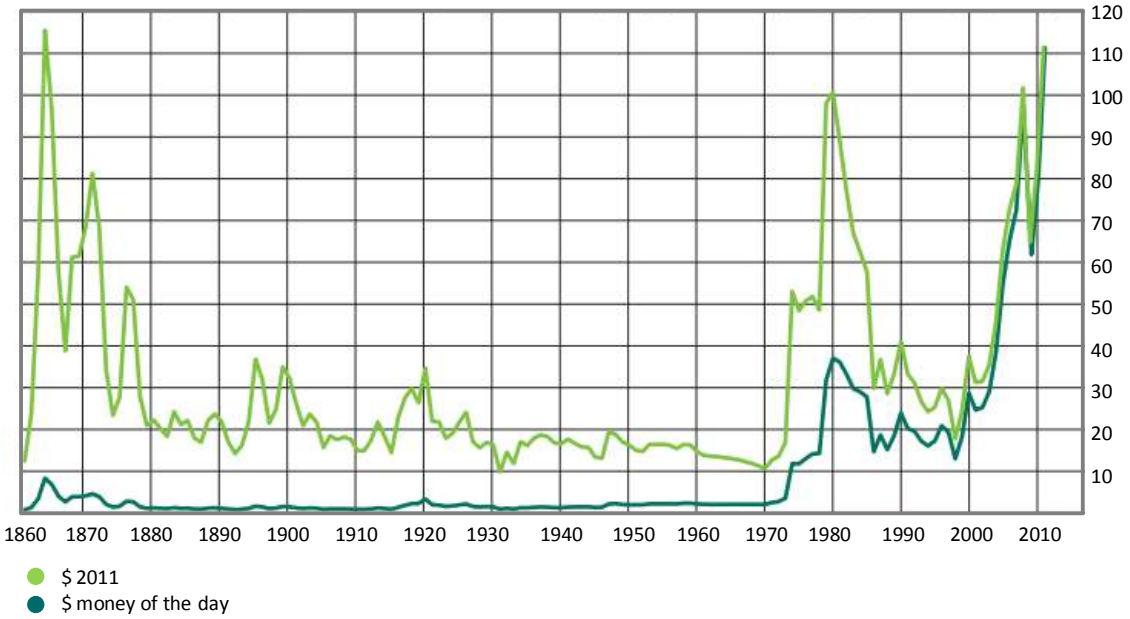

Figure 1: Crude oil prices 1861-2011. Statistical Review of World Energy June 2012. Website: http://www.bp.com/statisticalreview.

Because petroleum is a non-renewable resource, and because of increasing demand, it is estimated that petroleum will run out in 50 years or less (Soetaert & Vandamme, 2009). Petroleum was formed by chemical processes that took place during millions of years on the earth, and therefore, it is a limited, non-renewable resource. Refineries were at first operating in areas of easy access. As easily accessed reserves are being exhausted, the process of extracting petroleum becomes more challenging. On the other hand, the forecasted demand of crude oil is increasing as a natural consequence of increases in population and in development. The U.S. Energy Information Administration

(Website: http://www.eia.gov) forecasts a steady projection in the global demand of liquid fuel, and an increase in the demand of liquid biofuels (Figure 2). In conclusion, the limited capacity of crude oil supply, together with the increase in crude oil price, creates an urgent necessity to develop alternative transport fuels.

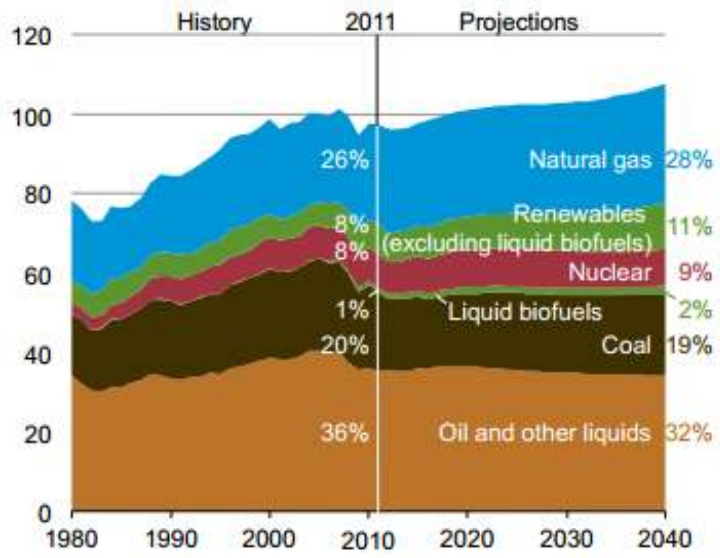

Figure 2: Forecast of global demand by fuel type (U. S. Energy Information Administration. Independent Statistics and Analysis. AEO2013 Early Release Overview. Website: http://www.eia.gov)

But petroleum does not have just economical and availability issues, it is also unsafe to the environment. The petrochemical industry has been related to CO_2 emissions, air pollution, and acid rain (Union of Concerned Scientists – Clean Energy. Website: http://www.ucsusa.org). Carbon dioxide is produced by the combustion of fuels and is related to global warming. Although there are multiple sources for carbon dioxide emissions, studies reveal that these emissions have increased about 35% when compared to pre-industrial times (Environmental Protection Agency. Website: http://www.epa.gov), suggesting a relationship with the increased use of fuels. According to the U.S. department of energy, CO_2 emissions related to energy are connected to over 80% of the greenhouse emissions (See Figure 3 for detail of other sources). Air pollution is another

negative side effect of using petroleum, causing damage to the health of humans. Burning fossil fuel generates several harmful emissions, among them carbon monoxide, nitrogen oxides and sulfur oxides. These emissions are related to health issues such as headaches, irritation of lungs, bronchitis, and respiratory infections. Finally, some of these emissions cause additional damage to the environment, such as acidic rain. Acidic rain has a negative impact on water, aquatic animal life, soils, and vegetation.

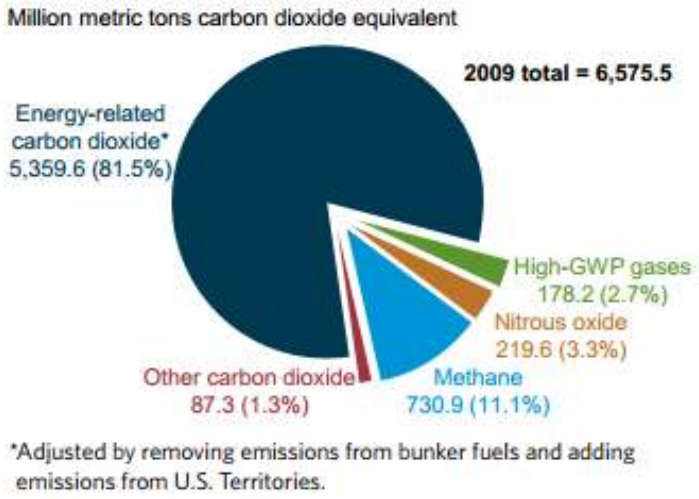

Figure 3: Greenhouse gas emissions by gas, 2009 (Emission of greenhouse gases in the United States 2009. U.S Energy Information Administration, Dec 2009. Website: ftp://ftp.eia.doe.gov)

1.1.2 Biofuels

The expected increase in the price of crude oil, together with the inevitable running out of it and the environmental damage associated with this industry, has lead several countries to make efforts in incorporating alternatives. Although different kinds of renewable energy are being explored, among them nuclear energy, solar energy, wind power, and biofuels, the last one is the most appropriate for transportation (Zidansek et al., 2009). For instance, solar and wind power are not very reliable as they depend on external conditions, and nuclear energy still has some safety issues that would delay any

implementation for several years (Zidansek et al., 2009). In contrast, biofuels have proven to be appropriate for transport energy and some countries are already incorporating them. In addition, biofuels are made from biomass, which can also provide substitutes for some derivatives of the petrochemical industry, making biofuels even more attractive as a replacement of fossil products.

Production of biofuels, and specifically of ethanol and biodiesel, was triggered by economic and environmental factors. After the oil crisis of 1973, Brazil decided to incorporate ethanol as an energy source for transport, and now it is one of the countries with the highest production of ethanol in the world (Leland, 2009; Reijnders & Huijbregts, 2009). Following the example of Brazil, the U.S. implemented a program to stimulate the use of ethanol in 1978, and is currently the other main producer of ethanol in the world (Leland, 2009; Reijnders & Huijbregts, 2009). The U.S. Department of Energy expects to quadruple the consumption of renewable biofuels in the coming years, from 9 billion gallons in 2008 to 36 billion ethanol-equivalent gallons in 2022 (U.S. Department of Energy, 2012), and other countries (such as Canada, South Africa and Germany) are also implementing similar strategies to replace part of traditional fuel consumptions (Reijnders & Huijbregts, 2009).

1.1.3 Glycerol and glucose as feedstocks for ethanol and chemicals production

Traditionally feedstocks for the production of biofuels have been cane and corn, for the production of ethanol, and oil crops, for production of biodiesel (Fischer et al., 2008). Cane and corn contain sucrose and starch respectively, which can be broken down into sugars, mainly glucose and fructose, and then be fermented to produce ethanol. Sugar fermentation is a relatively simple process that can take place in yeast and other

organisms. However, in order to make biofuels economically viable, it is necessary to develop new and more efficient processes to use glucose and other less expensive biofuels. One way to achieve this is in the use of alternative feedstock, such as cellulose, syngas, fatty acids, and glycerol, all of which have been proposed as alternatives to reduce cost in the production of biofuels (Dellomonaco et al., 2010; Fischer et al., 2008; Yazdani & Gonzalez, 2007). Another way to make biofuels more attractive economically is to concentrate on the production of advanced biofuels, which contain higher energy density than traditional fuels. In this thesis two approaches are studied: 1) the use of glycerol as a cheaper carbon source to produce biofuels and chemicals and 2) the use of a newly discovered metabolic pathway, the reversal of the β-oxidation cycle, to produce advanced biofuels and other chemicals. The reason for this selection is explained in the following two paragraphs.

Glycerol is a 3-carbon molecule that has two important and promising properties for the production of biofuels: low price and a high degree of reduction (Yazdani & Gonzalez, 2007). Glycerol is a by-product in the production of biodiesel, and its production is 10% (weight) of the biodiesel product. The increase in production of biodiesel in recent years has lead to a 10- fold decrease in the price of glycerol between 2004 and 2006 (Yazdani & Gonzalez, 2007), and its current price is even lower ($0.005 per pound. 01/2013; www.thejacobsen.com). The low price of glycerol makes it competitive when compared to sugars. Furthermore, the highly reduced nature of carbon atoms in glycerol (higher than sugars) makes it even more attractive for the production of biofuels. For instance, glycerol presents a maximum theoretical yield twice as large as the one produced when glucose is used as the carbon source in the anaerobic fermentation in

E. coli (Dharmadi et al., 2006). **Regardless of experimental efforts that have been conducted to improve the utilization by *E. coli* of glycerol for the productions of biofuels and chemicals, no mathematical modeling has been conducted previous to this thesis, a task that is imperative for further understanding and optimization of this process.**

The reversal of the β-oxidation cycle is a newly engineered process that results in the efficient synthesis of long chain chemicals, including advanced biofuels. While the β-oxidation cycle is the most commonly used metabolic pathway for the utilization of fatty acids as energy and carbon sources, the reversal of this process is possible by metabolically engineering the pathway. It experimental implementation in *E. coli* using glucose as carbon and energy source was demonstrated in 2011 by Dellomonaco and collaborators (Dellomonaco et al., 2011). The implementation of this pathway resulted in the production of long chain linear alcohols and fatty acids at higher yields than those reported using other pathways, a highly the attractive aspect of this pathway (Dellomonaco et al., 2011). **In order to increase the understanding of the reversal of the β-oxidation cycle in *E. coli* as well as to explore its capabilities to enhance the optimal production of a variety of long chain chemicals, the implementation of mathematical model is essential, a task that has been undertaken in this thesis.**

1.2 Selection of microorganism: *E. coli* as platform

The production of biofuels requires a platform capable of transforming the feedstock into the desired product. The complexity of this operation, together with the high efficiency that biological systems provide when compared to chemical catalysts, resulted in the decision to use biological microorganisms, which have proven to be able

to synthesize biochemicals. In addition, several tools have been developed in the field of biotechnology during the last 40 years (starting with the discovery of restriction enzymes in the 1970s), focused on the modification of wild strains in order to improve their original properties. Biotechnological tools allow, for instance, modifying the tolerance of cells to external conditions, adding or removing reactions from the original pathway in order to increase the production of the desired product, overexpressing or underexpressing native genes, and modifing proteins characteristics (reversibility, activity, among others).

Although different microorganisms are able to produce biofuels, this study focuses on one in particular: *Escherichia coli*. *E. coli* is a gram negative bacterium that has been widely studied for applications in biotechnology. Several properties make *E. coli* an ideal organism for the production of biochemicals on an industrial scale. First, *E. coli* can easily grow in attractive industrial conditions. It can grow with and without oxygen, use several substrates, and use inexpensive media components (Clomburg & Gonzalez, 2010). Second, the large amount of information on the metabolism of these bacteria allows efficient manipulation of it using gene transformation, regulation of gene expression, and protein engineering (Stephanopoulos, 2007). Furthermore, the development of "omics" technology (genomics, transcriptomics, and proteomics) has been applied extensively to *E. coli*, allowing an increase in the understanding of this bacterium. This accumulated knowledge has allowed mathematical modeling of part of the metabolism of *E. coli*, the remarkable examples being the central carbon metabolism for glucose utilization (Chassagnole et al., 2002) and genome-scale modeling (Orth et al., 2011).

Most importantly, recent studies confirm that *E. coli* is able to ferment glycerol in the absence of external electron acceptors, an ability shared only by a few organisms (Dharmadi et al., 2006), which can lead to the production of ethanol other products. In addition, *E. coli* can produce long chain chemicals (including advanced biofuels) utilizing a newly engineered pathway: the reversal of the β-oxidation cycle (Dellomonaco et al., 2011).

1.3 The use of mathematical modeling in the study of biological systems

Prior to the utilization of mathematical models in biological systems, biological parts (genes, proteins, reactions, and metabolites) were studied in a limited way with laboratory technology. Most of the experiments consisted of the modification of one single element (a gene, for instance) and then the observation of the effect over other components of the system. This approach has changed in recent years, and several efforts have been made to apply mathematical models to the study of biological systems as a whole.

The use of mathematical models allows a deeper understanding of the roles of different parts of the system, and how their manipulation can increase the production of a desired product under specific conditions. For example, a mathematical model can allow the identification of the limiting steps in a system, while otherwise it would be necessary to performance multiple experiments in the laboratory, which are expensive and time consuming, to reach the same conclusion. Gombert and Nielsen reviewed the two main approaches in modeling metabolic pathways: stoichiometric models and kinetic models (Gombert & Nielsen, 2000). Furthermore, some models incorporate the genetic

regulatory network in order to represent different conditions that suppose the expression of different genes (see for example Ramakrishna et al., 1996 and Moisset et al., 2012).

1.4 Objectives

The main goal of this thesis is the development of mathematical models for the understanding of microbial utilization of glycerol and the implementation of a functional reversal of the β-oxidation in *E. coli* related to the production of biofuels and other valuable chemicals. This was done using two approaches: kinetic modeling and genome-scale modeling. In particular, the following tasks were performed:

- **Implementing a kinetic model for the fermentative metabolism of glycerol**. This model was used to elucidate the control structure in this pathway, to create predictions, and to propose genetic modifications for increasing the production of biofuels.
- **Implementing a genome-scale (stoichiometric) model (GEM) for the fermentative metabolism of glycerol.** This model allowed the identification of active pathways and engineered pathways for the efficient conversion of glycerol into biofuels and other chemicals.
- **Implementing a GEM for the utilization of glucose to produce long chain chemicals using the reversal of the β-oxidation cycle**. This model allowed for the evaluation of different strategies for the production of a variety of advanced biofuels and other long chain chemicals. These strategies include the evaluation of adding and removing reactions.

1.5 Organization of the thesis: Overview of the chapters

The next section of this thesis is **Background and literature review**. That section starts by reviewing metabolic information available for *E. coli*, which includes detailed studies of pathways related to utilization of glycerol and glucose. Specific pathways for the consumption of glycerol and glucose are explained. Different pathways that have been proposed to produce advance biofuels and other chemicals are explained, including the β-oxidation cycle as well as its engineered reversal for the production of long chain products. Then, mathematical models for metabolic pathways are presented, including approximate models and applications.

Two mathematical methods were selected for this study: kinetic modeling and GEM. **Materials and Methods** explains why these methods were selected and gives further details of their implementations. Also, detailed experimental protocols are presented for the validation of predictions and other relevant findings.

The next three sections present **Results**, which consist of 1) a kinetic model for glycerol fermentation, 2) a GEM for glycerol fermentation, and 3) a GEM for glucose metabolism for the production of medium and long chain products using the reversal of the β-oxidation cycle. The kinetic model accounts for the glycerol transport and dissimilation, glycolysis, and ethanol synthesis, and it represents correctly the experimental data. This model was used to study the control structure of glycerol fermentation and predictions were experimentally validated. The GEM for glycerol in *E. coli* accurately represents glycerol fermentation. Implementation of this model allowed increasing the understanding of glycerol fermentation, as well as investigating the synthesis of additional products using optimal strategies. The GEM for the reversal of the

β-oxidation cycle was used to evaluate this pathway as an efficient platform for the production of a variety of medium and long chain products, including advanced biofuels, and it increases the understanding of redox balance and energy requirements of this pathway. In addition, a GEM was used to simulate the use of different platforms for the production of medium and long chain products. It was concluded that the reversal of the β-oxidation cycle predicts higher productivities based on a higher energetic efficiency.

To conclude, **Final Remarks and Future Directions** presents a summary of the main findings exposed in this thesis, as well as suggestions about future experimental work to corroborate the findings of this work. In future experimental work it is suggested that a variety of genetic modifications be implemented, leading to i) corroboration of the existence of new unstudied pathways and ii) production of biofuels and chemicals at optimal levels. Some future directions in the use of mathematical models in metabolic engineering, in particular en the area of production of biofuels and chemicals are also suggested.

2 Background and literature review

This chapter describes fundamentals for building mathematical models for glycerol fermentation and respiratory utilization of fatty acids in *E. coli*. First, the metabolism of *E. coli* is described, with special emphasis on glycerol and glucose utilization. The fermentative metabolism of glycerol and glucose includes glycolysis and production of fermentative products, among others. The problem of achieving redox balance is explained, and how this affects both the cell growth and the maximum theoretical yield for biofuels production. Then, the use of mathematical tools to model metabolism is explained, including different approaches that have been used. A special emphasis is given to models that have been successfully applied to *E. coli* and to models for glycerol fermentation that have been developed in other organisms. Then, the advantages and challenges of producing advanced biofuels and other long chain chemicals are presented, including the newly reported reversal of the β-oxidation cycle. This provide a comprehensive vision of the different efforts to model the metabolism of *E. coli* and the utilization of glycerol and glucose for the synthesis of biofuels and chemicals.

2.1 Metabolism of *E. coli*

The cellular metabolism consists of all reactions that uptake nutrients from the environment, and then utilize them for cell function and reproduction. Metabolism can be divided into two main processes: catabolism and anabolism. The catabolism includes all those reactions that break down large molecules in order to obtain energy and building blocks. Building blocks are used in the anabolic pathways in order to produce

macromolecules that enable the maintenance and reproduction of cells, such as proteins, polynucleotides (DNA and RNA) and lipids. Energy and redox power are two important concepts that govern the metabolism, as they are involved in a vast number of pathways.

2.1.1 *E. coli*

This study utilizes the bacterium *E. coli* K-12, on whose metabolism a vast number of studies have been performed. These studies cover both specific pathways and genome scale studies. While studies of the metabolism started from studies of particular pathways, such as glycolysis and TCA cycle, genome scale studies attempt to include all reactions in the metabolism. This section first explains available genome scale information for this microorganism and then it explains specific pathways related to the utilization of glycerol and fatty acids.

Genome scale studies

Prior to the publication of the genome scale project for *E. coli*, just 1,853 genes had been identified in this organism. In 1997 the genome scale project revealed that *E. coli* has 4,288 ORFs (potential genes) (Blattner et al., 1997), and this number has been updated to 4,499 genes (Keseler et al., 2013). ORFs potentially encode information for proteins, whose main functional categories are metabolism (enzymes), transportation (across cellular membranes), regulation, and structure. The database **EcoCyc** collects the information related to each of these ORFs of *E. coli* and presents it in a user-friendly and integrated way (Keseler et al., 2013). Both sequence analysis and experiments are used to assign the biochemical function of a gene product (Karp et al., 2007). By 2006 EcoCyc curators finished performing a literature review of each of the ORFs of *E. coli*, and they keep updating the database (Karp et al., 2007; Keseler et al., 2013). Among the genes that

E. coli has, 76% of them have a biochemical function assigned, and in most of those cases there are experiments that support the function (Karp et al., 2007). In addition, EcoCyc present all known metabolic pathways of *E. coli*, and it also presents related information for each enzyme in a reaction, such as activators, inhibitors, and cofactors. By 2012, EcoCyc cited 23,909 distinct references, and included 300 metabolic pathways, which is considerably more than the 194 metabolic pathways reported by this site in 2007 (Karp et al., 2007). A classification of these pathways is complicated given the complexity of the metabolic network, but a general classification considers biosynthetic pathways, degradation pathways, detoxification, generation of precursor metabolites and energy, and signal transduction pathways (taken from EcoCyc website).

The information presented in EcoCyc has been used and compared with the metabolic model built by the group of Palsson (Karp et al., 2007). The final result of this effort is a **GEM**, named the iJO1366**,** that accounts for all known metabolic pathways presented in EcoCyc (Orth et al., 2011). In addition, this model includes spontaneous reactions that are not catalyzed by enzymes, and therefore they are not part of the EcoCyc database. The model includes 2,251 reactions and 1,366 ORFs, representing the effort of 21 years working on the reconstruction of the complete metabolic network of *E. coli* (Figure 1).

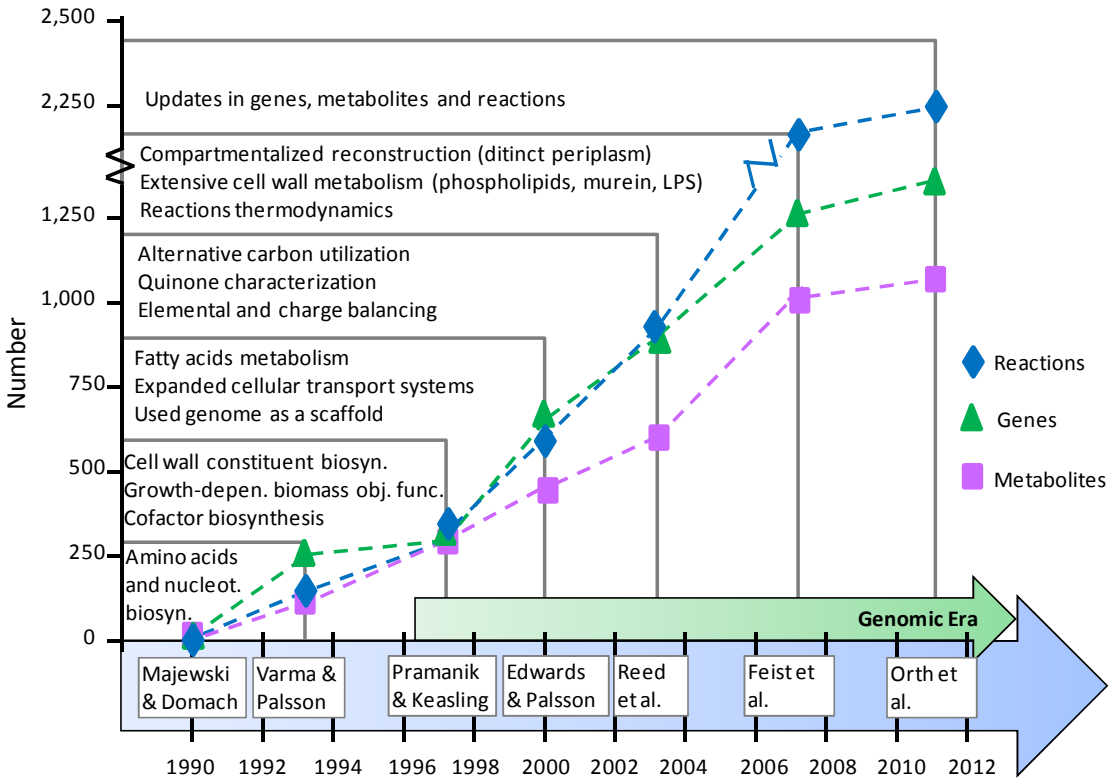

Figure 4: Seven milestones efforts in the construction of metabolic network of *E. coli* (Feist & Palsson, 2008). This figure was updated to include the information from the last released GEM for *E. coli*, the iJO1366 (Orth et al., 2011).

Another relevant source of information in the study of the metabolism of *E. coli* is the BRaunschweig ENzyme DAtabase, most commonly referred to as **BRENDA** (Schomburg et al., 2013). This database collects detailed enzymatic information, such as biochemical and molecular information, from nearly 500 organisms. As with EcoCyc, BRENDA curators collect information from literature. BRENDA is not specific to any organism, but for each enzyme, it offers the option to restrict the displayed information to a specific organism, among them *E. coli*. This database is especially useful for collecting kinetic information, as it links to articles that have reported rate law, reversibility, kinetic parameters, and possible inhibition of the corresponding reaction.

Glycolysis and fermentative pathways

Pathways in the central metabolism are especially relevant in this study, as they allow the utilization of different carbon sources, such as glucose, malate, succinate, and acetate. Glucose and other sugars have been widely studied, as they represent an efficient cellular growth. Anaerobic fermentation of glucose uses the glycolysis and fermentative pathways in order to obtain energy (in the form of ATP), and it results in the production of lactate, ethanol, and other fermentative products (Sawers & Clark, 2004). In the case of aerobic utilization of glucose, the tricarboxylic acid cycle (TCA cycle) is also incorporated, which results in a higher production of ATP and therefore a more efficient cell growth. Glycolysis and fermentative pathways are explained in the next paragraphs.

Glycolysis is for the most part a linear pathway that starts from the metabolite glucose-6-phosphate (G6P) and culminates in the production of pyruvate (Figure 5). Glucose can be transported and phosphorylated into G6P by the phosphotransferase system (PTS), a well studied mechanism that is also related to catabolic repression of the utilization of other carbon sources (Romeo & Snoep, 2005). Other carbon sources, such as galactose and maltose, are first transformed in an intermediate metabolite, glucose-1-phosphate (G1P), which is then converted into G6P by the action of a phosphoglucomutase (Pgm) (Romeo & Snoep, 2005). The first reaction in glycolysis is the conversion of G6P into fructose-6-phosphate (F6P) mediated by phosphoglucose isomerase (Pgi). F6P is an essential metabolite that either goes to the pentose phosphate pathway (PP pathway) or continues in the glycolytic pathway by adding a second phosphorylation that results in fructose-bi-phosphate (FBP). The interconversion of F6P and FBP is considered a regulatory step in the glycolysis, as it is catalyzed by two

phosphofructokinases (Pfk-1 and Pfk-2) that present allosteric and genetic regulation (Romeo & Snoep, 2005). Pfk-1 and Pfk-2, are encoded by the genes *pfkA* and *pfkB* respectively, the first being responsible for 90% of the enzymatic activity in this step (Romeo & Snoep, 2005). FBP is reversibly dissociated into two metabolites, glyceraldehyde-3-phosphate (GAP) and di-hydroxyacetone-phosphate (DHAP). DHAP can be transformed into GAP by the action of a triosephosphate isomerase (TPI) and continue with the glycolytic pathway, or it can be transformed into the toxic metabolite methylglyoxal (MG). GAP is interconverted through four successive reactions into phosphoenolpyruvate (PEP), resulting in the production of one molecule of ATP and one molecule of NADH (equivalent to two reducing equivalent, H) (Romeo & Snoep, 2005). The last reaction in glycolysis is the conversion of PEP into pyruvate (PYR), producing one ATP. This reaction is catalyzed by the action of two pyruvate kinases (PykF and PykA), both subject to genetic and allosteric regulation (Romeo & Snoep, 2005). In the case of glucose utilization, glycolysis represents the production of two NADH (four reducing equivalents, H) given that one molecule of glucose allows the production of two molecules of PYR. These molecules of NADH need to be reoxidized to maintain redox poise, which is achieved either by using fermentative pathways or by the action of an external electron acceptor.

In the absence of external electron acceptors, *E. coli* utilizes **fermentative pathways** to generate products that are more reduced than the starting metabolite, resulting in a pathway that oxidizes the reducing equivalents generated during the glycolysis. Fermentative pathways can produce a variety of products, such as acetate, carbon dioxide, dihydrogen, ethanol, formate, lactate, and succinate (Sawers & Clark,

2004). Figure 5 shows how these fermentative pathways connect to the glycolysis, starting from either PEP or PYR.

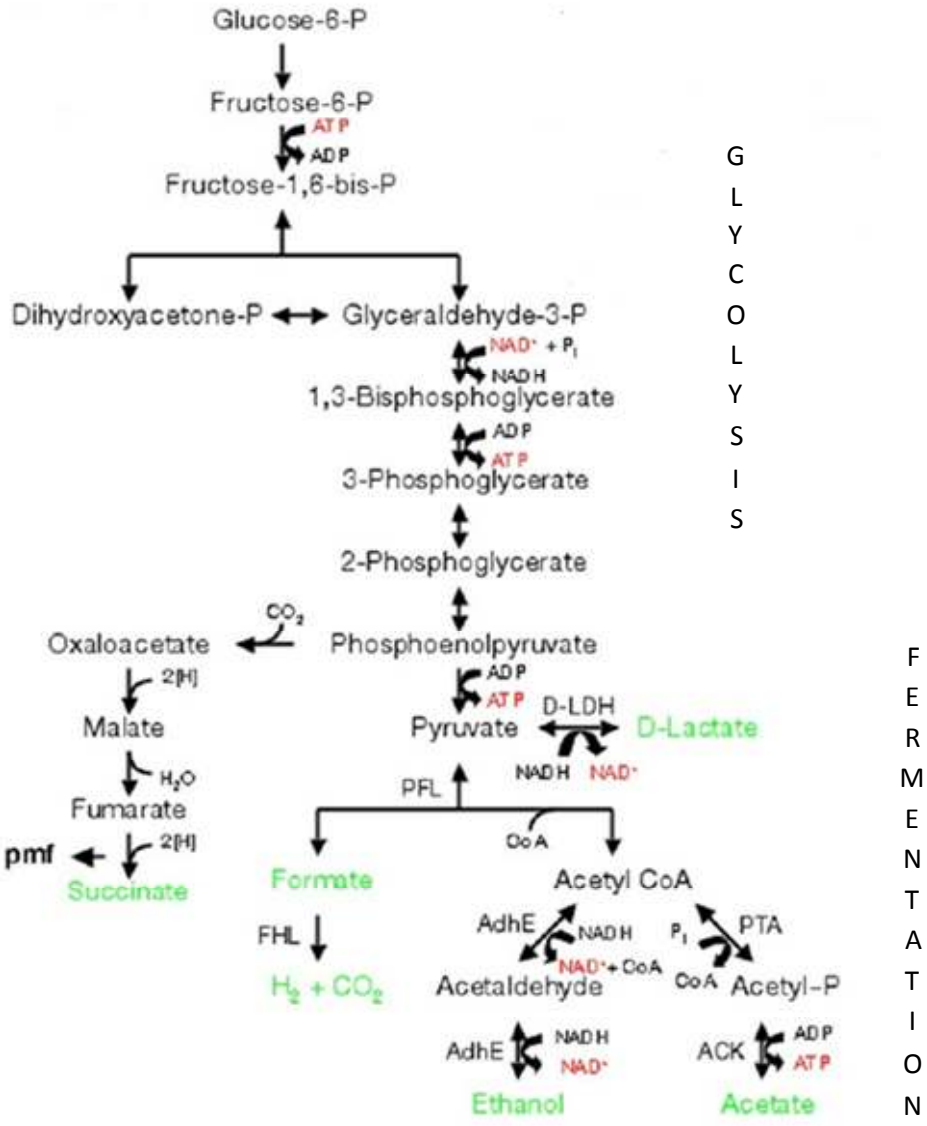

Figure 5: Glycolysis and fermentative pathways for *E. coli*. Intermediate metabolites are shown in black and fermentative products appear in green. (Sawers & Clark, 2004).

In order to understand how the fermentative pathways allow the cell to achieve redox balance, it is necessary to consider the degree of reduction of carbon molecules in substrates, products, and biomass production. The degree of reduction per carbon in a molecule can be calculated in three steps: 1) define a set of reference compounds with a

degree of oxidation equal to zero, 2) calculate the oxidation number of each element in the reference system, and 3) calculate the degree of reduction by adding the number of oxidation in the molecule and dividing it by the amount of carbons (Ratledge & Kristiansen, 2001). Selection of H_2O, H^+, HCO_3^-, SO_4^{2-}, and H_2SO_4 as reference compounds results in the following oxidation number per element: O = -2, H = 1, C = 4, S = 6, and N = -3. Table 1 shows the degree of reduction per carbon in substrates, metabolites, products, and biomass. Thus, the 2 molecules of NADH generated in the glycolysis during glucose utilization can be reoxidized by transforming PYR into some of the products with a higher degree of reduction, such as ethanol or lactate. The amount of reducing equivalent that each of the fermentative pathways generates is shown in Figure 5.

Table 1: Oxidation state and degree of reduction of various substrates, intermediate, products, biomass and reactions.

Compound	Formula	Degree of reduction
Substrates		
Glucose	$C_6H_{12}O_6$	4
Xylose	$C_5H_{10}O_5$	4
Glycerol	$C_3H_8O_3$	4.67
Intermediate		
PYR	$C_3H_3O_3$	3
Products		
Acetic Acid	$C_2H_4O_2$	4
Ethanol	C_2H_6O	6
Formic acid	CH_2O_2	2
Lactic acid	$C_3H_6O_3$	4
Succinic acid	$C_4H_6O_4$	3.5
1,2-PDO	$C_3H_8O_2$	5.33
1,3-PDO	$C_3H_8O_2$	5.33
Carbon dioxide	CO_2	0
Biomass	$CH_{1.9}O_{0.5}N_{0.2}$	4.3

Although different fermentative pathways allow achieving redox balance, not all of them are efficient in energy production. For instance, one molecule of PYR going to ethanol consumes 2 molecules of NADH and does not produce energy; in contrast, production of acetate from PYR produces one molecule of ATP, but it does not consume any reducing equivalent. Since glucose utilization allows the production of two molecules of PYR, producing 50% ethanol and 50% acetate is an option that both achieves redox balance and produces ATP.

So far the analysis of redox balance has been done without including the production of biomass. The degree of reduction of reactions can be calculated as the difference of degree of reduction of products and substrates, weighted by the stoichiometric number and the amount of carbons. Thus, if glucose is used for the production of biomass, it results in the consumption of part of the reducing equivalents generated during glycolysis. On the other hand, if the carbon source is more reduced than the biomass (e.g. glycerol), the fermentative pathways need to be able to reoxidize the reducing equivalents generated during glycolysis and biomass production.

In the presence of an external electron acceptor, such as oxygen, fermentative pathways are no longer required to achieve redox balance, and metabolites generated in the glycolysis can go to the TCA cycle. This cycle is part of the aerobic respiration process, and it generates energy (as ATP) by reducing metabolites and subsequently increasing the number of reducing equivalents (Alberts, 2002). The final electron acceptor in respiration is oxygen, which allows the reoxidation of reducing equivalents.

2.1.2 Glycerol fermentation

Glycerol fermentation is an attractive system to produce biofuels because of its potentially high efficiency. When compared with common sugars such as glucose and xylose, the highly reduced nature of glycerol (Table 1) represents a higher theoretical yield of ethanol (Dharmadi et al., 2006). This section presents the current knowledge of glycerol fermentation in bacteria.

Glycerol fermentation in bacteria

Among the few species that are able to ferment glycerol anaerobically, there are *Klebsiella*, *Enterobacter*, and *Citrobacter*. The mechanism that allows these bacteria to ferment glycerol has been studied for years. In these organisms, the fermentation of glycerol is linked to the ability to metabolize glycerol through two pathways: reductive and oxidative (Lin, 1976; Zhu et al., 2002). Figure 6 shows the two pathways that allow the utilization of glycerol: the oxidative pathway produces DHAP and the reductive pathway produces 1,3-propanediol (1,3-PDO). In the oxidative pathway, glycerol is dehydrogenated by a NAD-dependent glycerol dehydrogenase (glyDH-I), resulting in the formation of dihydroxyacetone (DHA). Then, DHA is phosphorylated by a DHA kinase (DHAK), resulting in the formation of DHAP, which is incorporated to the glycolysis. DHAK requires either PEP or ATP to donate the phosphate group (Yazdani & Gonzalez, 2007). Additionally, fermentation of glycerol in these members of the *Enterobacteriaceae* family is linked to their ability to produce 1,3-PDO. Production of 1,3-PDO starts with the dehydration of glycerol by the coenzyme B_{12}-dependent glycerol dehydrogenase (GlyD) resulting in the production of 3-hydroxypropionaldehyde (3-

HPA). This molecule is then reduced to 1,3-PDO by the action of the NADH-dependent 1,3-PDO dehydrogenase (1,3-PDODH) (Yazdani & Gonzalez, 2007).

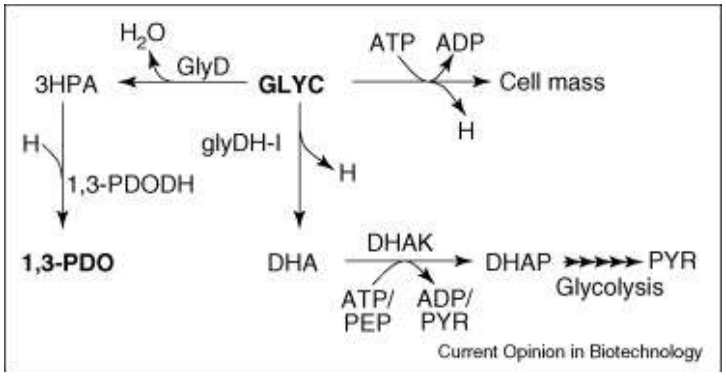

Figure 6: Glycerol utilization model for species of the *Enterobacteriaceae*. 1,3-PDO: 1,3-propanediol, GLYC: glycerol, DHA: dihydroxyacetone, 3HPA: hydroxypropionaldehyde, DHAP: di-hydroxyacetone phosphate, PYR: pyruvate, DHAK: di-hydroxyacetone kinase (Yazdani & Gonzalez, 2007).

To understand why glycerol fermentation requires the production of 1,3-PDO in members of the *Enterobacteriaceae* family, it is necessary to understand how to achieve redox balance. First, the degree of reduction of glycerol and biomass (shown in Table 1) indicates that glycerol is more reduced than biomass (4.67 versus 4.3), which is the opposite case than in the utilization of glucose. Consequently, biomass production starting from glycerol generates reducing equivalent. In addition, production of ethanol is redox balanced when glycerol is the carbon source (Figure 5). Although the ethanol fermentation pathway is able to consume the reducing equivalents generated during uptake of glycerol and glycolysis, this pathway is not able to consume any of the extra reducing equivalents that would be generated during cell growth; therefore, a different pathway is necessary. Production of 1,3-PDO allows the reoxidation of reducing equivalents but this pathway does not generate energy; consequently, both pathways (production of ethanol and 1,3-PDO) need to be combined to enable maintenance and cell growth.

A few other organisms have been reported to ferment glycerol without producing 1,3-PDO, such as *Propionibacteria freudenreichii* and *Propionibacteria acidipropionici ssp shermanii*, (Bories et al., 2004). Nevertheless, the pathways that enable these organisms to ferment glycerol have not been well studied.

Glycerol fermentation in E. coli

E. coli does not have the ability to produce 1,3-PDO; consequently, it was believed that this organism fermented glycerol only in the presence of an external electron acceptor. Aerobic utilization of glycerol starts with the transport of glycerol into the cell using passive diffusion or facilitated diffusion by the aquaglyceroporin GlpF (Heller et al., 1980). The gene encoding this enzyme (*glpF*) belongs to the same operon as the gene *glpK*. The product of *glpK* is an ATP-dependent glycerol kinase (GlpK) that catalyzes the conversion of glycerol into glycerol-3-phosphate (G3P) (Booth, 2005). Two glycerol 3-phosphate dehydrogenases (GlpD and GlpABC, for aerobic and anaerobic conditions respectively) allow the oxidation of G3P into DHAP (Booth, 2005). These enzymes are membrane-bound flavin-dependent, and the reaction results in the production of one reduced ubiquinone (ubiquinol). In the absence of external electron acceptors, the second reaction cannot proceed as there are no later steps to reoxidize the ubiquinol, resulting in the accumulation of G3P in toxic levels (Booth, 2005). Figure 7 shows this pathway.

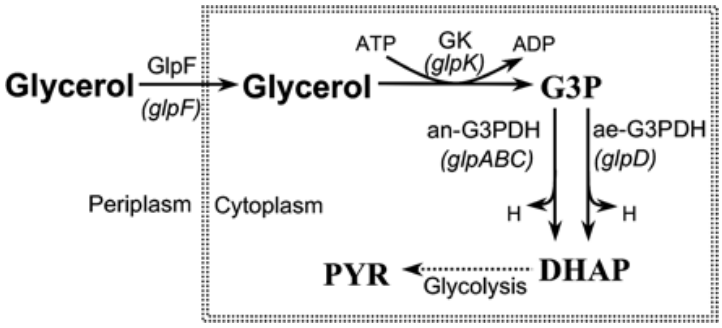

Figure 7: Respiratory utilization of glycerol by *E. coli*. PYR: pyruvate, G3P: glycerol-3-phosphate, DHAP: di-hydroxyacetone phosphate. G3P: glycerol-3-phosphate, an-G3PDH: anaerobic G3P dehydrogenase, ae-G3PDH: aerobic G3P dehydrogenase (Murarka et al., 2008).

The discovery that *E. coli* is able to consume glycerol in the absence of external electron acceptors motivated several studies to understand the experimental conditions as well as the pathways required in this process, since *E. coli* is a highly attractive host for the production of chemicals and biofuels. The first experiment that showed fermentative utilization of glycerol in *E. coli* utilized a rich medium (Dharmadi et al., 2006), but later experiments were performed in a minimum medium supplemented with tryptone, sodium selenite, and Na_2HPO_4 (Murarka et al., 2008). In these batch experiments, the initial concentration of glycerol was 110 mM at 37°C. The optimum pH was identified as 6.3, although alkaline conditions were tolerable when a supplemented minimum medium was used. Fermentation of near 80% of the glycerol took 96 hours, with a maximum specific growth rate of 0.04 h^{-1} (Murarka et al., 2008). Figure 8 shows the utilization of glycerol in 96 hours, and the corresponding production of biomass, ethanol and other byproducts. Products of this process are 1,2-propanediol (1,2-PDO), acetic acid, succinic acid, formic acids (minor amounts), carbon dioxide, hydrogen, and ethanol, the latter corresponding to the most abundant (other than hydrogen and carbon dioxide) (Gonzalez et al., 2008; Murarka et al., 2008). Ethanol corresponds to nearly 95% of the fermentative products, while 1,2-PDO presents a very low concentration (0.5 ±0.15 mM in stationary phase)

(Gonzalez et al., 2008). These results contrast with the products of glucose fermentation in *E. coli*, where the main product is lactate (not observed in glycerol fermentation), ethanol represents only a 29%, and there is no evidence of 1,2-PDO production (Sawers & Clark, 2004).

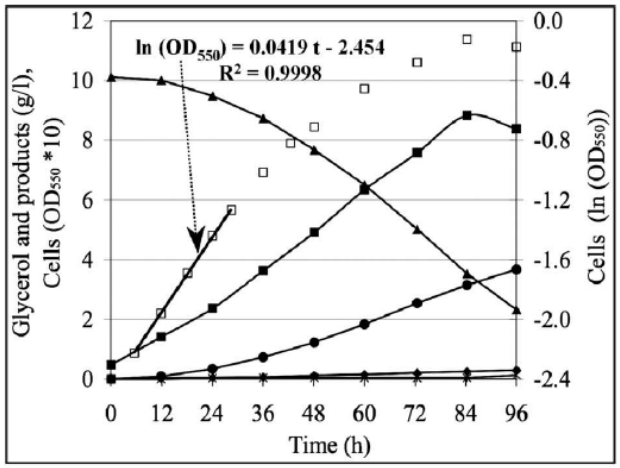

Figure 8: Glycerol fermentation by *E. coli* MG1655. Cell density: black squares. Cell density log-linear: white squares. Ethanol: black circles. Glycerol: triangles. Succinic acid: rhombus. Formic plus acetic acids: cross. 1 OD = 0.34 gCDW/L.

Glycerol fermentation in *E. coli* starts with the conversion of glycerol into DHA catalyzed by the enzyme glycerol dehydrogenase (glyDH), a type two glycerol dehydrogenase encoded by the gene *gldA* (Gonzalez et al., 2008). The existence of this gene was known before the discovery of *E. coli* being able to ferment glycerol, but it was considered cryptic (Truniger & Boos, 1994). The discovery that *E. coli* can express this enzyme is key in the fermentation of glycerol, and it constitutes one of the essential enzymes of this process (Gonzalez et al., 2008). The next step is the phosphorylation of DHA into DHAP by the action of the PEP-dependent di-hydroxyacetone kinase (DHAK). This enzyme, likewise glyDH, is essential for the utilization of glycerol in the absence of external acceptors (Gonzalez et al., 2008).

Studies were conducted to investigate the effect of alternative pathways for the breakdown of glycerol, as well as the branches to different products. Disruption of the gene *glpK* (responsible for the conversion of glycerol into G3P) decreased the maximum specific growth rate in 17.5% (Murarka et al., 2008), suggesting that although this enzyme is not essential, it contributes to the process. In addition, deletion of fermentative pathways indicates that ethanol production is essential for glycerol fermentation, while disruption of acetate production (deletion of gene *pta*) resulted in a decrease in the maximum specific growth rate of nearly 30% (Murarka et al., 2008). Disruption of the enzyme formate-hydrogen lyase (FHL), responsible for the conversion of formate into hydrogen (H_2) and carbon dioxide (CO_2), results in a significant reduction of cell growth, a phenomenon than has been attributed to the necessary presence of CO_2 in the media and the negative effects of H_2, as it affects the redox balance (Gonzalez et al., 2008; Murarka et al., 2008).

Given the inability of *E. coli* to produce 1,3-PDO, and the finding that 1,2-PDO is a byproduct of glycerol fermentation, a new model linked to 1,2-PDO production was proposed to explain the fermentation of glycerol (Gonzalez et al., 2008). Figure 10 presents two pathways that could allow the production of 1,2-PDO in *E. coli*. They both start with the conversion of DHAP into MG, a highly toxic compound for *E. coli* (Booth, 2005). MG can be converted into 1,2-PDO via production of either hydroxyacetone (HA) or lactaldehyde (Lald), both reducing steps that result in the consumption of one NADH (or NADPH). Experimental data support the production of 1,2-PDO through HA rather than through Lald, as genetic disruption in the first branch decreases the production of 1,2-PDO to nearly 65% of original values, while disruption in the second branch does not

have any effect (Gonzalez et al., 2008). Interestingly, the enzyme that catalyzes the reduction of HA to 1,2-PDO is glyDH (encoded by *gldA*), the same that oxidizes glycerol to DHA in the first step of glycerol breakdown under fermentative conditions, which highlights the importance of this enzyme.

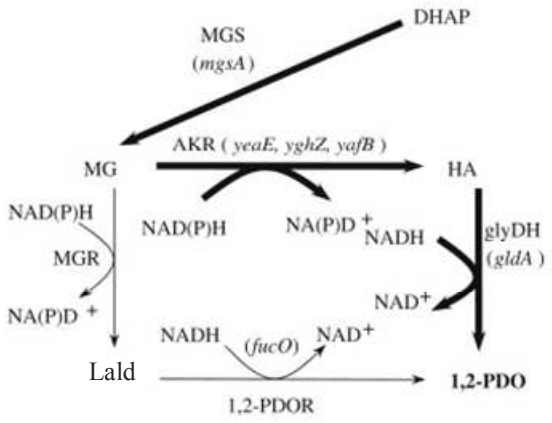

Figure 9: Metabolic pathways for the production of 1,2-PDO in *E. coli*, starting form DHAP. Tick lines represent the most probably pathway for glycerol fermentation in *E. coli* (Gonzalez et al., 2008). DHAP: di-hydroxyacetone phosphate, MG: methylglyoxal, HA: hydroxyacetone, Lald: lactaldehyde, 1,2-PDO: 1,2 propanediol.

Figure 10 presents the glycerol uptake pathway, combining with the production of fermentative products and 1,2-PDO. The transformation of DHA to DHAP via a PEP-dependent (DHAK) requires that this reaction combines with the last step in the glycolysis, which is responsible for the conversion of PEP into PYR. A simple stoichiometric analysis predicts that PEP is converted into PYR at the same rate that DHA is converted to DHAP, but this is incompatible with the fact that part of the flux is going to the production of 1,2-PDO. One pathway that could partially explain it is the conversion of glycerol into DHAP going through G3P, a pathway that requires the already mentioned GlpK and GlpABC. Nevertheless, disruption of this pathway only results in a decrease in the cell growth, not in a total inability to ferment glycerol. Therefore, these experimental findings indicate that additional pathways may play an important role in the fermentation of glycerol in *E. coli*, a fact that emphasizes the

importance of conducting additional studies in glycerol fermentation in order to identify all pathways involved in the process. Despite experimental studies of glycerol fermentation in *E. coli*, no mathematical analysis of glycerol fermentation has been conducted previous to this thesis.

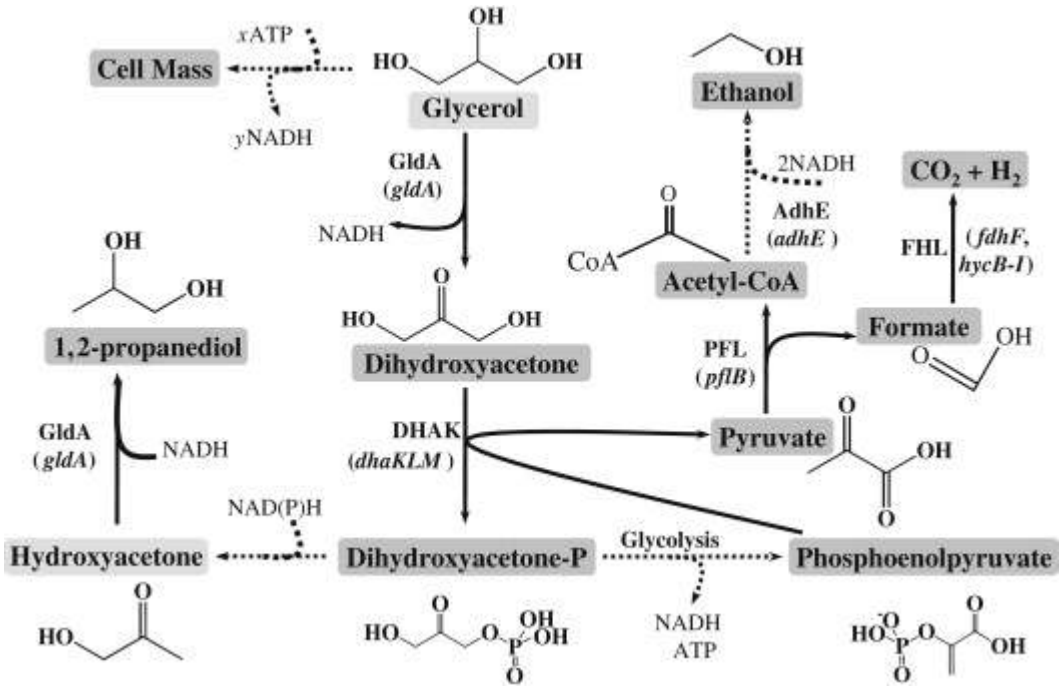

Figure 10: Proposed model for glycerol fermentation in *E. coli*. Production of ethanol and 1,2-PDO is essential to support cell growth as a combined synthesis of these two products supports the generation of ATP and the consumption of reducing equivalents. GldA: glycerol dehydrogenase, DHAK: di-hydroxyacetone kinase, FHL: formate hydrogen lyase, PFL: pyruvate formate lyase, AdhE: alcohols/aldehyde dehydrogenase (Gonzalez et al., 2008).

2.1.3 Glucose utilization and the production of advanced biofuels

The mechanism that carries the consumption of glucose in *E. coli* has been well documented, as glucose is a preferred substrate by this and many other microorganisms. The incorporation of glucose into *E. coli* utilizes the phosphotransferase system (PTS), which results in the transport and phosphorylation of glucose to produce G6P using PEP as the phophoryl group-donor (Mayer & Boos, 2005). The PTS consist of the general

component and the sugar-specific component. The general component includes the enzyme I (EI), encoded by the gene *ptsI*, and the histidine protein (HPr), encoded by the gene *ptsH*. The sugar-dependent component includes the enzyme complexes II, corresponding to enzymes EIIA, encoded by the gene *crr*, and EIIBC, encoded by the gene *ptsG*. The phosphoryl group is subsequently transferred from PEP to EI, HPr, EIIB, and then to glucose, resulting in the production of G6P. The domain EIIC is responsible for the transport of glucose across the membrane into the cell (Mayer & Boos, 2005). Once G6P is in the cytoplasmatic compartment, it can be metabolized in the glycolysis as explained above (page 18), or go into the pentose phosphate pathway (PPP) to produce the essential metabolites ribose-5-phosphate, sedpheptulose-7-phosphate and erythrose-4-phospthate (Ecocyc website).

The PTS system is also involved with the gene expression regulation system. In the absence of glucose, the predominantly present phosphorylated EIIA causes catabolic repression of genes involved in the transport and utilization of sugars. In contrast, the presence of glucose increases the concentration of nonpnosphorylated EIIA, which prevents the use of other substrates by inhibiting the activity of non-PTS sugar transport system (Mayer & Boos, 2005).

Glucose has been utilized for the production of advanced biofuels in *E. coli*. Advanced biofuels are molecules with a higher energy density than traditional biofuels, making them more comparable to traditional fuels. For example, ethanol, the most widely used biofuels, only contains 70% of the energy density of gasoline, while butanol, an advance biofuel, contains 84% of the energy density of gasoline (Atsumi et al., 2008a; Peralta-Yahya & Keasling, 2010). However, for most advanced biofuels there is no

natural pathways to produce them (butanol being the exception), but in recent years a number of efforts have been made in experimental work to implement the production of advanced biofuels in bacteria, and specifically in *E. coli*. The following paragraphs review the most remarkable pathway to convert glucose into advanced biofuels: the fatty acid (FA) biosynthesis pathway, the α-keto acid pathway, and the reversal of the β-oxidation cycle.

E. coli has been metabolically engineered to produce long chain chemicals using the **FA biosynthesis pathway** and **proper termination enzymes** (Steen et al., 2010). The FA biosynthesis pathway is a well studied process in *E. coli*, in which one molecule of AcCoA is converted into malonyl-ACP (malACP) using energy, and then the malACP is utilized to elongate an acyl-ACP molecule (Cronan & Rock, 2008). A diagram of this pathway is shown in Figure 11. The mechanisms that converts AcCoA into malACP requires the genes *accC*, *accAD*, *acpH*, *acpS* and *fabD*, and it uses the energy of one phosphoryl group from ATP (Figure 11-A). The molecule malACP can be combined with one molecule of AcCoA (using enzyme FabH) to produce acetoacety-ACP, which initiate FA synthesis, or it can be used as carbon donor in the elongation cycle (Figure 11-B). The elongation cycle for FAs consists of four reactions: reduction (catalyzed by enzyme FabG), dehydrogenase (catalyzed by enzyme FabZ), reduction (catalyzed by enzyme FabI), and elongation (catalyzed by enzymes FabB and FabF) (Cronan & Rock, 2008).

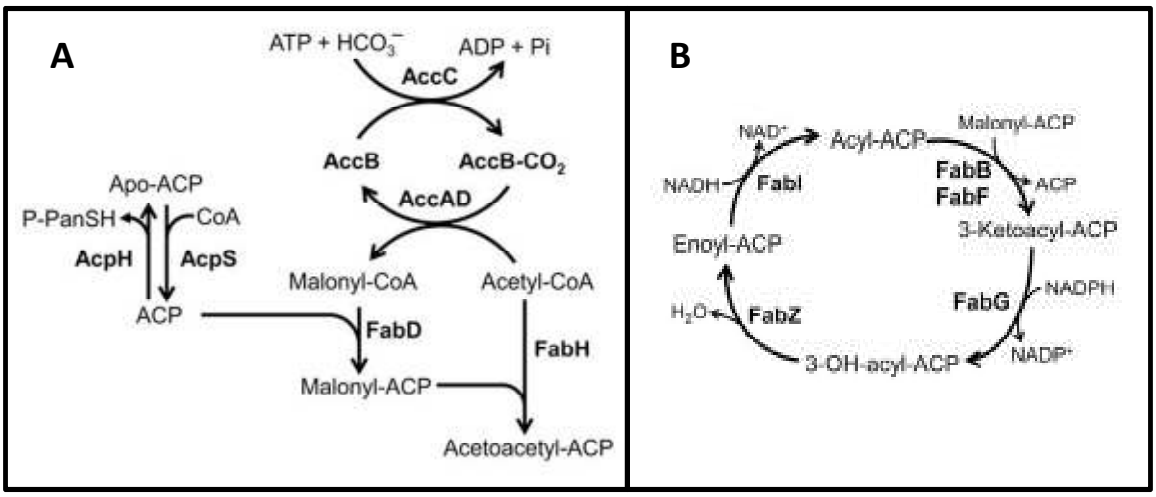

Figure 11: FA biosynthesis pathway. Panel A shows the production of malACP and acetoacetyl-ACP for elongation and initiation of the production of fatty acids. Panel B shows the elongation cycle, which incorporates the two carbon molecules from mal-ACP to produce acyl-ACP (Cronan & Rock, 2008).

Using the FA biosynthesis pathway and metabolic engineering, Steen and collaborators proved the production of a variety of long chain products, such as fatty alcohols and fatty esters (Steen et al., 2010). Figure 12 shows a diagram that summarizes this pathway and the genetic modifications involved. Synthesis of desired products resulted from the overexpresion of thioesterases (TES) and acyl-CoA ligases (ACL) to produce AcCoA, and the different products were obtained by overexpressing fatty-acyl-CoA reductase (FAR) for the production of fatty alcohols, and acyltransferase (AT) for the production of esters. Other products were also produced in this study, including biodiesels. Production of long chain FAs was obtained at a yield of 6% (w/w), while production of long chain fatty alcohols was not reported in yields, a 2% (w/v) of glucose was converted into 60 mg/l, which correspond to a yield of 3% (w/w) assuming that all the glucose was consumed (not reported) (Steen et al., 2010).

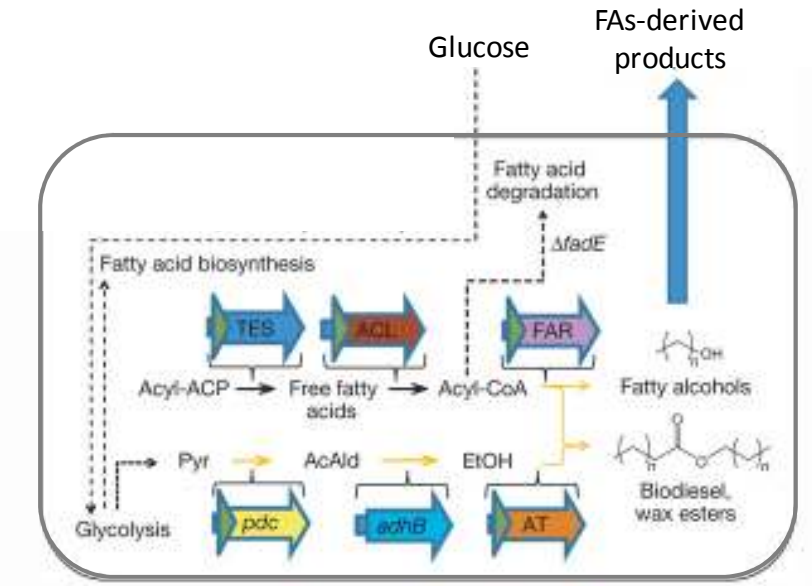

Figure 12: Metabolic pathway for the production of long chain products using the FA biosynthesis pathway. Figure is an adaptation from Steen and collaborators. TES: Thioesterase, ACL: Acyl-CoA ligases, FAR: fatty-acyl-CoA reductase, pdc: pyruvate decarboxylase, adhB: alcohol dehydrogenase, AT: Acyltransferase, Pyr: pyruvate, EtOH: ethanol, AcAld: acetaldehyde (Steen et al., 2010).

A different approach that has been implemented for the production of synthesis of long chain products is the **α-keto acid pathway**, which unlike the FA biosynthesis pathway, incorporates one molecule of carbon per cycle. This pathway was developed in Dr. James Liao's research center, and it modifies an aminoacids biosynthesis pathway for the production of linear alcohols. Figure 13 shows a diagram of how this pathway converts glucose into butanol. Using this strategy the production of butanol consists of using the biosynthesis pathway for the production of threonine, converting this molecule into 2-ketobutyrate, and then elongating 2-ketobutyrate incorporating one molecule of acyl-CoA and releasing one molecule of CO_2 (utilizing genes *leuA*, *leuCD* and *leuB*), resulting in the production of the intermediate 2-ketavalerate. Finally, production of butanol is achieved by reducing 2-ketovalerate using genes *kivd* (from *Lactococcus lactis*) and ADH2 (from *Saccharomyces cerevisiae*) (Figure 13) (Shen & Liao, 2008). Thus, the combination of gene *leuA*, *leuCD* and *leuB* allows the elongation in one

molecule of carbon, and it extension to produce hexanol has been proved (Marcheschi et al., 2012).

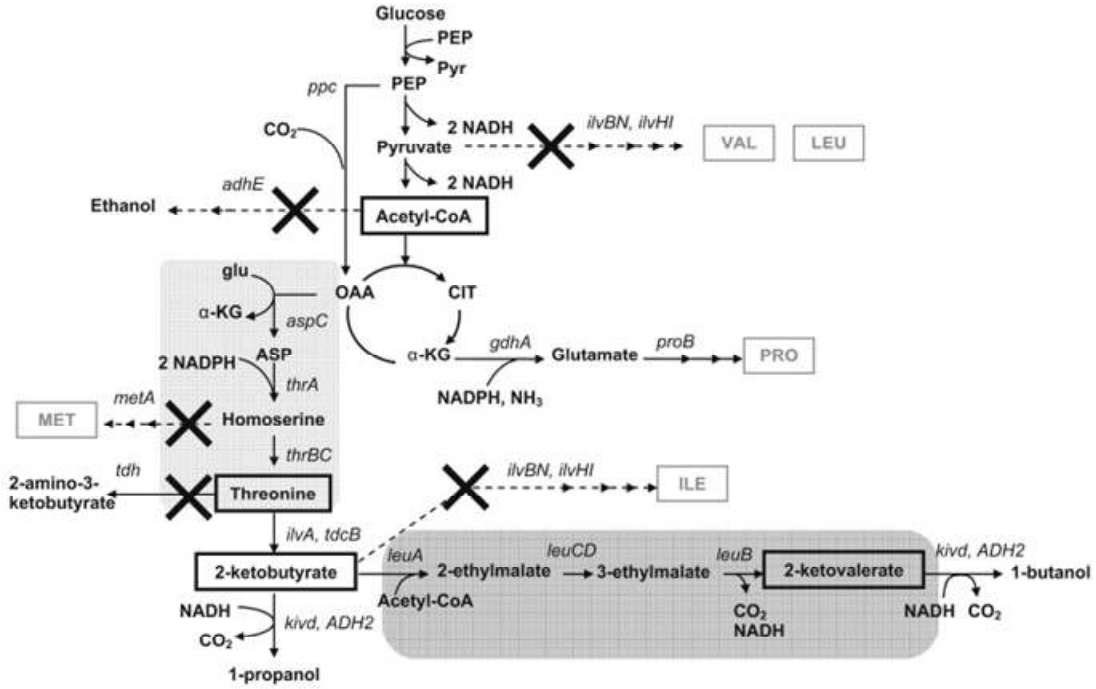

Figure 13: Schematic illustration of the production of propanol and butanol utilizing the threonine biosynthesis pathway (Shen & Liao, 2008). Enzymes LeuA, LeuCD and LeuB elongate the intermediate product in one carbon, and it can be utilized to produce 1-pentanol and 1-hexanol.

More recently a new promising pathway has been implemented for the synthesis of long chain products in *E. coli*: the **reversal β-oxidation cycle**. In 2011, Dellomonaco and collaborators engineered the β-oxidation cycle, which normally breaks down fatty acids into AcCoA molecules, to produce medium and long chain products (includying alcohols and fatty acids) starting from glucose (Dellomonaco et al., 2011). The implementation of this pathway required the modification of the regulatory pathway in wild type *E. coli* in order to activate this pathway in the absence of natural substrate (i.e., fatty acids) and the presence of glucose. The metabolic pathway requires the breakdown

of glucose into AcCoA, a molecule that is used both as starting point for the reversal β-oxidation cycle, and as carbon donor for the elongation step in this cycle (Figure 14).

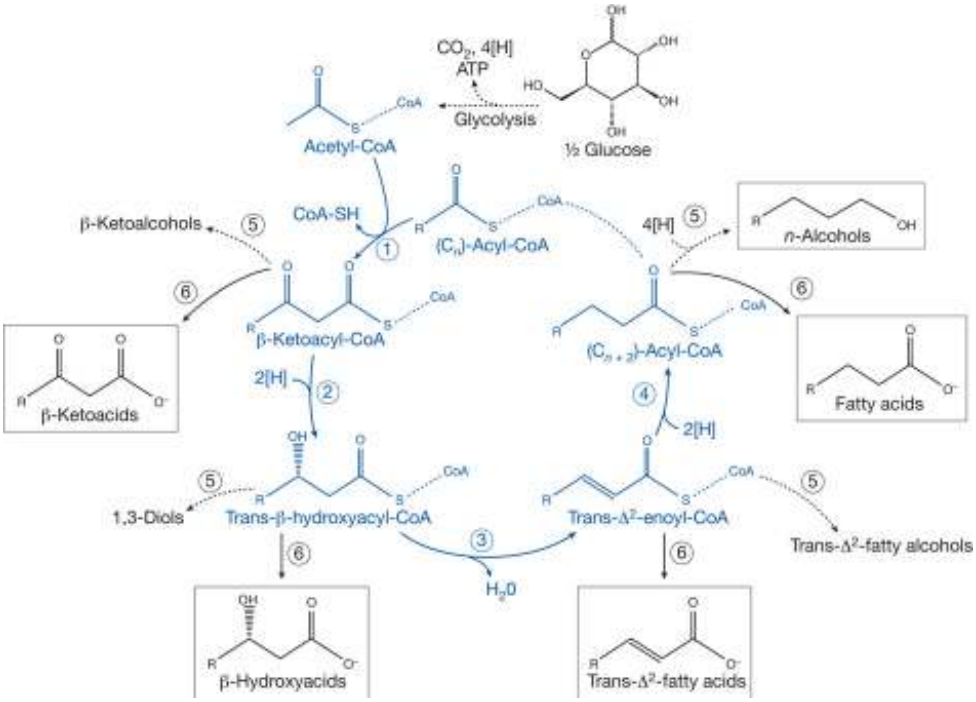

Figure 14: Illustration of the reversal β-oxidation cycle to synthesize long chain products. Glucose is first break down into acetyl-CoA in the glycolysis, a process that results in production of ATP and reducing equivalents. Then acetyl-CoA is utilized to produce the primer of the cycle, and also as elongation molecule in the cycle. Expression of proper termination enzymes results in the production of alcohols and fatty acids (Dellomonaco et al., 2011).

The primer of the reversal β-oxidation cycle is synthesized by the enzyme acetyl-CoA acetyltransferase (AtoB), which catalyze the conversion of two molecules of acetyl-CoA into one molecule of acetoacetyl-CoA (a ketoacyl-CoA). The reversal β-oxidation cycle has 4 steps in addition to the starting point: elongation, reduction (first), dehydration and reduction (second). Ketoacyl-CoA molecule is reduced by the action of FadB, producing a molecule of hydroacyl-CoA. The reaction oxidizes one molecule of NADH in turn. Hydroacyl-CoA is dehydrated by the action of FadB. A second reduction occurs by the action of *enoyl-CoA reductase*, a reaction that has been proposed to use ferredoxins as reducing equivalents, associated to the gene *ydiO*. The expression of

proper termination enzymes resulted in the production of long chain FAs at yields of 28% (w/w), and of higher chain liner alcohols (C6-C10) at 8.3% (w/w). These values are higher than those reported using other the FA biosynthesis pathway and the α-keto acid pathway, which was proposed to be due energetic efficiencies of this pathway (Dellomonaco et al., 2011). More recently additional experimental efforts have been done using this pathway, especially in order to have a more controllable system for the regulatory system (Clomburg et al., 2012), but previous to this thesis no studies have been done using mathematical models. The utility of these models, as well as the state of art of pertinent mathematical models, is the focus of the following section of this chapter.

2.2 Mathematical modeling of microbial metabolism

Mathematical modeling of metabolism in microbial organisms consists in expressing in mathematical language the interaction between biochemical reactions, metabolites, substrates, and products. Biochemical reactions are those reactions that interconvert metabolites (or substrates) into other metabolites (or products). Because these reactions take place in a microorganism, they are often catalyzed by enzymes. From a structural point of view, there are two main categories of mathematical modeling of metabolism: stoichiometric models and kinetic models (Gombert & Nielsen, 2000). These two models differ in complexity and applicability, and they provide answers to questions such as what is the transient answer of the system when an external variable is changed, which are the control reactions in a specific pathway, what is the maximum theoretical yield of biomass, and what pathways need to be activated or deleted in order

to increase product yield. These two kinds of models are complementary to each other as they study the metabolism from different points of view.

2.2.1 Stoichiometric modeling

Stoichiometric models require the definition of a set of metabolites and the reactions that interconnect these metabolites. Each reaction should keep the law of conservation of mass; in other words, there must be a valid stoichiometric relationship in each reaction. In addition to this, stoichiometric models assume that the system is in a steady state, and therefore there is no accumulation of any internal metabolite. A stoichiometric matrix (S) contains all the stoichiometric parameters, in which rows represent reactions and columns represent metabolites. Because this matrix is used for mathematical calculus, linearly dependent cofactors (such as ATP and ADP) are included just once in the stoichiometric matrix in order to avoid having a linearly dependent matrix. Figure 15 represent the implementation of stoichiometric modeling for a metabolic network. In steady a state, it is valid to say that the net rate of formation of each metabolite minus the dilution rate associated with that metabolite ($\mu \cdot M_i$) is equal to zero (Figure 15, c). The dilution term is usually neglected because levels of intracellular metabolites are small; therefore, this flux is also small when compared with other fluxes of production and consumption of metabolites (Stephanopoulos et al., 1998). This leads to an equation system, in which the vector of fluxes **v** contains the unknown rates (Figure 15, c). Nevertheless, the system is often underdetermined and additional tools should be included.

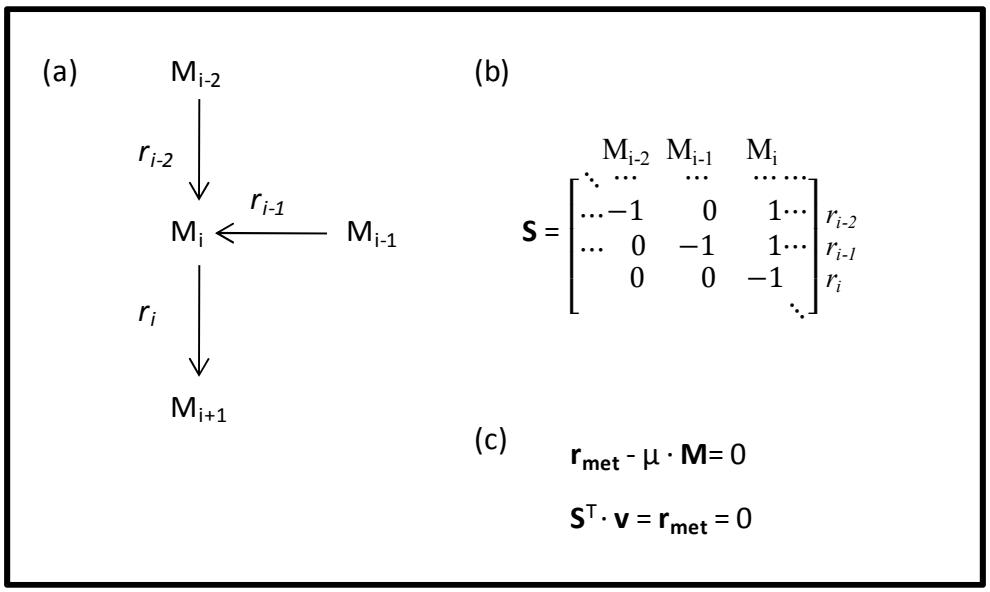

Figure 15: Stoichiometric Modeling. (a) Shows a segment of the structure of a metabolic network that is modeled. The metabolic network is translated into a matrix (b) in which rows represent metabolites and columns correspond to reactions. Finally, the stoichiometric matrix is used to write a system of equations in steady-state (c).

Stoichiometric models are used to find a list of feasible reactions that satisfy steady state conditions, but it is necessary to include more information in order to come near to realistic solutions. Because of this, stoichiometric models are often combined with **Metabolic Flux Analysis (MFA)**, which incorporates measurements of fluxes (external and/or internal) in order to reduce the degrees of freedom of the system. The application of MFA to a metabolic pathway has been explained by Stephanopoulos et al., and a summary of that method is presented here (Stephanopoulos et al., 1998).

Depending on the system and on the number of measured fluxes, the system might be determined, underdetermined, or overdetermined. Suppose that there are K metabolites and J fluxes in the system. In the matrix form, this means that the dimension of **v** is Kx1 and the dimension of **S** is JxK. The second equation in Figure 15, c presents a system with a degree of freedom F = J – K. To have a determined system, we need to measure F independent fluxes, which will reduce the freedom of the system to zero.

Assume F fluxes were measured and storage in the vector v_m, and the vector v_c storages the remaining unknown fluxes. Then the second equation in Figure 15, c can be re-written as:

$$0 = S^T \cdot v = S_m^T \cdot v_m + S_c^T \cdot v_c \quad (1)$$

which lead to a unique solution for the unknown fluxes:

$$v_c = -(S_c^T)^{-1} \cdot S_m^T \cdot v_m \quad (2)$$

The matrix S_c^T can be inverted since this is a square matrix of dimension KxK, and the solution is unique. If the system is overdetermined (the number of measured fluxes is greater than J – K) and there is little noise in measurements, the system can be determined using the Moore-Penrose pseudo-inverse matrix of S_c^T, named $(S_c^T)^{\#}$, which is square matrix. In this case we have:

$$v_c = -(S_c^T)^{\#} \cdot S_m^T \cdot v_m \, , \quad (3)$$

where $(S_c^T)^{\#}$ can be calculated as:

$$(S_c^T)^{\#} = (S_c \cdot S_c^T)^{-1} \cdot S_c \, . \quad (4)$$

If the system is underdetermined, optimization might be combined with MFA in order to elucidate the fluxes. In stoichiometric modeling, the system is linear; therefore, all theory from linear optimization can be applied. Here is presented a brief description of linear optimization, but it will be further explained together with Flux Balance Analysis (FBA). A linear optimization problem requires the definition of an objective function and a set of constraints. The objective function is usually the optimization of cell growth (Stephanopoulos et al., 1998), although other functions have also been proposed, such as optimization of product formation. Then, the system is restricted to the space of valid solutions that are allowed for each flux rate.

MFA requires the incorporation of measured fluxes. There are two ways to do this: measurement of external fluxes (without labeling) and measurement of internal fluxes (requires labeling). When this information is incorporated, the degrees of freedom of the system decrease. Measurement of internal metabolites increases the complexity of experiments but it also increases the quality of the calculus. In order to do this, substrates are labeled and then the labeled state of internal metabolites is measured. One widely used method for the determination of intracellular fluxes is the incorporation of isotopes of carbon (^{13}C or ^{14}C) in a specific position of a substrate. This results in an introduction of an asymmetry in the distribution of labeled carbon, which can be detected and used to calculate internal fluxes (Stephanopoulos et al., 1998). Distribution of internal metabolites is measured using either gas chromatography-mass spectrometry (GC-MS) or Nuclear Magnetic Resonance (NMR).

Stoichiometric modeling has also been used in conjunction with **flux balance analysis (FBA)**. This method uses optimization in order to simulate microbial metabolism (Kauffman et al., 2003). The fundamental difference between MFA and FBA is the scope: while MFA focuses on the determination of metabolic fluxes for one experimental condition, the goal of FBA is to predict metabolic fluxes of a system under new conditions (Llaneras & Pico, 2008). Optimization of a linear problem requires, as was already stated, the definition of an objective function and a set of constraints for the unknown fluxes. The objective function is a linear combination of other fluxes in the system, and the objective must either maximize or minimize that function. The mathematical formulation of this is as follows:

$$Objective\ Function = \frac{Max}{Min} \sum_{i=1}^{J} \alpha_i \cdot v_i \quad , \qquad (5)$$

where J is the number of fluxes of the system and α_i is the coefficient associated with the flux v_i. The objective in FBA is usually the maximization of biomass production, and other possible objective functions are the maximization of ATP production and maximization of a desired product (Kauffman et al., 2003). The use of Biomass as Objective Function (BOF) has been validated experimentally; in fact, FBA applied to *E. coli* using BOF has shown a quantitative prediction of growth in 86% (68 out of 79) of mutants examined by Edwards and Palsson (Edwards & Palsson, 2000). Constraints refer to the range of valid values that each flux can take. For instance, those reactions that are known to be irreversible should be restricted to the range of positive values. In general this requirement can be written in the following mathematical form:

$$l_i \leq v_i \leq u_i$$

where l_i and u_i represent the lower and upper admissible values for flux v_i. Other constraints that can be included are regulatory constraints (which fluxes are allowed under specific circumstances) (Covert et al., 2001) and incorporation of thermodynamics constraints (Beard et al., 2002).

Once the metabolic network has been established in conjunction with the stoichiometric relationship, flux constraints, and an objective function, the problem can be solved using a mathematical software. Figure 16 represents a hypothetical case in which v_1 and v_4 are unknown fluxes. Each of these fluxes has been restricted to a positive value, and the maximum value is as shown in the figure. Inclusion of additional restrictions coming from stoichiometric relationships defines the space of admissible solutions, also called solution space (area in color). The objective function is a linear

combination of fluxes of the system. Optimization of the objective function finds a solution (if possible), but in some cases multiple solutions are found.

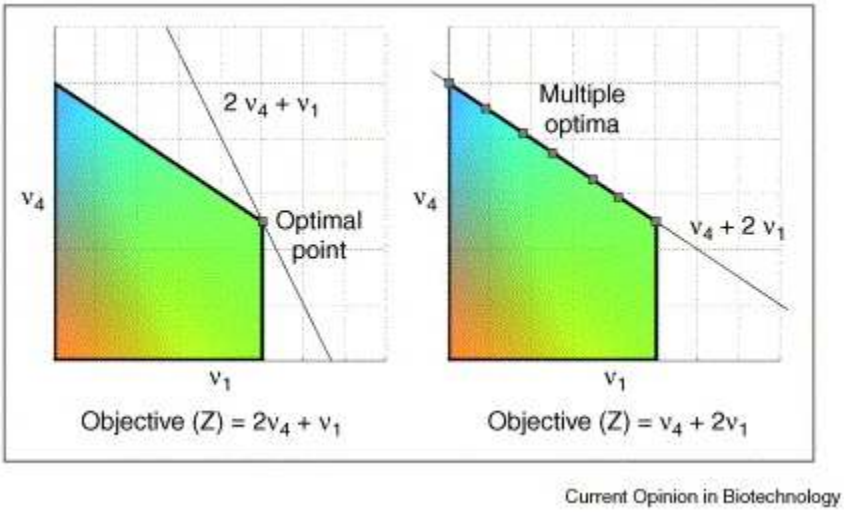

Figure 16: Linear optimization in a constraint system. Left figure represent a situation in which the optimum is unique, and right figure correspond to a case in which there are multiple optimum solutions (Kauffman et al., 2003).

Linear optimization is also used to find alternative metabolic fluxes that satisfy a desired condition (called **flux variability analysis**) and to perform **flux coupling analysis** (Zomorrodi et al., 2012). In the first case, flux variability analysis (FVA) identifies the minimum and maximum flux values for each reaction that will support certain condition of the optimal function (e.g., 95% of maximum specific growth rate). The second case uses FVA to identify if two fluxes vary independently of each other or not. Two fluxes are coupled if they depend on each other. These two tools are used to predict and study possible flux distributions.

The increase in information on metabolic networks, driven by genome sequencing of several organisms and "-omics" technologies, has allowed the implementation of a new kind of stoichiometric modeling: Genome Scale Models (**GEMs)**. These models represent large scale metabolic networks, and they utilize FBA to predict phenotypes. At

present at least 35 organisms have been modeled with this approach, including *E. coli* (Orth et al., 2010). Implementing a GEM requires an extensive literature review and a detailed consideration of reactions to be included. Figure 17 represents the four fundamental steps to build one of these models: (1) searching metabolic information in databases ("-omics), (2) reconstruction of the biochemical network, (3) *in silico* modeling, and (4) experimental validation. The construction of the model is complicated due to the large number of reactions that are included. In fact, after a draft metabolic network is built, the consistency of it must be checked to ensure that the model is not breaking thermodynamic laws (e.g. generation of energy in cycles), and that there are no missing reactions that prevent the model from being functional (Durot et al., 2009).

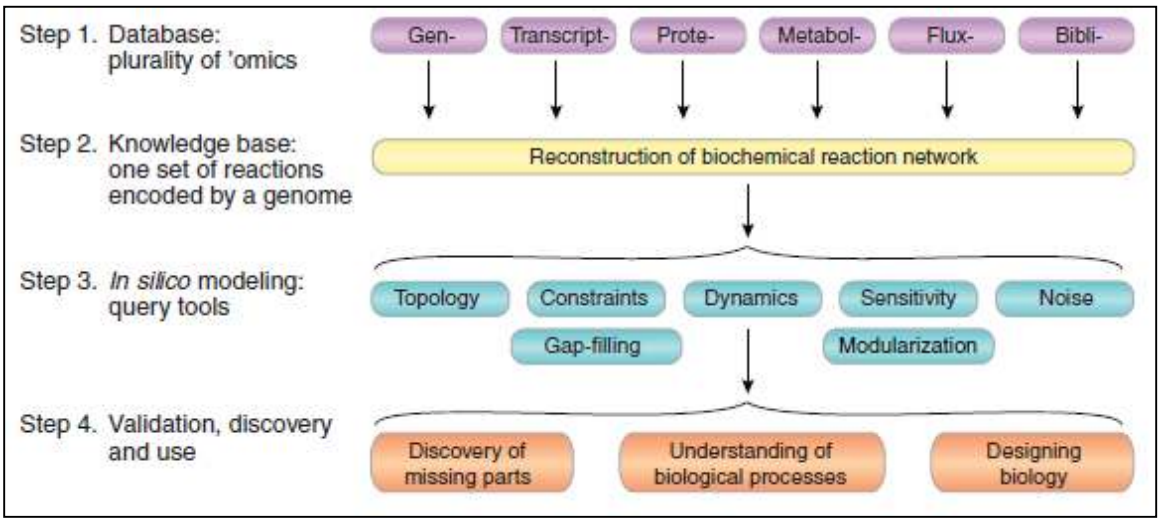

Figure 17: Genome-scale model construction. The scheme shows four steps for the construction a model, which include (1) bibliographic search with special focus in "omics" technology, (2) construction of the model, (3) *in silico* modeling and (4) validation and applications (Feist & Palsson, 2008).

GEMs have multiple applications for the study of microbial organisms and in metabolic engineering. The large number of metabolic interconnections included in a GEM allows consideration of the multiple requirements of the system. For instance, the biomass equation can contain a detailed account of the different building blocks that are

necessary. The main use of GEMs is to quantitatively identify physiological states of wild-type and mutant microorganisms (Feist & Palsson, 2008). The use of these models allows the identification of essential reactions and metabolites in a specific condition (Feist & Palsson, 2008). GEMs are also used in metabolic engineering because it can identify necessary changes to produce new products. (Feist & Palsson, 2008). In addition, GEMs can be used to drive biological discoveries, as these models allows the identification of gaps between the computational model and experimental information (Feist & Palsson, 2008). For instance, if the experimental data supports the existence of a pathway that creates a metabolite, but computational data does not reflect that, efforts can be made to identify the function of unknown ORFs that may be involved in that pathway.

The introduction of GEMs has laid the foundation for the development of optimization tools for the synthesis of desired products, remarkable being the **OptKnock** tool, which defines a bilevel linear optimization problem to propose reaction deletions that will result in optimizing the synthesis of a desired product and in coupling synthesis of the product to cell growth (Burgard et al., 2003). The bilevel problem consists on an outer and an inner problem: the outer problem is to find the optimal production rate of a desired chemical, and the inner problem is to optimize production of biomass (Figure 18-a). The expected solution identifies target reactions to knockout in order to optimize the synthesis of the desired product, and to couple it to biomass production. This expected result is exemplified in mutants A, B and C for the synthesis of succinate in Figure 18-b.

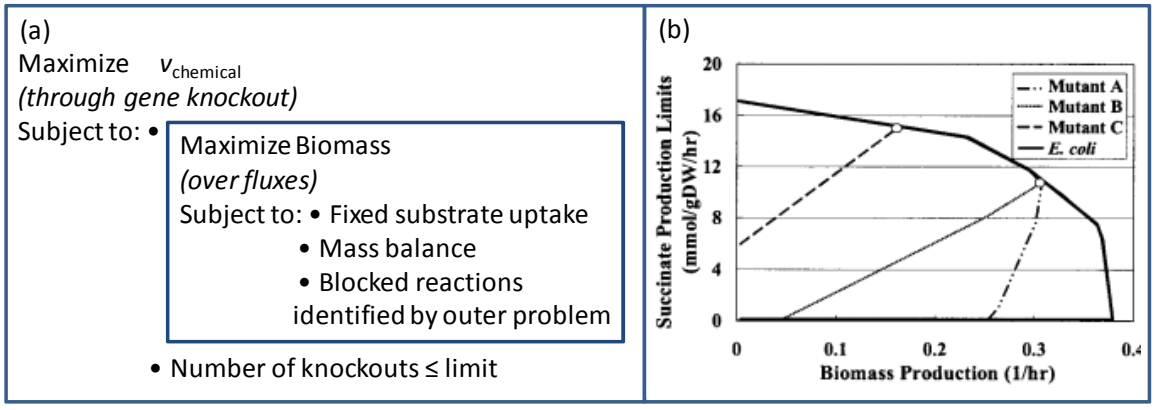

Figure 18: Optnock framework. a) The bilevel optimization structure of optKnock consists of two optimization problems that are solved simultaneously: optimization of the production of a chemical ($v_{chemical}$) and maximization of biomass (the inner problem). The achievement of these two objectives is facilitated by deleting reactions. b) One example of solution shows different mutants that result in the coupled production of succinate and biomass after removing reactions (Burgard et al., 2003).

2.2.2 Kinetic modeling

Kinetic Modeling includes, in addition to the stoichiometric balances, the kinetics of each of the reactions that are present in the model. Because the system is a microorganism, many of the reactions are catalyzed by enzymes. The kinetics of one reaction is defined by the rate law of the reaction plus the value of all involved kinetic parameters. For example, the most widely used kinetics of enzymes comes from the derivation of Michaelis-Menten, which describes an enzymatic kinetic reaction to transform irreversibly one substrate into one product. Figure 19 shows a scheme of the derivation of this kinetic model. A mass balance for each metabolite (or substrate or product) is defined as an ordinary differential equation (ODE) system using the stoichiometric relationships and the kinetics of each reaction. Figure 20 schematizes the fundamental steps to define a kinetic model:

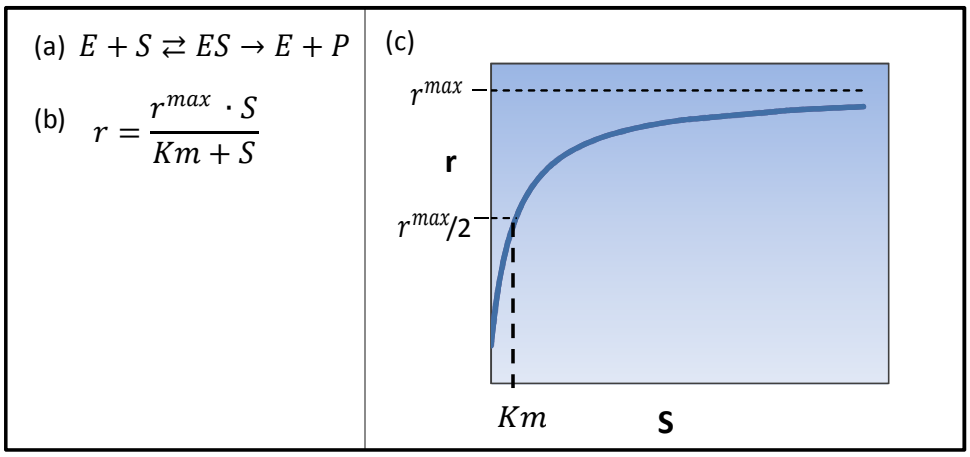

Figure 19: Michaelis-Menten enzymatic reaction. (a) Irreversible enzymatic mechanism. E represent Enzyme, S is the substrate and P is the product. ES is an intermediate complex formed by the enzyme and the substrate. (b) Rate expression. (c) Plot of reaction rate as a function of substrate concentration.

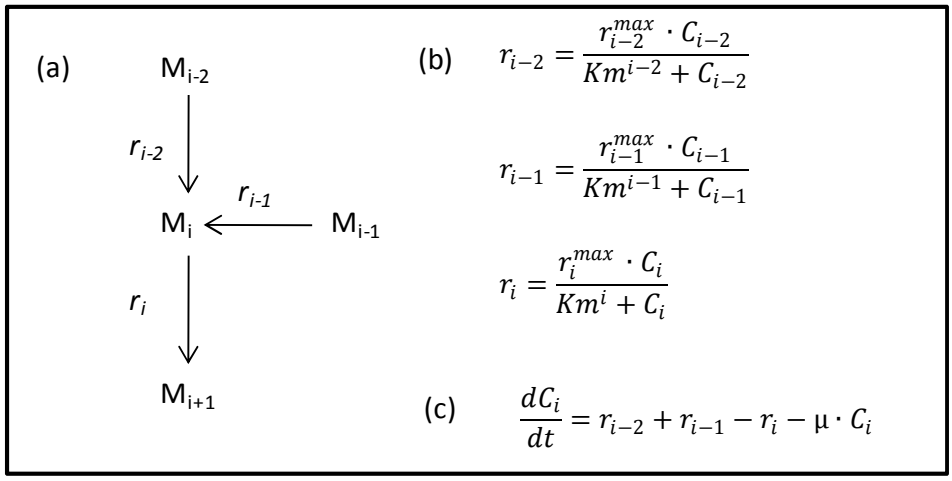

Figure 20: Kinetic Modeling. (a) Shows a segment of the structure of a metabolic network. For each reaction a kinetic is associated (b). Finally, a system of ordinary differential equations is writing for each metabolite, which represents the dynamic behavior of the system (c). Figure adapted from Gombert and Nielsen (Gombert & Nielsen, 2000).

Defining all the kinetic reactions is a complex problem, and it often limits the applicability of kinetic models. Each of the rate laws and parameters came from detailed experimental studies (*in vitro*), which are not always available. Nevertheless, some organisms and some pathways have been more extensively studied, and kinetic information is available in literature. For instance, the central carbon metabolism is of great importance, and many of the reactions involved in this pathway have been studied in different organisms. But *in vitro* parameters do not always represent a good fit for *in*

vivo conditions, and additional adjustments are necessary. A good example of an adjustment is the mathematical modeling of the central carbon metabolism of *Saccharomyces cerevisiae* developed by Rizzi et al. (Rizzi et al., 1997). In their paper they considered a generic form for each kinetic reaction r_i:

$$\boldsymbol{r_i = r_i^{max} \cdot f_i(C, P)}\ , \qquad (6)$$

where r_i^{max} is the maximum rate of the reaction r_i and $f_i(C, P)$ is a function that depends on metabolite concentrations *C* and on a set of parameters P. For instance, in the example of Figure 20, the following equation is valid for metabolite *Ci* in steady state:

$$\boldsymbol{\frac{C_i}{dt} = r_{i-2} + r_{i-1} - r_i - \mu \cdot C_i = 0}\ , \qquad (7)$$

where μ is the dilution rate. From this equation the maximum reaction rate (r_i^{max}) can be calculated as:

$$r_i^{max} = \frac{r_i + r_{i-1} - \mu \cdot C_i}{f_i(C,P)} \qquad (8)$$

The next step presented by Rizzi et al. was to perform a glucose pulse experiment, and to measure the response of the system within a few minutes. It can be assumed that in this time the concentration of enzymes does not change; therefore, the value for the maximum reaction rate remains constant. Then the data collected is used to calculate the value of maximum reaction rates in sequential steps, starting from the first reaction in the pathway. As a result, this method allows calculating values of maximum reaction rates when the other kinetic parameters are known, by measuring internal metabolite concentrations after a perturbation.

A complementary method to improve the quality of parameters in kinetic modeling is presented in the paper of Chassagnole et al., who modeled the central carbon

metabolism of *E. coli* using glucose as a carbon source (Chassagnole et al., 2002). In that paper, the authors used the approach presented by Rizzi et al. to calculate the maximum reaction rates, and they used mathematical optimization for the other kinetic parameters using the software packages ACSL and OPTDESX (Parkinson & Balling, 2002). These two packages allow modeling, simulation, and optimization of dynamical systems. Another software that has been used for the estimation of parameters is a nonlinear least-square routine from Matlab (lsqnonlin.m), which minimizes the sum-squared error of the simulated results versus experimental data (Tholudur et al., 1999).

Kinetic modeling can be combined with **Metabolic Control Analysis (MCA)** theory in order to elucidate the control structure of the pathway. MCA studies the effects of perturbations on a system in steady state (Stephanopoulos et al., 1998). Metabolic models are complex systems; therefore, it is not obvious which reactions are controlling the complete system. It is important to emphasize that this theory only applies to steady (or pseudo) state systems (Stephanopoulos et al., 1998). Two important concepts arise from MCA theory: flux control coefficients (FCCs) and concentration control coefficients (CCCs). FCCs represent the normalized change in the flux, given an infinitesimal change in an enzyme, and CCC is the normalized change in the concentration of a metabolite, given an infinitesimal change in one enzyme concentration. FCCs and CCCs are properties of the metabolic system, and their elucidation establishes the control structure of the pathway. Mathematical formulas for each FCC and CCC are as follow:

$$FCC_i^{J_k} = \frac{E_i}{J_k}\frac{\partial J_k}{\partial E_i} \qquad (9)$$

$$CCC_i^{X_j} = \frac{E_i}{X_j}\frac{\partial X_j}{\partial E_i} \qquad (10)$$

where E_i refers to enzymatic activity of *i*-th enzyme, *k* represents the *k*-th reaction in the pathway *J*, and X_j is the concentration of the metabolite *j*. Additional concepts and theories must be introduced in order to calculate FCCs and CCCs.

The flux-control summation theorem stipulates that the sum of all the FCCs of a specific flux J_k is equal to one. The mathematical expression for this theorem is:

$$\sum_{i=1}^{L} FCC_i^{J_k} = 1 \qquad k \in \{1, 2, \dots, L\} \tag{11}$$

A FCC close to one means that the corresponding enzyme is the rate-limiting of the system, although more frequently the control of the flux is distributed among more than one enzyme (Fell, 1998). The summation theorem for CCCs establishes that the sum of all the CCCs of one metabolite is equal to zero for any metabolite. For a system with M metabolites, this expression is as follows:

$$\sum_{i=1}^{L} CCC_i^{X_j} = 0 \qquad j \in \{1, 2, \dots, M\} \tag{12}$$

Calculation of FCCs and CCCs requires the introduction of elasticities. The elasticity is defined as the normalized change of a rate v_i (for the enzyme *i*), given an infinitesimal change in the concentration of metabolite *j*, X_j (Fell, 1992):

$$\varepsilon_{X_j}^{i} = \frac{X_j}{v_i} \frac{\partial v_i}{\partial X_j} \tag{13}$$

Many of these elasticities take null values because not all the metabolites are part of the kinetics of each enzyme.

The connectivity theorem for flux-control and concentration-control relate control coefficients to the elasticities (Fell, 1992). For a linear pathway, the connectivity theorem for FCCs is as follows (Fell, 1992):

$$\sum_{i=1}^{L} FCC_i^{J_k} \cdot \varepsilon_{X_j}^i = 1 \qquad k \in \{1, 2, \dots, L\};\ j \in \{1, 2, \dots, M\} \qquad (14)$$

The connectivity theorem for CCCs takes two different expressions depending on weather the metabolite in the CCC is the same or a different one than the metabolite in the elasticity. The mathematical expression is as follows (Fell, 1992):

$$\sum_{i=1}^{L} CCC_i^{X_A} \cdot \varepsilon_{X_B}^i = 0 \qquad A \neq B \qquad A, B \in \{1, 2, \dots, M\} \qquad (15)$$

$$\sum_{i=1}^{L} CCC_i^{X_A} \cdot \varepsilon_{X_A}^i = 1 \qquad A \in \{1, 2, \dots, M\} \qquad (16)$$

Connectivity theorems change for pathways that are not linear, such as branches and cycles.

When MCA is applied to a kinetic model, all the elasticities can be calculated analytically from the kinetic expression of each reaction. The use of the connectivity and summation theorems allows writing a system of equations, which leads to finding values for all the FCCs and CCCs of the system. MCA allows understanding the control steps in a metabolic pathway; therefore, it provides essential information to lead metabolic engineering efforts to increase the production of a desired product.

2.2.3 Approximative kinetic models

Kinetic modeling has great utility in the study of dynamics, simulation, and control structure. Nevertheless, its implementation requires detailed kinetic information for each of the reactions, most of them non linear in metabolite concentration. Rate laws and kinetic parameters are often not available depending on the microorganism and pathway that are being studied. Because of this, several theories have been developed in order to obtain similar results to those obtained with a kinetic model, but using less information. The simplest case is a linearization of rate law in the proximity of a known

solution using Taylor expansion, which results in a simple expression for a rate, but is not very useful because the validity of a linear approximation in most metabolic cases is just for infinitesimal changes. The main formats that have been applied for metabolic modeling are **logarithmic-linear (log-linear), power law-Generalize Mass Action (GMA-power law), synergistic system (S-systems), thermokinetic, linear-logarithmic (lin-log), and structural kinetic**. The last format differs from the previous ones because this model does not attempt to solve the steady state and dynamic behavior, but it rather focuses in the study of stability, oscillation, and existence of chaos (Steuer et al., 2006). Heijnen compared most of these formalisms (log-linear, GMA-power law, S-systems, lin-log, and thermodynamic), and he concluded that the lin-log model is the most powerful approximation (in terms of simplicity in amount of kinetic parameters), providing proper description of rate behavior, and existence of analytical solution (Heijnen, 2005). Nevertheless, all these formats have been proposed for metabolic modeling; therefore, here is given a brief description of each of them.

Log-linear approximation was developed by Hatzimanikatis and Bailey, and it is based on the Taylor expansion of the logarithmic rate expression, using the approximation $\ln(y) \approx y - 1$ (Hatzimanikatis & Bailey, 1997). Main qualities of this approximation are the existence of an analytical solution for dynamic and steady state, and for control coefficients of MCA (Hatzimanikatis & Bailey, 1997). Nevertheless, the applicability of this approximation is limited to study cases with small changes in enzymatic activities (Heijnen, 2005), which do not correspond to most cases of genetic engineering where big changes are desired (Heijnen, 2005).

GMA-power law uses power law kinetics to describe each reaction in an unbranched metabolic pathway. This form of power law is useful to describe reactions with several metabolites. Following this approximation, each reaction r_i can be written as a function of metabolite concentrations (x_j) in a power law form:

$$r_i = k_i \cdot e_i \cdot \prod_{j=1}^{m} x_j^{a_{ij}} \cdot \prod_{k=1}^{n} c_j^{b_{ik}} \qquad (17)$$

where k_i and e_i are kinetic parameters and enzymatic activities respectively, and a_{ij} and b_{ij} are exponential factors. The second product in the formula contains factors that are independent of concentrations (c_j). GMA-power law applies to cases with small changes in metabolite concentration, as the function for kinetic rate is unbounded, contrasting with enzymatic reactions that have a limited value for maximum rate (Heijnen, 2005).

Another limitation of GMA-power law is the applicability to unbranched pathways, which is rarely the case in metabolic networks. Modifications to include branched pathways resulted in the introduction of **S-systems** formalism. In this formalism, all the reactions that originate a metabolite x_i are combining in one rate law, and the same is valid for all reactions that consume the metabolite. Thus, for any metabolite, the differential expression is (Torres & Voit, 2002):

$$\frac{dx_i}{dt} = \alpha_i \cdot \prod_{j=1}^{m} x_j^{g_{ij}} - \beta_i \cdot \prod_{k=1}^{m} x_j^{h_{ik}} \qquad (18)$$

where α_i and β_i are kinetic parameters, and g_{ij} and h_{ik} are exponents. The use of this formalism allows analytical solutions of the dynamics and steady states, as well as the study of sensitivity and stability (Alvarez-Vasquez et al., 2000). A good example of the application of this model was developed for citric acid production in *Aspergillus niger*, in which the model was used to develop strategies of optimization (Alvarez-Vasquez et al.,

2000). As previous approximative models, S-systems model is limited to small changes in enzymatic activities, and it cannot simulate deletions of enzymes in one branch as that would annul the complete output flux (Heijnen, 2005).

The **thermokinetic** format is a linear approximation for kinetic description of enzymes based on Gibbs free energy (Nielsen, 1997). By approximating kinetic rates (r_i) to a linear combination of affinities, a general mathematical formulation is obtained (Nielsen, 1997):

$$r_i = a_i \sum_{j=1}^{m} k_{ij} \cdot \ln(x_j) + b_i \qquad (19)$$

where a_i, b_i and k_{ij} are kinetic parameters. This generic equation allows the presence of effectors, in which case the kinetic parameters need to be calculated empirically (Nielsen, 1997). In the absence of effectors, the term a_i becomes equal to the slope in the inflection point of the rate, and b_i is minus the product of the slope and the affinity (both evaluated in the inflection point) (Nielsen, 1997). Also, the kinetic coefficients k_{ij} should keep the stoichiometric relationships. This formalism better approximates enzymatic equations than power-law format, exemplified in a simple Michaelis-Menten kinetics (Figure 21). MCA can be applied to thermokinetic format in order to obtain the control structure of the pathway.

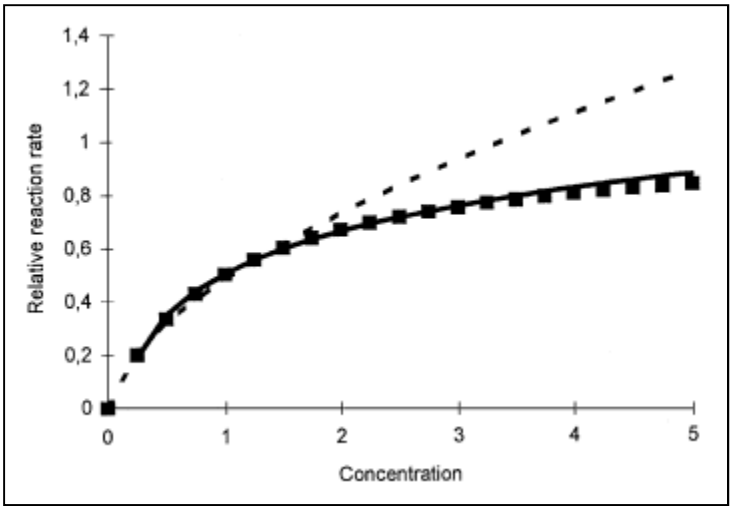

Figure 21: Comparison between Michaelis-Menten equation (square points), best fit using power-law kinetics (broken line), and best fit using thermokinetic format (solid line) (Nielsen, 1997).

The thermokinetic format inspired another format, the **lin-log** format, in which the main change is that the kinetic coefficients k_{ij} do not need to keep stoichiometric relationships (Visser & Heijnen, 2003). In addition, the enzymatic activity (e_i) is explicitly introduced, leading to the following equation (Heijnen, 2005):

$$r_i = e_i(b_i + \sum_{j=1}^{mx} a_{ij} \cdot \ln(x_j) + \sum_{j=mx}^{mc} a_{ij} \cdot \ln(c_j) \quad (20)$$

where x_j and c_j refer to intracellular and extracellular metabolites, respectively. Parameters are found using experimental data (Visser & Heijnen, 2003). This formalism retain the good qualities of the thermokinetic format (good adjustment, analytical solution, study of control structure), and it adds flexibility in the adjustment of parameters. Moreover, it allows finding analytical solutions for steady state and dynamic states when there are large changes in enzymatic activities (Heijnen, 2005).

Finally, **structural kinetic** models focuses in the study of the dynamic behavior of the system, in terms of stability, oscillations and possibility of chaos (Steuer et al., 2006). This format focuses in the construction of the Jacobian matrix (referred to the

vector of reaction rates) of a metabolic system in the steady state. Elements of the matrix can be calculated using experimental data (Steuer et al., 2006).

2.2.4 Remarkable models for *E. coli* central carbon metabolism and glycerol fermentation

This section presents models that have been built to represent the metabolism of *E. coli* and glycerol fermentation. *E. coli* has been the subject of study for several years, and a number of mathematical models have been built to describe its metabolism. Among the most remarkable are the stoichiometric model for glucose fermentation (Chassagnole et al., 2002) and the GEM (Feist et al., 2007). To date there are no kinetic models for the glycerol fermentation in *E. coli*, but a model has been proposed to describe this process in *Klebsiella pneumonia* (Sun et al., 2008), one of the few microbial organisms that is able to ferment this carbon source. There is one effort that has been made for the glycerol fermentation of *E. coli*, and it is a stoichiometric model using FBA (Murarka, not published). Nevertheless, this model just represents a set of 78 reactions, and in view of the recent development of GEMs, it is more useful to describe accurately the fermentation of glycerol using a GEM. Furthermore, that stoichiometric model was built assuming certain pathways without having experimental confirmation of them.

2.2.4.1 Kinetic modeling of the central carbon metabolism of E. coli

A kinetic modeling of central carbon metabolism of *E. coli* was developed by Chassagnole and collaborators in 2002, and it represents the most cited kinetic model for the study of central carbon metabolism in *E. coli* (over 180 citations to date, according to Web of Knowledge – Thomson Reuters) (Chassagnole et al., 2002). The goal of this project

was to present a dynamical model that allows quantitatively predicting the physiological behavior of *E. coli* when there are changes in the glucose supply. Moreover, the model allows the study of stability and control structure (using MCA).

The experimental conditions consisted in the aerobic growth of *E. coli* K-12 strain W3110, in a continuous culture. The metabolic network included the phosphotransferase system (PTS) to uptake glucose, the glycolysis (also known as embden-meyerhof-parnas pathway), the pentose-phosphate pathway (PPP), and reactions for the production of amino acids and polysaccharides (Figure 22). The PTS is a PEP-dependent system that allows *E. coli* to uptake carbohydrates, such as hexoses and disaccharides. The vast number of studies performed to elucidate the mechanisms of enzymes in the central carbon metabolism of *E. coli* allowed the construction of a detailed kinetic model. Most of the kinetic rates of glycolysis were taken from analytical experiments reported in the literature. Unknown rates were proposed using Michaelis-Menten kinetics. Some kinetic expressions that were utilized are reversible Michaelis-Menten, allosteric regulation, and Hill equation.

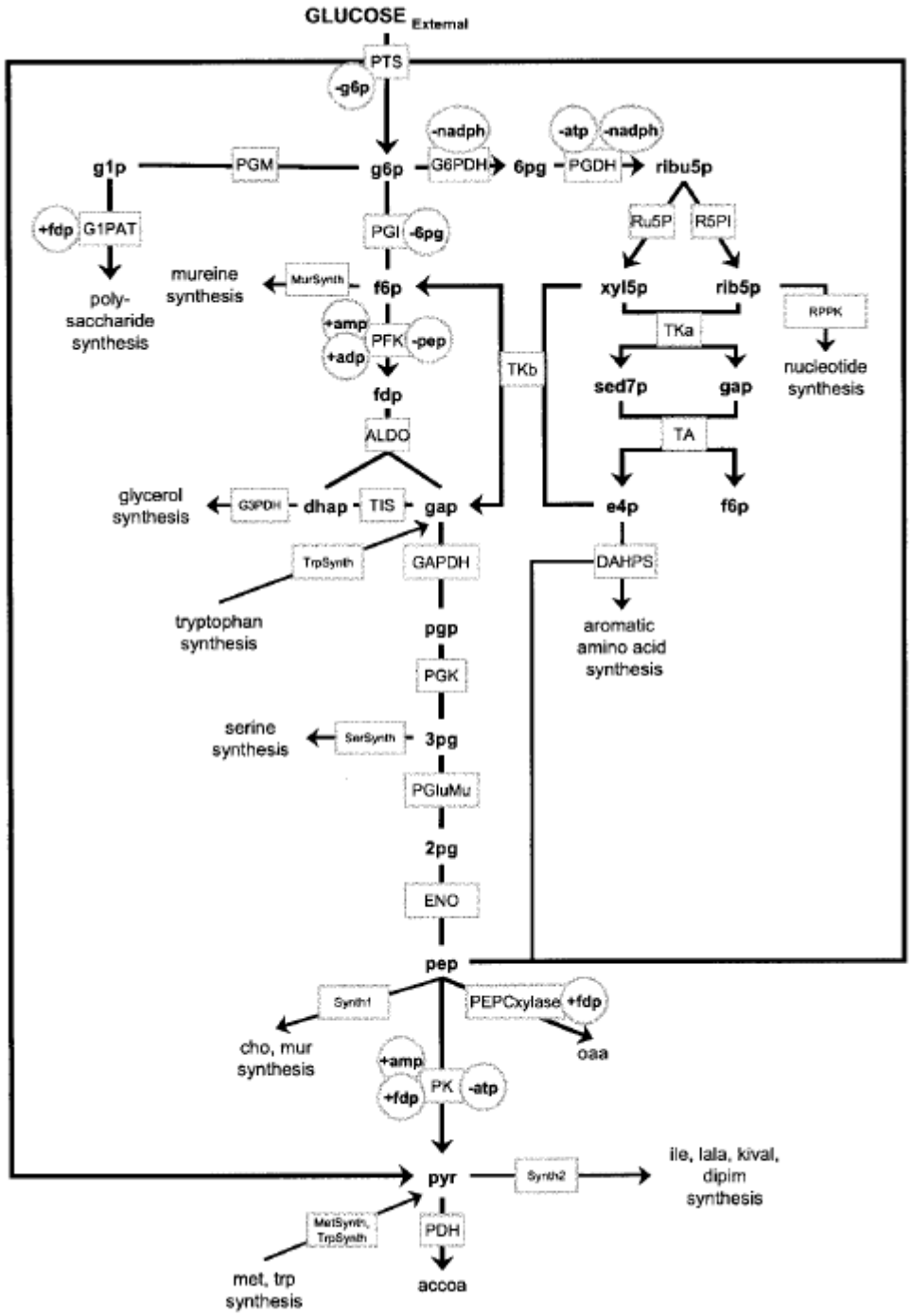

Figure 22: Metabolic network of kinetic model for central carbon metabolism in *E. coli*. Squares: enzymes, circles: regulatory effects (Chassagnole et al., 2002). See Nomenclature for abbreviations (page 214).

Kinetic parameters were adjusted using experimental data and computational optimization. Maximum reaction rates were calculated by using experimental data of

intracellular metabolite concentrations after a glucose pulse experiment, and by applying the methodology presented by Rizzi et al. (Rizzi et al., 1997). Computational softwares ACSL and OPTDESX were used to optimize values of other kinetic parameters. Unbalanced co-metabolites (energy balance and redox balance) were fitted with analytical expression, and they were not part of the ODE system used to solve the dynamic state of the system.

As a result, the kinetic model fits most of the experimental data of intracellular metabolite concentrations after a pulse of glucose. The main difference was found for PYR, which could be caused by errors in measurements together with wrong assumptions in the mechanistic model. The stability of the model was studied by evaluating the model's recovery after a glucose pulse. As a result, the model did not come back to the original steady state, but the experiments did not either, indicating that there might be instabilities. In addition, the model allowed the calculation of the theoretical natural frequency of oscillation (analysis of eigen values of the system), which result was of the same order of magnitude than previous studies of oscillation in *E. coli*.

The model was used to elucidate the control structure in the pathway by using MCA. The result showed that the control of glucose utilization is shared by the PTS (FCC=0.42) and, to a lesser extent, by glucose-6-phosphate dehydrogenase, phosphofructokinase, and pyruvate dehydrogenase.

2.2.4.2 Kinetic modeling of glycerol fermentation in K. pneumonia

K. pneumonia is one the few organisms that can ferment glycerol in the absence of electron acceptors. As already stated, the utilization of glycerol in this species requires the combination of two pathways: oxidative and reductive pathways. Glycerol oxidation allows the formation of DHAP, which will later go to the glycolysis pathway, while reductive pathway of glycerol produces 1,3-PDO. Sun and collaborators developed a kinetic model for this process, which includes the oxidative and reductive pathway (Figure 23) (Sun et al., 2008).

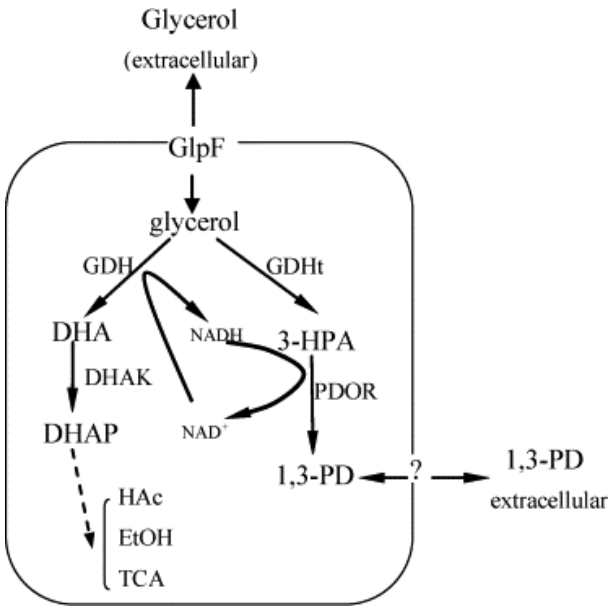

Figure 23: Anaerobic pathways for metabolism of glycerol. GlpF: glycerol facilitator, GDH: glycerol dehydrogenase, DHA: dihydroxyacetone, DHAP: di-hydroxyacetone phosphate, HAc: acetate, EtOH: ethanol, GDHt: glycerol dehydratase, 3-HPA: 3-hydroxypropionaldehyde, PDOR: 1,3-PD oxydoreductase, 1,3-PD: 1,3-propanediol (Sun et al., 2008).

The model represents anaerobic metabolism of glycerol at 37°C, and it applies to batch and continuous cultures. This is a small kinetic model, in which the emphasis is in the reducing pathway that allows the formation of 1,3-PDO. In fact, the model just represents four reactions of the reducing pathway (toward formation of 1,3-PDO). Among them, one is glycerol transport, two are Michaelis-Menten (proposed in this

work), and the last one is diffusion of 1,3-PDO. The oxidative pathway (toward formation of DHAP) was considered a black box. In addition, the complexity of the model increases for multiple growth inhibitions that affect *K. pneumonia* under fermentative conditions. In particular, *K. pneumonia* growth is inhibited by glycerol, 1,3-PDO, ethanol, and acetate.

The kinetics of transport of glycerol is a combination of simple diffusion and facilitated transport mediated by a permease. Facilitated transport is modeled as Michaelis-Menten kinetics, according to studies performed in the equivalent permease in *E. coli*. The two intracellular reactions were modeled as Michaelis-Menten reactions with inhibition by 3-HPA (the intermediate metabolite of this pathway) in agreement with experimental data. The Monod equation with multiple inhibitions for batch cultures was used for the specific growth rate. Kinetic parameters were found using experimental data, and utilizing the method of multi-dimensional unconstrained nonlinear minimization (Matlab). How the black box was set for the oxidative pathway is not presented in the model, nor is the simulated production of acetate and ethanol as fermentative products.

Simulations using the model are compared with experiments of batch and continuous cultures. The model represents correctly concentrations of biomass, glycerol, 3-HPA, 1,3-PDO, ethanol, and acetate. In batch cultures, simulation curves of glycerol and biomass appear displaced to the right and left, respectively, indicating that the model is predicting a slower utilization of glycerol and production of biomass. In addition, the model predicts an abrupt consumption of glycerol in the late stage of batch cultures, which is in disagreement with experimental data. The authors did not go into the

explanation of this phenomenon, but it could be caused by the use of an erroneous glycerol transport rate.

Finally, the model suggests that 1,3-propanediol oxidoreductase (PDOR) (Figure 23) may be the limiting step because simulating data shows accumulation of 3-HPA (in agreement with experimental data).

Other models developed to study the dynamics of glycerol fermentation include the implementation of an S-system model to study the regulatory and metabolic pathway in *K. pneumonia* (Sun et al., 2012).

2.2.4.3 Genome-scale metabolic model for E. coli

In 2011, the last version of a GEM applied to *E. coli* was released and developed within the group of Dr. Bernhard Palsson. This version is an upgrade of the previous versions, which were presented in 2000 by Edwards and Palsson, 2003 by Reed et al., and 2007 by Feist et al. (Edwards & Palsson, 2000; Feist et al., 2007; Reed et al., 2003). By 2008 these three models had been used in more than 60 studies of metabolism (Feist & Palsson, 2008), and their utilization has continued in recent years.

The last version of the GEM for *E. coli*, named i1366, includes 1,366 functional ORFs, 97% of which are experimentally based, and 3% of which present functions computationally predicted. Different intracellular compartments were included, and transport reactions allowed them to be connected. The model contains 2,251 reactions; among them, 1,382 correspond to metabolic reactions catalyzed by enzymes, and 706 correspond to transport reactions catalyzed by enzymes. As for metabolites, the model contains 1,136 unique metabolites (regardless of their intracellular location).

The iJO1366 model is an updated version of the previous GEM for *E. coli*, the iAF1260, which was presented in 2007 by Feist et al. The construction of the iJO1366 model included the metabolic information of *E. coli* contained in the EcoCyc Database and biochemical studies performed over enzymes of this bacterium (Keseler et al., 2009). Gene associations were made for each reaction when there was an identified enzyme associated with a reaction. Besides, thermodynamic information for each reaction was calculated using an intracellular metabolite concentration (of an estimated 1 mM) to perform thermodynamic consistence analysis that could ensure feasibility in the directionality of each reaction, following the system developed by Feist et al. (Feist et al., 2007). For instance, the reactions of export and import of ions were considered reversible at first, but thermodynamic analysis and literature review confirmed that export of ions is a separate mechanism that requires energy. Then, the model was curated by filling gaps in pathways for the formation of essential metabolites starting from a minimum medium. Finally, the construction of the model used experimental data to propose a reaction for biomass production, and also to determine growth associated maintenance energy (GAM) and non-growth associated maintenance energy (NGAM). This resulted in a calculated NGAM of 3.15 mmol ATP/gCDW/h and a GAM of 53.95 mmol ATP/gCDW/h.

FBA was used to perform different studies, and biomass was used as objective function. The predicting capability of the iJO1366 model was validated using two approaches: first, to study a vast variety of possible substrates using the model, and second to study single gene deletions using glucose and glycerol in minimal media. Both approaches proved the highly accurate in predicting phenotypes using the iJO1366 (Orth et al., 2011).

3 Materials and methods

The present project consists of mathematical modeling of *E. coli* using two recently developed platforms: glycerol fermentation and the reversal β-oxidation cycle utilizing glucose. These two approaches have recently been reported experimentally and this study expands their capabilities as platforms to produce biofuels (including advanced biofuels) and biochemicals. Mathematical models need to be validated experimentally; therefore, a section for experimental conditions is also included. Finally, the workflow will be explained.

3.1 Modeling

In the previous section, different mathematical models of metabolism were explained. The present project uses two of them: kinetic modeling and GEM.

Kinetic modeling allows the detailed study of one pathway, and it can be implemented as long as the pathway has been identified and kinetic information has been determined. Given the fact that the main pathways in glycerol and in fatty acids metabolisms have been well characterized in *E. coli*, it is possible to implement this kind of model for glycerol fermentation. This approach allows a dynamic study of the system and the elucidation of the control structure of the pathway by applying MCA.

GEM, a stoichiometric model, gives a global vision of the complete metabolic network. The use of FBA together with this model allows finding the maximum theoretical growth under a given condition, and which pathways should be used to achieve such state. Identification of active pathways that allow the fermentative utilization of glycerol and the use of the reversal of the β-oxidation cycle is fundamental

for a deeper understanding of these processes. Predictions presented using GEMs can lead experimental efforts in metabolic engineering. The vast amount of studies performed in *E. coli* has allowed the construction of a GEM for this organism(Orth et al., 2011). This model is available online and it can be modified to represent different conditions, such as adding or deleting pathways, or changing the chemical composition of the medium.

Both kinds of models are used to study the metabolism of *E. coli* from different perspectives, two fundamental tasks for understanding glycerol fermentation and the reversal of the β-oxidation cycle, and to engineer this microorganism for the efficient production of biofuels.

3.1.1 Kinetic modeling and MCA

This section explains the steps in the construction of a kinetic model without going into details of the specific pathways that are studied. Further details are part of results (chapters 4, 5 and 6).

3.1.1.1 Kinetic modeling

The fundamental steps in the construction of kinetic modeling are:

1. **Set computational system**. Use of Matlab v7.11.0 (R2010b, The Mathworks, Inc.).
2. **Define metabolic network**. This step defines which metabolites and reactions are part of the model. This information is available and it was presented in the previous section (Background and Literature Review).

3. **Define kinetics of each reaction**. This information is available for all the reaction.
4. **Define system of ODE**. The system is obtained by applying a mass balance in each substrate, metabolite, product, and biomass.
5. **Define initial conditions**. It is necessary to define initial concentrations of substrates, internal metabolites, products, and biomass. The substrates, products, and the biomass concentrations are known for these experiments. In contrast, values of internal metabolites need to be obtained experimentally or estimated. In many cases, estimated values can be obtained from the literature, and the mathematical model is not sensitive to these values after the first few seconds. This is because the mathematical solution of the system quickly adjusts values of the internal metabolites.
6. **Parameter optimization**. *In vitro* kinetic parameters can be obtained from the literature for most of cases, and they can be estimated in the other cases. These values were used as an initial estimate of the real values. An analysis of sensitivity was performed over all parameters of the system. Sensitive parameters were optimized using Matlab and simulations.
7. **Solve the system**. The program Matlab was used to write the ODE system that needs to be solved.

3.1.1.2 MCA

MCA theory applied to cycles represents some variations with respect to linear pathways, which will be explained below.

Construction of matrix method for MCA

FCCs and CCCs can be calculated when elasticities are known. The system of equations is linear and allows the construction of a matrix equation. Since a metabolic pathway may be linear, branched or cyclic, the system of equations will vary for the different cases. Matrix method for linear and branched pathways were developed by Sauro and Fell (Sauro et al., 1987). Extension of this method to conserved cycles requires to apply the principles presented by Fell and Sauro, and Hofmeyr et al. (Fell & Sauro, 1985; Hofmeyr et al., 1986).

Linear pathways (Sauro et al., 1987)

For a linear pathway of 3 reactions and 4 metabolites (Figure 24), equation 21 presents the system of equations that apply.

$$X_0 \xrightarrow{E_1} X_1 \xrightarrow{E_2} X_2 \xrightarrow{E_3} X_3$$

Figure 24: Linear pathway

$$\begin{bmatrix} 1 & 1 & 1 \\ \varepsilon_1^1 & \varepsilon_1^2 & 0 \\ 0 & \varepsilon_2^2 & \varepsilon_2^3 \end{bmatrix} \cdot \begin{bmatrix} FC_1 & CC_1^{X_1} & CC_1^{X_2} \\ FC_2 & CC_2^{X_1} & CC_2^{X_2} \\ FC_3 & CC_3^{X_1} & CC_3^{X_2} \end{bmatrix} = \begin{bmatrix} 1 & 0 & 0 \\ 0 & -1 & 0 \\ 0 & 0 & -1 \end{bmatrix} \quad (21)$$

Extension of this system to bigger systems is intuitive. The first matrix, named M, present a first row with just ones, coming from the summation theorem for FCCs and for CCCs. The following rows in M contain the elasticities with respect to the metabolites (rows) and enzymes (columns), which come from the connectivity relationships between FCCs and elasticities, and connectivity relationships between CCCs and elasticities.

Branched pathways (Sauro et al., 1987)

Equation 22 applies for a branch point of 3 reactions and 4 metabolites, in which the branches take fluxes of aJ and (1-a)J as shown in Figure 25. $CCC_1^a, CCC_2^a,$ and CCC_3^a correspond to branch distribution coefficients.

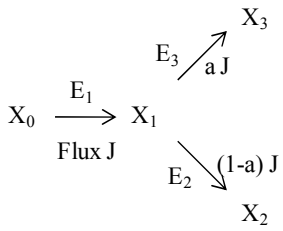

Figure 25: branched pathway

$$\begin{bmatrix} 1 & 1 & 1 \\ \varepsilon_1^1 & \varepsilon_1^2 & \varepsilon_1^3 \\ 0 & (1-a) & -a \end{bmatrix} \cdot \begin{bmatrix} FCC_1 & CCC_1^{X_1} & CCC_1^a \\ FCC_2 & CCC_2^{X_1} & CCC_2^a \\ FCC_3 & CCC_3^{X_1} & CCC_3^a \end{bmatrix} = \begin{bmatrix} 1 & 0 & 0 \\ 0 & -1 & 0 \\ 0 & 0 & 1-a \end{bmatrix} \quad (22)$$

Moiety-conserved cycles (Hofmeyr et al., 1986)

A cycle in a metabolic pathway is a special case of a branched pathway. Consider the case represented in Figure 26.

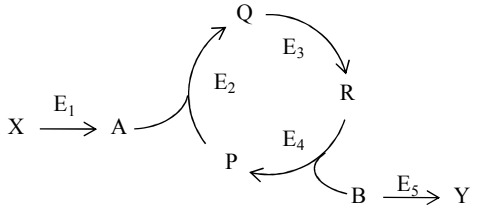

Figure 26: Cyclic pathway

While the summation theorem for FCCs does not change, connectivity theorem equations are modified as follows:

$$FCC_1 \cdot \varepsilon_A^1 + FCC_2 \cdot \varepsilon_A^2 = 0 \quad (23)$$

$$FCC_2 \cdot \varepsilon_Q^2 + FCC_3 \left(\varepsilon_Q^3 - \varepsilon_R^3 \cdot \frac{Q}{R}\right) - FCC_4 \cdot \varepsilon_R^4 \cdot \frac{Q}{R} = 0 \quad (24)$$

$$FCC_3 \cdot \varepsilon_R^3 + FCC_4 \left(\varepsilon_R^4 - \varepsilon_P^4 \cdot \frac{R}{P}\right) - FCC_2 \cdot \varepsilon_P^2 \cdot \frac{R}{P} = 0 \quad (25)$$

$$FCC_4 \cdot \varepsilon_B^4 + FCC_5 \cdot \varepsilon_B^5 = 0 \quad (26)$$

Notice that elasticities with respect to Q and R were combined in one equation, the same for elasticities with respect to R and P. The result of combining all these equations leads to the following system of equations to calculate the FCCs for the system presented in Figure 26:

$$\begin{bmatrix} 1 & 1 & 1 & 1 & 1 \\ \varepsilon_A^1 & \varepsilon_A^2 & 0 & 0 & 0 \\ 0 & \varepsilon_Q^2 & \left(\varepsilon_Q^3 - \varepsilon_R^3 \frac{C_Q}{C_R}\right) & -\varepsilon_R^4 \frac{C_Q}{C_R} & 0 \\ 0 & -\varepsilon_P^2 \frac{C_R}{C_P} & \varepsilon_R^3 & \left(\varepsilon_R^4 - \varepsilon_P^4 \frac{C_R}{C_P}\right) & 0 \\ 0 & 0 & 0 & \varepsilon_B^4 & \varepsilon_B^5 \end{bmatrix} \cdot \begin{bmatrix} FCC^1 \\ FCC^2 \\ FCC^3 \\ FCC^4 \\ FCC^5 \end{bmatrix} = \begin{bmatrix} 1 \\ 0 \\ 0 \\ 0 \\ 0 \end{bmatrix} \quad (27)$$

The FCC can then be calculated by solving this system of equations.

3.1.2 Stoichiometric modeling

As already stated, a GEM is available for *E. coli* to represent the metabolism of glucose under aerobic conditions. The model was modified to represent the conditions that are the focus of this study. Below are the steps involved in the modification and use

of this model to the study of glycerol fermentation, and of the reversal of the β-oxidation cycle.

1. **Set computational system**. The COBRA toolbox v2.0 was used, which is a toolbox for Matlab that has been developed specifically to manipulate genome-scale programs (Schellenberger et al., 2011). COBRA stands from "Constraint-Based Reconstruction and Analysis", and it provides a friendly platform to perform diverse studies in GEM, such as FBA, FVA, addition and deletion of reactions, and OptKnock. The latest version of COBRA (v2.0) includes a linear programming kit (GLPK), libSBML, SBML toolbox, and glpkmex, all of which are necessary for the proper functioning of COBRA. In order to use Optknock from COBRA, the solver Gurobi 5.0 was implemented.
2. **Set experimental conditions**. For glycerol fermentation, oxygen and glucose utilization were set as unavailable, and glycerol was set as available. For the glucose fermentation using the reversible β-oxidation cycle, glucose was set as available, and oxygen was set as unavailable. In both cases it was assumed minimal medium.
3. **Model curation.** This was a repetitive process. First, the model was checked to ensure that all the reactions in the main pathways are present, and with the right directionality. Then, reactions that were not feasible under the current conditions were eliminated. Some of these reactions were amino acids degradation, nucleotides degradation, and ion exchange. Degradation of amino acids and nucleotides does not take place under normal conditions, as these processes require the expression of involved enzymes. Ion exchange is subject

to thermodynamic restrictions. This process was facilitated by using FBA with biomass as the objective function, evaluating if the results are feasible, and modifing the model if necessary.

4. **Perform Flux Balance Analysis (FBA) and Flux Variability Analysis (FVA) of base case**. Biomass was used as the objective function (BOF), and FBA was used to identifying the main pathways that are predicted for the production of maximal theoretical cell growth. FVA was used to identify alternative optimal solutions and to generate solution spaces, which represent productivity versus biomass production.
5. **Perform FBA of additional pathways.** In addition to simulate flux distribution of the base case (wild type *E. coli* for glycerol fermentation, and a modified *E. coli* containing the reversal β-oxidation cycle for glucose fermentation), additional pathways are incorporated as a way to optimize the synthesis of desired products.
6. **Perform OptKnock to optimize synthesis of desired products.** This tool was used to identify possible reactions to knockout that would result in the coupling production of biomass and a desired product. In each case, up to 8 reactions were permitted as target to knockout, and the minimal specific growth rate was set as 0.07 h-1. The solver Gurobi 5.0 was used in combination with the COBRA toolbox.

3.2 Experimental work

Experimental validation is a fundamental step in the construction and adaptation of mathematical models to predict cellular phenotypes. In particular, the results from MCA for glycerol fermentation were used to predict changes in the metabolic network when enzymatic activities are modified, and experiments were conducted to corroborate the predictions. Below are the protocols for strain and genetic methods, culture medium and cultivation, analytical methods and enzymatic activities. The protocol for glycerol fermentation was taken from the experiments performed by Dharmadi et al. (Dharmadi et al., 2006) and Gonzalez et al. (Gonzalez et al., 2008) unless otherwise is indicated. All the experimental work of this thesis was performed by James Clomburg.

Glycerol fermentation – strains, plasmids and genetic methods

Wild-type strains *E. coli* K12 strain MG1655 was used as wild type, and mutants were constructed using the transposon-mediated mutagenesis method (Kang et al., 2004). Table 2 shows the strain and plasmids used in this study. The protocols for the contraction of plasmids pZSBlank (Yazdani & Gonzalez, 2008), pZSKLMgldA (Yazdani & Gonzalez, 2008), pZSKLM (Bachler et al., 2005), pZSgldA (Yazdani & Gonzalez, 2008), and pZSadhE (Clomburg & Gonzalez, 2011) have been previously described. For construction of plasmids pZSpflB, pZStpiA, and pZSglpF, the genes *pflB*, *tpiA*, and *glpF* were PCR amplified from MG1655 genomic DNA. The resulting products were then cloned into pZSKLMgldA (Yazdani & Gonzalez, 2008) digested with *Kpn*I and *Mlu*I using the InFusion PCR cloning kit (Clontech Laboratories, Inc., Mountain View, CA).

Table 2: Strains and plasmids used in this study.

Strain/Plasmid/ Primer	Description/Genotype/Sequence	Source
MG1655	F- λ- *ilvG- rfb*-50 *rph*-1	(Kang et al., 2004)
pZSblank	oriR pSC101*, tetR, *cat,* contains $P_{LtetO-1}$	(Yazdani & Gonzalez, 2008)
pZSKLMgldA	*E. coli dhaKLM* and *gldA* genes under control of $P_{LtetO-1}$(tetR, oriR SC101*, cat)	(Yazdani & Gonzalez, 2008)
pZSKLM	*E. coli dhaKLM* genes under control of $P_{LtetO-1}$(tetR, oriR SC101*, cat)	(Yazdani & Gonzalez, 2008)
pZSgldA	*E. coli gldA* gene under control of $P_{LtetO-1}$(tetR, oriR SC101*, cat)	(Yazdani & Gonzalez, 2008)
pZSadhE	*E. coli adhE* gene under control of $P_{LtetO-1}$(tetR, oriR SC101*, cat)	(Clomburg & Gonzalez, 2011)
pZSglpF	*E. coli glpF* gene under control of $P_{LtetO-1}$ (tetR, oriR SC101*, cat)	This Study (James Clomburg)
pZSpflB	*E. coli pflB* gene under control of $P_{LtetO-1}$ (tetR, oriR SC101*, cat)	This Study (James Clomburg)
pZStpiA	*E. coli tpiA* gene under control of $P_{LtetO-1}$ (tetR, oriR SC101*, cat)	This Study (James Clomburg)

Manufacturer protocols and standard methods (Miller, 1972; Sambrook et al., 1989) were followed for DNA purification (Qiagen, Valencia, CA), restriction endonuclease digestion (New England Biolabs, Ipswich, MA), and DNA amplification (Stratagene, La Jolla, CA and Invitrogen, Carlsbad, CA). The strains were kept in 32.5% glycerol stocks at -80°C. Plates were prepared using LB medium containing 1.5% agar, and when appropriate chloramphenicol was included at 34 µg/mL.

Glycerol fermentation – culture medium and cultivation conditions

Culture conditions of strains were minimal medium (Neidhard.Fc et al., 1974) supplemented with 10 g/L tryptone (Difco, USA), 10 g/L glycerol, 5 g/L yeast extract, and 1.32 mM Na2HPO4 in place of K2HPO4. Pre-culture medium was supplemented with MOPS. Chemicals were obtained from Fisher Scientific (Pittsburg, PA) and Sigma-Aldrich Co. (St. Louis, MO).

Anaerobic conditions as well as 37ºC will be kept. The pH was maintained at 6.3 (optimum) using NaOH and H_2SO_4. Fermentations were conducted in a SixFors multi-

fermentation system (Infors HT, Bottmingen, Switzerland) with six 500 mL working volume fermenters and independent control of temperature, pH, and stirrer speed (200 rpm). The system will be designed to prevent evaporation and to keep anaerobic conditions, as previously reported (Dharmadi et al., 2006). Strains were streaked onto LB plates and incubated overnight, and then a single colony was used to inoculate 17.5 Hungate tubes completely filled with medium (Murarka et al., 2008). The tubes were incubated at 37ºC until they achieved an OD550 of 0.4, and washed pellet was used to inoculate each of the six fermenters with the target starting optical density of 0.05 at 550 nm (Dharmadi et al., 2006).

Glycerol fermentation – analytical methods and enzyme activities

The methodology for the analytical methods was presented by Dharmandi et al. (Dharmadi et al., 2006). Cell growth, substrate (glycerol) concentration and products concentrations were monitored during the experiments. Cell concentration were estimated measuring optical density at 550 nm (1 OD = 0.34 g DW/L). Samples were centrifugated and the supernatant was stored at -20ºC for further analyses. The substrate (glycerol) and products (lactate, acetate, formate, succinate, and ethanol) were measured with ion-exclusion HPLC as previously reported (Dharmadi et al., 2006).

The activity of glycerol dehydrogenase on glycerol oxidation was measured as described previously (Gonzalez et al., 2008), with potassium carbonate (pH 9.5) as the buffer. PEP-dependent dihydroxyacetone kinase activity was assayed using the method reported by Kornberg and Reeves (Kornberg & Reeves, 1972), with minor modifications as previously described (Yazdani & Gonzalez, 2008).

3.3 Workflow

Figure 27 shows the workflow diagram that was followed to implement the mathematical models. The process starts collecting relevant data to the study (literature review), and it finishes with a validated model that can be used in metabolic engineering. The process is iterative in comparing computational simulations/predictions with experimental data, and major differences require to review and to modify the model.

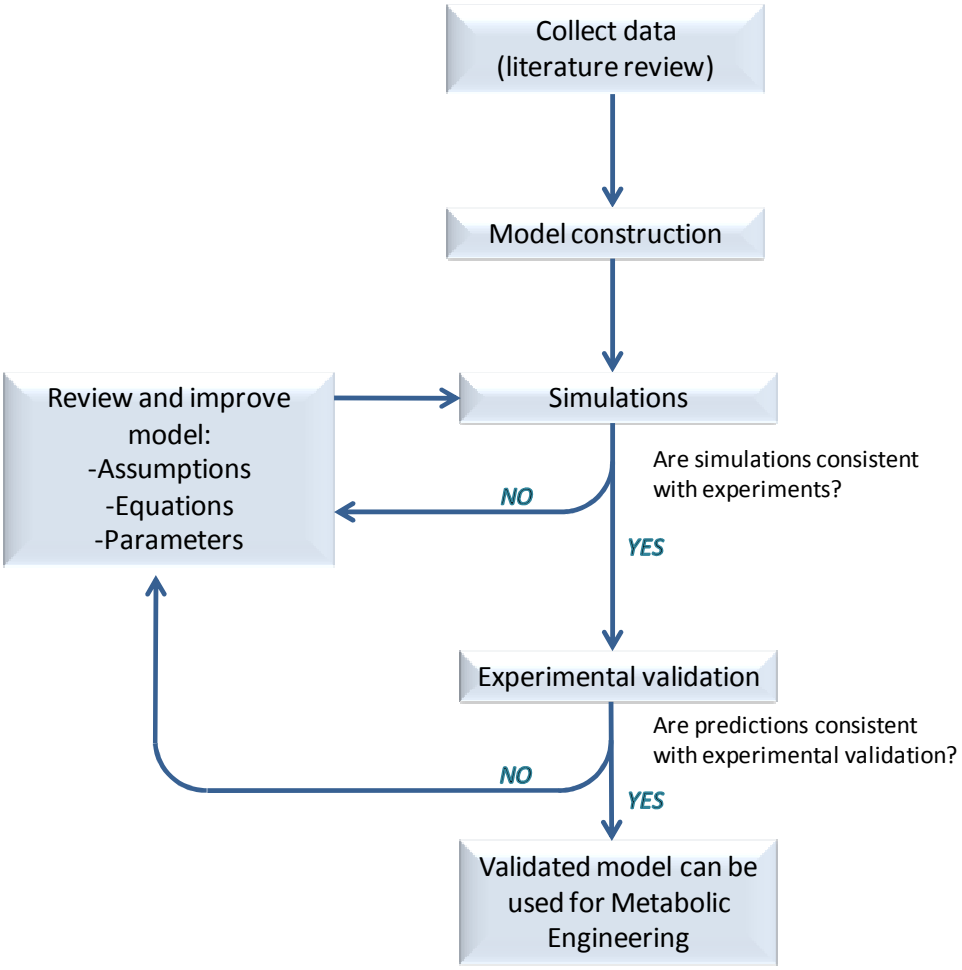

Figure 27: Workflow diagram for mathematical model construction.

4 Results I: Kinetic modeling and metabolic control analysis of the fermentative metabolism of glycerol fermentation.

This chapter presents the development and results of a kinetic model for the fermentative metabolism of glycerol in *E. coli*, as well as the use of the model for the elucidation of the control structure of the associated metabolic pathway. The anaerobic fermentation of glycerol was believed for many years to be exclusive to those organisms having the ability to produce 1,3-propanediol (1,3-PDO), and the recent discovery that *E. coli* is able to ferment glycerol even though it is unable to produce 1,3-PDO has drawn interest from the scientific community as a possible platform for the production of biofuels (see for example (Yazdani & Gonzalez, 2007). Despite efforts to establish pathways and mechanisms of glycerol fermentation in *E. coli*, the quantitative analysis of this metabolic process had not been performed before this thesis.

Kinetic models quantitatively describe dynamics and steady state of a metabolic network (metabolites, substrates, products, and fluxes) by defining a system of ordinary differential equations (ODEs) and using kinetic information for specific enzymatic and transport reactions. Once a kinetic model has been established, Metabolic Control Analysis (MCA) can be introduced to calculate flux control coefficients (FCCs).

The following are sections of this chapter: *Model development*, *Parameter estimation*, *Result of modeling*, *MCA of glycerol fermentation*, *Experimental validation* and *Conclusions*. Model development presents the metabolic pathway and the kinetic equations for each step, together with the system of ODEs. Parameter estimation explains in detail the problem of obtaining reliable parameters and the approach used in this work

to optimize those parameters. Once the model has been established and the parameters have been defined, results of the model are presented for glycerol, ethanol, biomass and internal metabolites, and compared to experimental data. The next section presents MCA of the model, which allows elucidating that the first two enzymes (glycerol dehydrogenase and di-hydroxyacetone kinase) are controlling the flux through the pathway. Experimental verification shows that in fact these two enzymes are responsible for the control over this pathway, and overexpression of these two enzymes resulted in doubling the rate of glycerol utilization and ethanol synthesis.

4.1 Model development and simulations

The model construction focused on the anaerobic fermentation of glycerol at a pH of 6.3 (optimum) in a minimum medium supplemented with 10% of tryptone, 5 g/L of yeast and 10 g/l of glycerol (see section 3, *Material and Methods* for further details); where negligible amounts of glycerol goes to by-products or biomass (Gonzalez et al., 2008). The model considered ethanol as the only product of this fermentation since it accounts for over 95% of carbon recovery. This metabolic pathway is NADH balanced and produces ATP, two essential functions to support cell growth. The model was constructed using information from previous publications, the details of which will be given later in this section. Kinetic structures and parameters were taken from studies conducted in *E. coli* unless otherwise specified. Figure 28 shows the metabolic pathway of the model, which is comprised of 11 reactions starting with the passive transport of glycerol across the cell membrane (Heller et al., 1980). Under fermentative conditions, intracellular glycerol is converted to the glycolytic intermediate dihydroxyacetone phosphate (DHAP) in a two-step pathway involving glycerol dehydrogenase (glyDH) and

dihydroxyacetone kinase (DHAK), as previously reported (Gonzalez et al., 2008). The native *E. coli* DHAK is a phosphoenolpyruvate (PEP)-dependent enzyme that utilizes PEP as the phosphate group donor for the phosphorylation of dihydroxyacetone (DHA) (Gutknecht et al., 2001). The conversion of DHAP into PEP takes place in five steps through the action of common glycolytic enzymes (Romeo and Snoep, 2006). While the glycolytic enzyme pyruvate kinase converts PEP into pyruvate during metabolism of other carbon sources (Romeo & Snoep, 2005), a unique characteristic of glycerol metabolism is that the conversion of PEP into pyruvate is coupled to DHA phosphorylation (i.e. due to the fact that DHAK uses PEP as the phosphate group donor). This coupled reaction is a critical component of glycerol fermentation in *E. coli* and generates a cycle in the metabolic pathway (Figure 28) which for the purpose of the model allows the assumption of negligible pyruvate kinase activity. The synthesis of acetyl-CoA (AcCoA) from pyruvate can take place through two different enzymes, the pyruvate dehydrogenase complex (PDHC) and pyruvate formate lyase (PFL). However, considering the high NADH/NAD+ ratios observed during glycerol fermentation (Murarka et al., 2008) and given that NADH negatively regulates PDHC (Sawers & Clark, 2004), PFL is expected to play a primary role. The dispensable nature of pyruvate dehydrogenase during glycerol fermentation has been verified in our laboratory (Clomburg and Gonzalez, unpublished). The final reactions in the model consist of the two-step conversion of AcCoA into ethanol through the action of acetaldehyde/alcohol dehydrogenase (ALDH/ADH) (Sawers & Clark, 2004).

The kinetic rate expressions considered for each of the reaction are presented below with their sources and justifications. For a given reaction i and metabolite j, the

following notation will be used: r_{max}^{i} for the maximum rate(mM/s), Keq_i for the equilibrium constant, Km_i^j for the Michaelis-Menten constant (mM) and C_j for the metabolite concentration (mM). X represents cell concentration (g CDW/L). Other notations are presented for some specific reactions, which will be noted later.

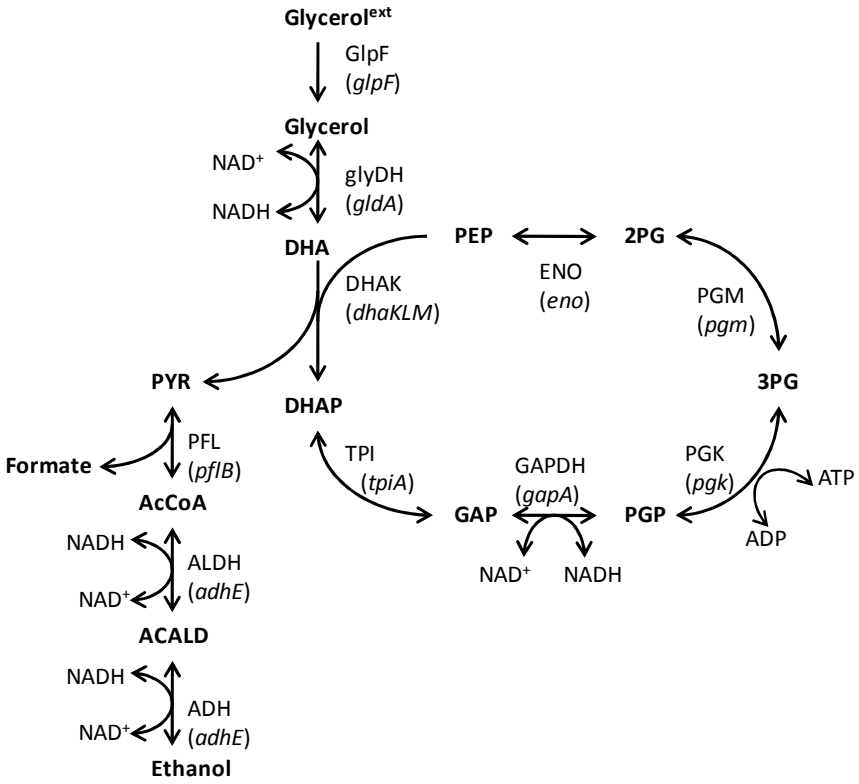

Figure 28: Model of Glycerol Fermentation under anaerobic conditions in *E. coli*. Reactions: ADH, acetaldehyde dehydrogenase; ALDH, alcohol dehydrogenase; DHAK, dihydroxyacetone kinase; ENO, enolase; GAPDH, glyceraldehyde 3-phosphate dehydrogenase; glyDH, glycerol dehydrogenase; GlpF, glycerol transport; PFL, pyruvate formate-lyase; PGM, phosphoglycerate mutase; PGK, phosphoglycerate kinase; TPI, triose phosphate isomerase. Metabolites: 2PG, 2-phosphoglycerate; 3PG, 3-phosphoglycerate; AcCoA, acetyl-CoA; ADP, adenosine diphosphate; ATP, adenosine triphosphate; DHA, dihydroxyacetone; DHAP, dihydroxyacetone phosphate; GAP glyceraldehyde-3-phosphate; NADH, dihydrodiphosphopyridine nucleotide; NAD^+, diphosphopyridine nucleotide; PGP, 1,3-diphosphateglycerate; PYR, pyruvate.

Kinetic rate expressions

Glycerol Transport: The first step in glycerol fermentation is the transport of glycerol, as shown in Figure 28. Transport is possible through passive transport across the membrane, aided by the action of the aquoporin GlpF which allows facilitated

diffusion of glycerol in both directions of the membrane (Lu et al., 2003). Although flux mediated by GlpF has been modeled as Michaelis-Menten (Voegele et al., 1993), those studies assume unidirectional transport. Nevertheless, since the next reaction (glycerol dehydrogenase) has a high Michaelis-Menten constant comparative to the concentration of external glycerol (Table 3), it is most likely that the intracellular concentration of glycerol (GLYC in the kinetic equation) will be high compared with the external concentration (GLYC_ext in the kinetic equation), and flux in both directions is expected. On the other hand, GlpF has also been modeled as diffusion, following a two-parameter formalism for this enzyme (Kleinhans, 1998). Therefore, a simple diffusion equation was used in this project, where D (s^{-1}) is the diffusivity constant (which includes simple diffusion and facilitated diffusion):

$$r_{GlpF} = D \cdot \left(C_{GLYC\_ext} - C_{GLYC}\right) \tag{28}$$

Oxidation of glycerol: glyDH is one of the key enzymes that allow glycerol fermentation, as was previously stated. Reversible Michaelis-Menten reaction is used for this step (Subedi et al., 2008):

$$r_{glyDH} = \frac{\frac{r_{max}^{glyDH}}{Km_{glyDH}^{GLYC}} \cdot \left(C_{GLYC} - \frac{C_{DHA}}{Keq_{glyDH}}\right)}{1 + \frac{C_{GLYC}}{Km_{glyDH}^{GLYC}} + \frac{C_{DHA}}{Km_{glyDH}^{DHA}}} \tag{29}$$

Phosphorylation of DHA: DHAK in *E. coli* is a PEP-dependent kinase. This reaction allows the simultaneous conversion of DHA into DHAP, and PEP into PYR, creating a cycle in the metabolic pathway (Figure 28). It must be mentioned that there is another enzyme, the ATP-dependent pyruvate kinase (PYK), which is also able to convert PEP into PYR. However, a simple mass balance indicates that all the flux to produce PYR must go through the action of DHAK in this simplified model. The kinetics

of DHAK has been modeled as an irreversible Michaelis-Menten (Gutknecht et al., 2001). This kinetics assumes that DHA is the limiting reactant, and that there is an excess of PEP. Other kinetic expressions are available with competitive inhibition from L-D glyceraldehyde (Garcia-Alles et al., 2004), but since glyceraldehyde is not part of the metabolic pathway the former kinetics was considered to be appropriate:

$$r_{DHAK} = \frac{r_{max}^{DHAK} \cdot C_{DHA}}{Km_{DHAK} + C_{DHA}} \tag{30}$$

Isomerization of DHAP: The enzyme triose phosphate isomerase (TPI) mediates the conversion of DHAP into glyceraldehyde-3-phosphate (GAP). Its kinetics correspond to a reversible Michaelis-Menten (Richter et al., 1975):

$$r_{TPI} = r_{max}^{TPI} \cdot \frac{C_{DHAP} - \frac{C_{GAP}}{Keq_{TPI}}}{Km_{TPI}^{DHAP} \cdot \left(1 + \frac{C_{GAP}}{Km_{TPI}^{GAP}}\right) + C_{DHAP}} \tag{31}$$

Oxidation of GAP: The conversion of GAP into 1,3-diphosphoglycerate (PGP) is mediated by the enzyme glyceraldehyde-3-phosphate dehydrogenase (GAPDH). Its kinetics is modeled according to a two-substrate reversible Michaelis-Menten mechanism (Chassagnole et al., 2002) and represented by the following expression:

$$r_{GAPD} = r_{max}^{GAPD} \cdot \frac{C_{GAP} \cdot C_{NAD} - \frac{C_{PGP} \cdot C_{NADH}}{Keq_{GAPD}}}{\left(Km_{GAPD}^{GAP} \cdot \left(1 + \frac{C_{PGP}}{Km_{GAPD}^{PGP}}\right) + C_{GAP}\right) \cdot \left(Km_{GAPD}^{NAD} \cdot \left(1 + \frac{C_{NADH}}{Km_{GAPD}^{NADH}}\right) + C_{NAD}\right)} \tag{32}$$

Phosphorylation of PGP: This reaction allows converting PGP into 3-phosphoglycerate (3PG), and it is catalyzed by the enzyme phosphoglycerate kinase (PGK). The kinetics of this enzyme is modeled according to a two-substrate reversible Michaelis-Menten mechanism (Chassagnole et al., 2002). Concentration of ATP and

ADP were kept constant, as these metabolites are unbalanced in the modeled pathway. Below is the equation for this reaction.

$$r_{PGK} = r_{max}^{PGK} \cdot \frac{C_{ADP} \cdot C_{PGP} - \frac{C_{ATP} \cdot C_{3PG}}{Keq_{PGK}}}{\left(Km_{PGK}^{ADP} \cdot \left(1 + \frac{C_{ATP}}{Km_{PGK}^{ATP}}\right) + C_{ADP}\right) \cdot \left(Km_{PGK}^{PGP} \cdot \left(1 + \frac{C_{3PG}}{Km_{PGK}^{3PG}}\right) + C_{PGP}\right)} \quad (33)$$

Isomerization of 3PG: The enzyme phosphoglycerate mutase (PGM) allows the conversion of 3PG into 2-phosphoglycerate (2PG), and its kinetics corresponds to a reversible Michaelis-Menten (Chassagnole et al., 2002):

$$r_{PGM} = \frac{r_{max}^{PGM} \cdot \left(C_{3Pg} - \frac{C_{2PG}}{Keq_{PGM}}\right)}{Km_{PGM}^{3PG} \cdot \left(1 + \frac{C_{2PG}}{Km_{PGM}^{2PG}}\right) + C_{3PG}} \quad (34)$$

Dehydration of 2PG: The enzyme enolase (ENO) allows the interconversion of 2PG and PEP, and its kinetics is modeled as a reversible Michaelis-Menten (Chassagnole et al., 2002):

$$r_{ENO} = \frac{r_{max}^{ENO} \cdot \left(C_{2PG} - \frac{C_{PEP}}{Keq_{ENO}}\right)}{Km_{ENO}^{2PG} \cdot \left(1 + \frac{C_{PEP}}{Km_{ENO}^{PEP}}\right) + C_{2PG}} \quad (35)$$

PYR cleavage: PYR can be converted into AcCoA using two different enzymes: Pyruvate dehydrogenase complex (PDHC) or Pyruvate formate lyase (PFL). The first one is associated with an oxidative process, which generates one molecule of NADH, while PFL is activated under anaerobic conditions and does not produce NADH. In addition, PDHC is negatively regulated by NADH, which makes this enzyme inactive under fermentative conditions (Sawers & Clark, 2004). Therefore, PFL is expected to be the only active enzyme that performs this step under fermentative conditions. The kinetics of

PFL has been modeled as a ping-pong mechanism by Knappe et al. (Knappe et al., 1974), which expression is given below:

$$r_{PFL} = \frac{r_{fmax}^{PFL} \cdot C_{PYR} \cdot C_{CoA}}{C_{PYR} \cdot C_{CoA} + Km_{PFL}^{Pyr} \cdot C_{CoA} + Km_{PFL}^{CoA} \cdot C_{PYR}} - \frac{r_{rmax}^{PFL} \cdot C_{AcCoA} \cdot C_{Form}}{C_{AcCoA} \cdot C_{Form} + Km_{PFL}^{AcCoA} \cdot C_{Form} + Km_{PFL}^{Form} \cdot C_{AcCoA}}$$

(36)

Under anaerobic fermentation of glycerol, formate was not detected (Dharmadi et al., 2006) causing the second term to be negligible.

Reduction of AcCoA: Alcohol dehydrogenase, encoded by *adhE*, is able to catalyze the conversion of AcCoA into acetaldehyde (ACALD), and then ACALD into ethanol. This first reaction, acetaldehyde dehydrogenase (ALDH), has been modeled as a bi-uni-uni-uni ping-pong mechanism (Shone & Fromm, 1981). While an explicit expression of the reverse reaction is presented in this paper, the forward reaction is obtained from Segel (Segel, 1975). Both reactions are simplifications from the original mechanism, assuming absence of products or absence of substrates, respectively. All kinetic parameters are obtained from Shone and Fromm (Shone & Fromm, 1981), except for the case of Kia, a kinetic constant of this mechanism (see details in Segel, 1975). Concentration of Coenzyme-A (CoA) was also considered as a constant. The kinetic expression results having the following equation:

$$r_{ALDH} = r_{max}^{ALDH} \cdot \frac{C_{AcCoA}}{Km_{ALDH}^{AcCoA} + C_{AcCoA} \cdot \left(1 + \frac{Km_{ALDH}^{NADH}}{C_{NADH}} + \frac{Km_{ALDH}^{NADH} \cdot C_{ACALD}}{K_{ia} \cdot C_{NADH}}\right)} - \frac{r_{max}^{ALDH}}{Keq_{ALDH}} \cdot \frac{C_{ACALD} \cdot C_{NAD} \cdot C_{COA}}{K_{ia} \cdot {K_m}^{NAD} \cdot C_{CoA} + {K_m}^{COA} \cdot C_{ACALD} \cdot C_{NAD} + {K_m}^{NAD} \cdot C_{ACALD} \cdot C_{CoA} + {K_m}^{ACALD} \cdot C_{NAD} \cdot C_{CoA} + C_{ACALD} \cdot C_{NAD} \cdot C_{CoA}}$$

(37)

Reduction of acetaldehyde: ACALD is reduced into ethanol by the enzyme alcohol dehydrogenase (ADH), which has been modeled as reversible Michaelis Menten (Membrillo-Hernandez et al., 2000):

$$r_{ADH} = \frac{r_{max}^{ADH}}{Km_{ADH}^{ACALD}} \cdot \frac{\left(C_{ACALD} - \frac{C_{EtOH}}{Keq_{ADH}}\right)}{1 + \frac{C_{ACALD}}{Km_{ADH}^{ACALD}} + \frac{C_{EtOH}}{Km_{ADH}^{EtOH}}} \quad (38)$$

Cell growth: The specific growth rate (μ) was adjusted using Monod equation (see equation 39), where μ_{max} is the maximum specific rate and $Km_{gly}^{Growth}$is the Monod coefficient. Biomass production was calculated from the specific growth rate according to equation 40:

$$\mu = \frac{\mu_{max} \cdot C_{GLYC\ ext}}{Km_{GLYC}^{Growth} + C_{GLYC\ ext}} \quad (39)$$

$$\mu = \frac{1}{X} \cdot \frac{dX}{dt} \quad (40)$$

Mass Balances: ODE

Once all the kinetic equations are defined, these rates are integrated in a system of ODEs. The ODEs for a batch system are listed below. Equations for substrates and products are divided by the density, as they are presented in different units than internal metabolites.

$$\frac{d\,C_{GLYC\ ext}}{dt} = -r_{GlpF} \cdot X/\text{density} \quad \text{-- Substrate} \quad (41)$$

$$\frac{d\,C_{GLYC}}{dt} = r_{GlpF} - r_{glyDH} - \mu \cdot C_{GLYC} \quad (42)$$

$$\frac{d\,C_{DHA}}{dt} = r_{glyDH} - r_{DHAK} - \mu \cdot C_{DHA} \quad (43)$$

$$\frac{d\,C_{DHAP}}{dt} = r_{DHAK} - r_{TPI} - \mu \cdot C_{DHAP} \quad (44)$$

$$\frac{d\,C_{GAP}}{dt} = r_{TPI} - r_{GAPDH} - \mu \cdot C_{GAP} \quad (45)$$

$$\frac{d\,C_{PGP}}{dt} = r_{GAPDH} - r_{PGK} - \mu \cdot C_{PGP} \quad (46)$$

$$\frac{d\,C_{3PG}}{dt} = r_{PGK} - r_{PGM} - \mu \cdot C_{3PG} \quad (47)$$

$$\frac{d\,C_{2PG}}{dt} = r_{PGM} - r_{ENO} - \mu \cdot C_{2PG} \quad (48)$$

$$\frac{d\,C_{PEP}}{dt} = r_{ENO} - r_{DHAK} - \mu \cdot C_{PEP} \quad (49)$$

$$\frac{d\,C_{PYR}}{dt} = r_{DHAK} - r_{PFL} - \mu \cdot C_{PYR} \quad (50)$$

$$\frac{d\,C_{AcCoA}}{dt} = r_{PFL} - r_{ALDH} - \mu \cdot C_{AcCoA} \quad (51)$$

$$\frac{d\,C_{ACALD}}{dt} = r_{ALDH} - r_{ADH} - \mu \cdot C_{ACALD} \quad (52)$$

$$\frac{d\,C_{EtOH}}{dt} = (r_{ADH}) \cdot X/\text{density} \quad \text{--Product} \quad (53)$$

$$\frac{d\,X}{dt} = \mu \cdot X \quad \text{--Biomass} \quad (54)$$

This system of ODEs was solved using Matlab v7.11.0 (R2010b, The Mathworks, Inc.), using function ode23t (suitable for moderately stiff problems). Concentration of ATP and ADP were kept constant as these metabolites are unbalanced in the modeled pathway. Concentrations of ATP, ADP, NADH and NAD were taken from the model of glucose metabolism, with values of 4.27 mM, 0.595 mM, 0.1 mM, and 1.47 mM, respectively (Chassagnole et al., 2002). Concentration of the coenzyme-A (CoA) was assumed constant and equal to 0.1 mM. Initial concentrations of other metabolites were assumed to be 0.1 mM, although this assumption does not affect the response of the system after one minute of simulation. The total time of simulation was 100 hours. See Appendix 0 for details.

4.2 Parameters estimation: *In vitro*, *in silico* and optimization

The problem of finding reliable parameters for the model is non-trivial. While it is desirable to know the *in vivo* parameters, in practice there is no sufficient technology that allows do that, and *in vitro* or *in silico* experiments approach the real values. *In vitro* parameters are obtained in three defined steps: 1) assignments of a rate law, 2) measurements of involved molecules, and 3) parameter calibration (Dreger et al., 2009). Since this procedure requires studying an isolated part of the system, and also assuming one specific rate law, differences with respect to the *in vivo* parameters are expected. To obtain the maximum rate using *in vivo* information, data of internal metabolites concentration together with the kinetic expressions are used (Rizzi et al., 1997). On the other hand, parameters can be calculated by defining a model, and then finding the parameter values that allow representation of experimental observations in the best possible way (optimization). Different strategies have been proposed to solve the problem of the optimization, among them Monte Carlo methods (random optimization) and Evolutionary Algorithms (Dreger et al., 2009). Different models differ in complexity and performance and, depending on the system to be modeled, one or another method may be more convenient (Dreger et al., 2009). Whereas *in vitro* parameters and optimization attempt to solve the same problem, often differences are found, and optimized parameters differ even in several orders of magnitude with respect to *in vitro* parameters (Chassagnole et al., 2002; Teusink et al., 2000). In this work, I combined both approaches to find parameters for the glycerol fermentation model.

Values from literature were used as an initial approach, followed by sensitivity analysis and optimization of relevant parameters. For Michaelis –Menten parameters, the

approach was to use *in vitro* information from *E. coli* when available. For maximum rate parameters there were two main strategies: 1) for glycolytic enzymes shared with glucose fermentation, parameters from Chassagnole et al. were used (Chassagnole et al., 2002), which were calculated using measurements of metabolites in addition to the kinetic rate laws and optimization; 2) for others enzymes, which are specific to glycerol utilization (glyDH and DHAK) and ethanol synthesis (ALDH and ADH), information of specific activity *in vitro* from experiments in our group was used.

A sensitivity analysis was performed over all the parameters in order to increase the quality of these, using a Matlab program (Garcia, 2002). Some parameters have been shown to have a different value in modeling optimization (Chassagnole et al., 2002), others were obtained in different experimental conditions, and a third group was proposed in this paper. The sensitivity analysis allowed identifying the parameters that have an influence over the three measured variables (glycerol, ethanol, and biomass). As a result of this, the following parameters were identified: r_{max}^{glyDH} , Km_{glyDH}^{DHA} , Keq_{glyDH} , r_{max}^{DHAK}, Km_{DHAK} , μ_{max}, and Km_{glyc}^{Growth}. Among these parameters, the Michaelis-Menten constants were considered more reliable than the maximum rates. In addition, μ_{max} has been calculated from the anaerobic fermentation of glycerol (Murarka et al., 2008), while in contrast there is no reliable data for Km_{gly}^{Growth}. Therefore, an optimization was performed over r_{max}^{glyDH}, r_{max}^{DHAK}, Km_{glyc}^{Growth}. First, random parameters were generated in order to identify the range of best fit for these three parameters. Then, a grid was prepared in order to find the values of these three parameters that minimized the error (difference between simulated and experimental concentrations of glycerol, ethanol and

biomass). The resulting parameters are presented in Table 3, along with all the other kinetic parameters used in this model and their sources.

Table 3: Kinetic parameters for glycerol fermentation in *E. coli*.

Reaction	Parameters	Source
GlpF	D = 1	This study.
glyDH	$r_{max}^{glyDH} = 1.33$ mM/s $Km_{glyDH}^{gly} = 56\ mM$ $Km_{glyDH}^{DHA} = 0.3\ mM$ $Keq_{glyDH} = 0.006977$[a]	This study. (Subedi et al., 2008). (Subedi et al., 2008). (Subedi et al., 2008).
DHAPK	$r_{max}^{DHAPK} = 0.72$ mM/s $Km_{DHAPT} = 45 \cdot 10^{-3} mM$	This study. (Gutknecht et al., 2001).
TPI	$r_{max}^{TPI} = 68.7\ mM/s$ $Keq_{TPI} = 0.04$ $Km_{TPI}^{DHAK} = 2.8\ mM$ $Km_{TPI}^{GAP} = 0.3\ mM$	(Chassagnole et al., 2002). (Babul et al., 1993). (Babul et al., 1993). (Babul et al., 1993)
GAPDH	$r_{max}^{GAPDH} = 921.6\ mM/s$ $Keq_{GAPDH} = 0.67$ $Km_{GAPDH}^{GAP} = 0.15\ mM$ $Km_{GAPDH}^{Pgp} = 0.1\ mM$ $Km_{GAPDH}^{NAD} = 0.45\ mM$ $Km_{GAPDH}^{NADH} = 0.02\ mM$	(Chassagnole et al., 2002) (Bakker et al., 1997). (Bakker et al., 1997). (Bakker et al., 1997). (Bakker et al., 1997). (Bakker et al., 1997).
PGK	$r_{max}^{PGK} = 3021.77 mM/s$ $Keq_{PGK} = 1800$ $Km_{PGK}^{ADP} = 0.18$ $Km_{PGK}^{ATP} = 0.24\ mM$ $Km_{PGK}^{Pgp} = 0.006$ $Km_{PGK}^{3Pg} = 0.17$	(Chassagnole et al., 2002). (Ni & Savageau, 1996). (Molnar & Vas, 1993). (Fifis & Scopes, 1978). (Lavoinne et al., 1983). (Schmidt et al., 1995).
PGAM	$r_{max}^{PGAM} = 89.0497\ mM/s$ $Keq_{PGAM} = 0.1$ $Km_{PGAM}^{3Pg} = 0.2$ mM $Km_{PGAM}^{2Pg} = 0.369\ mM$	(Chassagnole et al., 2002). (Pettersson, 1990). (Britton et al., 1972). (Grana et al., 1989).
ENO	$r_{max}^{ENO} = 330.448\ mM/s$ $Keq_{ENO} = 6.7$ $Km_{ENO}^{2Pg} = 0.1\ mM$ $Km_{ENO}^{PEP} = 0.135\ mM$	(Chassagnole et al., 2002). (Bakker et al., 1997). (Spring & Wold, 1971). (Duggleby, 1994).
PFL	$r_{rmax}^{PFL} = 656\ mM$ $r_{fmax}^{PFL} = 0.46 \cdot r_{rmax}^{PFL}/1.33$ $Km_{PFL}^{Pyr} = 2.05\ mM$ $Km_{PFL}^{CoA} = 0.0068\ mM$ $Km_{PFL}^{Form} = 24.5\ mM$ $Km_{PFL}^{AcCoA} = 0.051\ mM$	Calculated from Zhu and Shimizu (Zhu & Shimizu, 2004) Calculated from data presented in Knappe et al. (Knappe et al., 1974). (Knappe et al., 1974). (Knappe et al., 1974). (Knappe et al., 1974). (Knappe et al., 1974).
ALDH	$r_{max}^{PDH} = 2311\ mM$ $Keq_{PDH} = 1$ $Km_{PDH}^{AcCoA} = 0.007\ mM$ $Km_{PDH}^{NADH} = 0.025\ mM$ $K_{ia} = 1$	This study. (Hoefnagel et al., 2002). (Shone & Fromm, 1981). (Shone & Fromm, 1981). This study.

	$Km_{PDH}^{NAD} = 0.080\ mM$ $Km_{PDH}^{CoA} = 0.008\ mM$ $Km_{PDH}^{Acetal} = 10.0\ mM$	(Shone & Fromm, 1981). (Shone & Fromm, 1981). (Shone & Fromm, 1981).
ADH	$r_{max}^{ADH} = 2311\ mM/s$ $Keq_{ADH} = 12354.9$ $Km_{ADH}^{Acetal} = 5.4\ mM$ $Km_{ADH}^{EtOH} = 2.4\ mM$	This study. (Hoefnagel et al., 2002) (Membrillo-Hernandez et al., 2000). (Membrillo-Hernandez et al., 2000).
Biomass	μ_{max}= 0.04/3600 s^{-1} Km_{gly}^{Growth}= 159.2 mM Density = 476.762[b]	(Murarka et al., 2008) This study (Sundararaj et al., 2004)

[a] By definition, Keq_{glyDH} = ($C_{DHA\ eq}$/Cgly eq) = ($r_{\max\_f}^{glyDH}$ / $r_{\max\_r}^{glyDH}$) (Km_{glyDH}^{DHA}/ Km_{glyDH}^{gly}). Here Keq_{glyDH} was calculated as ($k_{cat\ f}$ /$k_{cat\ r}$) (Km_{glyDH}^{DHA}/ Km_{glyDH}^{gly}) given that kcat = r_{max} /[E], where [E] is the enzymatic concentration.

[b]Density appears in Equations (41) and (53) as a conversion factor to use biomass in proper units. It was calculated using data from CyberCell Database (CCDB) (Sundararaj et al., 2004). Density ¼ cell-dry-weight/cell-cytoplasm-vol = $3*10^{-13}$ g / $6.7*10^{-6}$ L.

4.3 Results of modeling

Figure 29 shows the solution to the system of ODEs for glycerol, ethanol, and biomass, and compares them to experimental data. Data at time zero was not included to adjust the curves, and predictions of biomass in the interval zero to 12 hours are an extrapolation using the model. The model is able to describe correctly glycerol metabolism, ethanol production, and biomass. Also, simulated glycerol utilization shows a smooth curve in the late stages in agreement with experimental data, being it a direct consequence of using simple diffusion in the kinetic expression for glycerol transport. In contrast, when a Michaelis-Menten kinetics was tested for the transport of glycerol (in accordance with report from Voegele et al. (1993)), there was an abrupt decrease in glycerol concentration at later stage of fermentation (results not shown), which is in disagreement with experimental data. The fact that the simulated curve for ethanol is above experimental data in late stages can be attributed to evaporation of ethanol in experimental measurements and exclusion of by-products.

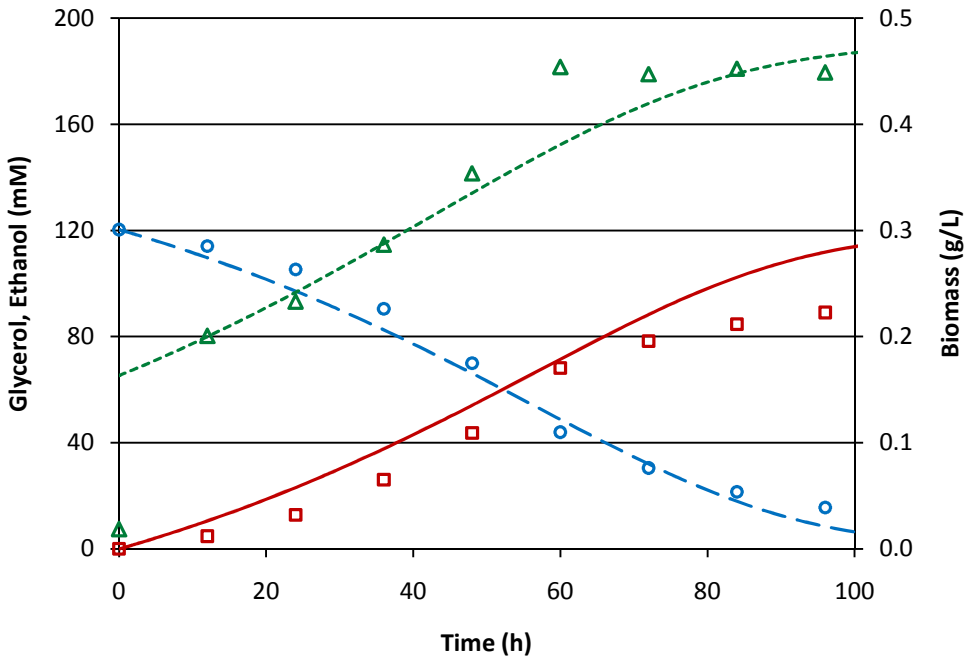

Figure 29: Glycerol fermentation by *E. coli*. Experimental concentration of glycerol (blue circles), ethanol (red squares) and cells (green triangles). Simulated concentration of glycerol (blue dashed line), ethanol (red continuous line) and biomass (green dotted line).

Figure 30 presents predictions for internal metabolite concentrations. The internal metabolite concentrations can be classified into two main groups based on their concentrations similarities throughout the fermentation. The first group, which includes 3PG, PEP and AcCoA (dashed lines in Figure 30), corresponds to metabolites that experience an almost step-increase in concentration at the beginning of the fermentation, and then their concentration exponentially decreases converging to a value close to 1 mM. However, it is noteworthy that the most dramatic decreases in the concentrations of these intracellular metabolites takes place within the first 24 hours, during which the cells have not reached the exponential growth phase. Once exponential growth has been reached, these metabolites appear to be in quasi-steady state as the change in their concentrations is small compared to that of the extracellular metabolites (Figure 30). Interestingly, the concentrations of these metabolites were also reported to change in a

coordinated manner in response to changes in the metabolism of glucose (Schaub & Reuss, 2008). The second group of metabolites, which includes DHA, DHAP, 2PG, ACALD, PYR, GAP and PGP (continuous lines in Figure 30), corresponds to metabolites that are not predicted to have dramatic changes in their concentrations throughout the fermentation period. Overall, after 24 hours all internal metabolites are considered to have achieved a quasi-steady state, as the change in their concentrations is less than 2% the change in concentrations of external metabolites (glycerol and ethanol). Internal concentration of glycerol was not included in Figure 30 because it has the same behavior (and values) of external glycerol concentration, which is caused by the high value of the Michaelis-Menten constant of the enzyme glyDH.

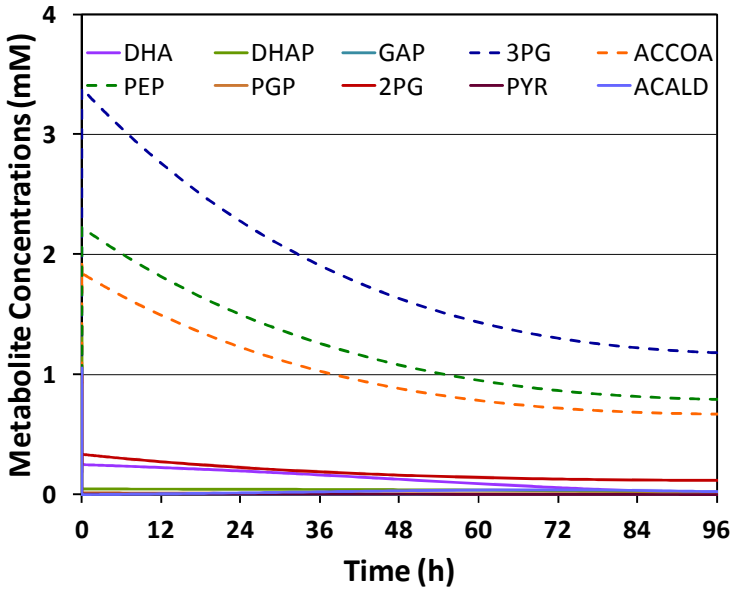

Figure 30: Prediction of changes in the concentration of intracellular metabolites. Two groups of intracellular metabolites are distinguished for the behavior: group 1 (3PG, AcCoA and PEP), dashed lines, have the greater variation during first 24 hours, and group 2 (DHA, DHAP, GAP, PGP, 2PG, PYR and ACALD), continuous lines, have lower concentrations and they remain in quasi-steady state during the fermentation. Reactions: ADH, acetaldehyde dehydrogenase; ALDH, alcohol dehydrogenase; DHAK, dihydroxyacetone kinase; ENO, enolase; GAPDH, glyceraldehyde 3-phosphate dehydrogenase; glyDH, glycerol dehydrogenase; GlpF, glycerol transport; PFL, pyruvate formate-lyase; PGM, phosphoglycerate mutase; PGK, phosphoglycerate kinase; TPI, triose phosphate isomerase.

4.4 Metabolic control analysis of the fermentative utilization of glycerol

MCA is a theory developed to elucidate the control structure of a metabolic pathway. The main concept that arises from this theory is the Flux Control Coefficients (FCCs), as they represent the normalized change in each flux given an infinitesimal change in an enzyme concentration. The flux-control summation theorem stipulates that the sum of all the FCCs of one flux J is equal to one. Because of this, a FCC close to one means that the corresponding enzyme is the rate-limiting of the system, although more frequently the control of the flux is distributed among more than one enzyme (Fell, 1998). FCCs are properties of the metabolic system.

The cyclic pathway in the glycerol fermentation pathway presented in Figure 28 falls into the classification of conserved cycle, because the total concentration of its components does not change. This cycle can be treated as a mioetyc cycle because there is a conserved component in the cycle (the three carbon chain with one aldehyde group) that is neither synthesize nor breakdown (Sauro, 1994) For a system where moiety-conserved cycles are present, Hofmeyr et al. presented the theories that allow calculating FCCs using a matrix system. See *Material and methods* (chapter 3) for the theory and Appendix 10.1 for the matrix system applied to the glycerol fermentation pathway. Elasticities were calculated using the kinetic expressions for each reaction, and using predicted values of internal metabolites from quasi-steady state, at time equal to 50 hrs (Figure 30). This point was considered quasi-steady state because the concentration of intracellular metabolites changes at a rate that is less than 2% of that of external metabolites. The resulting FCCs calculated using this approach are shown in Figure 31.

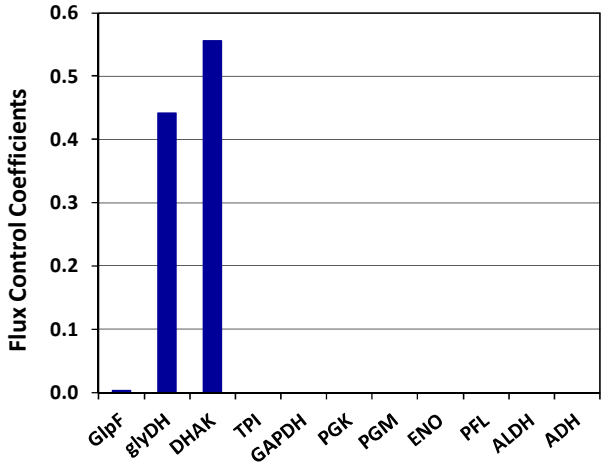

Figure 31: Calculated Flux Control Coefficients (FCC^j, where j represents the reaction specified by the listed enzyme) for the glycerol fermentation pathway represented in Figure 28. Reactions: ADH, acetaldehyde dehydrogenase; ALDH, alcohol dehydrogenase; DHAK, dihydroxyacetone kinase; ENO, enolase; GAPDH, glyceraldehyde 3-phosphate dehydrogenase; glyDH, glycerol dehydrogenase; GlpF, glycerol transport; PFL, pyruvate formate-lyase; PGM, phosphoglycerate mutase; PGK, phosphoglycerate kinase; TPI, triose phosphate isomerase.

Discussion of limiting steps

Values of FCCs reveal that the control of the flux in the glycerol fermentation pathway is shared by two steps: glyDH and DHAK, with values of FCC 0.44 and 0.56, respectively. All other FCCs have null (or near to null) values, meaning that no control is performed by the corresponding enzymes. These findings reveal a very different control structure than found for similar analyses of glucose metabolism. For example, using a kinetic model Chassagnole and collaborators calculate the FCCs of glucose respiration in *E. coli*, and they reported that for glucose metabolism the control of the flux through the pathway is mainly in the phosphotransferase system (PTS), with an FCC of 0.4, and in a smaller but still significan degree in the enzymes phosphofructokinase (PFK), glucose-6-phosphate dehydrogenase (G6PDH), and pyruvate dehydrogenase (PDH), due to their inhibtory effects on the PTS (Chassagnole et al., 2002). In addition, Koebmann and collaborators used an experimental approach to study the control structure of *E. coli* in

glucose respiration, and they have postulated that the majority of control of the glycolytic flux resides outside of the pathway, with the enzymes that hydrolyze ATP, as the authors were able to significantly increase the glycolytic flux through the specific induction of ATP hydrolysis (Koebmann et al., 2002). Both of these findings using glucose contrast the control structure elucidated for glycerol metabolism, as the transport reaction for glycerol (GlpF) was found to have very little control on the overall flux, and two key pathways enzymes, glyDH and DHAK, were found to have nearly total control of the overall pathway flux.

Based on the results of the MCA for glycerol fermentation in *E. coli* (Figure 31), it is predicted that changes in the enzymes glyDH and DHAK will reduce the time of glycerol fermentation toward the production of ethanol in *E. coli*, while overexpression of other enzymes involved in the pathway will have no effect in this metabolic process.

4.5 Experimental verification

The purpose of this section is to corroborate the predictions performed using the MCA, in which it was proposed that overexpression of the enzymes glyDH and DHAK should accelerate the fermentation of glycerol toward ethanol, and overexpression of other enzymes of this pathway should not affect the rate of glycerol consumption and ethanol production.

Experiments were performed by collaborator James Clomburg in order to corroborate the effect of overexpressing DHAK, glyDH, and both. Figure 32 shows the effect in glycerol consumption and ethanol production when the enzymes glyDH and DHAK were overexpressed. It is clear that both enzymes have a noticeable effect in reducing the time to ferment glycerol. The effect of increasing DHAK is bigger than

increasing glyDH, in agreement with values of FCCs of these two enzymes. In addition, overexpression of both enzymes has a synergistic effect over this process, as the time to ferment glycerol decrease more than the simple addition of time reduction in the overexpression of these enzymes separately. Table 4 shows the measured enzyme activities and metabolic fluxes for strains for the control strain (MG1655 pZSblank), and for strains overexpressing glyDH (MG1655 pZSgldA), DHAK (MG1655 pZSKLM), or both (MG1655 pZSKLMgldA). The increase of metabolic fluxes for glycerol consumption and for ethanol production is maximal for the overexpression of glyDH and DHAK.

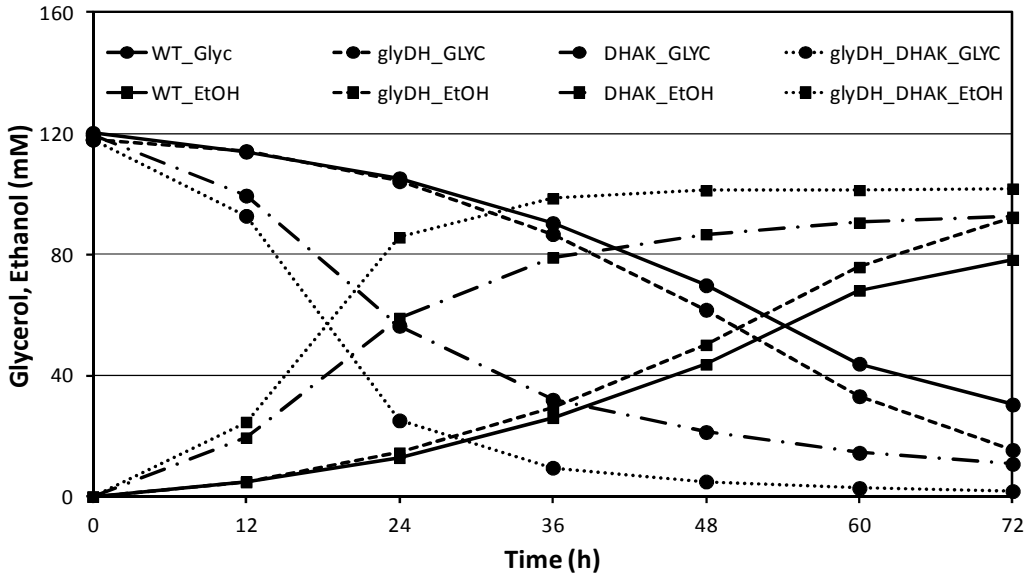

Figure 32: Effect of overexpressing enzymes glyDH, DHAK, and both (glyDH_DHAK) in the fermentation of glycerol in *E. coli*. Concentrations of glycerol (circles) and ethanol (squares) are shown. Results are compared to wild type (WT). Experiments were performed by James Clomburg.

Table 4: Enzyme activities and glycerol-utilization and ethanol-synthesis fluxes for wild-type MG1655 and strains overexpressing glycerol-utilization enzymes. Experiments and calculations were performed by James Clomburg.

Strain	Enzyme activity[a]		Metabolic fluxes[b]	
	glyDH	DHAK	Glycerol utilization	Ethanol synthesis
MG1655 (pZSblank)	0.114±0.002	0.0157±0.001	4.6±0.7	4.1±0.5
MG1655 (pZSgldA)	0.62±0.03	NM	4.3±0.9	3.9±0.8
MG1655 (pZSKLM)	NM	0.028±0.03	6.4±0.9	6±2
MG1655 (pZSKLMgldA)	0.41±0.01	0.037±0.001	10.7±0.8	10±1

[a] Activities (µmol/mg protein/min) were measured during active growth as described in Materials and Methods. NM: not measured.
[b] Fluxes (mmol/g CDW/h) represent average values for fluxes calculated during the active growth phase.

Finally, to further demonstrate that the control of the metabolic pathway is not shared with the other enzymes that were predicted to have FCCs close to zero, experiments increasing expression of genes *tpiA*, *adhE* and *glpF* (separately) were performed, resulting in no apparent change after 72 hours of fermentation. These results confirmed that these enzymes do not have participation in the control structure of glycerol fermentation (Figure 33).

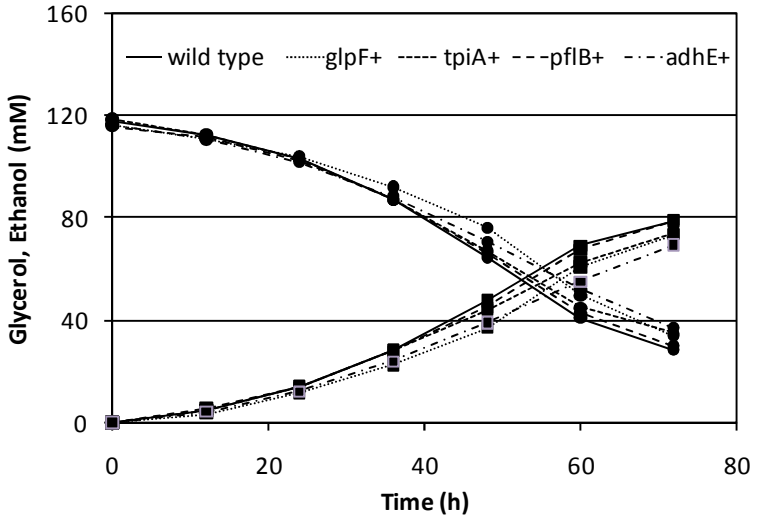

Figure 33: Effect of overexpression of enzymes/proteins involved in glycerol metabolism. Overexpression of genes *glpF*, *tpiA*, *pflB* and *adhE*. Concentrations of glycerol (circle) and ethanol (square) are shown. Experiments were performed by James Clomburg.

4.6 Conclusions

A kinetic model for glycerol fermentation in *E. coli* was developed. The model includes the main 11 reactions that allow the conversion of glycerol into ethanol, a process that is NADH balanced and generates ATP. One interesting property of this metabolic pathway is the appearance of a cycle, as the second reaction, phosphorylation of DHA to produce DHAP, is catalyzed by a PEP-dependent kinase that also converts PEP into PYR.

The model is able to correctly represent the utilization of glycerol and synthesis of ethanol and biomass. In addition, the model was used to identify the control structure of the pathway, indicating that reactions glyDH and DHAP are the limiting steps in glycerol fermentation in *E. coli.* Experiments were conducted to corroborate these results. It was found that separate overexpression of glyDH and DHAK accelerate the fermentation of glycerol, being DHAK the one that has a bigger impact in accordance with the FCCs values. The combined overexpression of both enzymes has a higher impact in increasing the fermentation rate of glycerol than the mere addition of overexpressing enzymes glyDH and DHAK separately. In addition, overexpression of other enzymes in the pathways did not affect the kinetics of glycerol fermentation, which further corroborates the predictions of the model.

In conclusion, the use of metabolic control analysis combined with kinetic modeling is a powerful tool to guide rational strain design to optimize the synthesis of desired products. For example, the kinetic model presented in this chapter was developed using only kinetic equations from the literature and measurements of the external concentrations of glycerol, ethanol and biomass. This information was later used to

optimize the kinetic parameters, predict internal metabolite concentrations, and calculate flux control coefficients, which were used to decide which genes needed to be overexpressed in order to reduce the fermentation time for glycerol conversion to ethanol. Thus, the implementation of a kinetic model is useful in saving time and resources in experimental work.

In summary, the main results and findings presented in this chapter are:

- Implementation of a kinetic model of the fermentative metabolism of glycerol in *E. coli.* The model consists of 11 reactions that represent the conversion of glycerol into ethanol, the main product of this process.
- Optimization of parameters in the model, by using sensitivity analysis and minimizing the error between predictions and experimental data for external variables (glycerol, ethanol and biomass).
- Predict internal metabolite concentrations.
- Identification of the control structure of the fermentation of glycerol, by calculating flux control coefficients, which identified that the enzymes glyDH and DHAK share the control of the flux through the pathway. Use of these results to predict changes in the production of ethanol after overexpressing key genes.
- The results were experimentally validated by a collaborator, and the experimental production rate of ethanol doubled its original value after overexpressing genes associated with glyDH (*gldA*) and DhaK (*dhaKLM*). Overexpression of other genes was tested and, as predicted, it did not have an impact on the production rate of ethanol.

5 Results II: Genome-scale modeling of the fermentative metabolism of glycerol and assessment of its potential as a platform for fuel and chemical production

This chapter presents the study of glycerol fermentation in *E. coli* using a genome -scale model (GEM) as a mean to study the metabolism from a comprehensive approach. The most recent GEM model for *E. coli*, named iJO1366, was used as a base to model fermentative metabolism of glycerol in this organism (Orth et al., 2011). Flux Balance Analysis (FBA) was used to predict flux distribution and cell growth by maximizing biomass production (called Biomass Objective Function, of BOF). The use of a GEM to study glycerol in *E. coli* has two main purposes: 1) to understand which products and reactions are important in this metabolic process, and 2) to develop strategies for the production of desired fuels and chemicals. It was of special interest to identify which secondary pathways would allow the production of 1,2-PDO, a product that has been suggested as essential to achieve redox balance when biomass is produced and whose production pathway is not well established (Gonzalez et al., 2008). Unlike the kinetic model presented in the previous section, in which one of the assumptions was that glycerol is used exclusively to produce ethanol (the scenario using rich medium), in this analysis I used a GEM to simulate the use of minimal medium. It is important to note that experimental efforts for using minimal medium for glycerol fermentation have been unsuccessful in wild-type *E. coli*, although two strategies had led to ferment glycerol in minimal medium: engineering a strain to overproduces 1,2-PDO or modifying the medium by adding acetol, which leads to the synthesis of 1,2-PDO(Gonzalez et al.,

2008). These results suggest that there is a correlation between the capacity to ferment glycerol in minimal medium and the capacity to produce 1,2-PDO. Thus, this analysis used a GEM to elucidate which pathways are associated with production of 1,2-PDO in order to achieve redox balance when biomass is produced. In addition, the GEM was used to determine the effect of deleting products and reactions, and to identify the function associated with key reactions.

Another objective in the use of a GEM was to develop strategies for the production of desired fuels and chemicals from glycerol, besides ethanol. Products that were targeted in this analysis included native products (lactate, 1,2-PDO and succinate), and non-native products (1,3-PDO, butanol, propionic acid, and propanol). In all cases, the GEM model was used to evaluate the introduction and/or deletion of reactions that would result in an increased productivity yield of the desired products. The development of the strategies incorporated knowledge of pathways that would increase the yield of the desired products, as well as the utilization of mathematical optimization tools that would identify efficiently reactions that need to be removed.

The following are sections of this chapter: 1) *model implementation*, 2) *results A: understanding glycerol fermentation*, 3) *results B: assessing the capabilities of glycerol fermentation as a platform for the synthesis of fuels and chemicals*, and 4) *conclusions*. Model implementation defines the external conditions that were simulated in the model, as well as its curation in order to model glycerol fermentation properly. Results I describes the predicted pathways for glycerol fermentation using a GEM, in good agreement with the experimental data, it proposes a pathway for the production of 1,2-PDO, and it reviews the role of different reactions. Results II describes simulations and

development of strategies for the production of 1,2-PDO, 1,3-PDO, succinate, lactate, butanol, propionic acid, and propanol. Finally, the conclusions discuss the implications of using this kind of model to increase the understanding of glycerol fermentation and to simulate genetic modifications.

5.1 Model Implementation

The implementation of the GEM to represent glycerol fermentation in *E. coli* requires three steps: 1) defining a starting GEM, 2) defining external conditions, and 3) curating the model. Below I elaborate in each of these points.

5.1.1 Define a starting GEM.

The genome scale iJO1366 for *E. coli* K-12 MG1655 was used as starting point, as it represents the most updated GEM for this bacterium (Orth et al., 2011). Table 5 presents some of the properties of iJO1366. The model includes 1,366 genes; among them 1,328 have an experimentally based function and 38 have a computationally predicted function. These genes represent 91% of total genes/ORF with an assigned enzymatic function (Serres et al., 2004) (http://genprotec.mbl.edu/overview.html, updated on Aug 2007). These genes support the production of 1,254 unique functional proteins, including complex enzymes and isoenzymes. The system has 2,251 reactions, which can occur in the cytoplasm, periplasm, or extracellular compartment. The presence of different cellular compartments requires the inclusion of transport reactions. In addition to protein-associated reactions, some reactions occur spontaneously. The correlation between experimental data and *in silico* results allowes the establishment of a growth associated maintenance (GAM) of 53.95 mmol ATP/gCDW/h and a non-growth

associated maintenance (NGAM) of 3.15 mmol ATP/gCDW/h. It is interesting to note that the previous model, named iAF1260, contains a higher value of GAM and NGAM, which indicates that different sets of experimental data may result in different calculations of these parameters. However, from a modeling point of view, the values used in the model iJO1366 were considered sufficient for the purpose of this section, while it is acknowledged that a more accurate set of these values (specific for glycerol fermentation) would increase the quantitative prediction power of the model.

Table 5: Main properties of the GEM iJO1366 (Orth et al., 2011).

Included genes	1366
Experimentally based function	1328
Computationally predicted function	38
Unique functional proteins	1254
Reactions	2251
Metabolic reactions	1473
Transport reactions	778
Exchange reactions	330
Unique metabolites	1136

5.1.2 Definition of External Conditions.

In order to properly use this model to represent glycerol fermentation, it is necessary to adjust the external conditions and to curate the model. The external conditions were set to represent minimal medium under anaerobic conditions (no external electron acceptor). In a GEM, external conditions are defined by changing the lower bound limit of the corresponding exchange reaction, usually setting the value to -1000 mmol/gCDW/h for non limiting nutrients. Table 6 shows a list of the nutrients that were considered as part of the minimal medium, with the corresponding exchange reaction and

lower bound, as defined elsewhere (Feist et al., 2007; Orth et al., 2011). Glycerol was the only limiting nutrient, and its value was set to -20 mmol/gCDW/h.

Table 6: External conditions for the GEM to represent glycerol fermentation. All reactions correspond to "exchange" reactions, which represent the presence of these molecules in the medium.

Exchange Reaction	Lower bound (mmol/gCDW/h)	Exchange Reaction	Lower bound (mmol/gCDW/h)
Calcium exchange	-1000	Sodium exchange	-1000
Chloride exchange	-1000	Ammonia exchange	-1000
Co2+ exchange	-1000	Ni2+ exchange	-1000
Cu2+ exchange	-1000	Phosphate exchange	-1000
Fe2+ exchange	-1000	Selenate exchange	-1000
Fe3+ exchange	-1000	selenite exchange	-1000
H+ exchange	-1000	Sulfate exchange	-1000
H2O exchange	-1000	tungstate exchange	-1000
K+ exchange	-1000	Zinc exchange	-1000
Mg exchange	-1000	Glycerol exchange	-20
Mn2+ exchange	-1000	Cob(I)alamin exchange	-0.01
Molybdate exchange	-1000		

5.1.3 Model curation

Initially, no additional modifications were made to the model. However, the preliminary predictions of flux distribution and cell growth (using FBA) did not match experimental data at the redox balance level. Therefore, the model iJO1366 was curated to represent glycerol fermentation properly.

As already discussed in the introduction of this thesis, the fermentation of glycerol by *E. coli* is particularly challenging because of the highly reduced nature of glycerol. The ethanol-1,2-PDO model has been proposed to explain glycerol fermentation in *E. coli*. The synthesis of ethanol from glycerol is NADH-balanced and hence supports generation of ATP through substrate-level phosphorylation in the glycolytic pathway. Conversion of glycerol to 1,2-PDO results in the consumption of the extra reducing

equivalents generated during cell growth on glycerol (Gonzalez et al., 2008). However, the initial use of FBA identified ethanol as the only essential fermentative product, and a non-permissible pathway under the simulated conditions was consuming the reducing equivalents generated during cell growth. A recursive process of identifying non-permissible sinks for reducing equivalents and then eliminating them from the model resulted in the identification of the following pathways:

a) Amino acid degradation and nucleotide degradation.

b) Sulfate reduction.

c) Iron reduction.

d) Spermidine and 5-methylthio-D-ribose production.

In addition to these modifications, other modifications were introduced to account for changes specific to the use of glycerol, or changes that were overseen by the starting model iJO1366. These modifications correspond to:

e) Activation of formate hydrogen-lyase (FHL) toward formation of CO_2.

f) Irreversibility of reaction NADP-dependent glycerol-3-phosphate dehydrogenase.

g) Removal of pyruvate synthase reaction linked to oxidation of flavodoxin.

h) Modification of pyridine nucleotide transhydrogenase (PntAB).

i) Essentiality of DHAK in glycerol fermentation.

Modifications a) through d) were made to remove non-permissible electron sinks under the current conditions from the model. Below these modifications are explained in detail.

a) The first non-permissible pathway identified in the consumption of reducing equivalents was the simultaneous production and degradation of amino acids and nucleotides. Amino acids and nucleotides are essential cellular components, and therefore their production is required when a minimal medium is used. However, the simultaneous activation of synthesis and degradation pathways of these building blocks would be energetically expensive. In fact, the activation of enzymes involved in amino acids degradation is highly regulated (Reitzer, 2005) and degradation of nucleotides is also subject to regulation (Jensen et al., 2008). Therefore, the model was curated to eliminate all reactions catalyzed by enzymes unique to amino acid degradation and to nucleotide degradation. It is interesting to note that although FBA assumes that optimization of the production of biomass allows the prediction of flux distribution and cell growth, FBA uses linear optimization and cannot incorporate the non-linear effect that would result in incorporating specific enzyme production for each reaction. Inclusion of these non-linear factors would help to reject a solution that includes inefficiencies associated with the simultaneous production of enzymes for the synthesis and degradation of molecules. In other words, if a non-linear optimization model was used (which incorporates a burden associated with the production of enzymes in each active reaction), then the model would likely exclude the simultaneous use of biosynthetic and degradation pathways for amino acids and nucleotides, as it is inefficient. However, a non-linear problem would greatly increase the complexity of the system and finding a solution for a GEM would be impracticable.

b) After removing the degradation of amino acids and nucleotides, *in silico* simulations using FBA used sulfate as an electron acceptor. While some organisms are

known to use sulfate as an electron acceptor for anaerobic respiration (Klenk et al., 1997; Matias et al., 2005), *E. coli* has not been reported to use sulfate as an electron acceptor. However, *in silico* results using FBA indicated that *E. coli* assimilate sulfur by converting sulfate into hydrogen sulfide. Therefore, in order to ensure fermentative conditions, the export of hydrogen sulfide was deleted as a way to prevent the respiratory utilization of sulfate.

c) The presence of iron is intended as a nutrient in the minimal medium, although some organisms (including *E. coli*) are capable of using iron as an electron acceptor by oxidizing Fe(III) to Fe(II) (Appenzeller et al., 2005; Sugio et al., 1987). I modified the GEM to prevent the export of Fe(II), and therefore Fe(II) would be used only as a nutrient.

d) Finally, simultaneous production of spermidine and 5-methylthio-D-ribose consumed reducing equivalents in some of the situations simulated using FBA, in a pathway that involves production of methionine, an essential amino acid. Experimental data support that spermidine is toxic and consequently *E. coli* does not accumulate it (Limsuwun & Jones, 2000). In addition, there is no experimental evidence that indicate production and accumulation of 5-methylthio-D-ribose in wild type *E. coli* for glycerol fermentation. Therefore, I decided to remove the exchange reactions of spermidine and 5-methylthio-D-ribose, thus still allowing their production for other intracellular processes, but preventing their production as an end product.

Modifications e) to h) were made to specific reactions in order to represent proper regulation under glycerol fermentation.

e) The reaction formate hydrogen-lyase (FHL) was considered unfeasible toward formation of CO_2 and H in the original model (Feist et al., 2007; Orth et al., 2011). However, this enzyme is active under acidic conditions and, in particular, it has been experimentally shown to be active in glycerol fermentation under optimal (acidic) conditions (Bagramyan et al., 2002; Murarka et al., 2008). Therefore, this reaction was modified in the model in order to allow conversion of formate into carbon dioxide and molecular hydrogen.

f) The reaction NADP-dependent glycerol-3-phosphate dehydrogenase was considered as reversible in the iJO1366 GEM, but when glycerol is fermented this reaction is expected to be inhibited by glycerol-3-P (G3P), and for that reason the flux was modified to be irreversible toward production of G3P (Edgar & Bell, 1978).

g) The pyruvate synthase reaction was included in the iJO1366 GEM associated with the oxidation of flavodoxin. However, experimental evidence associates this reaction with the oxidation of ferredoxin (and not flavodoxin) (Charon et al., 1999), a molecule that is not part of the GEM. Since there is no purpose in adding this reaction as this is the only reaction that uses ferredoxins, this reaction was eliminated from the model.

h) The reaction pyridine nucleotide transhydrogenase (PntAB) converts NADH into NADPH using a proton exchange pump, was modified to do the conversion using transport of only one proton, and not two as included in the original GEM. Modification of PntAB was made to represent the reaction as it is more widely accepted (Fjellstrom et al., 1997; Pedersen et al., 2008).

i) Experimental information for the dissimilation of glycerol into DHAP was incorporated. Preliminary predictions of flux distribution using FBA and FVA identified two optimal pathways to metabolize glycerol into the glycolytic intermediate dihydroxyacetone phosphate (DHAP). Figure 34 shows the flux distribution in two scenarios for optimal solutions. The first pathway consisted of two steps, using a glycerol dehydrogenase and then converting the dihydroxyacetone (DHA) into DHAP by the action of the enzyme PEP-dependent DHAK. This pathway has been experimentally shown to have a key role in glycerol fermentation (Gonzalez et al., 2008). The second pathway, which will be called the "fructose phosphate bypass" from here on, converts glycerol into DHAP in three steps that start with consuming glyceraldehydes-3-P and end with producing it again. The first reaction of the fructose phosphate bypass converts DHA and glyceraldehyde-3-P into fructose-6-P (F6P) by the action of a fructose-6-P aldolase (*fsaA*, *fsaB*). F6P is then phosphorylated into fluctose-1,6-bisphosphate (FDP) by a ATP-dependent phosphofructokinase (*pfkA*, *pfkB*) and FDP splits into DHAP and glyceraldehyde-3-P by the action of a fructose-bisphosphate aldolase (*fbaA*, *fbaB*). Both pathways achieve the conversion of DHA into DHAP with the same ATP efficiency, but the first pathway does it in one step through the PEP-dependent DHAK, while the fructose phosphate bypass does it in three steps in a PEP-independent manner, allowing more flexibility in lower stages of the glycolytic pathway. Preliminary results using FBA showed that DHAK was not essential (see fluxes in Figure 34), although experimental data have proven the importance of these enzymes (Gonzalez et al., 2008). Therefore, the model was modified to restrict the flux through the fructose phosphate bypass to up to 4 mmol/gCDW/hr, wherein DHAK and glyDH become essential. This modification is also

supported by the fact that the control flux of the glycerol fermentation pathway is in reactions DHAK and glyDH, and overexpression of those enzymes results in increasing the flux of the overall pathway, indicating that the glyDH-DHAK is the main pathway (Cintolesi et al., 2012).

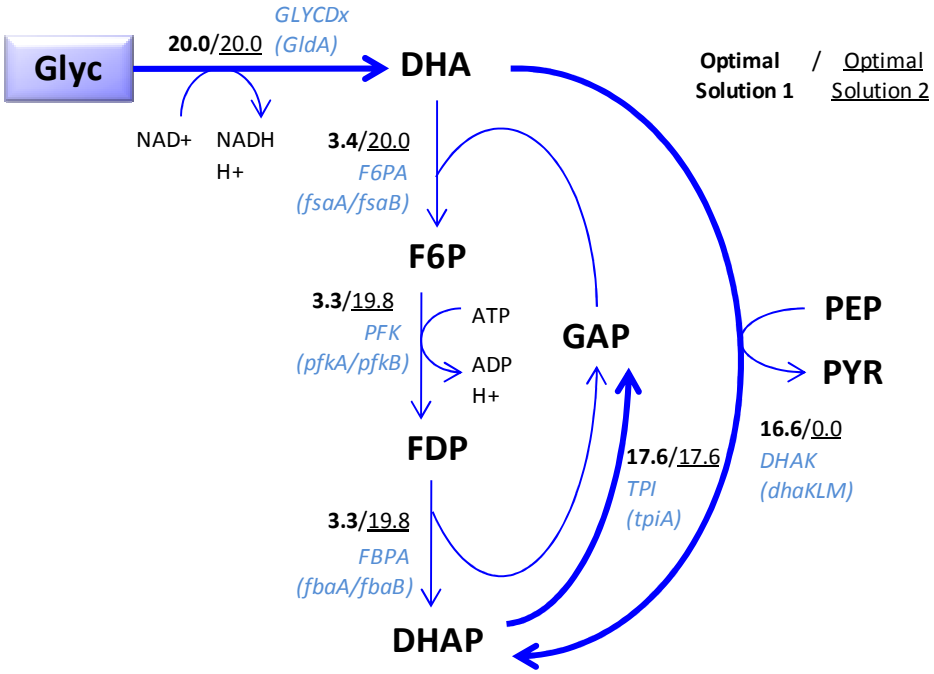

Figure 34: Alternative optimal flux distributions in preliminary results for the conversion of glycerol into DAHP. Optimal solution 1 is marked in bold, and optimal solution 2 is underlined. Optimal solution 1 converts DHA into DHAP using mainly enzyme DHAK, while optimal solution 2 converts DHA into DHAP using only fructose phosphate bypass pathway. See Nomenclature for details (page 214).

j) Finally, using Flux Variability Analysis (FVA) I identified three alternative pathways for the conversion of fructose-6-P (F6P) into DHAP and glyceraldehydes-3-P (GAP), as shown in Figure 35.

- Pathway A converts F6P into DHA and GAP is catalyzed by the enzyme F6P aldolase (F6PA), and then DHA is phosphorylated to produce DHAP by the enzyme DHA phosphotransferase (DHAK), which is finally converted into GAP by the action of TPI.

- Pathway B phosphorylates F6P into fructose diphosphate (FDP) by the action of a phosphofructokinase (PFK), and FDP is converted into DHAP and GAP by the enzyme fructose bi-phosphate aldolase (FBPA) and finally DHAP is converted to GAP by TPI.
- Pathway C combines erythrose 4-phosphate (e4p) and F6P to produce sedoheptulose 7-phosphate (S7P) and GAP by the action of the enzyme transaldolase, and then S7P is phosphorylated by phosphofructokinase (PFK_3) into sedoheptulose 1,7-bisphosphate (S17BP), which is then split into DHAP and e4p by the enzyme S17BP glyceraldehyde-3-phosphate-lyase (FBPA3). Finally, DHAP is converted into GAP by the action of TPI.

These three pathways were identified with simulations of glucose fermentation (and hence the three pathways start from F6P, and intermediate of that metabolism), and their possible relevance for glycerol fermentation are analyzed below. The three pathways have the same net effect of converting F6P into GAP and DHAP, but pathway A does it in a PEP-dependent way, while pathways B and C perform this conversion in an ATP-dependent way. After analyzing the feasibility of these three pathways, I found that pathway A was relevant to this study, as DHAK has shown to be essential. Pathway B can combine with pathway A to produce glycolytic intermediates (DHAP and GAP) independent of conversion of PEP into PYR, and thus it seems reasonable to keep it. Pathway C, however, corresponds to the S7P bypass pathway, which uses some of the same enzymes as the traditional central carbon metabolism, and it seems more likely to active in the glucose fermentation, but not in glycerol fermentation (Nakahigashi et al.,

2009). Therefore, for simplicity pathway C was no longer considered in the simulation for glycerol fermentation.

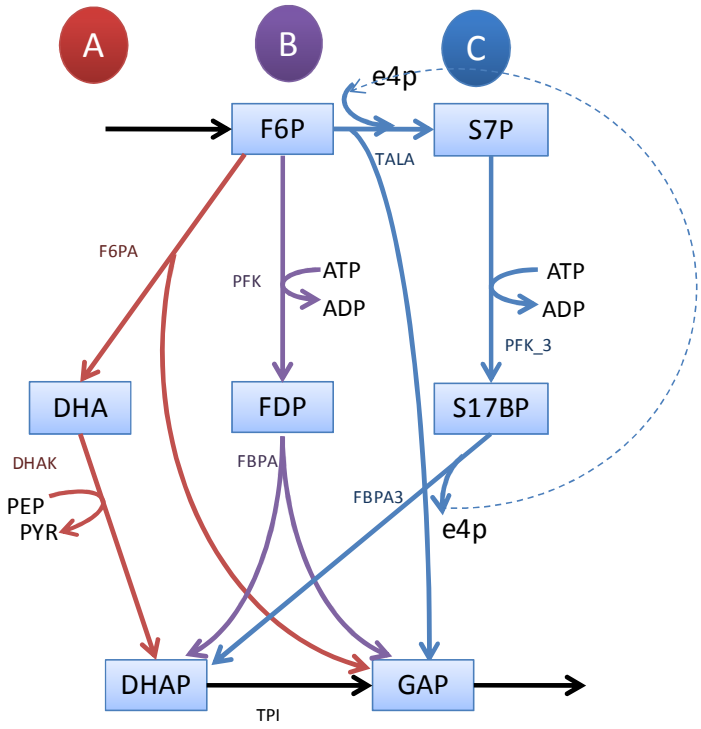

Figure 35: Alternative pathways for the conversion of F6P to GAP. Pathway A goes through DHA, pathway B goes through FDP and pathway C goes through S17BP (sedoheptulose bisphosphate bypass). See Nomenclature for details (page 214).

Hexanoate production was also removed from the model as this was not a product of interest in this study.

The modifications presented in this section were implemented in the iJO1366 model by modifying the upper and/or lower boundaries of the corresponding reactions, and a detail of these modifications is presented in the Appendix 10.2. The resulting model is referred to as glyc-GEM. The model was used to predict cell growth and flux distribution, and, when possible, these predictions were contrasted with available experimental data. Results generated using the glyc-GEM are also referred to as *in silico* results. The next two sections of this chapter present the results generated by the glyc-

GEM to increase the understanding of glycerol fermentation, and to evaluate glycerol as a platform for the production of valuable chemicals. See Appendix 10.10 for details of the Matlab function of the model glyc-GEM.

5.2 Results A: Understanding glycerol fermentation

The glyc-GEM was used in combination with FBA to predict cell growth and product synthesis during metabolism of glycerol under fermentative conditions. Optimizing cell growth resulted in production of biomass at a specific growth rate of 0.15 h^{-1}. Table 7 presents a complete list of substrates/products of this simulation; many of which are consumed/produced in small amounts to satisfy cell growth requirements. The exceptions are consumption of glycerol (fixed at 20 mmol/gCDW/h), production of ethanol (15.48 mmol/gCDW/h), production of 1,2-PDO (2.21 mmol/gCDW/h), production of carbon dioxide (16.05 mmol/gCDW/h), production of hydrogen (16.12 mmol/gCDW/h) and production of water.

Table 7: Substrates and products of glycerol fermentation. Positive values correspond to production rates, and negative values correspond to consumption rates.

Reaction	Reaction name	Consumption or production rate (mmol/gCDW/h)
EX_12ppd-R(e)	(R)-1,2-PDO exchange	2.210076
EX_ca2(e)	Calcium exchange	-0.00078
EX_cl(e)	Chloride exchange	-0.00078
EX_co2(e)	CO2 exchange	16.04787
EX_cobalt2(e)	Co2+ exchange	-3.7E-06
EX_cu2(e)	Cu2+ exchange	-0.00011
EX_etoh(e)	Ethanol exchange	15.48282
EX_fe2(e)	Fe2+ exchange	-0.00124
EX_fe3(e)	Fe3+ exchange	-0.00117
EX_glyc(e)	Glycerol exchange	-20
EX_glyclt(e)	Glycolate exchange	0.0001
EX_h(e)	H+ exchange	1.478851

EX_h2(e)	H2 exchange	16.11898
EX_h2o(e)	H2O exchange	6.246339
EX_k(e)	K+ exchange	-0.02928
EX_meoh(e)	methanol exchange	3E-07
EX_mg2(e)	Mg exchange	-0.0013
EX_mn2(e)	Mn2+ exchange	-0.0001
EX_mobd(e)	Molybdate exchange	-1.9E-05
EX_nh4(e)	Ammonia exchange	-1.62002
EX_ni2(e)	Ni2+ exchange	-4.8E-05
EX_pi(e)	Phosphate exchange	-0.14469
EX_so4(e)	Sulfate exchange	-0.03783
EX_succ(e)	Succinate exchange	0.049716
EX_zn2(e)	Zinc exchange	-5.1E-05

The *in silico* results presented in this section were compared with the experimental studies that have been done previously in order to understand glycerol fermentation in *E. coli* (Dharmadi et al., 2006; Gonzalez et al., 2008; Murarka et al., 2008). The main topics that have been studied are glycerol dissimilation pathways, essential fermentative products, and the role of FHL. It is important to note that the first published study of glycerol fermentation was performed for *E. coli* K12 strain MG1655 in rich medium (Dharmadi et al., 2006), and that subsequent studies have been done for the same strain in minimal medium supplemented with 2 g/L of tryptone (Gonzalez et al., 2008; Murarka et al., 2008). In contrast, *in silico* analysis was done simulating minimal medium, and therefore some differences are expected. Here I will discuss how *in silico* results compare to previous experimental studies in terms of glycerol dissimilation, essential fermentative products, the role of FHL, and other single deletions that have been characterized.

5.2.1 Glycerol dissimilation

Different experimental studies have been conducted to understand glycerol dissimilation pathways in *E. coli*. These studies have shown that the main pathway involves two enzymes: glycerol dehydrogenase (glyDH) and DHAK (Gonzalez et al., 2008), which convert glycerol into DHA, and then DHA into DHAP.

Figure 36 shows flux distribution of the trunk and auxiliary pathways that were simulated using FBA in this study. The trunk pathway is responsible for the conversion of glycerol into glycolytic intermediates, and the auxiliary pathways enable glycerol fermentation by providing reactions to produce ATP and to achieve redox balance (Gonzalez et al., 2008). The enzyme glycerol dehydrogenase (glyDH) converts glycerol into DHA, and then DHA is metabolized through two pathways: one that converts 83% of DHA into DHAP by the action of the enzyme DHAK, and another branch that converts 17% of the flux of DHA into DHAP through two intermediate (F6P and FDP). As most of the flux of glycerol dissimilation is incorporated into the glycolytic pathway using enzymes glyDH and DHAK, deletion of these enzymes was evaluated using the glyc-GEM. Simulation of deletion of any of these two reactions gave no valid solution, correlating well with the fact that experimental results have shown the essential role of these enzymes and that deletion of either one of them would result in no glycerol fermentation (Gonzalez et al., 2008). It is necessary to mention that the enzyme DHAK was not essential before restricting the fructose phosphate bypass flux (Figure 34), as that pathway could support the same achievement of ATP and conversion of DHA into DHAP.

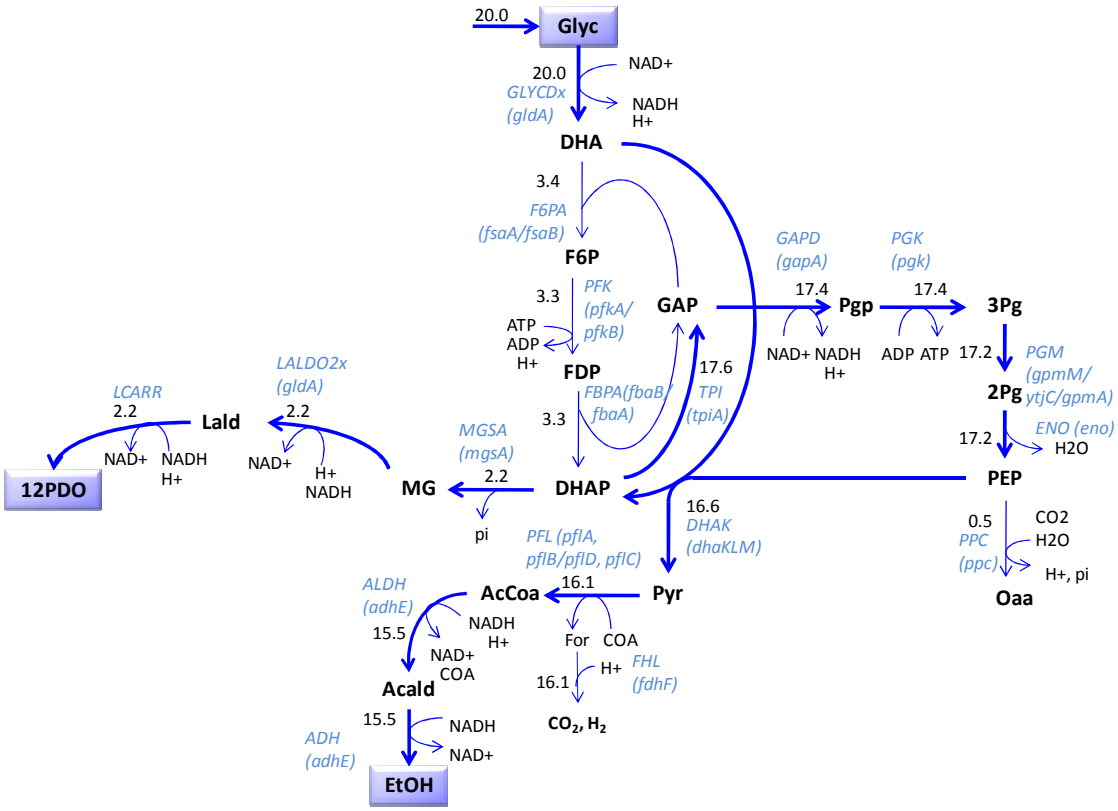

Figure 36: Prediction of flux distribution using FBA. Figure includes central carbon metabolism and main fermentative products. See Nomenclature for details (page 214).

Also, I explored the possible role of respiratory pathways in the fermentation of glycerol by *E. coli* using the glyc-GEM and I compared my *in silico* results with previous experimental studies. In previous studies the experimental deletion of genes *glpA*, *glpD* and *glpK* had been performed to study the role of associated reactions, all of which are involved in the respiratory metabolism of glycerol in *E. coli* (see Figure 7, page 26) (Gonzalez et al., 2008; Murarka et al., 2008). Gene *glpK* encodes enzyme glycerol kinase, and genes *glpA* and *glpD* encode enzymes glycerol-3-p dehydrogenase, anaerobic and aerobic, respectively. My simulations indicate that reactions associated with genes *glpA* (G3PD5, G3PD6, G3PD7) and *glpD* (G3PD5) and glpK (GLYK) were non-essential, in agreement with experimental results presented by Murarka and collaborators (Murarka et al., 2008).

5.2.2 Essential Products

Gonzalez et al. proposed a metabolic model for glycerol consumption associated with the production of ethanol and 1,2-PDO, which are essential products (Gonzalez et al., 2008). The results of flux predictions using the glyc-GEM supported their model. In fact, single knockout simulation of reactions alcohols dehydrogenase (ALDH, for production of ethanol) or methylglyoxal synthase (MGSA, for production of 1,2-PDO) resulted in no cell growth. Interestingly, while simulation of knockout of ALDH resulted in an unfeasible case, simulation of knockout of MGSA still allowed the model to find a solution in which production of ethanol was 20 mmol/gCDW/h (equal to the maximal theoretical yield) with no cell growth associated. These results indicated differences in the functional role of the production of ethanol and 1,2-PDO. While ethanol production is essential to satisfy minimal energetic requirements of the model in a redox balance manner, the role of 1,2-PDO production seems to be strictly associated with the consumption of the reducing equivalent generated during cell growth. This situation is shown in Figure 37, which shows the solution space associated with the production of ethanol, 1,2-PDO and biomass. The optimal solution (identified using FBA) corresponds to the highest production of biomass and lower biomass productions allow to produce ethanol and 1,2-PDO at different rates. The solution space shows graphically that production of ethanol is always essential, even if the specific growth rate is equal to zero (stationary phase), while production of 1,2-PDO is essential for optimal cell growth, but it is not necessary for cell growth.

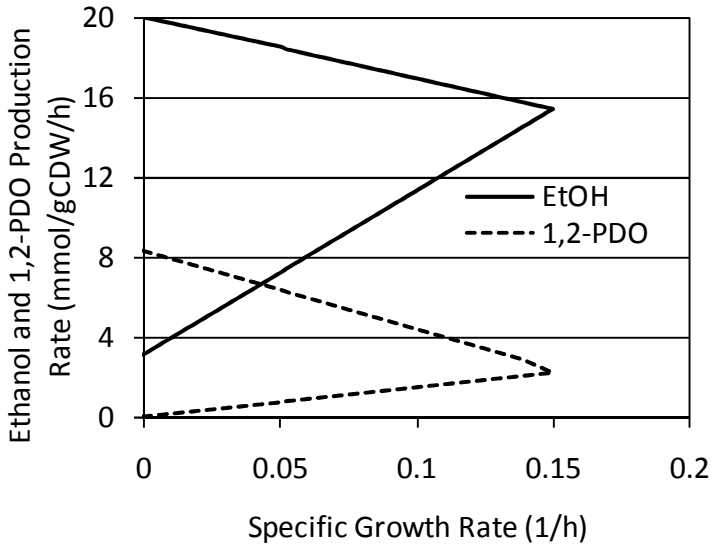

Figure 37: Predicted solution space for the production of 1,2-PDO, ethanol and biomass in wild type *E. coli*. Continuous line corresponds to the simulated solution space of ethanol production, and dashed line corresponds to the simulated solution space of 1,2-PDO.

FBA predicts production of ethanol at a yield of 0.77 mol/mol, and production of 1,2-PDO at a yield of 0.11 mol/mol. In contrast, experimental data show production of ethanol at a rate of 0.92 mol/mol (19% higher than the modeled value) and 1,2-PDO at a very low yield (not specified) (Murarka et al., 2008). In addition, the model predicted specific growth rate of 0.15 1/hr, which is significantly higher than the 0.04 1/hr experimental result (Murarka et al., 2008). However, the big difference in the predicted specific growth rate is in part explained by the fact that in the model I assumed a different glycerol consumption rate (20 mmol/gCDW/h) than the experimentally found (7.8 mmol/gCDW/h, calculated from Murarka et al., 2008). In fact, the ratio between glycerol consumption rate and specific growth rate using the model was 133 mmol glycerol/gCDW, versus an experimental value of 194 mmol glycerol/gCDW: only 31% smaller than the predicted value. Discrepancies in predicted result for ethanol, 1,2-PDO, and biomass were linked to each other. A simulated higher production of biomass

resulted in fewer resources to produce ethanol, at the same time that a higher production of biomass required a higher production of 1,2-PDO in order to consume the increased production of reducing equivalents from biomass. In addition, the glyc-GEM simulated growth in minimal condition at a fixed glycerol consumption rate, while experimental data correspond to growth under minimal supplemented data at a lower glycerol consumption rate.

While the glyc-GEM successfully predicted the necessity of producing 1,2-PDO, the pathway that it used is different from the one that has been experimentally verified (Gonzalez et al., 2008). Figure 36 shows the pathway that FBA selected as the most efficient (optimal), which consists of two dehydrogenase steps from MG to lactaldehyde, and then from lactaldehyde to 1,2-PDO. Each of these steps consumes one molecule of NADH. In contrast, experimental evidence shows that the pathway that produces 1,2-PDO in *E. coli* goes through hydroxyacetate, consuming one molecule of NADHP in the first step, and one molecule of NADH in the second step. Both pathways consume the same amount of reducing equivalents, but of different kinds. Deletion of the pathway going through lactaldehyde results in using a pathway going through hydroxyacetate with a slight reduction in cell growth prediction (3%), and with minimal impact in production of ethanol and 1,2-PDO. This result indicates that although a pathway for production of 1,2-PDO going through lactaldehyde was identified as optimal, both pathways (going through lactaldehyde and hydroxyacetate) have a very similar outcome.

In addition to the synthesis of ethanol and 1,2-PDO, previous experimental studies have evaluated the role of other metabolic products. Deletion of *pta* and *frdA*, involved in the production of acetate and succinate respectively, were properly predicted

as non-essential by the glyc-GEM, in agreement with experimental results (Murarka et al., 2008). However, some differences need to be considered. For the case of acetate production, the glyc-GEM predicted no acetate production in the original case, and therefore no effect was observed in the simulations after deleting reaction PTAr (corresponding to gene *pta*: phosphate acetyltransferase). However, the experimental deletion of gene *pta* caused a reduction in growth rate of 29% (Murarka et al., 2008). In the case of gene *frdA* for production of succinate, *in silico* results showed that the associated reactions, namely FRD2 and FRD3, were not being used, although there was experimental evidence that succinate was being produced in small amounts. Surprisingly, experimental deletion of *frdA* resulted in an increase of specific growth rate of 43%, but this could be associated with a higher rate of glycerol consumption, which was not simulated using the glyc-GEM. While it may be difficult to use glyc-GEM to predict differences in specific growth rate if they are associated with changes in glycerol uptake rate (the glycerol consumption rate is fixed in the *in silico* simulations), experimental results support the findings that the phenotypes of the mutants with deletion of *pta* or *frdA* are indistinguishable from the phenotype of the wild-type *E. coli* (Murarka et al., 2008).

5.2.3 Role of FHL

Simulation results also coincided with experimental data in identifying the enzyme formate-hydrogen lyase (FHL) as active in the dissimilation of formate to produce hydrogen and carbon dioxide (Dharmadi et al., 2006). It was proposed that the role of FHL in glycerol fermentation is to provide an acidic medium by increasing the concentration of carbon dioxide, which medium may be required for proper functioning

of enzymes or other processes. Interestingly, the *in silico* predictions indicated that FHL may have an energetic role linked to the conservation of protons, which could relate to the experimental function of keeping an acidic concentration of protons. Experimental deletion of FHL resulted in 70% reduction of glycerol fermentation and a 50% reduction in cell growth, while *in silico* deletion of FHL resulted in a reduction in cell growth of 27% (using a constant glycerol consumption rate). Deletion of FHL in the glyc-GEM predicted an increase in the production of protons (from 1.5 to 12.2 mmol/gCDW/h), while formate production appeared at a value of 17.0 mmol/gCDW/h (previously zero). The additional protons generated in the glyc-GEM were exported by the model using the reaction ATP hydroxylase, which used ATP to export protons at a rate of 4.9 mmol/gCDW/h (versus a rate of 0.9 mmol/gCDW/h before deletion of this reaction). This possitive correlation between energy and FHL has been reported experimentally by Akopian and collaborators (Akopian et al., 2006), although in their experiments the ATP hydroxylase worked in the opposite direction (as ATP synthase).

5.2.4 Production of 3-C intermediate metabolites

The previous section shows the importance of production of DHAP by converting glycerol to DHA, and then DHA to DHAP. However, this pathway imposes a stoichiometric constraint as conversion of DHA to DHAP is linked to conversion of PEP to PYR, a later step in the glycolytic flux. Therefore, the production of 1,2-PDO as well as precursors for the production of biomass require an additional pathway that would allow redirection of 3C metabolites between DHAP and PEP (namely DHAP, GAP, Pgp, 3Pg, 2Pg, and PEP) into other synthetic pathways. While this could be achieved using the enzyme PEP synthase that could convert PYR back into PEP using two phosphate groups

from ATP (one of them is released and the other one is transfer to PYR to produce PEP), *in silico* results identified a new pathway that could accomplish the generation of 3C intermediate metabolites in a more efficient way. This pathway, named the fructose phosphate bypass, is presented in Figure 36, and it converts glycerol into DHAP with no necessity to tie this conversion to the conversion of PEP into PYR. This new pathway converts DHA into DHAP going through F6P and FBP.

The fructose phosphate bypass consists of three steps and incorporates GAP as a pseudo carrier. The first steps binds DHA and GAP to produce F6P by the action of the enzyme F6P aldolase, the second step phosphorylates F6P into FDP catalyzed by the enzyme phosphofructokinase, and the last step converts FDP into DHAP and GAP by the enzyme fructose bisphosphate aldolase. The first step can be performed by one of the two enzymes F6P aldolase that have been identified in *E. coli*: FsaA and FsaB, encoded by genes *fsaA* and *fsaB* respectively (Schurmann & Sprenger, 2001). It is interesting to note that although the physiological role of F6P aldolases in *E. coli* is unknown (Schurmann & Sprenger, 2001), the gene *fsaB* is encoded in the same transcription unit as gene *gldA* (see Figure 38, taken from Ecocyc website), whose physiological function has recently been elucidated as a component of glycerol fermentation (Gonzalez et al., 2008). The fact that the gene *fsaB* is in the same transcription unit as gene *gldA* indicates that the physiological function of *fsaB* may also be in glycerol fermentation, an option that is now supported by the *in silico* results from the glyc-GEM. It is of further interest that there is a third gene in this transcriptional unit, *ptsA*, which encodes a protein whose function has been predicted to be a component of a phosphotransferase system, similar to the system that glucose and other sugars need in order to be metabolized (Reizer et al., 1995). Thus,

the role of genes *fsaB* and *ptsA*, both encoded in the same transcription unit as gene *gldA*, may be linked to the fermentation of glycerol. Last, the new fructose phosphate bypass has the equivalent effect of an ATP-dependent DHAK, such as the one in *Citrobacter freudii*, which converts DHA into DHAP in one direct step that consumes one molecule of ATP.

Figure 38: Transcription unit gldA-fsaB-ptsA in *E. coli*. The inclusion of these three genes in the same transcriptional unit suggests that they may be involved in the same process. The operon was taken from the Ecocyc website (Keseler et al., 2011).

5.2.5 Study of essential genes/reactions

In addition to those genes that were mentioned in previous sections, a complete study of essential genes of the model was conducted. Using single gene deletion the current study found that 15.7% genes were essential for cell viability (218 genes out of the 1366, see Appendix 10.4). I then focused on the reactions from the central carbon metabolism (Figure 36), and I performed a single reaction deletion (which often includes deletion of more than one gene). Results are summarized in Figure 39. As discussed in previous sections, reactions glyDH and DHAK were predicted to be essential by the model, as was the production of 1,2-PDO and ethanol. In addition to those reactions, all reactions involved in the glycolytic pathway for the transformation of DHAP up to AcCoA were also predicted to be essential, which is expected given that these reactions are required to produce ethanol and other essential intermediates. Deletions in the fructose phosphate bypass proved to be non-essential, although the predicted specific growth rate decreased by 16% after deletion of this pathway (see insertion in Figure 39),

and the reaction PEP synthase became active as a way to produce 3-C intermediates (although in a less efficient way, as this reaction consumes two phosphate groups from ATP, as oppose to the only one phosphate group that is required in the fructose phosphate bypass).

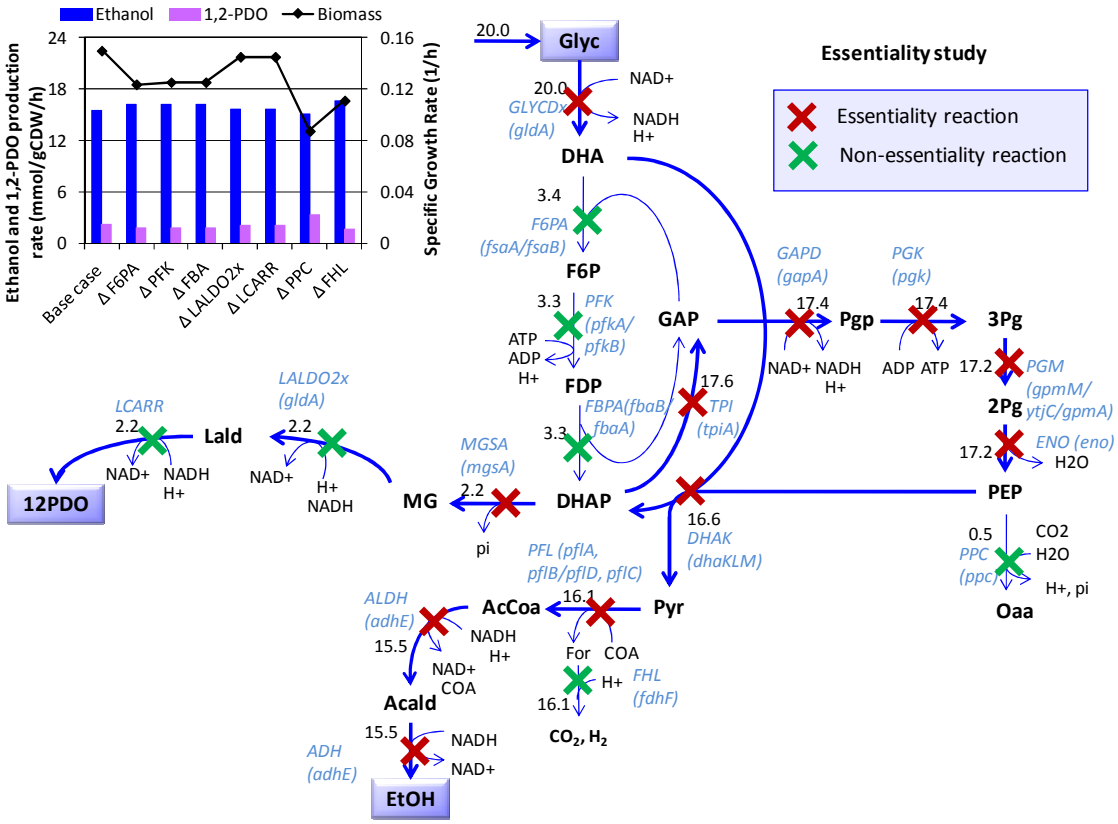

Figure 39: Analysis of reaction essentiality of central carbon metabolism of glycerol fermentation using FBA. Red crosses correspond to essential reactions for cell growth, and green crosses correspond to non-essential reactions. Insert on the left shows effect of removing non-essential reaction over ethanol and 1,2-PDO production, and specific growth rate. See Nomenclature for details (page 214).

5.2.6 Targets Identified for Experimental Validation

This section proposes experimental validation for two relevant results identified using the glyc-GEM: the fructose phosphate bypass, and the role of gene *ptsA*.

In order to validate the potential role of the new fructose phosphate bypass proposed in this thesis, I propose the following four steps:

1.- Measure activity of F6P aldolase.

2.- Measure activity of F6P aldolase after deleting *fsaB* gene.

3.- Delete *fsaA*/*fsaB* and perform glycerol fermentation.

4.- Delete genes *fsaA*/*fsaB* and *ppsA* . Deletion of fsaA/fsaB would prevent the fructose phosphate bypass, and deletion of *ppsA* would prevent PEP synthase. By removing these two pathways it is expected that cells cannot grow as at least one of these pathways is required.

The first two steps of this strategy will allow identification of the presence of F6P aldolase activity, and whether that activity is linked to the gene *fsaB*, as suggested in the results of this chapter. Step 3 will allow us to determine if genes *fsaA* and *fsaB* are essential for fermentation of glycerol. If they are not essential step 4 can identify the role of gene *ppsA* in providing a less efficient pathway to generate intermediate 3 carbon metabolites, as previously discussed.

In addition to experimentally validating the fructose phosphate bypass, I suggest validating the role of gene *ptsA* linked to the transport and utilization of glycerol, as part of a possible phosphotransferase system (PTS). It has been suggested that the gene *ptsA* encodes a fusion of two components of a PTS: the enzyme I (in the N-terminal) and the enzyme EIIA (in the C-terminal) (Reizer et al., 1995), although other genes may be

involved in this system as well. These components mediate the transport and phosphorylation of other sugars (such as glucose, as it is reviews in section 2.1.3). Since this gene is part of the same transcription unit as genes *gldA* and *fsaB* (Reizer et al., 1995), both of them have been proven or predicted to have a role in glycerol fermentation, it is now suggested that the product of gene *ptsA* is involved in the transport of glycerol. To prove this theory, construction of a *ptsA* deficient strain is suggested to test if fermentation of glycerol is affected. To further validate this strategy it is proposed to express gene *ptsA* in the strain deficient in this gene and repeat fermentations.

5.2.7 Other Models

In addition to the ethanol-1,2-PDO model that explains how wild type *E. coli* can ferment glycerol, other possible models could support glycerol fermentation in *E. coli*. In this section other models are explored by using a logical approach to generate models. Table 8 presents a list of possible products that *E. coli* could produce either as wild type or after adding exogenous reactions. Each product in Table 8 has an associated net ATP production, a net reducing equivalents production, and a conversion factor that indicates how many molecules of the product can be generated from one molecule of glycerol.

Table 8: Possible products whose synthesis could enable fermentative metabolism of glycerol by wild type or engineered *E. coli*. Negative values of ATP production or reducing equivalents production indicate that such molecules are being consumed in the pathway that converts glycerol to the associated product.

Product	Stoichiometric reaction	ATP produced	Reducing equivalent (2[H])	Conversion Factor
Ethanol	Glycerol → ATP + Ethanol + CO_2	1	0	1
Propanol	Glycerol + 4[H]→ Propanol	0	-2	1
Propanol (PckA*)	Glycerol + 4[H]→ Propanol + ATP	1	-2	1
Butanol	Glycerol → ATP + ½ Butanol + CO_2	1	0	0.5
Propionate	Glycerol → Propionate	0	0	1
Propionate (PckA*)	Glycerol → ATP + Propionate	1	0	1
Lactate	Glycerol → ATP + Lactate + 2[H]	1	1	1
Succinate	Glycerol + CO_2→ Succinate	0	0	1
Succinate (PckA*)	Glycerol + CO_2→ ATP + Succinate	1	0	1
1,2-PDO (through lactaldehyde)	Glycerol + ATP + 2[H] → 1,2-PDO	-1	-1	1
1,2-PDO (through acetol)	Glycerol + ATP + 2[H] → 1,2-PDO	-1	-1	1
1,2-PDO (glycerol directly to lactaldehyde)	Glycerol + 2[H] → 1,2-PDO	0	-1	1
1,3-PDO	Glycerol + 2[H] → 1,3-PDO	0	-1	1
Acetate	Glycerol → 1,2-PDO + 2ATP + 4[H]	2	2	1
Acetone	Glycerol + 2[H] → Acetone	0	-1	1

PckA*: reversible PEP kinase added.

Based on the information presented on Table 8, I calculated the possible combination of products that could produce ATP and consume reducing equivalents, as these are essential requirements to produce biomass. A total of 47 feasible models were predicted using this approach, and results are presented in Table 9. Interestingly, production of propanol combined with the addition of reversal PckA can produce ATP and consume reducing equivalents, resulting in this being the only product that could support production of biomass by itself. This caused production of propanol with the addition of reversal PckA to combine with any other products whether or not such a product helps in production of ATP and consumption of reducing equivalents.

Table 9: Predicted models that could support cell growth in *E. coli* under anaerobic fermentation of glycerol. This prediction table was constructed using the analysis of redox and ATP presented in Table 8. In grey are marked redundant models.

	Ethanol	Propanol	Propanol (reversible PckA added)	Butanol	Propionate	Propionate (reversible PckA added)	Lactate	Succinate	Succinate (reversible PckA added)	1,2-PDO (through Lald)	1,2-PDO (through acetol)	1,2-PDO (Glyc directly to Lald)	1,3-PDO	Acetate	Acetone
Ethanol	0	1	1	0	0	0	0	0	0	1	1	1	1	0	1
Propanol		0	1	1	0	1	1	0	1	0	0	0	0	1	0
Propanol (reversible PckA added)			1	1	1	1	1	1	1	1	1	1	1	1	1
Butanol				0	0	0	0	0	0	1	1	1	1	0	1
Propionate					0	0	0	0	0	0	0	0	0	0	0
Propionate (reversible PckA added)						0	0	0	0	1	1	1	1	0	1
Lactate							0	0	0	0	0	1	1	0	1
Succinate								0	0	0	0	0	0	0	0
Succinate (reversible PckA added)									0	1	1	1	1	0	1
1,2-PDO (through Lald)										0	0	0	0	0	0
1,2-PDO (through acetol)											0	0	0	0	0
1,2-PDO (Glyc directly to Lald)												0	0	1	0
1,3-PDO													0	1	0
Acetate														0	1
Acetone															0

The glyc-GEM was then used to validate the predicted models, finding 100% of the models envisioned based on redox balance and ATP analysis and 12 new models were identified (Table 10), corresponding to models producing 1,2-PDO (using conversion of glycerol into 1,2-PDO), 1,3-PDO and acetone. In these three cases biomass production was possible due to small amounts of ATP produced in non-substrate level phosphorylation reactions, such as the use of the proton pump (ATP synthase), and other minor reactions.

Table 10: Predictions of biomass optimization using glyc-GEM for predicted models that could support cell growth in *E. coli* under anaerobic fermentation of glycerol. Values correspond to specific growth rate predicted using FBA. In green are highlighted the models with a predicted specific growth rate greater than 0.15 (wild type). In red are highlighted the new predicted models that were identified using the glyc-GEM model, but which were not identified by the redox and ATP analysis. In grey are marked redundant models. See Appendix 10.11 for the Matlab function that was developed to find these models.

	Ethanol	Propanol	Propanol (reversible PckA added)	Butanol	Propionate	Propionate (reversible PckA added)	Lactate	Succinate	Succinate (reversible PckA added)	1,2-PDO (through Lald)	1,2-PDO (through acetol)	1,2-PDO (Glyc directly to Lald)	1,3-PDO	Acetate	Acetone
Ethanol	0	0.18	0.21	0	0	0	0	0	0	0.15	0.15	0.18	0.17	0	0.17
Propanol		0	0.08	0.18	0	0.21	0.07	0	0.08	0	0	0.07	0	0.11	0.01
Propanol (reversible PckA added)			0.08	0.21	0.21	0.21	0.15	0.08	0.08	0.08	0.08	0.11	0.08	0.21	0.08
Butanol				0	0	0	0	0	0	0.15	0.15	0.18	0.17	0	0.17
Propionate					0	0	0	0	0	0	0	0.09	0.02	0	0.06
Propionate (reversible PckA added)						0	0	0	0	0.16	0.15	0.21	0.19	0	0.20
Lactate							0	0	0	0	0	0.11	0.05	0	0.08
Succinate								0	0	0	0	0.05	0	0	0.01
Succinate (reversible PckA added)									0	0.05	0.05	0.10	0.06	0	0.06
1,2-PDO (through Lald)										0	0	0.05	0	0	0
1,2-PDO (through acetol)											0	0.05	0	0	0
1,2-PDO (Glyc directly to Lald)												0.05	0.05	0.15	0.05
1,3-PDO													0	0.08	0
Acetate														0	0.12
Acetone															0

Results presented in Table 10 are relevant to guiding efforts in metabolic engineering. Furthermore, among the 55 feasible models identified using FBA and the glyc-GEM, 16 models are predicted to allow *E. coli* to growth at a higher specific growth rate than *in silico* predictions of wild type *E. coli*.

5.3 Results B: Assessing the capabilities of glycerol fermentation as a platform for the synthesis of fuels and chemicals

This section assesses the capabilities of glycerol fermentation as a platform to produce valuable products. A number of experimental papers have been published in this direction, but previous works have not used mathematical models to support experimental strategies. GEMs are ideal to develop strategies for the production of desired products

and to improve existing strategies. GEMs allow prediction of the effect of adding and removing reactions of an existing metabolic network, without requiring any kind of experimental data or kinetic parameters.

In addition, mathematical optimization strategies have been developed using GEMs as a starting point, OptKnock being remarkable among them (Burgard et al., 2003). OptKnock is an optimization algorithm that identifies target reactions that would allow the coupling of cell growth to production of a desired product. Thus, OptKnock identifies a strategy that would more likely result in the cell being forced to produce the desired product in order to grow and a strategy with this quality can be further optimized using directed mutagenesis because growth and product will be optimized together (Burgard et al., 2003). Background and literature review (Chapter 3) presents further details of this tool. All OptKnock simulations considered a knockout number of up to 8 reactions, a computation time of up to 48 hours to find a result, and a minimal specific growth rate of 0.07 h^{-1}, unless otherwise specified. The solver Gurobi Optimizer 5.0 (Gurobi Optimization, Inc.) was used in combination with COBRA toolbox v2.0 (Schellenberger et al., 2011) in Matlab v7.11.0 (R2010b, The Mathworks, Inc.). The COBRA toolbox v2.0 includes a function for OptKnock.

Figure 40 shows the simplified pathways that would allow the production of 8 products with economical relevance, with 2 [H] representing one reducing equivalent (such as NADH) involved in the reaction conversion pathway. Since production and optimization of ethanol was already presented in the previous chapter using a kinetic model, here I present a mathematically supported strategy for the remaining 7 products, namely 1,2-PDO, 1,3-PDO, succinate, D-lactic acid, butanol, propanol, and propionic

acid. It is important to note that this list of products is not a complete list, as glycerol could be converted into various other products; however, this list represents a good sample to study the capabilities of glycerol for products that differ in energy and reducing equivalents being generated/consumed.

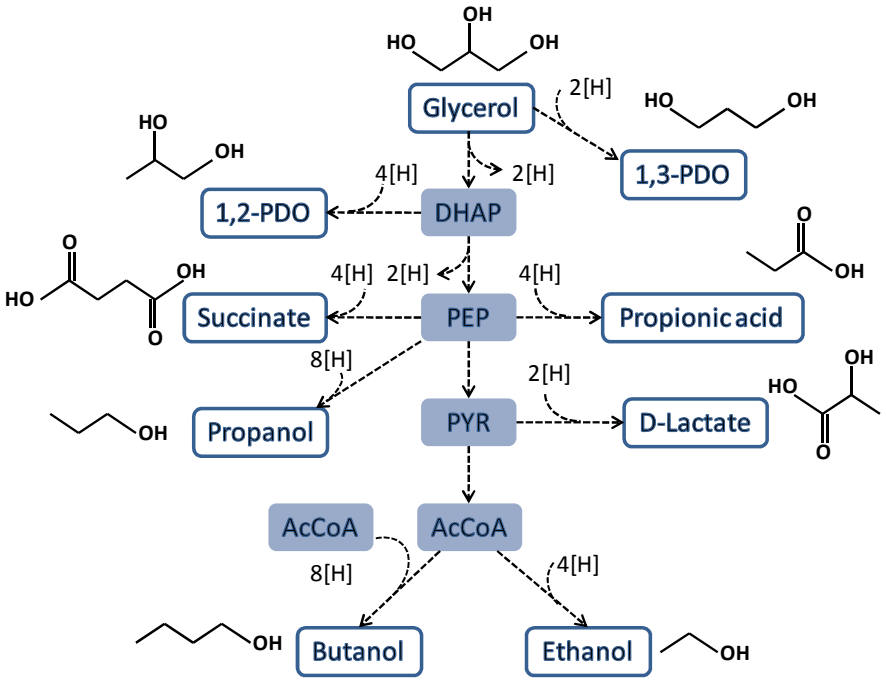

Figure 40: Glycerol as a platform for the production of biofuels and chemicals. Intermediated from the glycolytic pathway are presented in blue boxes, and final products are presented in white boxes. Dashed lines represent pathways for the production of each product from a glycolytic intermediate. 2 [H] represents reducing equivalents associated with each pathway. See Nomenclature for details (page 214).

In each study case a predicted solution space was generated using the glyc-GEM, which space represents the region where possible specific growth rate and product production could take place. In a solution space, the optimal solution (found by FBA) correspond to the highest specific growth rate, and the lower and higher curves of the space are found using Flux Variability Analysis (FVA).

5.3.1 1,2-PDO

Although 1,2-PDO is a natural product in the fermentation of glycerol by *E. coli*, it is naturally produced in very small amounts (Gonzalez et al., 2008). A strategy to increase the production of 1,2-PDO had already been developed in *E. coli* by Clomburg and collaborators using glycerol as carbon source (Clomburg & Gonzalez, 2011). In order to differentiate this and any other previous experimental strategy from experimental support that may be part of this thesis, any previous strategy will be referred as "pre-existing". In this thesis, the pre-existing strategy was simulated using the glyc-GEM in order to contrast how well the glyc-GEM can simulate this condition and also to identify if there is space for improvement of the pre-existing strategy.

Genetic modifications of the pre-existing strategy consisted of deleting key genes for the production of competing by-products and pathways, expressing one gene for the free production of 1,2-PDO, and overexpressing genes for the conversion of glycerol into DHAP, and then DHAP into 1,2-PDO (Clomburg & Gonzalez, 2011). In particular, the following genes were deleted: *ackA* (acetate kinase), *pta* (phosphate acetyltransferase), *ldhA* (D-lactate dehydrogenase) and *dhaK* (PEP-dependent DAH kinase). The insertion of enzyme ATP-dependent DhaK was simulated in order to allow production of 1,2-PDO uncoupled to production of ethanol. Finally, the pre-existing strategy overexpressed genes *mgsA* (methylglyoxal synthase) and *gldA* (L-1,2-propanediol dehydrogenase / glycerol dehydrogenase), both of them directly involved in the conversion of glycerol to 1,2-PDO. The simulation of this strategy was done by knocking down reactions corresponding to the gene knockout (namely ACKr, PTAr, LDH_D and DHAK in the glyc-GEM), and adding the reaction ATP-dependent DHAK to the model.

Overexpression of genes cannot be included in a GEM scale model; therefore, that information was not included.

Figure 41 shows the predicted solution space that was generated using the glyc-GEM for the pre-existing strategy from Clomburg and collaborators and its comparison to other *in silico* results and experimental results. The simulation indicates that 1,2-PDO is essential for the cell growth rate, as was already established in the previous section of this chapter (Results I). Two scenarios were simulated: wild type with no modifications, and wild-type with insertion of ATP-dependent DHAK and deletion of by-products, as established by the strategy of Clomburg and collaborators. Both platforms gave similar results and additional simulations removing the PEP-dependent DHAK for the second option was performed to confirm that the ATP-dependent DHAK was being used in that case. Although both scenarios provided a very similar prediction, pre-existing experimental results, however, support that adding ATP-dependent DHAK and deleting production of by-products is a better option. Discrepancies between experimental results and simulated results are likely due to limitations in maximum enzymatic rates that are not incorporated into the glyc-GEM. The results of these simulations were compared against the experimental yield reported of 0.213 w/w, which after converting to comparable units represent 2 mmol/gCDW/h (solid red circle in Figure 41). Details of all calculations can be found in Appendix 10.6.

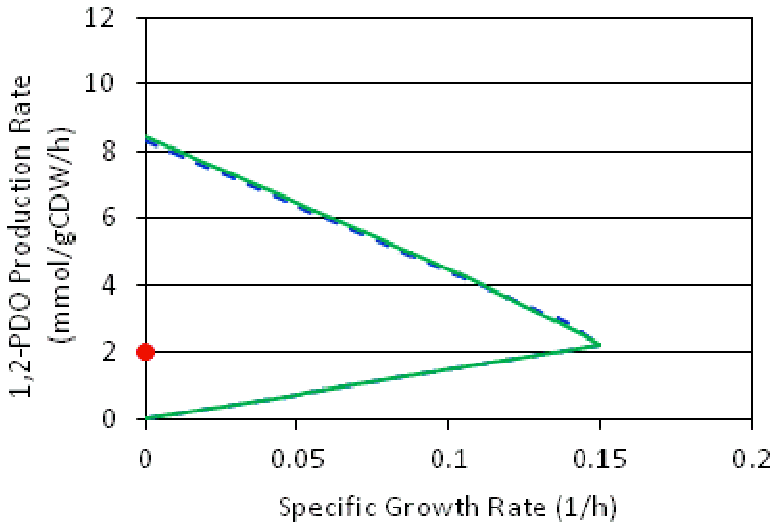

Figure 41: Predicted solution space for the production of 1,2-PDO and biomass. Two cases are simulated, which results overlap. The blue dotted line corresponds to the simulated solution space simulation of wild type *E. coli*. The green continuous line corresponds to the simulated solution space of adding an ATP-dependent DhaK and knocking out production of acetate and lactate (delete reactions ACKr, PTAr and LDH_D) in accordance with the pre-existing strategy. The solid red circle corresponds to the reported results using the pre-existing strategy (Clomburg & Gonzalez, 2011), in which there cells enter into stationary phase after 12 hours of fermentation (no cell growth).

While the experimental data of the pre-existing strategy are promising, the simulated solution space shows that it is theoretically possible to achieve a higher yield. This in turn motivated the use of OptKnock to identify different reactions whose deletion would result in a higher yield and productivity. Using OptKnock the following reactions were identified as targets for deletion: acetaldehyde dehydrogenase NADP (ALDD2y), malate dehydrogenase NADP (ME2), 6-phosphogluconolactonase (PGL), and two transhydrogenase periplasm (THD2pp and PntAB). Four of these deletions resulted in preventing the utilization of the cofactor NADP to generate the reducing equivalent NADPH, suggesting an important role in the kind of cofactors utilized. The use of this strategy, together with adaptive evolution (Fong et al., 2005) could result in an strategy leading to productivities close to 4.48 mmol/gCDW/hr of 1,2-PDO (productivity at maximal specific growth rate).

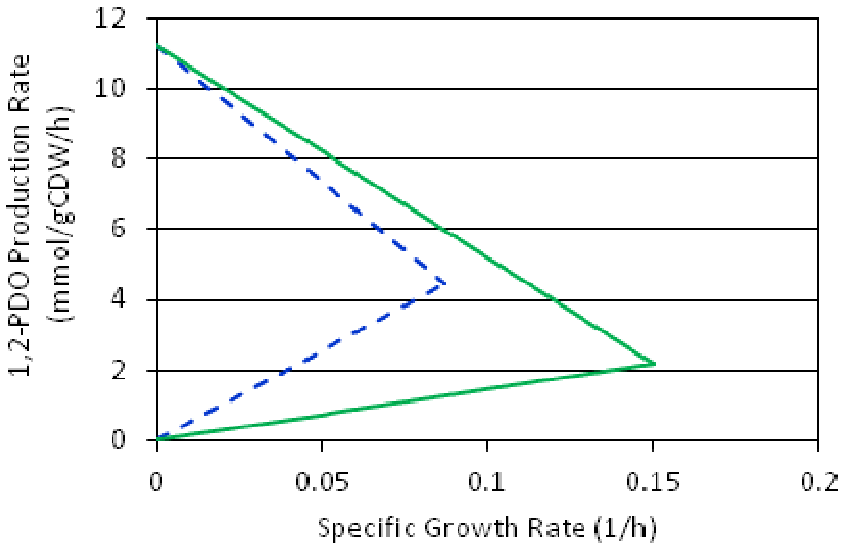

Figure 42: Predicted solution space for the production of 1,2-PDO and biomass. Green line corresponds to the simulated solution space of wild type *E. coli*. Blue line corresponds to the simulated solution space implementing the reduced OptKnock strategy (deletion of ALDD2y, ME2, PGL, THD2pp and PntAB).

5.3.2 1,3-PDO

For many years the fermentation of glycerol was linked to microorganisms with the capability to produce 1,3-PDO, a compound that could consume the reducing equivalents generated by the production of biomass from glycerol. *E. coli*, however, is not capable of producing 1,3-PDO, but metabolic engineering led Tang and collaborators to develop a strategy for the production of 1,3-PDO in *E. coli* (Tang et al., 2009), in which they inserted genes *dhaB1*, *dhaB2* and *yqhD* from *Clostridium butyricum*, mediating the conversion of glycerol into 1,3-PDO. Genes *dhaB1*, *dhaB2* encode a glycerol dehydratase enzyme and its activating factor, while gene *yqhD* encodes a 1,3-PDO oxidoreductase isoenzymes that can convert glycerol into 1,3-PDO, in the following manner:

Glycerol → 3-hydroxypropanal (3HPA) + h2o (glycerol dehydratase) (55)

3HPA + NADPH + h → 1,3-PDO + NADP (Oxidoreductase isoenzymes) (56)

In this section the pre-existing strategy developed by Tang and collaborators was implemented in the glyc-GEM by adding reactions glycerol dehydrogenase and 1,3-PDO oxidoreductase, as described above, and the simulated solution space was compared to the pre-existing experimental results. Figure 43, blue line shows the result of this comparison. From the experimental results presented by Tang et al. (2009) I calculated the estimated specific growth rate as 0.014 h^{-1}, and the production rate of 1,3-PDO as 1.42 mmol/gCDW/h (see details of calculations in Appendix 10.6). This values fall inside the predicted solution space (Figure 43, solid red circle), and it is observed that there is theoretically space for the improvement of the strategy. While the experimental implementation of this strategy resulted in the production of 1,3-PDO as main product, with small amounts of co-products pyruvate, acetate and others (Tang et al.), in the *in silico* results ethanol was the main product and 1,3-PDO was produced in small amounts. Deletion of ethanol as co-product resulted in a decrease in the simulated maximal growth rate of 50% (from 0.17 h-1 to 0.08 h-1), and a switch to 1,3-PDO being the main product (increased from 2.5 mmol/gCDW/h to 12.9 mmol/gCDW/h) for the optimal solution, and acetate being the main by-product (Figure 43, green line). The deletion of ethanol presents a significant improvement with respect to previous results by providing a required coupling between production of 1,3-PDO and cell growth. This strategy needs to be evaluated experimentally in order to assess any further modifications, and overexpression of genes *gldA* should be considered as this enzyme is a limiting step in the fermentation of glycerol by *E. coli*. However, overexpression of gene *gldA* could also increase production of 1,2-PDO due to the by-function of the protein associated with this gene;

therefore, it may be convenient to knockout out production of 1,2-PDO by knocking out gene *mgsA* and thus also preventing accumulation of the toxic methylglyoxal.

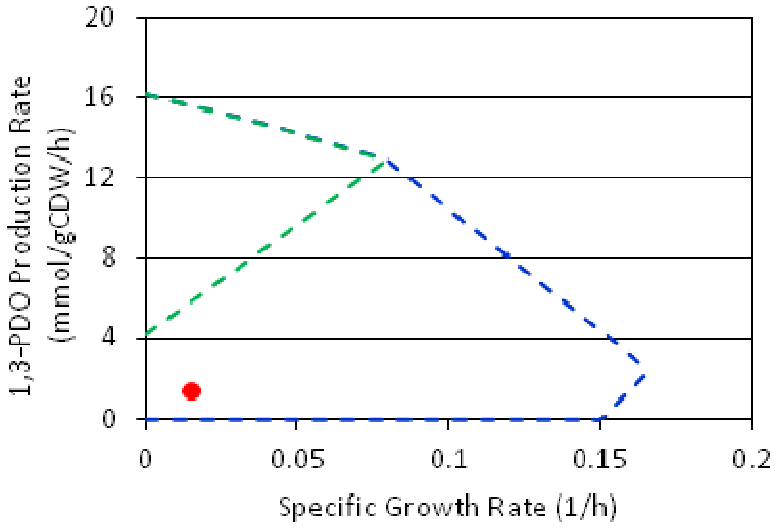

Figure 43: Predicted solution space for the production of 1,3-PDO and biomass. Blue line corresponds to the simulated solution space of the pre-existing strategy presented by Tang and collaborators (Tang et al., 2009). Green line corresponds to the simulated solution space removing ethanol production to the pre-existing strategy. The solid red circle corresponds to the reported results using the pre-existing strategy (Tang et al., 2009).

To explore alternative strategies for the production of 1,3-PDO, OptKnock was utilized. However, the outcome solution space of this strategy did not differ much from the outcome of the strategy deleting only ethanol production (as presented in previous paragraph), and the OptKnock strategy had the additional complexity of including 8 knockouts as opposed to only one knockout in the case of deleting only ethanol production. Therefore, the strategy of deleting ethanol production was considered sufficient.

5.3.3 Succinate

As in the case of previous products of this section, strategies to produce succinate in *E. coli* using glycerol have been implemented experimentally previously, and in this

thesis I evaluate two of them. Blankschien and collaborators used an approach using microaerobic conditions (Blankschien et al., 2010), and Zhang and collaborators used an anaerobic approach (Zhang et al., 2010).

Microaerobic approach

The strategy presented by Blankschien and collaborators also required the deletion of key genes toward the production of by-products (*adhE* for ethanol, *pta* for acetate, and *ldhA* for lactate). In addition to these deletions, the gene *poxB* (pyruvate oxidase) was deleted in order to ensure removal of acetate production. Gene *ppc* (PEP carboxylase) was deleted, and replaced by heterologenous gene *pyc* (pyruvate carboxylase) to drive production of succinate. This strategy also required the addition of carbon dioxide to the medium and the use of microaerobic conditions. The former condition provided carbon dioxide to be assimilated in the conversion of PEP into oxaloacetate (OAA), and the later condition provided a mean to oxidize reducing equivalents providing ATP.

In this thesis the aforementioned strategy was simulated using the glyc-GEM, and the *in silico* results were contrasted with the pre-existing strategy results. Simulation of microaerobic conditions was done by allowing oxygen consumption at a rate of 2 mmol/gCDW/h versus the 18.5 mmol/gCDW/h that has been used in GEMs to represent aerobic conditions (see for example (Feist et al., 2007)). The paper from Blankschien and collaborators reported a maximum succinate production rate of 3.45 mmol/gCDW/h, and the specific growth rate can be estimated as 0.038 h^{-1} (see Appendix 10.6). Figure 44 shows the solution space predicted by the use of the glyc-GEM (dotted blue line), and

how this space compares to the experimental results reported by the authors (solid red circle).

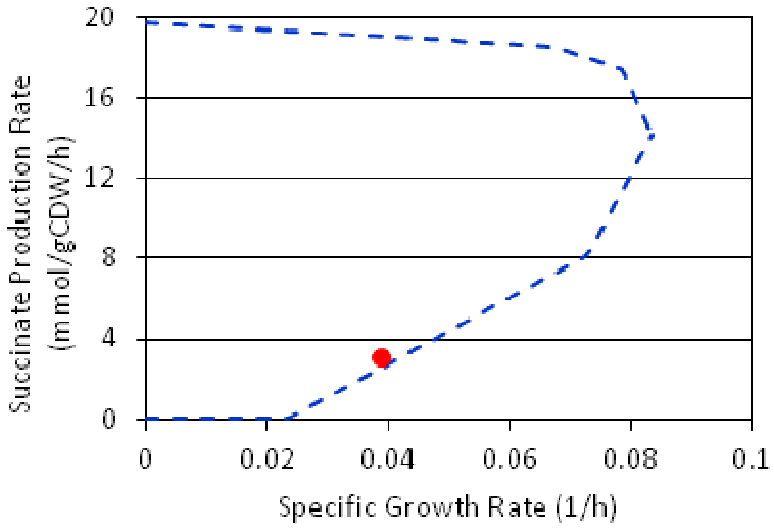

Figure 44: Predicted solution space for the production of succinate and biomass using pre-existing strategy simulated in the glyc-GEM. The solid red circle corresponds to the reported results using the pre-existing strategy (Blankschien et al., 2010).

The next step was to use OptKnock in order to evaluate possible target reactions for deletion, which could result in an increased succinate production coupled to biomass production. The OptKnock optimization was done including the same additions as in the strategy presented by Blankschien and collaborators, which consisted of addition of carbon dioxide to the media, microaerobic conditions, and addition of reaction from *L. lactis* pyruvate carboxylase (pyc). OptKnock identified 8 reactions and this set of reactions was further reduced to only three reactions, as their deletions contained the most relevant impact. The three reactions corresponded to aldehyde dehydrogenase (ALDH), D-lactate dehydrogenase (LDH_D), and pyruvate formate lyase (PFL), and the predicted solution space after incorporating these deletions is presented in Figure 45. This strategy allowed a prediction of 3-fold increase in productivity (from 3.45

mmol/gCDW/h to 10 mmol/gCDW/h) if the specific growth rate is maintained as in experimental results from Blankschien and collaborators. It is interesting to note that two of the reactions of the reduced OptKnock strategy correspond to deletions of the pre-existing experimental strategy, namely ALDH and LDH_D, for the production of by-products ethanol and lactate, respectively, and therefore the main contribution of OptKnock is to propose the deletion of PFL, and the non-deletion of POX and PPC.

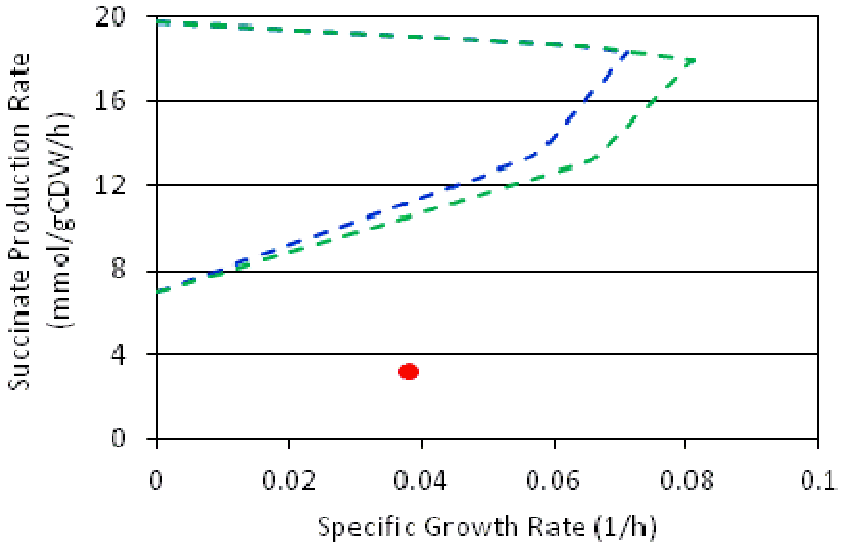

Figure 45: Predicted solution space for the production of succinate and biomass using OptKnock strategy. Blue line corresponds to the full OptKnock strategy (deletion of ACACT3r, ALDH, LDH_D, PFL, PPCSCT, SUCOA, THD2pp, and PntAB), and green line corresponds to the reduced OptKnock strategy (deletion of ADH, LDH_D and PFL). The solid blue circle corresponds to experimental results using preexisting strategy (Blankschien et al., 2010).

I propose validating this strategy by knocking out genes *adhE*, *ldhA* and *pflB*, corresponding to reactions ALDH, LDH_D and PFL, and including the additions mentioned by Blankschien and collaborators, namely addition of carbon dioxide to the media, microaerobic conditions, and addition of reaction pyc from *L. lactis*. An alternative to this strategy could consist of working in the same conditions, addition and deletions presented by Blankschien and collaborators, and deleting gene *pflB*, as this gene

represents the only new deletion of the strategy presented in this thesis in comparison to the strategy presented by Blankschien and collaborators.

Anaerobic approach

Zhang and collaborators proposed expressing a reversible PEP carboxykinase (PckA) that can convert PEP into OAA producing one molecule of ATP. This enzyme exists in *E. coli* and other organisms, such as *Bacillus subtilis*, and it performs the following reaction:

$$ADP + CO_2 + PEP <=> ATP + OAA \quad (57)$$

The advantage of introducing the reversible PckA is to produce one molecule of ATP, as opposed to dissipating energy by releasing one molecule of phosphate. The reversible PckA was incorporated into the glyc-GEM. This strategy also included a source of CO_2, which was modeled in the glyc-GEM by changing the lower boundary of the associated export reaction. In addition, the strategy evaluated different deletions, being be most efficient (for productivity) the deletion of genes *pflB* (pyruvate formate lyase) and *ptsI* (PTS enzyme I). Deletion of the gene *pflB* was simulated in the glyc-GEM by deleting the associated reaction in the model (PFL), as was the deletion of the gene *ptsI*, which was involved in more than 10 reactions (including DHAK), was simulated by using the function deleteModelGenes (in COBRA), that simulated the knock out of this gene.

The *in silico* results of the evaluation of this strategy using the glyc-GEM were contrasted with the pre-existing strategy results. Zhang and collaborators reported a maximum succinate yield of 0.8 w/w. The estimate a succinate production rate was

reported as 2.8 mmol/gCDW/h (see Appendix 10.6), and the specific growth rate was very low. The experimental result (represented as a solid red circle) is within the predicted solution space (Figure 46), which indicates that the glyc-GEM is simulating the implementation of this strategy properly.

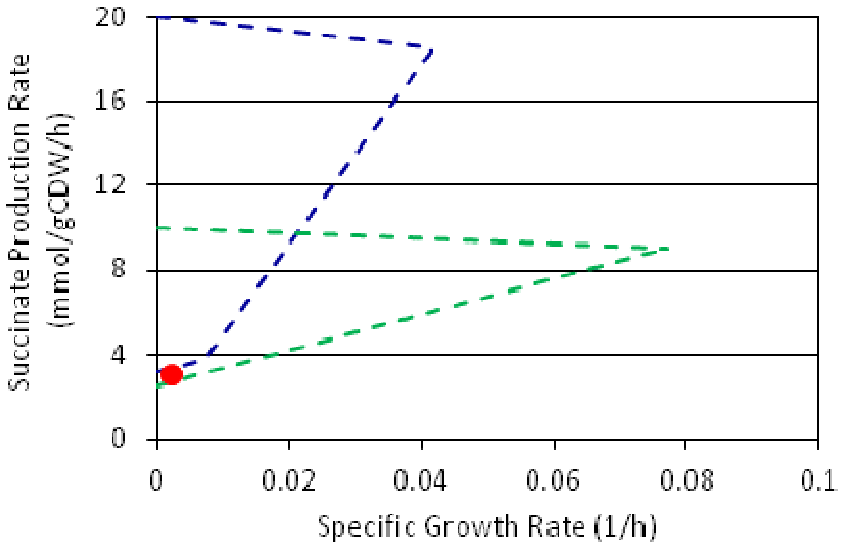

Figure 46: Predicted solution space for the production of succinate and biomass using pre-existing anaerobic strategy simulated in the glyc-GEM. The blue dotted line represent the simulation of the pre-existing strategy, and the green dotted line represent the OptKnock strategy. The solid red circle corresponds to the estimated results using the pre-existing strategy (Zhang et al., 2010).

The next step was to use OptKnock in order to evaluate possible target reactions for deletion, which could result in an increased succinate production coupled to biomass production. The OptKnock optimization was done by including the same additions as in the strategy presented by Zhang and collaborators. OptKnock identified 8 reactions, and this set of reactions was further reduced to only three reactions, as their deletions contained the most relevant impact. The three reactions corresponded to CO_2 transporter via diffusion (CO2tpp), FBPA, and formate transporter via diffusion (FORtppi). Figure 44 shows the predicted solution space using this strategy, in which there was an increase

in the maximum predicted growth rate, but there was a decrease in the predicted production rate of succinate.

The results using the microaerobic strategy presented more promising number for productivity and cell growth (experimental and *in silico* results), and therefore it is recommended that further studies are performed using the microaerobic strategy, as already discussed above.

5.3.4 D-Lactic acid

Production of lactic acid using glycerol as feedstock in *E. coli* has been reported by Mazumdar and collaborators (Mazumdar et al., 2010). This experimental strategy consisted of knocking out genes involved in production of by-products, specifically *frdA* (for succinate), *adhE* (for ethanol), and *pta* (for acetate). Deletion of the aerobic D-lactate dehydrogenase (*ldl*) was introduced in order to prevent lactate utilization. In addition, the gene *pflB* was deleted, which corresponds to pyruvate formate dehydrogenase, as deletion of this gene has been shown to result in accumulation of lactate (Durnin et al., 2009). Furthermore, the respiratory pathway GlpK-GlpD was overexpressed in order to increase production of DHAP, and the fermentative lactate dehydrogenase (*ldhA*) was overexpressed in order to increase production of lactate from pyruvate. Microaerobic conditions were used in this strategy. This strategy resultedin a maximum lactic acid production rate of 13.88 mmol/gCDW/h, and the specific growth rate can be estimated as 0.048 h^{-1} (see Appendix 10.6).

In this section this pre-existing strategy was modeled in the glyc-GEM, as explained below. First, the knockout of genes was simulated in the glyc-GEM by removing reactions associated with each gene, in the following way: reaction PFL for

gene *pflB*, reactions FRD2 and FRD3 for gene *frdA*, reaction ALDH for gene *adhE*, reaction LDH_D2 for gene *ldl*, and reaction PTAr for gene *pta*. Microaerobic conditions were simulated by allowing consumption of oxygen at an uptake rate up to 2 mmol/gCDW/h. Overexpression of genes was not incorporated in the model, as stoichiometric models do not incorporate that kind of information. Figure 47 shows the solution space corresponding to the modeling of this strategy in the glyc-GEM (dotted blue line) compared to the experimental result reported by Mazumdar and collaborators (solid red circle) (Mazumdar et al., 2010), and it is observed that the experimental data falls above the simulated solution space, with a productivity value 25% higher than the one obtained using the optimal solution optimizing biomass. The difference could have been caused by a variety of factors, including the use of an underestimated oxygen uptake factor in the model, a higher experimental consumption rate of glycerol, or the presence of unknown reactions that have not been included in the model. A more accurate modeling of this condition could be modeled in future works by performing continuous culture experiments, and in steady state conditions measuring glycerol uptake rate and oxygen uptake rate, to then be incorporated in the model. Oxygen consumption can be calculated by experimentally measuring kla, and then multiply it by dissolved oxygen at equilibrium.

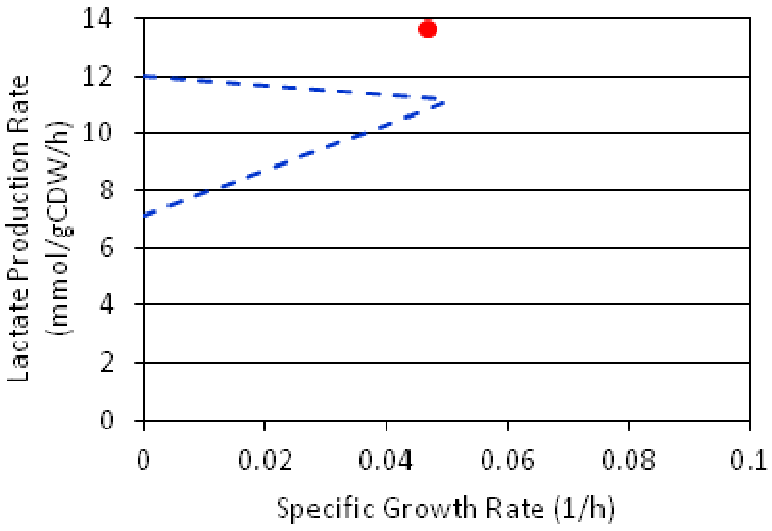

Figure 47: Predicted solution space for the production of lactate and biomass using the pre-existing strategy simulated in the glyc-GEM. The solid red circle corresponds to the reported results using the pre-existing strategy (Mazumdar et al., 2010).

The use of OptKnock in this case was unable to identify one solution that would satisfy the minimal requirements, even after 64 hours of simulation. The reason for that was not being able to satisfy minimal requirements for specific growth rate, which was set as 0.07 h^{-1}. However, OptKnock delivered a solution that was under-requirements, with a maximal production of biomass of 0.03 h^{-1} (57% below requirement). For the reasons mentioned above, the strategy presented by Mazumdar and collaborators is considered satisfactory.

5.3.5 Butanol

Production of butanol in *E. coli* has been done using different pathways, the most remarkable being α-keto acid using glucose (Atsumi et al., 2008a) and the reversal of the β-oxidation cycle starting from glucose (Dellomonaco et al., 2011). This section presents the simulations using one turn of the reversal β-oxidation cycle, as this pathway is more energy efficient than the α-keto acid pathway (more details of comparison of these

pathways is presented in the next chapter of this thesis). Following the same description of this pathway introduced by Dellomonaco and collaborators, reactions acyl-CoA dehydrogenase (ferredoxin) and pyruvate ferredoxin oxido reductase (PFOR) were added to the glyc-GEM as part of the reversal β-oxidation cycle. In addition, termination enzymes acyl-CoA reductase and aldehyde/alcohol dehydrogenase were added to produce n-butanol as final product (Dellomonaco et al., 2011). Each of the termination enzymes consumes one reducing equivalent of the form of NADH, making the pathway for the production of butanol redox balanced. Since ethanol is a natural competing by-product (same ATP production and redox balance), deletion of ethanol was simulated in the model by knocking out reaction aldehyde dehydrogenase (ALDH). Figure 48 shows the solution space of this strategy obtained using the glyc-GEM. As expected, production of butanol coupled to biomass production, which is a natural result of having removed ethanol as possible product, and introduced butanol production instead in a manner that produces ATP and is redox balanced, just as the natural product of this fermentation process (ethanol).

Another strategy that was evaluated was introducing knockouts of other by-products, namely succinate, acetate and lactate, in addition to ethanol. This strategy was introduced by Dellomonaco and collaborators when using glucose as carbon source, and it is reasonable to consider this as a proper strategy when glycerol is used instead (Dellomonaco et al., 2011). For this purpose the following genes were deleted: *frdA* (for succinate), *pta* (for acetate), *adhE* (for alcohol) and *ldh* (for lactate). The simulated solution space of this case corresponded exactly to the simulation of the solution space deleting only production of ethanol (remove reaction ALDH).

The use of OptKnock in this case was not able to identify any better strategy than the strategy presented in the previous paragraph, and therefore the aforementioned strategy is considered satisfactory.

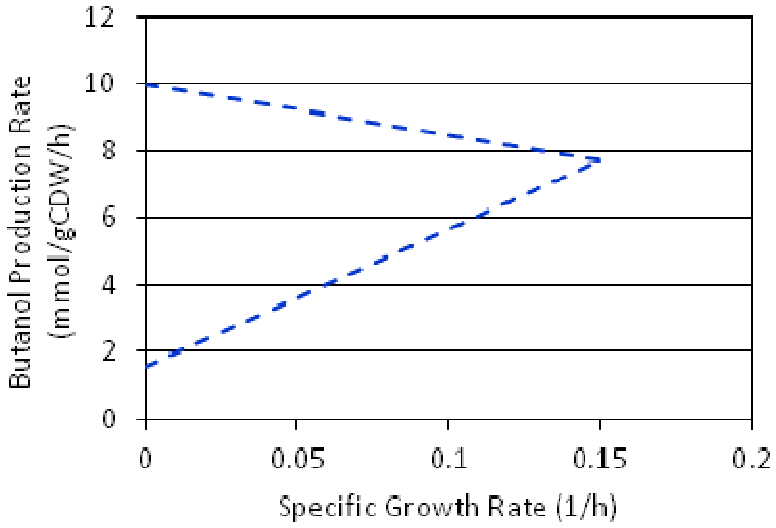

Figure 48: Predicted solution space for the production of butanol and biomass using one turn of the reversal of the β-oxidation cycle. This strategy simulates the deletion of competing by-product ethanol by removing reactions ALDH and ADH.

5.3.6 Propionic acid

This section and next section present the production of propionic acid and propanol, two products that have not been produced experimentally in *E. coli* using glycerol.

Production of propionic acid from glycerol has been reported in other organisms. For example, Barbirato and collaborators studied three strains, namely *Propionibacterium acidipropionici, Propionibacterium acnes,* and *Clostridium propionicum*, for this process (Barbirato et al., 1997). According to their results, *P. acidopropioncini* performed the best for the production of propionic acid. In this analysis it was hypothesized that *E. coli* could be genetically modified in order to produce this

product by including the reactions from *P. acidopropioncini* that convert succinate into propionic acid.

The production of propionic acid from the glycolytic intermediate PEP in this organism includes 4 steps: 1) conversion of PEP into OAA, 2) conversion of OAA into malate using NADH, 3) conversion of malate into succinate using NADH and producing ATP, and 4) conversion of succinate into propionate. The glyc-GEM already includes a set of equivalent reactions (using different co-factors) for the conversion of PEP into propionic acid. The glyc-GEM, however, lacks a transport system to export propionic acid, and therefore this reaction was added.

Another interesting step in this pathway is the conversion of PEP into OAA. Wild type *E. coli* completes this step using the enzyme PEP carboxylase, which fixes one molecule of carbon from bicarbonate and releases one phosphate group. In this section it is proposed to use a reversible PckA, which converts PEP into OAA and produces one molecule of ATP in this process (see reaction 57 in the for succinate production). The reversible PckA was incorporated into the glyc-GEM, and FBA was used to find the optimal solution. The initial solution indicated that ethanol was a competing product; therefore, the reactions ALDH essential for the production of ethanol was deleted. Figure 49 shows the solution of this strategy after deleting reaction ALDH (blue line). Production of propionic acid became essential after deleting production of the competing by-product ethanol. This is because production of propionic acid with the previously proposed strategy is redox balanced and produces one molecule of ATP per molecule of glycerol, having therefore the same net effect in terms of energy and redox balance as production of ethanol.

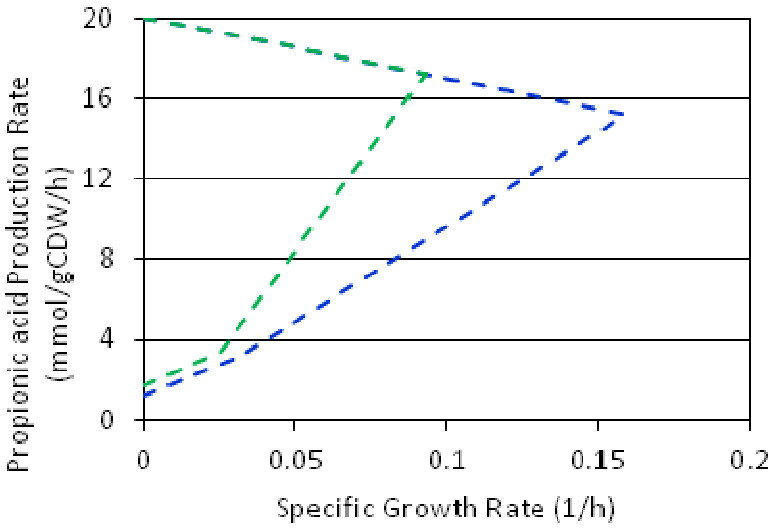

Figure 49: Predicted solution space for the production of propionic acid and biomass. Blue line corresponds to results after deleting competing pathway for the production of ethanol (deletion of ALDH). Green line corresponds to the solution space deleting the reactions identified by the OptKnock strategy (ALDH, GLYK and MDH).

OptKnock was used in order to other possible reactions to target as knockout, and that could increase the productivity (Figure 49, green line). Using OptKnock, the following three reactions were identified as target for deletion: aldehyde dehydrogenase (ALDH), glycerol kinase (GLYK) and malate dehydrogenase (MDH). This strategy can be implemented experimentally by knocking out the following genes: *adhE* (for reaction ALDH), *glpK* (for reaction GLYK) and *mdh* (for reactions MDH). While deletion of ALDH removed ethanol as a by-product, deletion of GLYK resulted in redirecting that flux to go through the DHAK reaction, which links phosphorylation of DHA to conversion of PEP into PYR, and PYR in turn is converted back to PEP by the action of the reaction PEP synthase (PPS in the glyc-GEM) using ATP. In addition, deletion of MDH forces the conversion of OAA into malonate to go through reaction malate oxidase (MOX), which produces oxygen.

In order to experimentally validate this strategy further research will be needed. I propose to introduce gene *pckA* (encoding reversible PEP carboxykinase), and to perform the gene knockout identified in the previous paragraph (*adhE*, *glpK* and *mdh*). Transport of propionate across the membrane is expected to occur spontaneously, and therefore no further genetic modifications are needed for that step.

5.3.7 Propanol

Production of propanol has been report in metabolically engineered organisms by extending natural pathways from 1,2-PDO (Jain & Yan, 2011) and from propionyl-CoA (Deng & Fong, 2011) , and using glucose as feedstock. In this section a strategy to produce propanol from glycerol is developed.

The glyc-GEM was used to simulate addition of both strategies mentioned in previous paragraph as follow:

1,2-PDO + cobamamide → h2o + 1-propanal (58)

1-propanal + NADH + h → 1-propanol + NAD (59)

Propanoyl-CoA (ppcoa) + NADH + h → 1-propanal + NAD + CoA (60)

Introducing both strategies and then using FBA to identify the optimal solution allows me to evaluate which one of the aforementioned strategies is expected to be more efficient. In addition to these modifications, a reversible PckA was introduced as explained in previous section (production of propionic acid).

FBA was used to predict flux distribution and cell growth after adding reactions 58-60, and the reversible PckA. The resulting solution space is presented in Figure 50, blue line. FBA selected production of propanol through propanoyl-CoA as the optimal solution (reactions 59 and 60), as oppose to production of propanol from 12-PDO

(reaction 58 and 59). Analysis of flux distribution of the solution identified ethanol as a competing by-product, and therefore this product was removed by simulation the deletion of reaction ALDH, a case that resulted in a clear coupling of the production of propanol and cell growth (Figure 50, red line). The optimal solution produces biomass at a specific growth rate of 0.21 h^{-1}, and propanol at a rate of 9.2 mmol/gCDW/h.

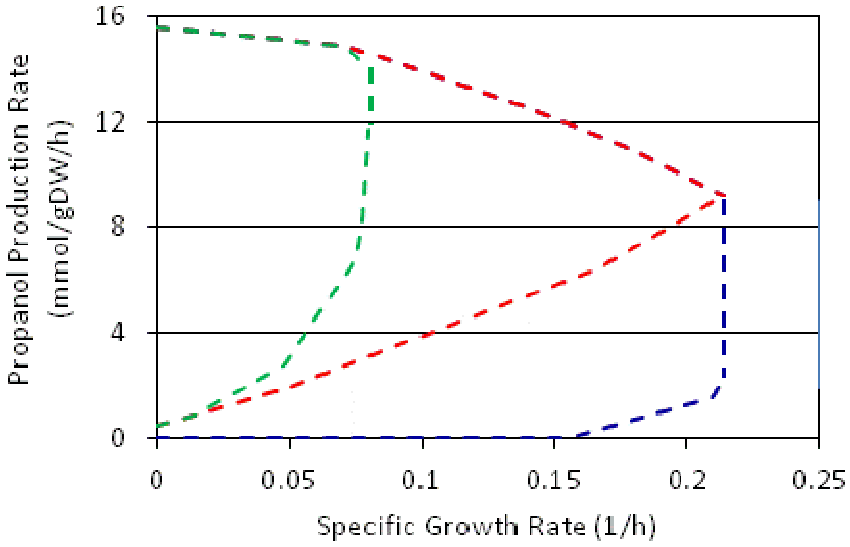

Figure 50: Predicted solution space for the production of propanol and biomass. Blue line corresponds to the solution before deleting competing by-products, and red line corresponds to the solution after deleting reaction ADH for the production of ethanol. Green line corresponds to OptKnock strategy (deletion of ALDH, ACt2rpp, D-LACtex, PYRt2rpp).

In order to explore the possibility of producing propanol at a higher yield, OptKnock was used. Using OptKnock the following four reactions were identified as target for deletion: aldehyde dehydrogenase (ALDH), acetate reversible transport via proton symport (ACt2rpp), D-lactate transport via diffusion (D-LACtex) and pyruvate reversible transport via proton symport (PYRtrpp). These four reactions are associated with production of ethanol, acetate, lactate and pyruvate, respectively. Deletion of these four reactions in the glyc-GEM increased production of propanol from 9.2

mmol/gCDW/h to a value between 11.7-14.1 mmol/gCDW/h (multiple optimal solutions), which represent an increase of 40% (Figure 50, green line).

The experimental validation of this strategy will require adding genes for the conversion of propanoyl-CoA into propanol, add a reversible PckA, and knockout genes toward the production of the undesired products identified using OptKnock. Production of propanol from propanoyl-CoA is expected to happen after adding the bifunctional aldehyde/alcohol dehydrogenase (gene *adhE2)* from *Clostridium acetobutylicum*, as presented by Deng and Fong (Deng & Fong, 2011). Thus, the associated protein could perform reactions 59 and 60. In addition, I propose to increase the expression of *pckA* from *E. coli,* encoding reversible PEP carboxykinase, using a promoter mutation (Zhang et al., 2010). The deletion of reactions identified using OptKnock cannot be implemented directly, as three out of the four reactions identified with this methodology do not have a specific gene associated. While deletion of reaction ALDH can be performed simply by knocking out gene *adhE*, the three other reactions identified by OptKnock correspond to transport reactions that would be difficult to remove. To this end I propose to knockout genes *pta*, and *ldhA* involved in the production of acetate and lactate respectively, as these deletions will have the same (or very similar) effect as deleting the transport reactions for acetate and lactate. Export of pyruvate will be more difficult to control, as pyruvate is an essential intermediate metabolite, and its transport occurs using generic transporters.

The following table shows a summary of the findings of this section, for the synthesis of different products.

Table 11: Summary table comparing production rates and specific growth rate for the synthesis of desired products using glycerol.

Product	Experimental results		*In silico* predictions	
	Production rate (mmol/gCDW/h)	Specific growth rate (1/h)	Production rate (mmol/gCDW/h)	Specific growth rate (1/h)
1,2-PDO	2[a]	0[a]	2.2	0.15
1,3-PDO	1.4[b]	0.014[b]	12.1	0.08
Succinate - microaerobic	3.5[c]	0.038[c]	18.31*	0.07*
Succinate - anaerobic	2.8[d]	0[d]	14.2	0.08
Lactic acid	13.88[e]	0.038[e]	11.1	0.05
Butanol			0.15	7.74
Propionic acid	-	-	17.2*	0.09*
Propanol	-	-	11.7-14.1*	0.08*

*** Optimal Strategy identified using OptKnock. a Clomburg & Gonzalez, 2011. b Tang et al., 2009. c Blankschien et al., 2010 . d Zhang et al., 2010. e Mazumdar et al., 2010.**

5.4 Conclusions

This chapter presented the modeling of glycerol fermentation in *E. coli* using a GEM. When available experimental data, the model simulated well the main features observed for this microorganism. Further, the use of a comprehensive metabolic network of this microorganism allowed exploring new unstudied pathways that appear to have a relevant role in glycerol fermentation. Of special interest was the prediction of the fructose phosphate bypass, which could support the production of 3C intermediate metabolites independently of PEP-dependent DhaK, providing a path for the production of 1,2-PDO and biomass. This theory is also supported by fact that the gene *fsaB*, which encodes enzyme F6P aldolase (necessary for the fructose phosphate bypass), belong to the same transcription unit as gene *gldA*, which has a key role in the fermentation of glycerol in *E. coli*, suggesting that both genes may be involved in the same process. Experimental validation of these results will need to be conducted in order to confirm the

role of the fructose phosphate bypass. The glyc-GEM validated the ethanol-1,2-PDO model for glycerol fermentation in wild type *E. coli*, by predicting these two products to be essential for cell growth. The glyc-GEM was also used to evaluate possible genetic modifications that would enable cell growth associated to the synthesis of other products, which identified a total of 59 possible models, 18 of them with a predicted maximum specific growth rate higher than the value predicted for wild type *E. coli*.

After studying fermentation of glycerol using the glyc-GEM, production of a variety of fuels and chemicals was addressed using the model. The simplicity of the method is remarkable when compare to other options, such as the use of a detailed kinetic model, or a purely experimental approach. Further, in most of the cases that were studied in this chapter, the simulated solution space generated by the model correlated well with pre-existing experimental data (data not used to curate the model), which highlight the predictive power of the glyc-GEM presented in this thesis. In most cases the use of the mathematical optimization algorithm OptKnock identified possible genetic manipulations that could increase the productivity of these desired chemicals.

While GEMs are powerful to study flux distributions without using experimental data, as well as to identify target genes to incorporate or delete in order to increase productivity of a desired product, its limitations can be complemented using kinetic models. One lacking aspect in the use of GEMs is the inability to predict the effect enzymes overexpression. The overexpression of enzymes plays a significant role in metabolic engineering, as it may result in increasing the flux on a desired pathway, or in re-directing part of the flux from one pathway to another one. Because of this, experimental implementations of strategies identified using GEMs may need to be

modified, in order to include possible gene overexpressions. One way to identify target genes to be overexpressed is the use of kinetic models, as presented in Chapter 3 of this thesis, which make these two kinds of models complimentary for the study and optimization in metabolic engineering.

In summary, the main results and finding presented in this chapter are:

- A detailed adaptation and curation of the genome scale model iJO1366 to represent glycerol fermentation in *E. coli*. The resulting model (glyc-GEM) represents well preexisting experimental data about the proposed Ethanol-1,2-PDO metabolic model of glycerol fermentation and corresponding essential genes and reactions.
- The glyc-GEM in conjunction with FBA identified a new possible dissimilation pathway to convert glycerol into DHAP independently of enzymes glycerol dehydrogenase and glycerol kinases. This pathway is potentially more efficient than alternative pathways, and it suggests that the physiological function of the gene *fsaB* (fructose bisphosphate alsolase) is to facilitate the anaerobic fermentation of glycerol. This gene is part of the same transcriptional unit as gene *gldA*, which is essential for glycerol fermentation in *E. coli.*
- The glyc-GEM in conjunction with FBA validated the ethanol-1,2-PDO model, which had been suggested to explain the anaerobic fermentation of glycerol in *E. coli*. Additional pathways were simulated in the model, using 15 conditions (products/pathways), and the viability of these pathways was evaluated. The glyc-GEM and FBA identified a total of 55

possible models using combinations of these conditions, 16 which predicted maximum specific growth rate higher than the value predicted for wild type *E. coli*.

- The glyc-GEM in conjunction with OptKnock evaluated and identified strategies for the optimal production of succinate, 1,2-PDO, 1,3-PDO, lactate, propanol, butanol and propionic acid.

6 Results III: Genome scale model for the reversal of the β-oxidation cycle

This chapter presents the *in silico* evaluation of the recently published reversal of the β-oxidation cycle in *E. coli* for the production of advanced biofuels with long hydrocarbon chains. This theoretical research expands upon the experimental work that was conducted by Dellomonaco and collaborators for the implementation of a functional of a reversal of the β-oxidation cycle (Dellomonaco et al., 2011). In order to produce long chain biofuels and biochemicals, it is necessary to elongate of a starting molecule or precursor, and to implement appropriate termination enzymes. Remarkable strategies for the elongation stage are the use of the fatty acids biosynthesis pathway (Schirmer et al., 2010; Steen et al., 2010), the engineering of the α-keto acid pathway for the production of alcohols (Zhang et al., 2008), and more recently the engineering of a functional reversal β-oxidation cycle (Dellomonaco et al., 2011). The latest has been shown to produce butanol and longer chain n-alcohols at higher yields than those reported previously, as it is energetically more efficient; therefore, it opens the door to a significant improvement in the productivity of a wide possibility of products.

The genome scale model iJO1366 was adapted for the *in silico* evaluation of the reversal β-oxidation cycle in *E. coli*. The production of several long chain product families was evaluated, including production of n-alcohols, alkanes and fatty acids. Flux Balance Analysis (FBA) and Flux Variability Analysis (FVA) were applied to the resulting genome-scale model (GEM) to generate predictions of flux distribution and

solution spaces. The iJO1366 model was also adapted to simulate the use of other platforms for the production of these products, and the results are contrasted.

The following are sections of this chapter: *model implementation*, *results* and *conclusions*. The model implementation presents the modifications that were done to the iJO1366 model in order to properly simulate the use of the reversal β-oxidation cycle to produce a variety of medium and long chain products, including alcohols, alkanes and fatty acids in *E. coli.* The model implementation section also presents the modifications that were done to represent alternative platforms for the production of the same products (for comparison purposes). Then, the results of the predicted performance of the reversal β-oxidation cycle for the production of desired products are presented. Deletions of native fermentation products were simulated in order to enhance the yields of desired products coupled to biomass growth. The energetic efficiency of this pathway allowed for the prediction of production of medium and long chains members of these product families, at significant productivities. The results are contrasted with other widely used pathways to verify the superiority of the reversal β-oxidation cycle under the circumstances evaluated in this project. In addition, the results of simulating the production of long chain products with a functionalized side chain are presented. Adding further modifications to the metabolic pathway in order to produce hydroxylated and carboxylated primers for the reversal β-oxidation cycle, allowed for the identification of efficient pathways for the production of diols, dicarboxylic acids and hydroxyacids. Finally, the conclusion section discusses the implications of using a GEM to quantitatively assess the metabolic capabilities of using the reversal of the β-oxidation cycle as an efficient platform for the production of long chain chemicals in *E. coli*.

6.1 Model implementation

The implementation of the GEM to represent the reversal β-oxidation cycle in *E. coli* for the production of long chain products requires four steps: 1) define a starting GEM, 2) define external conditions, 3) curate the model, and 4) add necessary reactions for the reversal β-oxidation cycle and termination reactions. The first three steps are similar to those presented in the previous chapter for the use of GEM to represent glycerol fermentation. The fourth step was implemented in three modules: Module I (priming), Module II (elongation, reduction, dehydration, reduction), and Module III (termination). Additional modifications to the Modules I, II and III were included for the production of chemicals with a functionalized side chains. Each of these points is expanded below.

6.1.1 Define a starting GEM

The genome scale model iJO1366 for *E. coli* K-12 1655 was used as starting point (Orth et al., 2011). See details of this model in section 5.1.1 (page 101).

6.1.2 Define External Conditions

The external conditions were set to represent glucose fermentation in minimal medium (no external electron acceptor). As stated in the previous chapter, external conditions are defined by changing the lower bound limit of the corresponding exchange reactions, usually setting the value to -1000 mmol/gCDW/h for non-limiting nutrients. Table 12 shows a list of the nutrients that were considered as part of the minimal medium, with the corresponding exchange reaction and lower bound, as defined

elsewhere (Feist et al., 2007; Orth et al., 2011). Glucose is the only limiting nutrient, and its value was set to -15 mmol/gCDW/h.

Table 12: External conditions for the GEM to represent glucose consumption. All reactions correspond to "exchange" reactions, which represent the presence of these molecules in the medium.

Exchange Reaction	Lower bound (mmol/gCDW/h)	Exchange Reaction	Lower bound (mmol/gCDW/h)
Calcium exchange	-1000	Sodium exchange	-1000
Chloride exchange	-1000	Ammonia exchange	-1000
Co2+ exchange	-1000	Ni2+ exchange	-1000
Cu2+ exchange	-1000	Phosphate exchange	-1000
Fe2+ exchange	-1000	Selenate exchange	-1000
Fe3+ exchange	-1000	selenite exchange	-1000
H+ exchange	-1000	Sulfate exchange	-1000
H2O exchange	-1000	tungstate exchange	-1000
K+ exchange	-1000	Zinc exchange	-1000
Mg exchange	-1000	Glucose exchange	-15
Mn2+ exchange	-1000	Cob(I)alamin exchange	-0.01
Molybdate exchange	-1000		

6.1.3 Model curation

The curation of the model was performed in order to represent glucose consumption. Some modifications identified in the GEM for glycerol fermentation (glyc-GEM) were considered as a starting point, as those modifications were done to prevent non-permisive pathways for the consumption of reducing equivalents (see section 5.1.3, page 103 for details). In particular, the following pathways were restricted to be equal to zero:

a) Amino acid degradation and nucleotide degradation.

b) Sulfate reduction.

c) Iron reduction.

d) Spermidine and 5-methylthio-D-ribose production.

Also, following the same rationale as in the curation of model glyc-GEM, pathway C for the conversion of fructose-6-phosphate (F6P) into glyceraldehyde-3-phosphate (GAP) (see Figure 35, page 111) was restricted to allow only the pathways that go through di-hydroxyacetone-phosphate (DHAP) (pathways A and B).

Pyruvate production was also removed from the model as this was not a product of interest in this study.

Finally, the iJO1366 model includes the reaction pyruvate oxidoreductase (POR5), which was modified. This reaction, although irrelevant in most of the cases studied in this chapter, was generating a non-permisive electron sink in some cases. Specifically, this situation was identified in preliminary results for the production of fatty acid after deleting competing by-products. An evaluation of this reaction identified that this reaction should be associated with ferredoxins, but the iJO1366 model has this reaction linked to flavodoxins. Because of this, the reaction was eliminated from the model, and instead a new reaction was added (named PFOR for pyruvate ferredoxin oxidoreductase), which uses ferredoxins (fd) as electron acceptor to convert pyruvate (PYR) into acetyl-CoA (AcCoA).

The next three subsections (6.1.4 - 6.1.6) present the implementation of the reversal β-oxidation cycle, implementation of alternative pathways (for comparison purposes), and implementation of termination pathways. The alternative pathways that are being considered in this thesis are the fatty acid (FA) biosynthesis pathway and the α-keto acid pathway, both of which are currently being used for the production of long chain products. Termination pathways were implemented to produce alcohols, alkanes, and fatty acids. Subsection 6.1.7 presents further modification to the iJO1366 model in

order to produce chemicals with a functionalized side chain using the reversal β-oxidation cycle.

6.1.4 Implementation of the reversal β-oxidation pathway

The production of long chain products using the reversal of the β-oxidation cycle consists of three modules: Module I (priming), Module II (elongation, reduction, dehydration, reduction), and Module III (termination). Figure 51 shows a scheme of the reversal β-oxidation cycle for the production of different families of products using the modularity system.

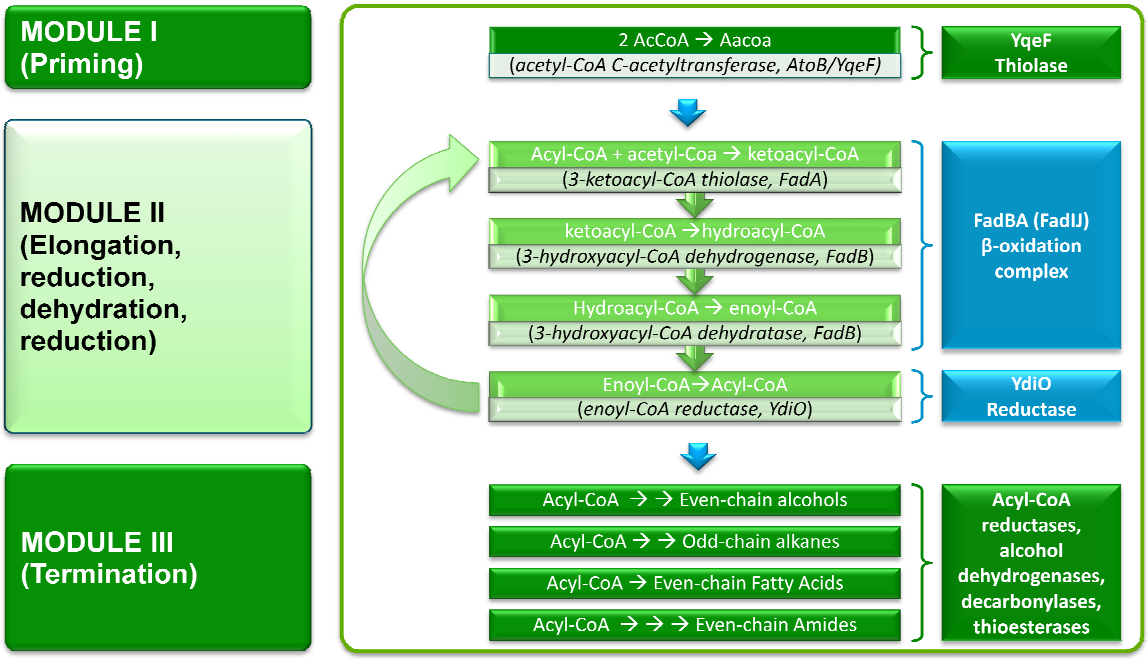

Figure 51: Pathway for reversal B-oxidation cycle. Modularity for the synthesis of different products.

The first module, priming, is already part of the iJO1366, and therefore no further modifications are necessary. The second module consists of 4 steps: elongation, reduction, dehydration, and reduction. Three of these steps already are included in the iJO1366 model with the proper reversibility. The fourth step, reduction of an enoyl-CoA,

was added coupled to the oxidation of a ferredoxin (fd) (see equation 61). Thus, the reversal β-oxidation cycle was fully implemented by adding the fourth step.

$$fd^{2-} + \text{enoyl-CoA} + H^{+} \rightarrow \text{AcCoA} + fd \qquad (61)$$

It is necessary to mention that the iJO1366 model already included the acyl-CoA dehydrogenase reactions, which were modified as part of this study. The iJO1366 includes reversible acyl-CoA dehydrogenases linked to the oxidation/reduction of a flavin adenine dinucleotide (fad) and to the gene *fadE*. However, previous evidence suggests that these reactions occur only in the direction of oxidation of the acyl-CoA *in vivo* conditions, and therefore this family of reactions was restricted to function only in that direction (Clark & Cronan, 2005).

As previously suggested (Dellomonaco et al., 2011), the redox balance of ferredoxins is achieved by adding the enzyme pyruvate ferredoxins oxidoreductase (PFOR), which transforms pyruvate (PYR) into acetyl-CoA (AcCoA) according to the following reaction:

$$PYR + CoA + fd \rightarrow AcCoA + CO^{2} + fd^{2-} + h^{+} \qquad (62)$$

Finally, the reaction acetyl-CoA carboxylase was restricted to have a flux no greater than 0.1 in order to prevent simultaneous activation of the reversal of the β-oxidation cycle and of the FA biosynthesis pathway.

6.1.5 Implementation of FA biosynthesis pathway and α-keto acid pathway

As stated in the introduction of this chapter, two pathways have been used for the production of long chain products: the FA biosynthesis pathway and the α-keto acid pathway. These two pathways were implemented in the GEM in order to benchmark the use of the reversal β-oxidation cycle.

The FA biosynthesis pathway is an essential pathway in wild type *E. coli*, and therefore it was already part of the iJO1366 model. This pathway requires malonyl-ACP for the production of the precursor acetoacyl-ACP and to act as carbon donor in the elongation of the fatty acids. Each cycle of this pathway elongates the four intermediates by 2 carbons.

The α-keto acid pathway is an engineered pathway in *E. coli* and it was implemented in the model for the production of n-butanol and n-hexanol, as reported (Atsumi et al., 2008b; Shen & Liao, 2011). To this end, I first verified that the production of 2-ketobutyrate using the L-threonine biosynthesis pathway was part of the iJO1366 model, and then I included the keto acid chain elongation cycle (Atsumi et al., 2008b; Shen & Liao, 2008), which consists of three steps: condensation (LeuA), isomerization (LeuCD) and oxidation (LeuB). Equations 63-65 show each of these reactions.

$$C_n\text{-keto acid} + \text{AcCoA} + \text{h2o} \rightarrow 2\text{-}C_n\text{-alkyl-malate} + \text{CoA} \quad (63)$$

$$2\text{-}C_n\text{-alkyl-malate} \rightarrow 3\text{-}C_n\text{-alkyl-malate} \quad (64)$$

$$3\text{-}C_n\text{-alkyl-malate} + \text{NAD} \rightarrow C_{n+1}\text{-keto acid} + CO_2 + \text{NADH} \quad (65)$$

Unlike the reversal β-oxidation cycle and the FA biosynthesis pathway, in which each cycle elongates the intermediate metabolites by 2 carbons, the α-keto acid pathway elongates the intermediate product by only one carbon molecule.

6.1.6 Implementation of termination pathways

Termination pathways were added for the **production of n-alcohols, alkanes and fatty acids**. These three product families are a sample of advanced fuels and chemicals that can be produced using the reversal of the β-oxidation cycle. The starting point for the termination steps will be either a fatty acyl-CoA (using the reversal of the β-oxidation

cycle), a fatty acyl-ACP (using the FA biosynthesis pathway), or an α-keto acid (using the α-keto acid pathway for production of n-butanol and n-hexanol). Acyl-CoA and acyl-ACP are structurally similar, as are the chemical reactions involved.

Using the reversal of the β-oxidation cycle, a fatty acyl-CoA can be converted into an alcohol by the action of two successive reduction steps catalyzed by an aldehyde-forming acyl-CoA reductase and an alcohol dehydrogenase (Dellomonaco et al., 2011). Likewise, an acyl-ACP (produced in the FA biosynthesis pathway) can be converted into an alcohol in two reducing steps catalyzed by an acyl-ACP reductase and an alcohol dehydrogenase (Schirmer et al., 2010). These reactions were implemented in the model as follows:

fatty acyl-CoA +h + NADH → CoA + NAD + aldehyde (66)

fatty acyl-ACP + h + NADH → ACP + NAD + aldehyde (67)

NADH + aldehyde + h → NAD + n-alcohol. (68)

Production of medium chain n-alcohols can also result from using the α-keto acid elongation pathway. The production of n-butanol and n-hexanol using the α-keto acid elongation pathway uses a 2-keto acid as starting point (Shen & Liao, 2011). The termination steps of this pathway include the decarboxylation of the 2-keto acid by the action of the enzyme 2-ketoisovalerate decarboxylase (KIVD), and dehydrogenation of the resulting aldehyde by the action of the enzyme alcohols dehydrogenase as previously described (see equation 68). The decarboxylation step is implemented as follows:

2-ketoacid (Cn) → aldehyde (Cn-1) + CO_2. (69)

The production of alkanes can be achieved by reducing an acyl-CoA or an acyl-ACP into an aldehyde as described in equation 66 and 67, followed by decarbonylatinon

of the aldehyde using a fatty aldehyde decarbonylase (Schirmer et al., 2010), in the following way:

aldehyde → alkane + CO. (70)

Production of fatty acids is achieved by hydrolysis of the thioester group in the acyl-CoA molecule (using the reversal of the β-oxidation cycle) or in the acyl-ACP molecule (using the FA biosynthesis pathway). *E. coli* possesses a number of thioesterases that can perform this function, and their overexpression has enhanced the production of fatty acids. For example, the enzyme TesA has been used to convert acyl-ACP into fatty acids (Steen et al., 2010) and acyl-CoA into fatty acids (Dellomonaco et al., 2011). Other enzymes, such as thioesterases TesB, FadM and YciA, have also been overexpressed to convert acyl-CoA into fatty acid (Dellomonaco et al., 2011). Accordingly, the hydrolysis of an acyl-CoA or an acyl-ACP is already part of the iJO1366 model. However, the original model only included a transport system for two molecules of this family: butyrate and hexanoate. Since experimental results suggest that *E. coli* is capable of producing longer chain FAs as final product, the transport reactions were added into the GEM as follows:

Fatty acid[c] + h[c] → fatty acid[p] + h[p]. (71)

where [c] and [p] indicate the location of the molecules: [c] for cytoplasm, and [p] for periplasm.

After adding the pathways for the production and transport of n-alcohols, alkanes and fatty acids, the final step in the model implementation is the addition of exchange reactions. In a GEM, the "exchange" reactions provide substrates and remove products to and from the media in order to simulate state conditions in the system. The iJO1366

model already includes the exchange reactions for fatty acids (as they are part of the possible natural substrates of *E. coli*). Addition of exchange reactions was necessary for all the new products, which consist of n-alcohols (C-4 to C-18, even chain length) and alkanes (C-3 to C-17, odd chain length), and for the by-product carbon monoxide. All these products possess a straight fatty chain and a terminal group, with no functional side chains.

6.1.7 Implementation of pathways for the synthesis of products with a functional side chain

The reversal β-oxidation cycle can also be used to synthesize products with a functional side chain. In the following sections two strategies are presented to this end. The first one consists of applying the termination pathways to different intermediates of the reversal β-oxidation cycle (beside the acyl-CoA metabolite). The second strategy utilizes a primer with a functional group in the omega end, a hydroxyl or a carboxyl, to produce 1,n-diols and dicarboxylic acids. The *in silico* implementation of these two strategies is explained next.

6.1.7.1 Strategy 1: Derive products from intermediate metabolites

The termination pathways described in previous sections can be applied to different intermediates of the reversal β-oxidation cycle, generating a variety of long chain products. This strategy can be experimentally implemented by using termination enzymes with different specificities and with the same catalytic function. Dellomonaco and collaborators already demonstrated that the use of thioesterases can act upon the intermediates β-keto acyl-CoA, trans- β-hydroxyacyl-CoA, and trans-d2-enoyl-CoA. The

resulting products of these reactions are β-ketoacids, β-hydroxyacids, and trans-d2-fatty acids (Dellomonaco et al., 2011). This experimental work is extended in this chapter, using mathematical modeling, to the production of other products using the same or other intermediates of the reversal β-oxidation cycle. Figure 52 shows a diagram of the products that result from applying the termination pathways presented earlier in this chapter to produce n-alcohols, alkanes and fatty acids. Box 1 in Figure 52 shows synthesis of products from an acyl-CoA; box 2 shows synthesis of products from a β-keto acyl-CoA, box 3 shows synthesis of products from a trans-β-hydroxy acyl-CoA, and box 4 shows synthesis of products from a trans-Δ-enoyl-CoA.

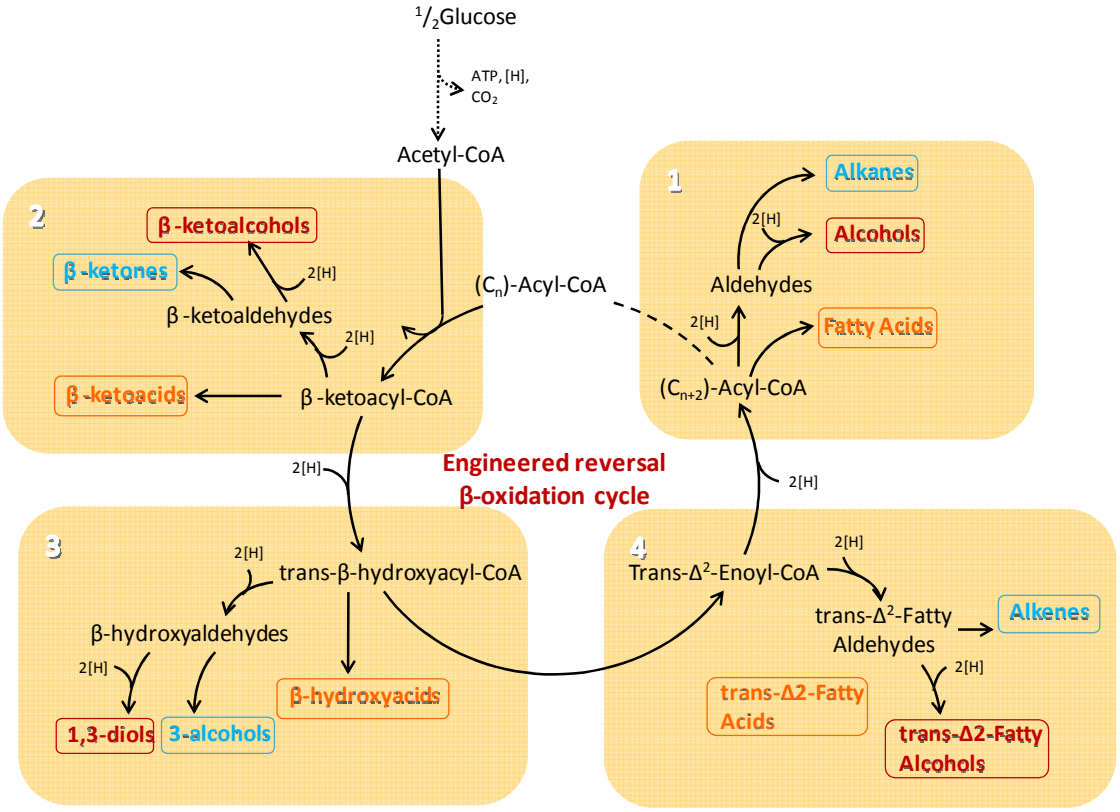

Figure 52: Production of long chain chemicals using the reversal of the β-oxidation cycle, starting from CoA intermediates. Four intermediates are used as inputs for the termination pathways: β-ketoacyl-CoA, trans- β-hydroxyacyl-CoA, trans-d2-fatty enoyl-CoA and acyl-CoA. Three set of termination pathways are implemented, each of them classified with a different color: red: alcohols termination, blue: alkane termination, and orange: carboxylic acid termination.

The mechanisms of the reactions involved in the termination pathways are the same mechanisms that were already presented using acyl-CoA as starting point. Thus, for the production of β-ketoalcohols, 1,3-diols and trans-d2-fatty alcohols, the termination pathway consists of two consecutive reductions performed by dehydrogenases, as presented in equations 66 and 68. Production of β-ketones, 3-alcohols and alkenes is achieved by the action of a decarbonylase as presented in equation 70. Production of β-ketoacids, β-hydroxyacids and trans-d2-fatty acids is achieved by hydroxylation of the thioester group of the starting metabolite, in the following way:

h2o + β-ketoacetyl-CoA → CoA + h + β-ketoacid (72)

h2o + trans-β-hydroxyaceyl-CoA → CoA + h + β-hydroxyacid (73)

h2o + trans-2-enoyl-CoA → CoA + h + trans-d2-fatty acid (74)

All these modifications were added to the iJO1366 model, and the results of adding these pathways are presented in the subsection 6.2.5 (*Synthesis of products with functionalized side chain*).

6.1.7.2 Strategy 2: Use hydroxylated and carboxylated primers

The final set of products that was evaluated using the functional reversal of the β-oxidation cycle consists of diols, hydroxyacids and dicarboxylic acids. The production of these products was simulated using a hydroxylated primer or a carboxylated primer, instead of using the original AcCoA as primer. Figure 53 shows a simplified diagram of the main reactions and pathways involved in this case, and corresponding reactions were added to the iJO1366 model when needed for the termination reactions and for the production of the primers.

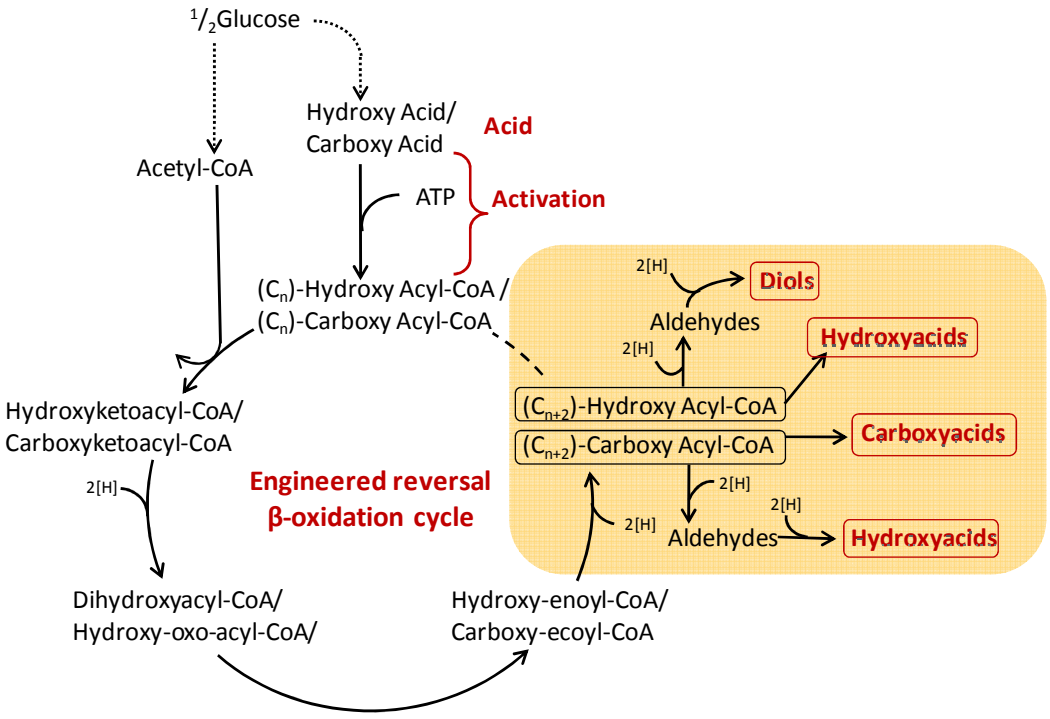

Figure 53: Simplified diagram of the use of hydroxylated and carboxylated primers in the reversal β-oxidation cycle to produce diols, hydroxyacids and dicarboxylic acids. Glucose is converted into a hydroxy acid (oxalate, malate and succinate) or a carboxy acid (hydroxy propionate and hydroxy propionate), and these molecules are activated using one molecule of ATP. The elongation of the molecule occurs using AcCoA.

This study evaluated the use of five primers that are CoA thioester derivatives: oxalyl-CoA, malonyl-CoA and succinyl-CoA, 4-hydroxybutyryl-CoA, and 3-hydroxypropionyl-CoA. Production of these primers can be achieved by activation of the corresponding hydroxy acid or carboxy acid. To this end, I first identified the primers and/or acids that the iJO1366 model can produce, and I found pathways for the production of the carboxylated primers oxalyl-CoA, malonyl-CoA, and succinyl-CoA. In the iJO1366 model, the production of oxalyl-CoA and succinyl-CoA is mediated by the activation of the corresponding acids: oxalate and succinate, respectively. The production of the hydroxylated primers 4-hydroxybutyryl-CoA and 3-hydroxypropionyl-CoA was

not part of any pathway in the iJO1366; therefore, their production was simulated in the model by extending existing pathways of the iJO1366 model.

The production of 4-hydroxybutyryl-CoA can be achieved by activating the hydroxy acid hydroxybutyrate, an intermediate molecule whose production is part of the iJO1366, into 3-hydroxypropionyl-CoA. This activation was simulated in the model by adding the reaction hydroxybutyryl-CoA synthetase, which is part of the 4-hydroxybutyrate cycle in some Archea (Berg et al., 2007), in the following way:

hydroxybutyrate + ATP + CoA → 4hydroxybutyryl-CoA + AMP + ppi (75)

The production of 3-hydroxypropionyl-CoA can be achieved by adding a 3-hydroxypropionyl-CoA synthase that converts the hydroxy acid 3-hydroxypropionate into the desired molecule. Since production of 3-hydroxypropionate is not part of the iJO1366 model, two pathways that would produce this molecule were added, following the diagram presented in Figure 54. Equations 76-80 show these reactions in detail, which correspond to malonyl-CoA reductase (eq. 76), hydroxypropionate:NADP+ oxidoreductase (eq. 77), glycerol dehydratase (eq. 78), 3-hydroxypropionaldehyde dehydrogenase (eq. 79) and 3-hydroxypropionate:CoA ligase (eq. 80). All of the reactions presented in equations 76-80 were added to the iJO1366 model by simulating the incorporation of exogenous genes encoding the proteins capable of performing these reactions (Berg et al., 2007; Daniel et al., 1998), and by adding the endogenous reaction 3-hydroxypropionaldehyde dehydrogenase (Jo et al., 2008).

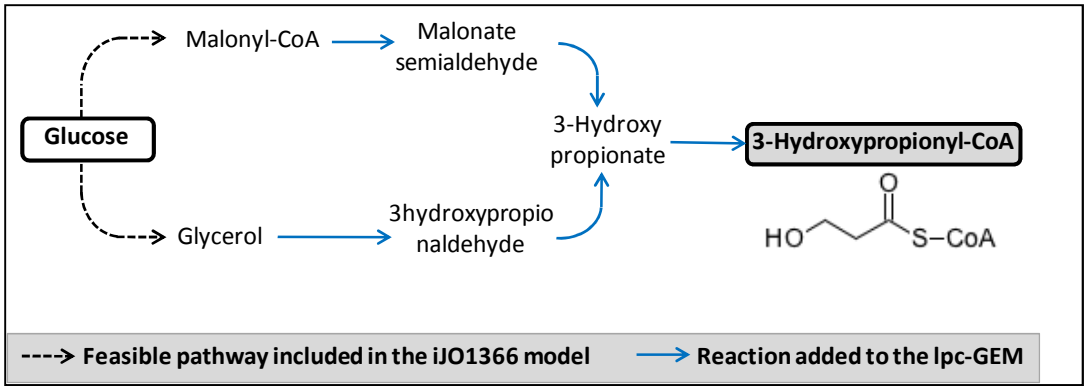

Figure 54: Addition of exogenous pathways in the iJO1366 model for the production of 3-hydroxypropionate (hydroxylated primer) and 3-hydroxypropionyl-CoA (activated primer) from glucose.

malCoA + NADPH + h → Malonate-semialdehyde + CoA + NADP (76)

Malonate-semialdehyde + NADPH + h → 3-hydroxypropionate + NADP (77)

glyc → 3-hydroxypropionaldehyde + h2o (78)

3-hydroxypropionaldehyde +NAD +h2o → 3-hydroxypropionate + NADH + 2 h (79)

3-hydroxypropionate + CoA + ATP → 3-hydroxypropionyl-CoA → ppi + amp. (80)

The next step consisted of the incorporating these primers into the reversal β-oxidation cycle reactions, as illustrated in Figure 53. The following equations represent the reactions for the incorporation of the primers:

hydroxyacetyl-CoA + AcCoA --> 4-hydroxyacetoacetyl-CoA + CoA (81)

3-hydroxypropionyl-CoA + AcCoA --> 5-hydroxy-3-oxopentanoyl-CoA +CoA (82)

4-hydroxybutyryl-CoA + AcCoA --> 6-hydroxy-3-oxohexanoyl-CoA + CoA (83)

oxaloacetyl-CoA + AcCoA --> 3-oxosuccinyl-CoA + CoA (84)

malonyl-CoA + AcCoA --> 3-oxoglutaryl-CoA + CoA (85)

succinyl-CoA + AcCoA --> 3-oxoadipyl-CoA + CoA. (86)

Finally, two termination pathways were incorporated into the model, starting from either a hydroxy-acyl-CoA or a carboxy-acyl-CoA (Figure 53). The first termination

pathway consists of two dehydrogenation steps toward the production of diols or hydroxyacids. The second termination pathway consists of a hydroxylation of the thioester group of the starting metabolite, resulting in the production of hydroxyacids or carboxyacids. It is important to note that the production of hydroxy acids was implemented in the model following two distinct pathways, as shown in Figure 53. The first pathway uses a hydroxylated primer to produce a hydroxyacyl-CoA in the reversal β-oxidation cycle, and then it converts the hydroxyacyl-CoA into a hydroxy acid by hydroxylation of the thioester group. The second pathway uses a carboxylated primer to produce a carboxyacyl-CoA in the reversal β-oxidation cycle, and then it converts the carboxyl-acyl-CoA into a hydroxy acid by two consecutive reductions. The use of FBA will identify the most efficient pathway.

All these reactions were added to the iJO1366 model in order to simulate the production of diols, hydroxyacids and dicarboxylic acids. The integration of both even and odd length primers enabled the simulated production of even and odd length chain products using the model. For the case of diols, the model was used to simulate production of all 1,n-diols from 4 carbon molecules (1,4-butanediol) to 18 carbon molecules (1,18-octadecanediol). For the case of hydroxyacids, the model was used to simulate all omega-hydroxyacids from 4 carbon molecules (4-hydroxybutyric acid) to 18 carbon molecules (18-hydroxyoctadecanoic acid). For the case of dicarboxylic acids, the model was used to simulate production of all omega dicarboxylic acids, from 4 carbon molecules (3-dicarboxylic propionic acid) to 18 carbon molecules (17-dicarboxylic heptadecanoic acid).

All the modifications presented in this section were added to the iJO1366 model. Appendix 10.3 shows a detail of the reactions that were added or removed. The resulting model is referred to as lcp-GEM in the rest of this chapter, where "lcp" stands for "long chain products". The following section (*Results*) shows the results of *in silico* simulations using the lcp-GEM for the production of alcohols, alkanes, FAs, and products with a functionalized side chain. Appendix 10.12 shows the Matlab function for the model lcp-GEM, and Appendices 10.13 and 10.14 show the Matlab functions for the GEM that simulates the synthesis of products with a functionalized chain.

6.2 Results: Production of alcohols, alkanes and fatty acids

The lcp-GEM was used in combination with FBA and FVA to predict production of long chain alcohols, alkanes, and FAs. In each case simulations were performed by allowing or deleting fermentative products. The deletion of native fermentation products was done to couple production of biomass to the desired product. For this purpose I considered the following as possible fermentative products: ethanol, lactate, acetate, succinate and acetate. Deletion of key enzymes was simulated by deleting the following reactions: ALDH (aldehyde dehydrogenase, *AdhE*), ADH (alcohol dehydrogenase, *adhE*), LDH_D (D-lactate dehydrogenase, *ldhA*), PTA2 (Phosphate acetyltransferase, *pta*), PTAr (phosphotransacetylase, *pta*), FRD2 (fumarate reductase, *frdA*, *frdB*, *frdC*, *frdD*), and FRD3 (fumarate reductase, *frdA*, *frdB*, *frdC*, *frdD*). In addition to these metabolic reactions, the following export reactions were deleted to ensure the eliminations of associated products: EX_ac(e) (for acetate), EX_PYR(e) (for pyruvate), and EX_hxa(e) (for hexanoate).

For the production of n-alcohols, simulations using the reversal β-oxidation cycle were contrasted against simulations using the FA biosynthesis pathway or the α-keto acid pathway. In a similar manner, for the production of alkanes and FAs, predictions using the reversal of the β-oxidation cycle were contrasted with predictions using the FA biosynthesis pathway.

All simulated solution spaces are presented for each product on carbon mole basis, in order to make the results comparable.

6.2.1 Production of alcohol

This section shows the simulated results for the production of alcohols using the reversal of the β-oxidation cycle, as well as the FA biosynthesis pathway and the α-keto acid pathway. The predicted performances of these three pathways were compared. In each case the solution space was simulated by allowing or deleting possible native fermentation products.

6.2.1.1 Use of the reversal β-oxidation cycle

Figure 55-A shows the predicted solution space associated with the production of alcohols using the reversal of the β-oxidation cycle. In each case the optimal specific growth rate was 0.39 h^{-1}, and the main products were acetate (11.7 mmol/gCDW/h) and ethanol (12.3 mmol/gCDW/h). Production of butanol and other longer chain alcohols was not found in the optimal solution, indicating that the native products (acetate and ethanol in this case) support a higher production of biomass than production of longer chain alcohols using the reversal of the β-oxidation cycle. Deletion of native fermentation products as explained above resulted in production of all alcohols considered in this study

coupled to cell growth (Figure 55-B), with an optimal growth rate equal to 0.26 ± 0.2 h^{-1}, and an alcohol production rate of 51.9 ± 0.5 mmol-C/gCDW/h (see Table 13 for more detailed values). Titers were calculated for all alcohols over a period of 24 hours (Table 13). See Appendix 10.8 for calculation of titers.

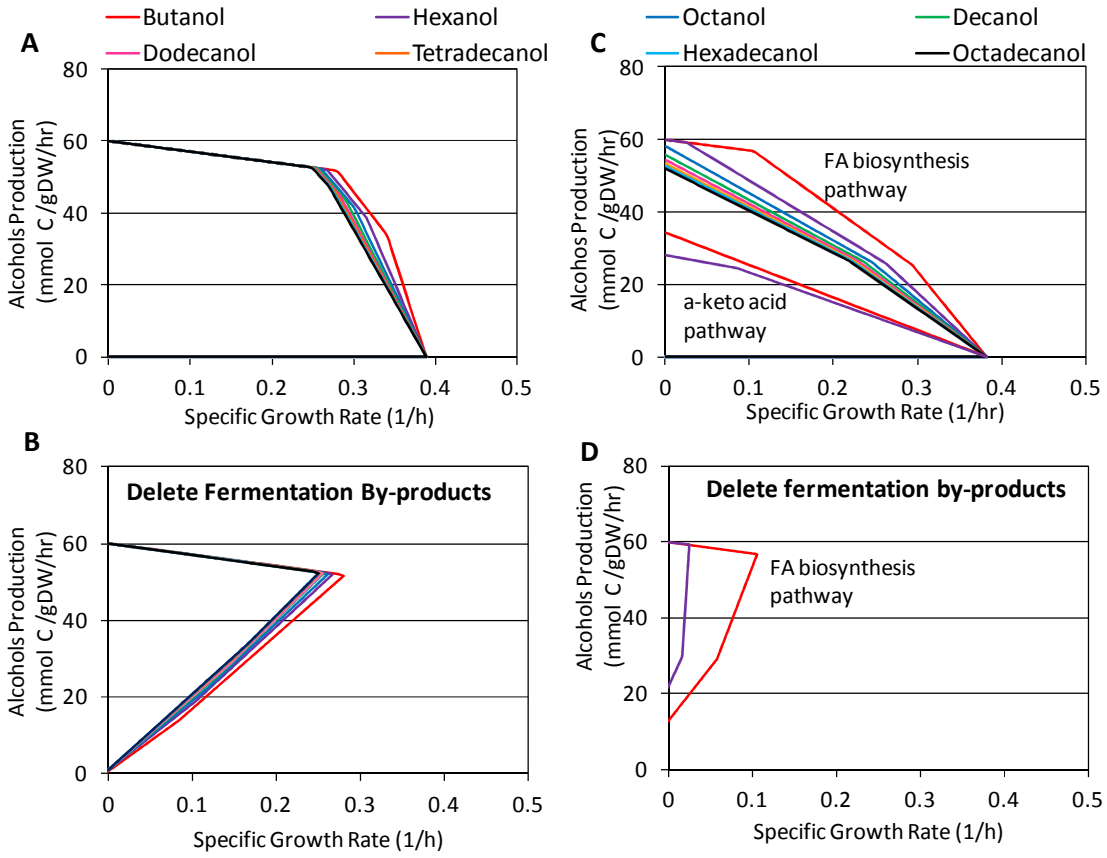

Figure 55: Predicted solution space for the production of alcohols using the reversal of the β-oxidation cycle (A, B), the FA biosynthesis pathway (C,D), and the α-keto acid pathway (C). Results are shown before deleting native fermentation products (A, C) and after simulating deletion of native fermentation products ethanol, acetate, lactate and succinate (B, D). There was no production of alcohols after deleting native fermentation products when the α-keto acid pathway was used.

Table 13: Model predictions for specific growth rate, production rate and titers. Production of alcohols using the reversal of the β-oxidation cycle, after blocking synthesis of native fermentation products.

Flux - Alcohols	C-4	C-6	C-8	C-10	C-12	C-14	C-16	C-18
Specific growth rate (1/h)	0.28	0.27	0.26	0.26	0.25	0.25	0.25	0.25
Production rate (mmol C/gDW/h)	51.4	51.8	52.0	52.1	52.2	52.2	52.3	52.3
Titer 24 hr (mol C/L)	152.9	118.0	103.6	95.8	90.9	87.6	85.2	83.3

Production of alcohols using the reversal of the β-oxidation cycle is redox balanced as expected; hence, no additional by-products were predicted as necessary to achieve redox balance. The expected amount of ATP produced in association with the production of alcohols using this pathway is presented in equation 87 (see details of calculations in Appendix 10.7):

$$n\ Glucose \rightarrow \frac{4n}{m}\ Alcohol\_Cm + 2n\ ATP, \quad (87)$$

where 'n' is the flux of glucose, 'm' is the number of carbons in the product, and Alcohol_Cm is the product (example: Alcohols_C8 is octanol). Since ATP production is independent of the produced alcohol, the model was expected to predict the same optimal solution for cell growth and production rate (per unit of carbon). However, although simulations in the production of all alcohols produced very similar solution spaces, production of shorter chain alcohols were simulated to allow a slightly higher specific growth rate (Figure 55-A,B). Analysis of flux distribution indicates that there is a connection between these minor differences and changes in flux distribution at the pyruvate node. Table 14 shows the flux distribution at the pyruvate node for the production of alcohols with different chain length. The longer the alcohol chain, the bigger the flux through PFOR and the smaller the flux through pyruvate dehydrogenase (PDH). This is because the redox balance is achieved in the two reduction steps of the reversal β-oxidation pathway plus the two reduction steps of the termination reactions. Consequently, a longer chain alcohol is associated with a smaller production per mole of product base and therefore more reducing equivalents are consumed in the cycle than in the termination steps. Since half of the reducing equivalents consumed in the β-oxidation cycle comes from ferredoxins, a higher consumption of reducing equivalents requires a

higher flux of ferredoxins to be oxidazed in the reaction PFOR. Considering that the reaction PFOR results in the generation of one proton (Charon et al., 1999), and that the reaction PDH was included in the iJO1366 without production of protons, the different flux distributions at the pyruvate node generate different production of protons. These protons under fermentative conditions need to be exported in order to maintain proton concentration inside the cell, a process that is catalyzed by the enzyme ATPase and that consumes energy (Cain & Simoni, 1989). Thus, simulation of the production of longer chain alcohols results in a slighter higher requirement of energy, which in turn lowers the efficiency in production of biomass. However, this situation may change if the enzyme PDH is modeled producing protons, as has been presented elsewhere (Bates et al., 1977), in which case both reactions (PFOR and PDH) would produce the same amount of protons.

Table 14: Analysis of flux partitioning at the pyruvate node and corresponding differences in specific growth rate during alcohol synthesis through the β-oxidation reversal. Abbreviations: PFOR (pyruvate ferredoxins oxidoreductase), PDH (pyruvate dehydrogenase), and PFL (pyruvate formate lyase).

Pyruvate Node	Alcohols							
(rates normalized with glucose rate)	C-4	C-6	C-8	C-10	C-12	C-14	C-16	C-18
PFOR	0.90	1.19	1.34	1.43	1.49	1.53	1.56	1.59
PDH	0.83	0.55	0.41	0.32	0.26	0.22	0.19	0.17
PFL	0.07	0.07	0.06	0.06	0.06	0.06	0.06	0.06

6.2.1.2 Use of the FA biosynthesis pathway

Figure 55-C shows the predicted solution space associated with the production of alcohols using the FA biosynthesis pathway. In each case the optimal specific growth rate was 0.38 h^{-1}, and the main products were acetate (12.2 mmol/gCDW/h) and ethanol (11.9 mmol/gCDW/h). Production of butanol and other longer chain alcohols was not found in the optimal solution, indicating that the native products (acetate and ethanol in this case)

support a higher production of biomass than production of longer chain alcohols using the FA biosynthesis pathway. Deletion of native fermentation products resulted in production of only butanol and hexanol coupled to cell growth (Figure 55-D). Values of simulated specific growth rate, production rate and titers after deleting native fermentation products are presented in Table 15. For the production of octanol and all other longer chain alcohols, the presence of by-products is predicted to be essential based on these results, which will reduce the yield of the desired alcohols.

Table 15: Model predictions for specific growth rate, production rate and titer during production of alcohols using the FA biosynthesis pathway, after deleting production of native fermentation products.

Flux - Alcohols	C-4	C-6
Specific growth rate (1/h)	0.11	0.03
Production rate (mmol C/gDW/h)	56.74	59.22
Titer 24 hr (mol C/L)	6.24	1.95

The simulated results using the FA biosynthesis pathway were compared to simulated results using the reversal of the β-oxidation cycle. Based in these simulations, the specific growth rates after deleting native fermentation products are predicted to be considerably smaller using the FA biosynthesis pathway (for butanol and hexanol), but the production rates are predicted to be slightly higher. The titer represents the total production of alcohols at the maximal specific growth rate after a period of time, and therefore it is a better parameter to compare both platforms. Over a period of time of 24 hours, predicted titers using the reversal of the β-oxidation cycle are 25 and 60 times higher that the predicted titers using the FA biosynthesis pathway for the production of butanol and hexanol, respectively. These results highlight the supremacy of the reversal β-oxidation cycle over the FA biosynthesis pathway for the production of alcohols.

The absence of other alcohols upon deletion of by-products using the FA biosynthesis pathway was unexpected, as theoretical analysis indicates that this pathway should produce ATP according to the following formula:

$$n\ Glucose \rightarrow (^{4n}/_{m})\ Alcohol\_Cm + (^{4n}/_{m})\ ATP, \quad (88)$$

where "m" is the number of carbon molecules in the product, and $n \leq 4m$. Detailed calculations are shown in Appendix 10.7. Therefore, for a glucose uptake rate of 15 mmol/gCDW/h, a maximal production of alcohols is associated with production of 60/m molecules of ATP (with m = 4 to 18), which is greater than the ATP required for maintenance (ATPM = 3.15 mmol/gCDW/h). However, analysis of flux distribution identified that in addition to the ATPM requirement, ATP is required to maintain pH homeostasis, a process in which protons are transported across the membrane and energy is consumed under fermentative conditions (Kasimoglu et al., 1996). This was identified by observing a significant and essential flux through the reversible enzyme ATP synthase in the lcp-GEM. Since production of butanol and hexanol using the FA biosynthesis pathway produces more ATP than production of octanol and other longer chain alcohols, only production of butanol and hexanol allowed satisfying the energetic requirements for ATPM and proton transport. Addition of a fictitious source of ATP resulted in production of longer chain alcohols. For example, Figure 56 shows the predicted flux distribution associated with the production of octanol using the FA biosynthesis pathway, adding a fictitious source of ATP, blocking the synthesis of native fermentation products. This example shows that the main sources of cytoplasmic protons is glycolysis, the termination pathway, and the conversion of NADH/NADP into NAD/NADPH. The addition of a fictitious source of ATP to the model allows the production of all other

alcohols using the FA biosynthesis pathway after deleting native fermentation products, supporting the conclusion that the ATP requirements for cell growth and cellular maintenance is preventing the efficient production of longer chain alcohols.

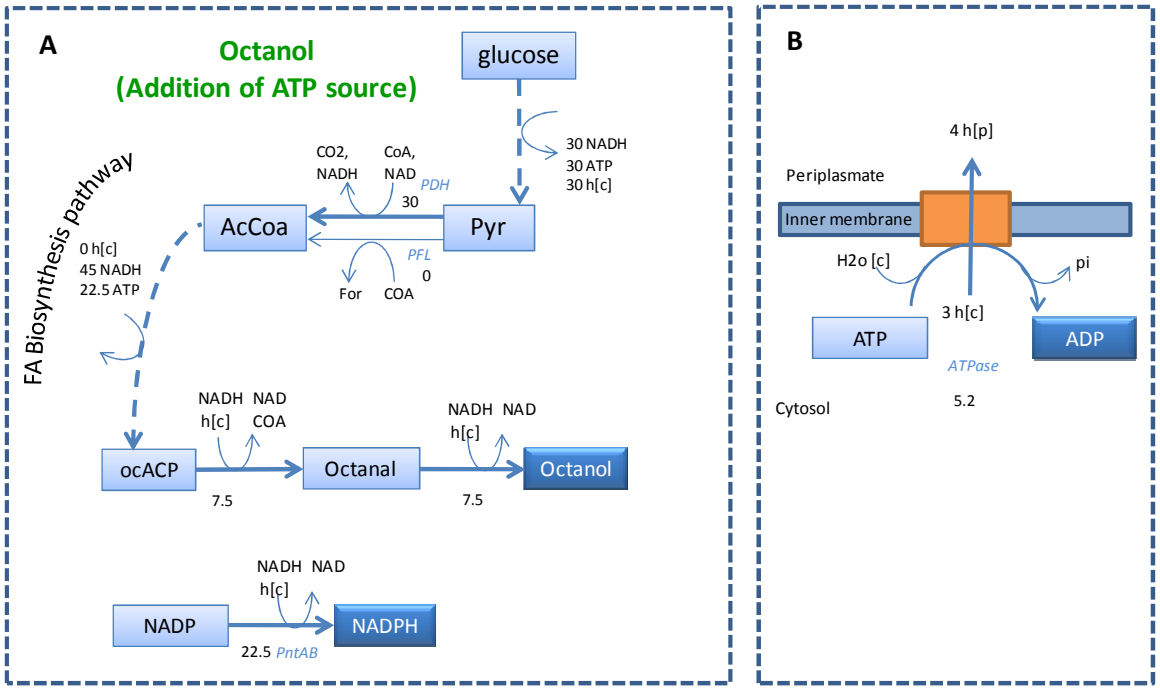

Figure 56: ATP requirements to maintain pH homeostasis (proton transport) during octanol synthesis via the FA biosynthesis pathway. A fictitious source of ATP was considered in the simulations.. FBA was used with octanol synthesis as the objective function. This figure includes the flux distribution from glucose to octanol (A), showing the production of protons, as well as the mechanism for proton transport across the membrane (B). Protons in the cytoplasm are called h[c], and protons in the periplasm are called h[p]. The overall balance for the production of octanol through the FA synthesis pathway is: ATP: 7.5; h[c]: 15; NADH: balance (A). See Nomenclature for details (page 214).

6.2.1.3 Use of the α-keto acid pathway

Figure 55-C shows the predicted solution space associated with the production of alcohols using the α-keto acid pathway. The optimal specific growth rate for the wild-type scenario was 0.38 h^{-1}, and the main products were acetate (12.2 mmol/gCDW/h) and ethanol (11.9 mmol/gCDW/h). Production of butanol and hexanol were not found in the optimal solution, indicating that the native products (acetate and ethanol in this case)

support a higher production of biomass than production of longer chain alcohols using the α-keto acid pathway. The solution space using this pathway is considerably smaller than the solution space for the same products using the FA biosynthesis pathway, or the reversal β-oxidation pathway.

Deletion of native fermentation products resulted in production of neither butanol nor hexanol using this pathway, indicating their requirement for pathway functioning. These simulations correlate well with experimental data, in which the strategies for production of 1-butanol include production of by-products, such as acetate (Shen & Liao, 2008). The analysis of the theoretical maximum production yield of butanol and hexanol allows the identification of the necessity for other fermentative products. The overall balance for production of alcohols, including ATP and reducing equivalents, and using the pathway presented by Shen et al., and Marcheschi et al. (Marcheschi et al., 2012; Shen & Liao, 2008) are as follows:

$$n\ \text{Glucose} + 2n[H] + n\ \text{ATP} \rightarrow n\ \text{butanol} + n\ \text{formate} \quad (89)$$

$$n\ \text{Glucose} \rightarrow n/2\ \text{Hexanol} + n/2\ \text{ATP} + n\ [H] + n\ \text{formate}, \quad (90)$$

where ‘n’ is the flux of glucose, ‘m’ is the number of carbons in the product, and [H] represents reducing equivalents (see Appendix 10.7 for details). The simulated flux distribution using FBA and the lcp-GEM supports these overall balances. Equation (89) shows that production of butanol consumes ATP, making imperative the production of an additional by-product that would result in an overall production of ATP. In addition, the consumption of reducing equivalents associated with the production of butanol requires the production of an additional by-product that produces reducing equivalents. Equation (90) shows that production of hexanol using the α-keto acid pathway produces reducing

equivalents and ATP. While the production of ATP would support the exclusive use of this pathway for cell growth, the high amount of reducing equivalents that would be generated would overcome the capacity to consume reducing equivalents associated with cell growth when using glucose as carbon source, making the production of additional fermentative products necessary to balance the reducing equivalents and to produce ATP in the case of butanol synthesis. Therefore, the *in silico* analysis using the lcp-GEM, as well as theoretical analysis using the overall pathway, indicate that production of butanol and hexanol using the α-keto acid pathway is less attractive than using the previously discussed pathways (reversal β-oxidation cycle and FA biosynthesis pathway), as essential production of by-products results in reducing the maximal theoretical yields.

6.2.2 Production of alkanes

This section shows the simulated results for the production of alkanes using the reversal β-oxidation cycle. In order to contrast performance, production of alkanes using the FA biosynthesis pathway was also simulated. In each case the solution space associated with each alkane was simulated allowing or deleting the synthesis of native fermentation products.

6.2.2.1 Use of the reversal of the β-oxidation cycle

The results of the predicted solution space associated with the production of alkanes using the reversal of the β-oxidation cycle are presented in Figure 57-A. Production of all alkanes is simulated by introducing a decarbonylase enzyme in the termination steps. Results for the production of alkanes is presented per unit on carbon mole basis “plus 1”, which make alkanes of all lengths comparable to each other. As with

the case of alcohols production, the predicted optimal solutions were not associated with the production of any alkane prior to deleting native fermentation products. Deletion of native fermentation products resulted in the production of all alkanes considered in this study coupled to cell growth (Figure 57-B), with an optimal growth rate equal to 0.24 h^{-1} in all cases. Table 16 shows predicted production rates and titers.

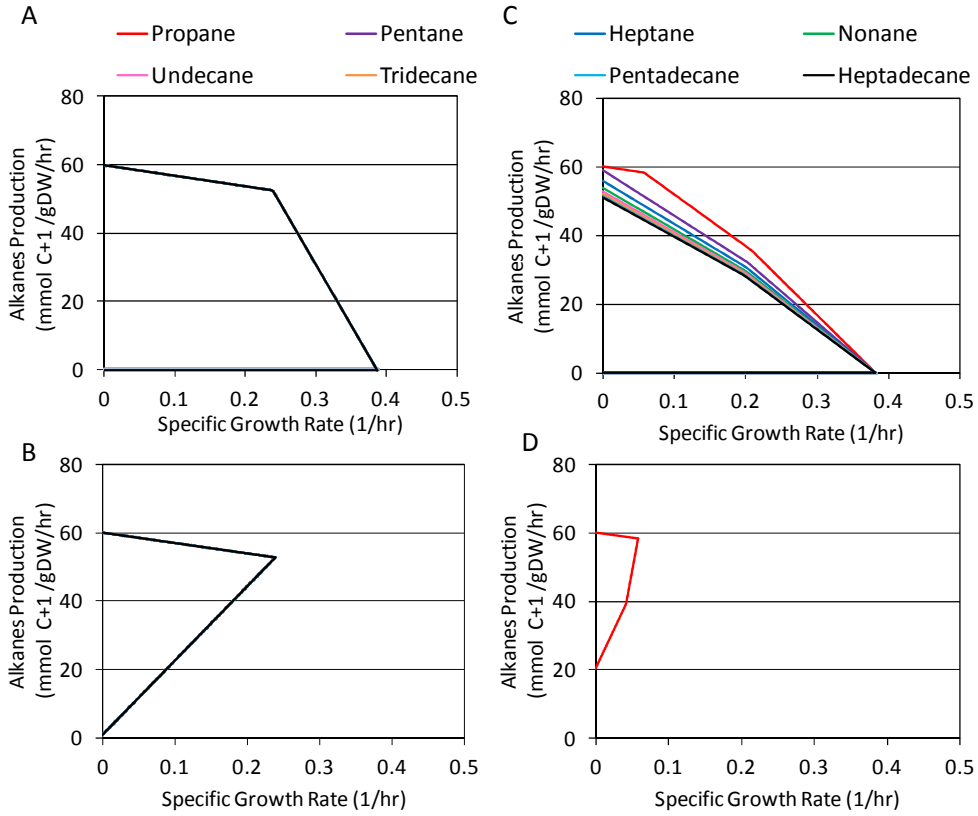

Figure 57: Predicted solution space for the production of alkanes using the reversal of the β-oxidation cycle (A, B) and the FA biosynthesis pathway (C,D). Results are shown before deleting native fermentation products (A, C) and after simulating the deletion of ethanol, acetate, lactate and succinate (B, D). For comparison purposes, all productions rates are plotted on carbon mole basis + 1.

Table 16: Model predictions of specific growth rate, production rate and titer. Production of alkanes using the reversal of the β-oxidation cycle, after blocking synthesis of native fermentation products.

Flux - Alkanes	C-3	C-5	C-7	C-9	C-11	C-13	C-15	C-17
Specific growth rate(1/h)	0.24	0.24	0.24	0.24	0.24	0.24	0.24	0.24
Production rate (mmol C/gDW/h)	39.5	43.9	46.1	47.4	48.3	48.9	49.4	49.7
Titer 24 hr (mol C/L)	51.2	56.9	59.8	61.5	62.6	63.4	64.0	64.5

To achieve redox balance the reversal β-oxidation cycle is combined with the conversion of PYR into AcCoA using the enzyme PFL (Table 14), which produces formate and not reducing equivalents. The conversion of glucose into an alkane produces ATP independently of the carbon chain length of the product, and the maximal theoretical equation for the production of alkanes is as follows (see Appendix 10.7 for details):

$$n\ \text{Glucose} \rightarrow (4n/m)\ \text{Alkane\_Cm-1} + 2n\ \text{ATP} + 4n/m\ \text{formate}, \qquad (91)$$

where 'n' is the flux of glucose, 'm' is the number of carbons in the product, and Alkane_Cm-1 is the product (example: Alkane_C7 is heptane). It is interesting to note that, unlike the case of alcohols productions, productions of all the alkanes coincide in the optimal solution (specific growth rate and production rate on carbon mole basis "plus 1"), which is explained by the fact that the different products are associated with the same protons production, and therefore there are no changes in the energetic requirements.

Table 17 shows the flux distribution at the pyruvate node for the production of alkanes with different chain length. The total flux is distributed between enzymes PFOR and PFL, and only PFOR produces reducing equivalents (as reduced ferredoxins). The longer the alkane chain, the bigger the flux through PFOR and the smaller the flux through PFL. This is because the redox balance is achieved in the two reduction steps of the reversal β-oxidation pathway plus the reduction step of the termination reactions. Consequently, a longer chain alkane is associated with a smaller production per mole of product base and therefore more reducing equivalents are consumed in the cycle than in the termination steps. Since half of the reducing equivalents consumed in the β-oxidation cycle come from ferredoxins, a higher consumption of reducing equivalents requires a higher flux of ferredoxins to be oxidized in the reaction PFOR. When compared with the

pyruvate node for the production of alcohols (Table 14), fluxes through PFOR are very similar, and the main change is in the use of PFL instead of PDH. This is because alkanes are less reduced than alcohols; therefore, a lower production of reducing equivalents at the pyruvate node enables a redox balanced system.

Table 17: Analysis of flux partitioning at the pyruvate node and corresponding differences in specific growth rate during alkane synthesis through the β-oxidation reversal. Abbreviations: PFOR (pyruvate ferredoxins oxidoreductase), PDH (pyruvate dehydrogenase), and PFL (pyruvate formate lyase).

Pyruvate Node	Alkanes							
(rates normalized with glucose rate)	C-3	C-5	C-7	C-9	C-11	C-13	C-15	C-17
PFOR	0.91	1.20	1.34	1.43	1.49	1.53	1.56	1.59
PDH	0.00	0.00	0.00	0.00	0.00	0.00	0.00	0.00
PFL	0.91	0.62	0.47	0.38	0.32	0.28	0.25	0.23

6.2.2.2 Use of the FA biosynthesis pathway

Figure 57-C shows the predicted solution spaces associated with the production of alkanes using the FA biosynthesis pathway. As in the case of alcohols production, the simulated optimal specific growth rate is 0.38 h^{-1}, and at the optimal solution there is no production of alkanes. The main products were acetate (12.2 mmol/gCDW/h) and ethanol (11.9 mmol/gCDW/h). Upon deletion of native fermentation products, only propane synthesis was predicted to be feasible and coupled to cell growth (Figure 57-D). Values of simulated specific growth rate, production rate and titer after deleting native fermentation products are presented in Table 18.

Table 18: Model predictions of specific growth rate, production rate and titer for the synthesis of alkanes using the FA biosynthesis pathway, after deleting production of native fermentation products. Propane is predicted to be the only feasible product.

Flux - Alkanes	C-3
Specific growth rate(1/h)	0.06
Production rate (mmol C/gDW/h)	43.7
Titer 24 hr (mol C/L)	2.28

A theoretical analysis of the production of alkanes using the FA biosynthesis pathway indicates that the production of ATP decreases with longer chain products, which explains why propane is the only product observed after simulating the deletion of native fermentation products. The overall equation for the maximal theoretical yield for the production of alkanes is as follows (see Appendix 10.7 for details):

$$n\ Glucose \rightarrow (4n/m)\ Alkane\_Cm\text{-}1 + (^{4n}/_{m})\ ATP + 4n/m\ formate, \quad (92)$$

where 'n' is the flux of glucose, 'm' is the number of carbons in the product and Alkane_Cm-1 is the product (example: Alkane_C3 is propane).

The simulated results using the FA biosynthesis pathway were compared to simulated results using the reversal of the β-oxidation cycle. The predicted solution space associated with the production of alkanes suggests higher production rates when the reversal of the β-oxidation cycle is used (Figure 57), both before and after deleting native fermentation products.

After deleting native fermentation products, the use of the FA biosynthesis pathway supports production of only propane, while the use of the reversal of the β-oxidation cycle supports production of all alkanes that were considered in this study. For the production of propane, the specific growth rate after blocking the synthesis of native fermentation products is predicted to be considerably smaller using the FA biosynthesis pathway (0.06 h^{-1} versus 0.24 h^{-1}), while the production rate is predicted to be slightly higher using the FA biosynthesis pathway (43.7 versus 39.5 mmol C/gCDW/h). Over a period of 24 hours, the predicted titer for propanol using the reversal of the β-oxidation cycle was 22 times higher than the predicted titer using the FA biosynthesis pathway, which highlights the supremacy of the reversed β-oxidation cycle. As in the case of

alcohol production, the inability of this pathway to produce longer chain alkanes is due the inability to satisfy ATP energetic requirements.

6.2.3 Production of fatty acids

The production of FAs was simulated using the reversal β-oxidation cycle implemented in the lcp-GEM. In order to contrast performance, the synthesis of FAs through the FA biosynthesis pathway was also simulated. In each case the solution space associated with each fatty acid was simulated in otherwise wild-type *E. coli* as well as a strain devoid of native fermentation pathways.

6.2.3.1 Use of the reversal β-oxidation cycle

Production of FAs was simulated using the reversal of the β-oxidation cycle, and the predicted solution spaces are presented in Figure 58-A. As in previous cases, the solutions for optimal specific growth rate were not associated with the production of any of the FAs included in this study. Instead, the optimal specific growth rate is associated with production of acetate and ethanol. When the synthesis of native fermentation products is blocked, the resulting solution spaces show coupling between FA production and the specific growth rate, making the production of FAs essential (Figure 58-B). Interestingly, the optimal solution is coupled to the production of 1,2-PDO in rates from 1.56 mmol/gCDW/h (for octadecanoate production) to 5.71 mmol/gCDW/h (for butyric acid production).

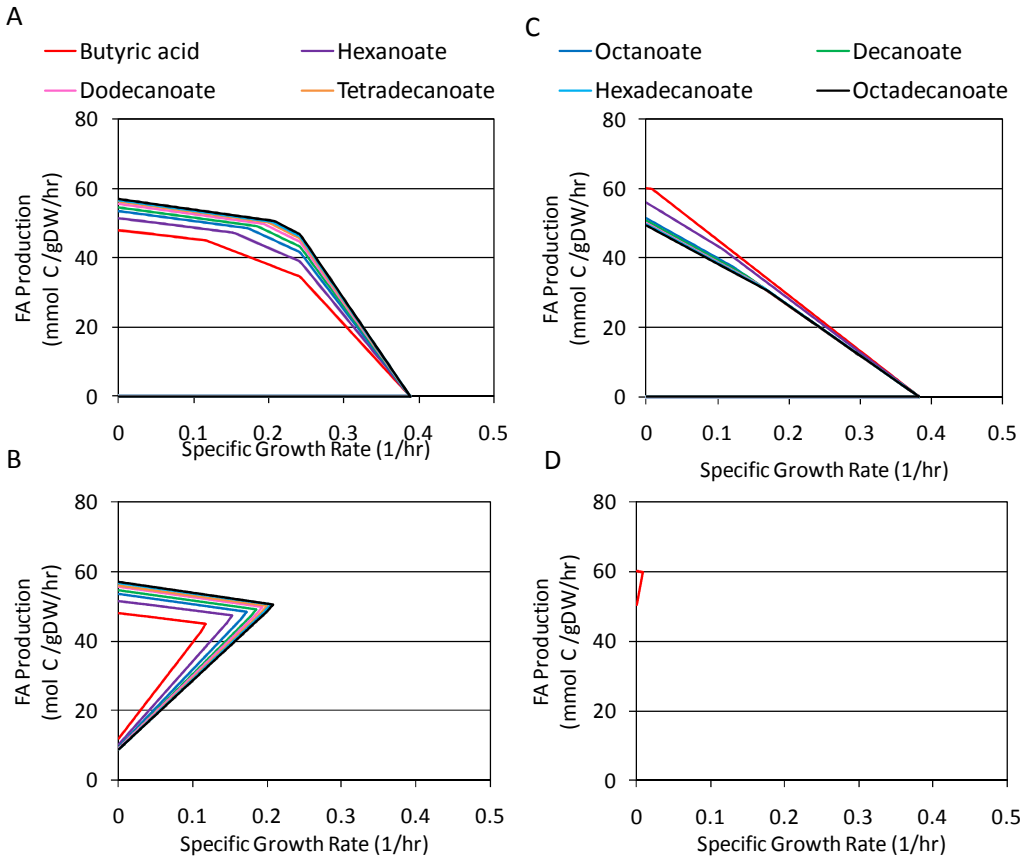

Figure 58: Solution space for the synthesis of fatty acids using reversal β-oxidation cycle (A, B) and FA biosynthesis pathway (C, D). Results are shown for both wild-type *E. coli* (A, C) and an engineered strain where pathways for native fermentation products ethanol, acetate, lactate and succinate were eliminated (B, D).

Table 19 shows simulated values for specific growth rate, production rate and titer associated with the optimal solution after the sysnthesis of native fermentation products was eliminated. The longer the carbons chain in the product, the higher the specific growth rate, the production rate, and the titer.

Table 19: Model predictions of specific growth rate, production rate and titer. Production of FAs using the reversal of the β-oxidation cycle, after blocking synthesis of native fermentation products.

Flux - Fatty acids	C-4	C-6	C-8	C-10	C-12	C-14	C-16	C-18
Specific growth rate(1/h)	0.12	0.15	0.17	0.18	0.19	0.20	0.20	0.21
Production rate (mmol C/gDW/h)	45.0	47.2	48.4	49.1	49.6	50.0	50.3	50.5
Titer 24 hr (mol C/L)	6.0	11.8	17.4	22.1	26.2	29.6	32.6	35.1

The differences in production rate and specific growth rate predicted for the different FAs can be explained by examining reactions that consume and produce

reducing equivalents. Table 14 shows that the conversion of PYR into AcCoA uses enzymes PFL, which does not produce reducing equivalents, and PFOR, which reduces ferredoxins. As in the production of alkanes, no flux goes through the enzyme PDH to prevent production of reducing equivalents in the form of NADH. Because the reversal of the β-oxidation cycle oxidizes reduced ferredoxins in the reduction of enoyl-CoA, an equivalent flux of ferredoxins needs to be reduced using the enzyme PFOR and, therefore, the only way to achieve redox-balance is through the production of a more reduced by-product. Simulations of the production of FAs, unlike the production of alcohols and alkanes, results in the production of the by-product 1,2-PDO, which acts as an electron sink in this process. The overall balance to produce FAs from glucose is presented in Appendix 10.7, and the resulting equation is as follows:

$$n\ Glucose = \frac{4n}{m+1} FA\_Cm + 2n\left(\frac{m-1}{m+1}\right) ATP + \frac{2n}{m+1} 1{,}2PDO + \frac{4n}{m+1} formate \qquad (93)$$

where 'n' is the flux of glucose and 'm' is the number of carbons in the product. Equation 93 shows that the longer the chain in the product (m), the smaller the production of 1,2-PDO, and the greater the production of ATP. Simulated results support this analysis, as production of longer chain FAs after deleting native fermentation products was associated with a smaller production of 1,2-PDO. Less production of the by-product 1,2-PDO and a higher production of ATP in turn support a higher production of biomass and of the desired product. Thus, this analysis explains the findings presented in Figure 58-A,B, in which production of longer chain FAs was predicted to result in higher specific growth rate and in higher production rates using the lcp-GEM.

Table 16 shows the flux distribution at the pyruvate node for the production of FAs with different chain length. As in the case of alkanes production, the total flux is

distributed between enzymes PFOR and PFL, and only PFOR produces reducing equivalents (as reduced ferredoxins). A longer chain FA is associated with a smaller production per mole of product base and therefore more reducing equivalents are consumed in the cycle than in the termination steps, which results in a larger flux through PFOR and a lower flux through PFL. Since half of the reducing equivalents consumed in the β-oxidation cycle come from ferredoxins, a higher consumption of reducing equivalents requires a higher flux of ferredoxins to be oxidized in the reaction PFOR. When compared with the pyruvate node for the production of alkanes (Table 14), fluxes through PFOR and PFL are smaller due to the fact that part of the glycolytic flux is being directed toward the production of 1,2-PDO to achieve redox balance.

Table 20: Analysis of flux partitioning at the pyruvate node and corresponding differences in specific growth rate during FA synthesis through the β-oxidation reversal. Abbreviations: PFOR (pyruvate ferredoxins oxidoreductase), PDH (pyruvate dehydrogenase), and PFL (pyruvate formate lyase).

Pyruvate Node	Fatty acids							
(rates normalized with glucose rate)	C-4	C-6	C-8	C-10	C-12	C-14	C-16	C-18
PFOR	0.77	1.07	1.23	1.34	1.41	1.46	1.50	1.53
PDH	0.00	0.00	0.00	0.00	0.00	0.00	0.00	0.00
PFL	0.77	0.55	0.43	0.35	0.30	0.27	0.24	0.22

6.2.3.2 Use of the FA biosynthesis pathway

Figure 58-C shows the predicted solution space associated with the production of FAs using the FA biosynthesis pathway. As in previous cases, the simulated optimal specific growth rate for otherwise wild type *E. coli* is 0.38 h^{-1}, with acetate and ethanol as main products, and no production of FAs at the optimal solution. Blocking the synthesis of native fermentation products led to coupling between product synthesis and cell growth only for the case of butyric acid (Figure 58-D). Values of simulated specific

growth rate, production rate and titer after blocking the synthesis of native fermentation products are presented in Table 21.

Table 21: Model predictions of specific growth rate, production rate and titer for production of FAs using the FA biosynthesis pathway after blocking synthesis of native fermentation products. Butyric acid is predicted to be the only feasible product.

Flux - Fatty acids	C-4
Specific growth rate (1/h)	0.01
Production rate (mmol C/gDW/h)	59.74
Titer 24 hr (mol C/L)	1.59

As in the case of alcohols and alkanes production, the production of longer chain FA decreases production of ATP, which explains why butyric acid is the only product observed after simulating the deletion of native fermentation products. The overall equation for the maximum theoretical yield for the production of FA is as follows (see Appendix 10.7 for details):

$$n\ \text{Glucose} \rightarrow (4n/m)\ \text{FA\_Cm} + (4n/m)\ \text{ATP} + 8n/m\ \text{formate}, \qquad (94)$$

where 'n' is the flux of glucose, 'm' is the number of carbons in the product and FA_Cm is the product (example: FA_C8 is octanoic acid).

The performance of the FA biosynthesis pathway for the production of FAs was compared with the performance of the β-oxidation cycle. The predicted solution spaces (before blocking the synthesis of native fermentation products) show higher production rates when the reversal β-oxidation cycle is used (Figure 58-A,C) for most products and for most specific growth rates. The only exceptions are the production of butyric acid and hexanoic acid, whose production rates are predicted to be slightly higher in the FA biosynthesis pathway than in the reversal of the β-oxidation cycle in the area close to null growth (see solution space in Figure 58-A,C at specific growth rates less than 0.10 h^{-1} for butyric acid and less than 0.04 h^{-1} for hexanoic acid).

After blocking the synthesis of native fermentation products, the simulations predict that only production of butyric acid is feasible using the FA biosynthesis pathway, while the use of the reversal β-oxidation cycle predicts production of all FAs that were considered in this study. For the production of butyric acid, the specific growth rate after blocking the synthesis of fermentation products is predicted to be considerably smaller using the FA biosynthesis pathway (0.01 h^{-1} versus 0.12 h^{-1}), while the production rate is predicted to be 33% higher using the FA biosynthesis pathway (14.9 versus 11.2 mmol /gCDW/h). Over a period of 24 hours, the predicted titer for propanol using the reversal of the β-oxidation cycle was 4 times higher than the predicted titer using the FA biosynthesis pathway. As in the previous cases, the inability of this pathway to produce longer chain alkanes is due the inability to satisfy energetic requirements.

6.2.4 Comparison of engineered β-oxidation reversal using ferredoxin- and NADH-dependent acyl-CoA dehydrogenases/trans-enoyl-CoA reductases.

The previous three sections of this chapter simulated the production of alcohols, alkanes and FAs using the reversal of the β-oxidation cycle, a platform that was simulated using endogenous enzymes to *E. coli*. Motivated by the unique constraint imposed on the pathway by the oxidation/reduction of ferredoxins, I decided to study the effect of changing the endogenous acyl-CoA dehydrogenase, a key enzyme of the pathway which is associated with ferredoxins (Dellomonaco et al., 2011), for an exogenous acyl-CoA dehydrogenase associated with NADH, such as the one from *Euglena gracilis* (Hoffmeister et al., 2005). The use of this enzyme should then release the constraint imposed by the ferredoxin balance. Simulation of alcohol, alkane and FA

synthesis using this pathway in otherwise wild-type *E. coli* predicted an optimal specific growth rate equal to 0.39 h^{-1}, and none of the aforementiones products was synthesized in the optimal solution. As in previous cases, blocking the synthesis of native fermentation products resulted in the coupling of each of the desired products to biomass production. Table 22 shows a summary of results for the production of short chains and long chain products, for alcohols, alkanes and FAs, after blocking the synthesis of native fermentation products. In all cases an increase in the specific growth rate was observed when compared to the use of the ferredoxin-dependent acyl-CoA dehydrogenase. In the case of production of alcohols and alkanes, the increase in the specific growth rate is contrasted with a small decrease in the production rate (less than 5%), and an increase in all titers of 20% or more (Table 22). For the production of FAs, the use of a NADH-dependent acyl-CoA dehydrogenase predicts an increase in the production rate of desired products, especially in those of shorter chain. For example, the production rate of butyric acid is simulated to increase from 11.2 to 13.1 mmol/gCDW/h. These increases in production rates, together with the increase in specific growth rate, result in an increase of the titer for the different products from 6 times (for octadecanoic acid) to 11 times (for butyric acid) (Table 22). The major contribution for the increase comes from releasing the restriction imposed at the redox balance level for ferredoxins, which was forcing a higher co-production of 1,2-PDO along with FAs, especially for short chain FAs (see discussion in section 6.2.3.1).

Table 22: Model predictions of specific growth rate, production rate and titer for production of FAs using the reversal of the β-oxidation cycle and a NADH-dependent acyl-CoA dehydrogenase after blocking synthesis of native fermentation products. The increase in titers with respect to the use of a ferredoxin-dependent acyl-CoA is presented.

Use of NADH-dependent Acyl-CoA dehydrogenase	Alcohols		Alkanes		Fatty acids	
Flux	C-4	C-18	C-3	C-17	C-4	C-18
Specific growth rate (1/h)	0.32	0.32	0.28	0.31	0.24	0.30
Production rate (mmol C/gDW/h)	50.14	50.14	38.49	47.60	52.53	50.66
Titer 24 hr (mol C/L)	341.81	341.81	118.83	272.61	72.05	243.49
Fold change in titer with respect to base case	1.2	3.1	1.3	3.2	11.1	5.9

6.2.5 Synthesis of products with functionalized side chain

The previous subsections focused on simulating the production of n-alcohols, alkanes and FAs using the reversal β-oxidation cycle. In all cases the primer or starter used to initiate the cycle was an AcCoA, and the final products were obtained by adding one or two termination steps to acyl-CoAs of different lengths (Figure 51). In this section the simulations and analysis of two additional functionalities of this platform are presented. The first one consists of using an AcCoA as a primer and deriving the final products from intermediate metabolites of the reversal β-oxidation cycle other than acyl-CoAs (i.e., β-keto acyl- CoAs, trans- β-hydroxyacyl- CoAs, and trans-d2-enoyl- CoAs). This strategy results in the production of alcohols, carboxylic acids, ketones and alkenes, as presented in the *Model Implementation* section (see Figure 52, page 167). The second functionality arises from the use of omega-hydroxylated or omega-carboxylated primers, as opposed to using AcCoA, and the products are produced from the hydroxylated acyl-CoA molecule or the carboxylated acyl-CoA molecules. This second functionality results in the production of diols, hydroxyacids and di-carboxylic acids, depending on the termination pathway being used.

6.2.5.1 Products derived from intermediate metabolites of the reversed β-oxidation cycle

This subsection reports the *in silico* predictions generated using the lcp-GEM and the implementation of the proper termination pathways from each of the intermediate metabolites of the reversal β-oxidation cycle, as explained in the section *Model Implementation* (see Figure 52, boxes 2, 3 and 4, page 167).

The lcp-GEM was used in combination with FBA and FVA to predict the solution spaces associated with the production of each of the products presented in Figure 52 after blocking the synthesis of native fermentation products. The results of these simulations are presented in Figure 59, which includes products derived from β-keto acyl-CoA, trans-β-hydroxy acyl-CoA, and trans-enoyl-CoA, a total of nine product families. Production of β-ketones, 3-alcohols and alkenes was plotted carbon mole basis "plus 1", in order to make products of different chain length comparable and due to the loss of one carbon molecule in the decarbonylation step. Based on the predicted solution spaces, I classified these nine families into four groups (Figure 59).

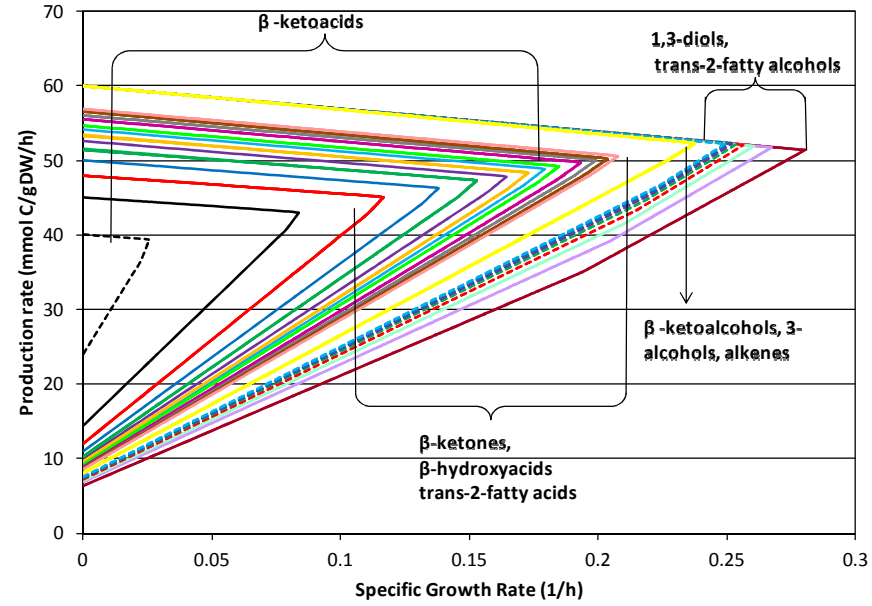

B

β-ketobut	β-ketohxa	β -ketoacids (group 1)
β-ketoocta	β-ketodca	
β-ketoddca	β-ketottdca	
β-ketohdca	β-ketoocdca	
β-ketobutanol	β-ketohexanol	β -ketoalcohols (group 3)
β-ketooctanol	β-ketodecanol	
β-ketododecanol	β-ketotetradecanol	
β-ketohexadecanol	β-ketooctadecanol	
acetone	2pentanone	β -ketones (group 2)
2heptanone	2nonanone	
2undecanone	2tridecanone	
2pentadecanone	2heptadecanone	
β-hydroxybut	β-hydroxyhxa	β-hydroxyacids (group 2)
β-hydroxyocta	β-hydroxydca	
β-hydroxyddca	β-hydroxyttdca	
β-hydroxyhdca	β-hydroxyocdca	
13butanediol	13hexanediol	1,3-diols (group 4)
13octanediol	13decanediol	
13dodecanediol	13tetradecanediol	
13hexadecanediol	13octadecanediol	
3propanol	3pentanol	3-alcohols (group 3)
3heptanol	3nonanol	
3undecanol	3tridecanol	
3pentadecanol	3heptadecanol	
trans-d2-but	trans-d2-hxa	trans-2-Fatty Acids (group 2)
trans-d2-octa	trans-d2-dca	
trans-d2-ddca	trans-d2-ttdca	
trans-d2-hdca	trans-d2-ocdca	
trans-d2-fatty-butanol	trans-d2-fatty-hexanol	trans-2-Fatty Alcohols (group 4)
trans-d2-fatty-octanol	trans-d2-fatty-decanol	
trans-d2-fatty-dodecanol	trans-d2-fatty-tetradecanol	
trans-d2-fatty-hexadecanol	trans-d2-fatty-octadecanol	
propene	pentene	Alkenes (group 3)
heptene	nonene	
undecene	tridecene	
pentadecene	heptadecene	

Figure 59: Solution spaces and classification of the production of nine product families derived from intermediate metabolites of the reversal β-oxidation cycle. Synthesis of native fermentation products was blocked. Panel A correspond to the solution spaces, including classification of the nine product families into four groups. Panel B corresponds to the legend of panel A, including the classification of the products per family and per group (on the right). The nine product families were grouped according to the shape of their solution space: group one (blue): β-ketoacids; group 2 (orange): β-hydroxyacids, trans-2-acids and β-ketones; group 3 (yellow): β-ketoalcohols, 3-alcohols and alkenes; and group 4 (green): 1,3-diols and trans-2-fatty alcohols.

Table 23 presents a summary of specific growth rates, production rates and titers in the optimal solution for short chain and long chain products of each of the nine families that resulted from the simulations. In accordance with results presented in Figure 59, the products are divided into four groups according to their predicted specific growth rate, production rate and titer.

Table 23: Model predictions of specific growth rates, production rates and titers for the synthesis of the nine product families derived from intermediate metabolites of the reversal β-oxidation cycle. Synthesis of native fermentation products was blocked. For each product family a short chain product (3 or 4 carbon molecules) and a long chain product (17 or 18 carbon molecules) are presented as they represent the behavior of each family. The products were classified in four categories according to their results, and four colors were used: group one (blue): β-ketoacids; group 2 (orange): β-hydroxyacids, trans-2-acids and β-ketones; group 3 (yellow): β-ketoalcohols, 3-alcohols and alkenes; and group 4 (green): 1,3-diols and trans-2-fatty alcohols.

Products from β-acyl-CoA	β-ketobut	β-ketoocdca	β-keto butanol	β-ketoocta decanol	acetone	hepta decanone
Specific growth rate(1/h)	0.03	0.18	0.24	0.24	0.12	0.21
Production rate (mmol C/gDW/h)	39.4	48.8	52.3	52.3	33.7	47.7
Titer 24 hr (mol C/L)	1.3	19.8	65.7	65.7	4.5	33.1
Products from trans-β-hydroxyalkane-CoA	β-hydroxy but	β-hydroxy ocdca	1,3buta nediol	1,3octa decanediol	3propanol	3hepta decanol
Specific growth rate(1/h)	0.12	0.21	0.28	0.25	0.24	0.24
Production rate (mmol C/gDW/h)	45.0	50.5	51.4	52.3	39.2	49.4
Titer 24 hr (mol C/L)	6.0	35.1	152.7	83.2	49.2	62.0
Products from trans-2-enoyl-CoA	trans-2-but	trans-2-ocdca	trans-2-fatty-butanol	trans-2-fatty-octadecanol	propene	hepta decene
Specific growth rate(1/h)	0.12	0.21	0.28	0.25	0.24	0.24
Production rate (mmol C/gDW/h)	45.0	50.5	51.4	52.3	39.2	49.4
Titer 24 hr (mol C/L)	6.0	35.1	152.7	83.2	49.2	62.0

Analysis of the four groups presented in Figure 59 and Table 23 indicates that a common characteristic of all members of each of the four groups is that they consume the same amount of reducing equivalents in the reversal β-oxidation cycle plus the termination steps. Table 24 shows the analysis of consumption of reducing equivalents for the production of one molecule of product starting from the precursor AcCoA. As the conversion of glucose to precursor AcCoA results in production of reducing equivalents, the achievement of redox balance depends mainly on consumption of reducing equivalents in the reversal β-oxidation cycle, in the termination pathway, and in the

potential synthesis of by-products. Simulations using the lcp-GEM identified 1,2-PDO as the preferred by-product to achieve redox balance in the synthesis of products from group 1 (β-ketoacids) and group 2 (β-hydroxyacids, trans-2-acids and β-ketones). Synthesis of products from group 3 (β-ketoalcohols, 3-alcohols and alkenes) and group 4 (1,3-diols and trans-2-fatty alcohols) does not require production of by-products, and the redox balance is achieved by switching the use of enzymes in the pyruvate node. For example, for short chain products, synthesis of products from group 3 is achieved by converting pyruvate into AcCoA using only the enzyme PFL (no production of reducing equivalents), while synthesis of products from group 4 uses a combination of enzymes PFL and PDH (production of reducing equivalents) to convert PYR into AcCoA. Longer chain products combine these enzymes with the enzyme PFOR, as PFOR is essential to complete cycles of the reversal β-oxidation cycle. Thus, this analysis identified that 1,2-PDO is a desired by-product to achieve redox balance in the synthesis of products from groups 1 and 2, and that a switch of enzymes in the pyruvate node allows achieving redox balance in the synthesis of products from groups 3 and 4.

Table 24: Consumption of reducing equivalents for the synthesis of short chain products (3 or 4 carbon molecules) derived from intermediates of the reversal β-oxidation cycle. The classification of groups is as presented in Figure 59. The consumption of reducing equivalents presented in this table corresponds to those consumed in the reversal β-oxidation cycle and in the termination pathways.

Group 1	β-ketobut	0 [H]
Group 2	acetone	-2[H]
	β-hydroxybut	-2[H]
	trans-2-but	-2[H]
Group 3	β-ketobutanol	-4[H]
	3-propanol	-4[H]
	propene	-4[H]
Group 4	1,3-butanediol	-6[H]
	trans-2-fatty butanol	-6[H]

6.2.5.2 Products derived from using hydroxylated and carboxylated primers

The *in silico* predictions for the production of diols, hydroxyacids and dicarboxylic acids using the reversal of the β-oxidation cycle are presented in this section. The lcp-GEM was used to simulate the production of hydroxylated primers and carboxylated primers to be utilized in the reversal of the β-oxidation cycle (see subsection 6.1.7.2 for details of the implementation of this strategy). The predicted solution spaces associated with the production of each of these product families are presented in Figure 60 (diols), Figure 61 (hydroxyacids), and Figure 62 (dicarboxylic acids), and discussed below.

The lcp-GEM was used to simulate **production of 1,n-diols**. It was found that all the diols considered in this study can be produced uncoupled to cell growth using the reversal of the β-oxidation cycle prior to blocking the synthesis of native fermentation products. In order to couple production of n-diols to biomass, reactions leading to the production of native fermentation products were deleted, and the results of these simulations are presented in Figure 60. Production of diols with less than 6 carbon atoms was not feasible after removing synthesis of native fermentation products, suggesting that native fermentation products are needed to achieve redox balance or to satisfy ATP requirements. Two distinct patterns were observed for the production of n-diols, depending on the chain length. Production of diols with an odd number of carbons follows one distinct pattern as presented in Figure 60-A, and production of diols with an even number of carbon molecules follows the pattern presented in Figure 60-B. The existence of two different patterns is due to the synthesis and use of different primers for the production of odd chain and even chain diols. Analysis of flux distribution allowed

me to identify that the production of odd chain diols is initiated by the primer 4-hydroxybutyryl-CoA. Production of even chain diols is initiated by the primer 3-hydroxypropionyl-CoA. For both even and odd chain diols, the longer the chain, the larger the predicted specific growth rate. This is a direct consequence of the ATP consumed in the production of the primers 4-hydroxybutyryl-CoA and 3-hydroxypropionyl-CoA, and the fact that the longer the chain in a product, the less primer is required to produce the same amount of product on carbon mole basis.

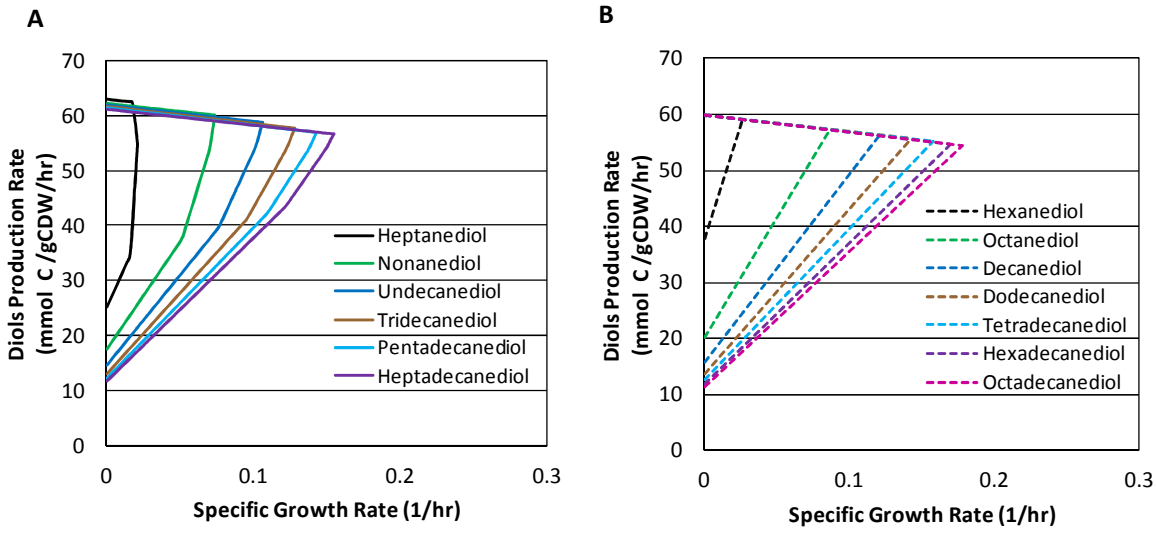

Figure 60: Simulated solution space for the production of (A) odd-chain length diols and (B) even-chain length diols. Reactions leading to the production of native fermentation products (LDH_D, PTAr, PTA2, ADH, ALDH, FRD2, FRD3, EX_ac(e)) were deleted. Production of diols coupled to cell growth was predicted for all the products with 6 or more carbon atoms. Simulations indicate that production of butanediol and pentanediol under present conditions is not feasible.

Production of 1,n-hydroxyacids was simulated using the lcp-GEM. As in the production of diols, when the synthesis of native fermentation products is allowed, the simulations indicate that production of all hydroxyacids considered in this study is feasible, although not coupled to biomass production. After the native fermentation products were deleted, the lcp-GEM predicted the production of hydroxyacids with 5 carbon atoms or more coupled to cell growth, and production of other products was not possible (Figure 61). Analysis of flux distribution indicates that all hydroxyacids were

produced using a carboxylated primer (and not a hydroxylated primer). This indicated that cell growth coupled to production of hydroxyacids is more efficient when the flux goes through the pathway involving carboxylated primers, as opposed to using a pathway that goes through hydroxylated primers. The two different patterns that were observed, and that are presented in Figure 61 (panel A and B), correspond to the use of malonyl-CoA as primer to produce hydroxyacids with an odd number of carbon molecules, and the use of succinyl-CoA as primer to produce hydroxyacids with an odd number of carbon molecules.

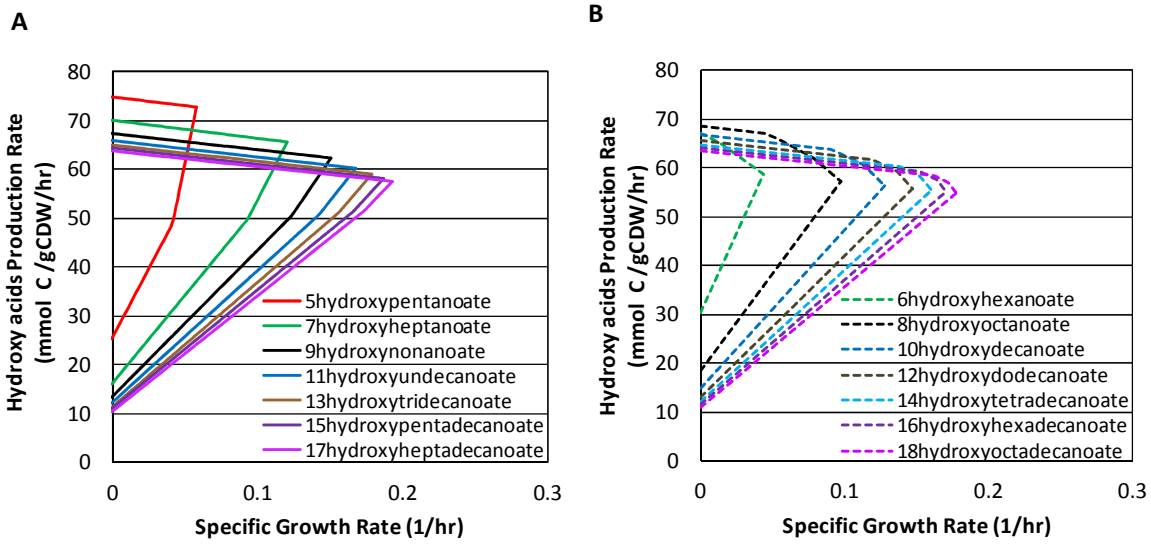

Figure 61: Simulated solution space for the production of (A) odd-chain length hydroxyacids and (B) even-chain chain hydroxyacids. Reactions leading to the production of native fermentation products (LDH_D, PTAr, PTA2, ADH, ALDH, FRD2, FRD3, EX_ac(e)) were deleted. Production of hydroxyl acids coupled to cell growth was predicted for all the products with 5 or more carbon atoms. Simulations indicate that production of 4-hydroxybutanoate under present conditions is not feasible.

As in the case of production of diols, the simulated optimal solution for the production of hydroxyacids after deleting native fermentation products predicts higher specific growth rate when associated with longer chain products. This is a direct consequence of the ATP consumed in the production of the primers malonyl-CoA and succinyl-CoA, and the fact that the longer the chain in the product, the less primer is required to produce the same amount of product per carbon atom.

Finally, the lcp-GEM was used to simulate the solution spaces for the production of **dicarboxylic acids**. The model successfully simulated production of all products included in this study prior to deleting native fermentation products, although not coupled to production of biomass. Deletion of native fermentation products resulted in production of dicarboxylic acids with 9 or more carbon atoms coupled to cell growth. Figure 62 shows the simulated solution spaces. Production of dicarboxylic acids with an odd number of carbon atoms (Panel A, left) is mediated by the primer malonyl-CoA, and production of dicarboxylic acids with an even number of carbon atoms (panel B, right) is mediated by the primer succinyl-CoA. As in the production of diols and hydroxyacids, production of dicarboxylic acids with longer chains is correlated with a higher specific growth rate at the optimal solution, a fact that is due to an smaller requirement of ATP to activate the smaller amount of primers of those cases.

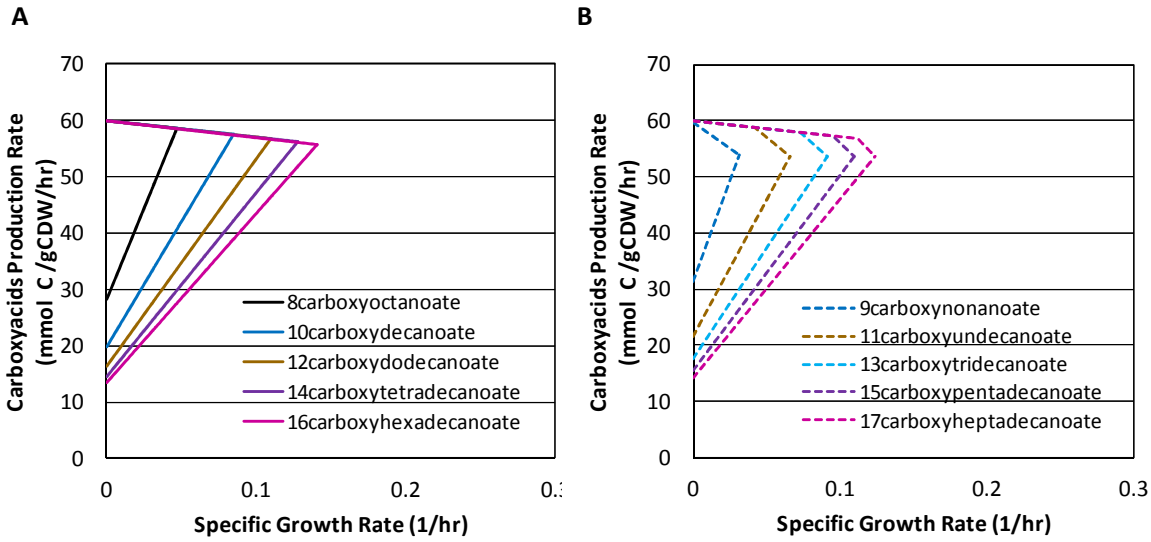

Figure 62: Simulated solution space for the production of (A) odd-chain length dicarboxylic acids and (B) even-chain length dicarboxylic acids. Reactions leading to the production of native fermentation products (LDH_D, PTAr, PTA2, ADH, ALDH, FRD2, FRD3, EX_ac(e)) were deleted. Production of dicarboxylic acids coupled to cell growth was predicted for all the products with 9 or more carbon atoms. There was no predicted production of 3-dicarboxylic propionate, 4- dicarboxylic butanoate, 5- dicarboxylic pentanoate, 6- dicarboxylic hexanoate and 7- dicarboxylic pentanoate under present conditions.

6.3 Conclusions

I have examined the metabolic capabilities of a functional reversal of the β-oxidation cycle using mathematical modeling. By implementing this pathway in a genome scale model, and using Flux Balance Analysis (FBA) and Flux Variability Analysis (FVA), I predicted productivities associated with products with different carbon chain lengths. First, I studied the production of three key product families for the biochemical industry: n-alcohols, alkanes and FAs. In each case, I simulated the synthesis of products with even chain lengths ranging from 3 or 4 carbon molecules to 17 or 18 carbon molecules. The results predict that the reversal β-oxidation cycle is capable of producing these products at attractive production rates and titers. Further research is needed on the experimental front in order to implement the strategies proposed in this chapter. The energy efficiency of this pathway seems to be the main factor that allowed obtaining significant improvement on the production of the longer chain products that were evaluated in this project. Further, the predictions generated by implementing the reversal of the β-oxidation cycle were contrasted with predictions of implemented alternative platforms (FA biosynthesis pathway and the α-keto acid pathway), and the results indicate that the use of the reversal β-oxidation cycle is significantly better than the evaluated alternatives in terms of production rate and titers.

In addition, the scope of using the reversal β-oxidation cycle was extended to the synthesis of products with a functionalized side chain using a genome-scale model (GEM) adapted to produce long chain products (the "lcp-GEM"). By modifying the first module (primer) and/or the third module (termination), I simulated the production of a vast number of products, such as diols, hydroxyacids and alkanes. The products with

functionalized side chain were classified in 12 product families. This highlights the versatility of the reversal β-oxidation cycle and suggests the need for experimental implementation.

While the simulations using the lcp-GEM represents a modeling analysis of the capabilities of *E. coli* using a functional of the reversal β-oxidation cycle, further steps will need to be taken to implement genetic manipulations that will prove these predictions.

The convenience of using *in silico* simulations relies on the potential to evaluate complex factors that have implications in the whole system rather than evaluating just a specific pathway. That is the case of ATP consumption/generation, redox balance, and other stoichiometric constraints. Finally, the use of GEM can guide the experimental design that will result in an optimal production of the desired product by identifying key reactions that need to be added, removed or modified.

In summary, the main results and findings presented in this chapter are:

- Modification of the GEM for *E. coli* to represent the synthesis of 15 product families of different chain lengths, using the reversal β-oxidation cycle. To this end, a total of 400 reactions were added to the iJO1366 model.
- The reversal β-oxidation cycle was simulated using a system of modules, which allows the diversification in the synthesis of final products.
- Simulations of optimal cell growth indicate that native fermentation products must be eliminated (knockout) in order to couple cell growth to production of desired products. To this end the following reactions were

eliminated: ALDH (*adhE*), ADH (adhE), ALDH (*adhE*), LDH_D (*ldhA*), PTA2 (*pta*), PTAr (*pta*), FRD2 (*frdA*, *frdB*, *frdC*, *frdD*), and FRD3 (*frdA*, *frdB*, *frdC*, *frdD*). In addition to these metabolic reactions, the following export reactions were deleted to ensure the eliminations of associated products: EX_ac(e) (for acetate), EX_PYR(e) (for pyruvate), and EX_hxa(e) (for hexanoate).

- Production of 1,2-PDO is an important electron sink associated with the synthesis of fatty acids, β-ketoacids, β-hydroxyacids, trans-2-acids and β-ketones.
- Identify optimal pathways for the production of long chains carboxylic acids, diols and hydroxyacids. These pathways include the production and utilization of hydroxylated and carboxylated primers from glucose.

7 Final remarks and future directions

This thesis addresses the problem of finding an economically viable alternative to petroleum-derived fuels and chemicals. The microbial production of biofuels and chemicals has become the most supported alternative to traditional fuels from petroleum because this alternative is renewable and environmentally friendlier than using petroleum-derived fuels and chemicals. However, the main drawback of using biofuels is the higher cost associated. While different approaches have been evaluated in recent years to synthesize biofuels and biochemicals, this thesis focuses in two specific strategies with economical potential: the fermentation of glycerol and the utilization of a reversal of the β-oxidation cycle.

In particular, the present thesis presents the modeling of the metabolic pathways in *E. coli* for the production of biofuels and chemicals using the recently experimentally reported glycerol fermentation and reversal β-oxidation cycle. Two platforms are very attractive to reduce the cost in the production of biofuels. Together with experimental work done by others, this study adds to the optimization of the synthesis of desired products. The use of mathematical models is fundamental to expand and optimize existing metabolic processes because mathematical tools can simulate the complexity of metabolic pathways resulting in a deeper understanding at a system level.

7.1 Summary of achievements presented in this thesis

The following is a summary of specific achievements of this thesis:

Kinetic model for the fermentative metabolism of glycerol in *E. coli.*

- Develop a kinetic model for the fermentative metabolism of glycerol in *E. coli,* which represents accurately the dynamic of external variables (substrate, product and biomass), and predicts the dynamic of concentration of internal metabolites.
- Use this kinetic model to determine the control structure of the pathway. This analysis predicted that two genes were controlling the flux through the pathway: glycerol dehydrogenase and di-hydroxyacetone kinase.
- Validate the predictions of the model by experimentally overexpressing the enzymatic activity of glycerol dehydrogenase and di-hydroxyacetone kinase, resulting in an remarkable increased production rate of ethanol from 4.1 mmol/gCDW/h to 10 mmol/gCDW/h (experiments performed by James Clomburg).

Genome-scale model for the fermentative metabolism of glycerol.

- Accurately represent glycerol fermentation in *E. coli* using a genome-scale model (modified from iJO1366 model).
- The problem of achieving redox balance for glycerol fermentation in *E. coli* was investigated in detail, as this is a critical challenge in this process that was not well understood previous to this work, and which has not been addressed before this thesis using genome-scale models. As a result, the genome-scale model was carefully curated to eliminate a number of pathways that lead to non-permisive consumption of reducing equivalents. The resulting model supports the

experimental finding of ethanol and 1,2-propanediol (1,2-PDO) being essential for cell growth under fermentative conditions (the ethanol-1,2-PDO model).

- Predict flux distribution and essential genes using Flux Balance Analysis (FBA). Elucidate a potential new optimal pathway for the incorporation of glycerol into the glycolytic flux linked to the ability to produce 1,2-PDO and essential intermediate metabolites, and propose a physiological function for genes *fsaB* (fructose aldolase) and *ptsA* (fused predicted PTS enzyme) based on experimental simulations.
- Evaluate the addition of genetic modifications as a way to support cell growth linked to the synthesis of different products. These modifications need to satisfy cellular requirement of ATP production and redox balance achievement. Using the genome-scale model I identified 59 models (including the ethanol-1,2-PDO model) linked to the production of native and non-native products as potential alternatives to support cell growth under fermentative conditions. With a few exceptions, most of these models are new predictions with experimental applications in the synthesis of biofuels and chemicals.
- Use the GEM to evaluate the synthesis of succinate, 1,2-PDO, 1,3-propanediol (1,3-PDO), lactate, butanol, propanol and propionic acid. I validated the model predictions by using pre-existing experimental data that was not used to curate the model. In most of these cases the solution spaces resulting from the GEM accurately represented the experimental data, being the only exception the production of lactic acid. These results corroborate the predictive capability of this model.

- Use FBA and OptKnock to propose strategies to optimize the synthesis of 1,2-PDO, 1,3-PDO, lactate, butanol, propanol and propionic acid (or to further improve existent strategies).

Genome-scale model for the reversal of the β-oxidation cycle utilizing glucose.

- Use genome-scale modeling to represent the reversal of the β-oxidation cycle in *E. coli* to synthesize medium and long chain products from glucose (modifications made to the iJO1366 model).
- Predict maximal cell growth rates and flux distribution for the production of 15 different products family, each family with products of different length chains. These product families include alcohols (advanced biofuels), alkanes, and fatty acids, among others. Predictions of the model indicate that the production of each product is essential and coupled to cell growth after deleting native fermentation products. This results indicate that the reversal of the β-oxidation cycle is superior in productivities than alternative platforms that I also evaluated using genome-models, a finding that corroborates which has been observed experimentally.
- Understand the main factors that affect production rates and cell growth for different product families and chain length. The main factors in finding an optimal strategy for the synthesis of desired products are 1) the ATP consumption of the biosynthetic pathway, which in the case of the reversal β-oxidation cycle is superior to other alternatives evaluated in this study, 2) the achieving of redox balance, and 3) stoichiometric constrains. Using the genome-scale model, I explain the mechanisms to achieve redox balance for all the possible products evaluated in this study. The use of a genome-scale model allowed the

identification of stoichiometric constraints, representing valuable information to consider in the search for optimal strategies to synthesize the desired products.

7.2 Future directions

A number a future directions are suggested as a result of this study, as are explained bellow.

The kinetic model presented for glycerol fermentation in *E. coli* can be expanded for the production of other products, including 1,2-PDO. The inclusion of this pathway could be highly relevant because the enzyme glycerol dehydrogenase, which mediates glycerol dissimilation, also plays a role in the production of 1,2-PDO. Inclusion of additional reactions and/or pathways may require a re-adjustment of parameters, using sensitivity analysis and mathematical optimization of parameters, as is explained in this thesis. The model could be used to calculate the flux control coefficient of the new system, a process that is achieved by calculating elasticities directly from the kinetic expressions and which does not require additional experiments.

In addition, the kinetic model can be modified to study the consumption of glycerol under different initial conditions (such as mixture of substrates, or presence of different metabolites) by incorporating the regulatory network. Once the model is expanded to include different conditions, it can be used to calculate the control structure of the new system, a task that builds on the kinetic model presented in this thesis, and which highlights the advantage of using mathematical modeling. In contrast, the control structure of the pathway could also be calculated by experimentally measuring elasticities, but in that case any modification to the system would require re-measuring

experimentally all the elasticities of the system because there is not building up on previous work.

Another aspect that will need to be investigated is finding a more suitable kinetic equation for biomass production than the widely used Monod equation. In this research the Monod equation was used to represent cell growth, as it fit properly the cell growth. However, this equation assumes that cell growth is a function of external substrate concentration (and possible inhibitors), but it does fit well the case in which engineering a strain may result in an increased rate of consumption of the substrate, with an associated increased specific growth rate (as it was the case of glycerol fermentation after overexpressing the limiting enzymes). This situation will have to be addressed by re-designing the cell kinetic growth equation. One option to do this could be to change the parameters of the Monod equation for functions, but then again it will need to be investigated which are the parameters of those functions. It seems reasonable to think that this new specific growth rate function will need to incorporate the rate at which ATP becomes available in the system, as ATP constraints certainly have an effect on cell growth, but other factors may need to be incorporated, such as the speed at which essential metabolites become available.

The genome-scale model presented for glycerol fermentation in *E. coli* indicates that glycerol is an attractive carbon source for the synthesis of several products, and further experimental validation is advised. In particular, it is recommended to experimentally implement the strategies for the production of succinate, 1,3-PDO, butanol, propanol and propionic acids, as they are predicted to increase production rates.

Other aspects of glycerol fermentation can be investigated using mathematical modeling. For example, Clomburg identified that acetate plays an important role in the fermentation of glycerol at high concentrations of glycerol (50 g/l) in a supplemented medium, and the reason for that remains unknown although some hypotheses were suggested, including the convenience of adding acetate to the media as a means to consume reducing equivalents when converted to ethanol (Clomburg, 2012). If this theory is true, the use of mathematical models could be used to investigate this and other possible factors involved in this phenomenon, such as the presence of another limiting reactant in the medium (stoichiometric constraints) that could be preventing the achieving of redox balance through production of 1,2-PDO.

The capabilities of the reversal β-oxidation cycle were explored using genome-scale models, and the *in silico* analysis supports the attractiveness of this pathway for the production of a variety of products (including advanced biofuels), many of which have not been synthesized experimentally yet. Based on these results it is advised to continue with further experimental implementation of pathways for the synthesis of the products explored in this thesis using the reversal of the β-oxidation cycle, as this pathway has a great capability to produce a variety of products at attractive productivities. It is also advised to utilize this model evaluate the synthesis of other products of interest.

Further mathematical analysis is recommended to study the reversal β-oxidation cycle, including the implementation of a kinetic model to elucidate the control structure of the pathway, and the analysis of using alternative feedstocks (such as glycerol).

Finally, the study presented in this thesis for the mathematical modeling of the fermentative metabolisms of glycerol and of glucose (using the reversal of the β-

oxidation cycle) is an important and necessary step toward the achieving of a higher goal: finding an ideal system for the production of fuels and chemicals that are currently derived from petroleum. The three mathematical models presented in this thesis are the first mathematical models implemented for the study of glycerol fermentation and the reversal β-oxidation cycle in *E. coli*, and the utility of these models to improve the production of biofuels and biochemicals and to reduce the cost associated is evident.

8 Nomenclature

a_{ij}	Exponential factor (power law), kinetic parameter (thermokinetic)
α_i	Coefficient associated with the flux vi, kinetic parameter (S-system)
b_{ij}	Exponential factor (power law), kinetic parameter (thermokinetic)
β_i	Kinetic parameter (S-systems)
C_{ij}	Concentration Metabolite i
c_j	Extracellular metabolite (lin-log)
e_i	Enzymatic activity (power law form, lin-log)
E_i	Enzymatic activity of *i*- th enzyme
$\varepsilon^i_{X_j}$	Elasticity , rate vi, metabolite j
$f_i(C,P)$	Function that depend on of metabolite concentrations C and on a set of parameters P
g_{ij}	Exponential factor (S-systems)
h_{ik}	Exponential factor (S-systems)
J	Pathway; number of fluxes
k_i	Kinetic parameter (power law form, thermokinetic)
k	*k*- th reaction
Keq_i	Equilibrium constrant, reaction i
Km^j_i	Michaelis-Menten constant, reaction i, metabolite j
Kia	Kinetic constant of bi-uni-uni-uni ping-pong mechanism
Km^{Growth}_{GLYC}	Kinetic constant for biomass production
l_i	Lower admissible values for flux vi
M_i	Metabolite
r^i_{max}	Maximum rate, reaction i
u_i	Upper admissible values for flux vi
S	Stoichiometric matrix
μ	Dilution rate
μ_{max}	Maximum specific growth rate
v	Vector of fluxes
$\mathbf{v_m}$	Vector of meassured fluxes
$\mathbf{v_c}$	Vector of unknown fluxes
X_j	Concentration Metabolite j
x_j	Intracellular metabolite (lin-log)

[H]	Reducing equivalents (ex: 2[H] = 1 NADH)
1,2-PDO	1,2-propanediol
1,3-PDO	1,3-propanediol
1,3-PDODH	NADH-dependant 1,3-PDO dehydrogenase
2PG	2-phosphoglycerate
3-HPA	3-hydroxypropionaldehyde
3PG	3-phosphoglycerate
5mtr	5-Methylthio-D-ribose
ACACT3r	Acetyl-CoA C-acyltransferase (hexanoyl-CoA) (reversible)
ACALD	Acetaldehyde
AcCoA	Acetyl-coenzymoA
Acetal	Acetaldehyde
ACKr	Acetate kinase
ACL	Acyl-CoA ligases
ACP	Acyl carrier protein
ACt2rpp	Acetate reversible transport via proton symport
Actp	Acetyl phosphate
ADH	Alcohols dehydrogenase
ADH2	Alcohols dehydrogenase (S.cerevisiae)
ADP	Adenosine Diphosphate
ALDD2y	Acetaldehyde dehydrogenase NADP
ALDH	Aldehyde dehydrogenase
ALR2	Aldose reductase (methylglyoxal)
ALR4x	Aldose reductase (HA)
AMP	Adenosine Monophosphate
AT	Acyltransferase
AtoB	Acetyl-CoA acetyltransferase
ATP	Adenosine Triphosphate
BOF	Bioamss as objective function
CCCs	Concentration control coefficients
CO2	Carbon dioxyde
CO2tpp	Transhydrogenase periplasm
CoA	Coenzyme-A
COBRA	COnstraints Based Reconstruction and Analysis (toolbox for Matlab)
DHA	Dihydroxyacetone
DHAK	Dihydroxyacetone kinase
DHAP	Di-hydroxyacetone-phosphate
D-LACtex	D-lactate transport via diffusion
e4p	D-Erythrose 4-phosphate
EI	Enzyme I, PTS system, PTS system

EIIA	Enzyme complexes II A, PTS system
EIIBC	Enzyme complexes II BC, PTS system
ENO	Enolase
EtOH	Ethanol
F6P	Fructose-6-phosphate
F6PA	Fructose 6-phosphate aldolase 2
FA	Fatty acid
FAD	Flavin adenine dinucleotide oxidized
FadB	3-hydroxyacyl-CoA dehydrogenase
FadM	Thioesterase
FAR	fatty-acyl-CoA reductase
FBA	Flux Balance Analysis
FBP	Fructose-bi-phosphate
FBPA	Fructose bi-phosphate aldoase
FBPA3	Sedoheptulose 1,7-bisphosphate D-glyceraldehyde-3-phosphate-lyase
FCCs	Flux control coefficients
fd	Ferredoxin (oxidized)
fd^{2-}	Ferredoxin (reduced)
FHL	Formate-hydrogen lyase
FORtppi	Formate transporter via diffusion
FRD2, FRD3	Fumarate reductase
FUM	Fumarase
FVA	Flux variability analysis
G1P	Glucose-1-phosphate
G3P	Glycerol-3-phosphate
G3PD2	NADPH-dependent glycerol-3-phosphate dehydrogenase
G6P	Glucose-6-phosphate
GAM	Growth associated maintenance energy
GAP	Glyceraldehyde-3-phosphate
GAPD	Glyceraldehyde 3-phosphate dehydrogenase
GC-MS	Gas chromatography-mass spectrometry
GEM	Genome-scale model
GK	Glycerol kinase
GlpABC	Anaerobic 3-phosphate dehydrogenase
GlpD	Aerobic 3-phosphate dehydrogenase
GlpF	Aquaglyceroporin
GlpK	ATP-dependent glycerol kinase
glu	Glutamate
Glyc	Glycerol
glyDH	NAD-dependent glycerol dehydrogenase

Glyc-GEM	Genome-scale model for glycerol femrentation
GLYK	Glycerol kinase
GMA-power law	Power law-Generalize Mass Action
H+, h	Proton
HA	Hydroxyacetone
HPr	Histidine protein, PTS system
ILE	Isoleucine
KIVD	2-ketoisovalerate decarboxylase
Lald	Lactaldehyde
LALDO2x	D-Lactaldehyde-NAD 1-oxidoreductase
LCARR	Lacaldehyde reductase (R-propane-1,2-diol forming)
lcp-GEM	Genome-scale model for the production of long chain products
LDH_D	D-lactate dehydrogenase
LEU	Leucine
lin-log	Linear-logarithmic
log-linear	Logarithmic-linear
malACP	Malonyl-ACP
MCA	Metabolic Control Analysis
MDH	Malate dehydrogenase
ME2	Malate dehydrogenase NADP
MET	Metionine
MFA	Metabolic Flux Analysis
MGSA	Methylglyoxal synthase
MOPS	4-Morpholinepropanesulfonic acid
MOX	Malate oxidase
mql8	Menaquinol 8
mqn8	Menaquinone 8
NAD	Nicotinamide adenine dinucleotide
NADH	Nicotinamide adenine dinucleotide - reduced
NADP	Nicotinamide adenine dinucleotide phosphate
NADPH	Nicotinamide adenine dinucleotide phosphate - reduced
NGAM	Non-growth associated maintenance energy
NMR	Nuclear Magnetic Resonance
OAA	Oxaloacetate
OD	Optical density
ODEs	Ordinary differential equations
PckA	Phosphoenolpyruvate carboxykinase
PDHC	Pyruvate dehydrogenase complex
PEP	Phosphoenol pyruvate
PFK (Pfl-1, Pfl-2)	Phosphofructokinases
PFL	Pyruvate formate lyase

PFOR	pyruvate ferredoxin oxidoreductase
Pgi	Phosphoglucose isomerase
PGK	Phosphoglycerate kinase
PGL	6-phosphogluconolactonase
PGM	Phosphoglycerate mutase
PGP	1,3-diphosphateglycerate
PntAB	Transhydrogenase periplasm
POX	Pyruvate oxidase
PP pathway	Pentose phosphate pathway
Ppa	Propionic acid
PPC	Phosphoenolpyruvate carboxylase
PPCSCT	Propanoyl-CoA: succinate CoA-transferase
ppi	Diphosphate
PP pathway	Pentose phosphate pathway
PRO	Proline
PTA2	Phosphate acetyltransferase
PTAr	Phosphotransacetylase
PTS	Phosphotransferase system
PYK	ATP-dependent pyruvate kinase
PYK (pykF, PykA)	Pyruvate kinases
PYR	Pyruvate
PYRtrpp	Pyruvate reversible transport via proton symport
S17BP	Sedoheptulose 1,7-bisphosphate
S7P	Sedoheptulose 7-phosphate
SBML	System Biology Markup Language
S-systems	Synergistic system
Succ	Succinate
SUCOA	Succinyl-CoA
TCA cycle	Tricarboxylic acids cycle
TES	Thioesterase
TesB	Thioesterase
THD2pp	Transhydrogenase periplasm
TPI	Triose phosphate isomerase
UQ	Ubiquinone
UQH2	Ubiquinol
VAL	Valine
YciA	Thioesterase
α-KG	α-ketoglutarate

9 References

Akopian M, Poladian A, Bagramian K (2006) Energy transformation coupled to formate oxidation during anaerobic fermentation. *Biofizika* **51:** 466-471

Alberts B (2002) *Molecular biology of the cell*, 4th edn. New York: Garland Science.

Alvarez-Vasquez F, Gonzalez-Alcon C, Torres NV (2000) Metabolism of citric acid production by Aspergillus niger: Model definition, steady-state analysis and constrained optimization of citric acid production rate. *Biotechnology and Bioengineering* **70:** 82-108

Appenzeller BMR, Yanez C, Jorand F, Block JC (2005) Advantage provided by iron for *Escherichia coli* growth and cultivability in drinking water. *Applied and Environmental Microbiology* **71**

Atsumi S, Cann AF, Connor MR, Shen CR, Smith KM, Brynildsen MP, Chou KJY, Hanai T, Liao JC (2008a) Metabolic engineering of *Escherichia coli* for 1-butanol production. *Metabolic Engineering* **10**

Atsumi S, Hanai T, Liao JC (2008b) Non-fermentative pathways for synthesis of branched-chain higher alcohols as biofuels. *Nature* **451:** 86-U13

Babul J, Clifton D, Kretschmer M, Fraenkel DG (1993) Glucose-metabolism in *Escherichia-coli* and the effect of increased amount of aldolase. *Biochemistry* **32:** 4685-4692

Bachler C, Schneider P, Bahler P, Lustig A, Erni B (2005) *Escherichia coli* dihydroxyacetone kinase controls gene expression by binding to transcription factor DhaR. *Embo Journal* **24:** 283-293

Bagramyan K, Mnatsakanyan N, Poladian A, Vassilian A, Trchounian A (2002) The roles of hydrogenases 3 and 4, and the F0F1-ATPase, in H-2 production by *Escherichia coli* at alkaline and acidic pH. *Febs Letters* **516:** 172-178

Bakker BM, Michels PAM, Opperdoes FR, Westerhoff HV (1997) Glycolysis in bloodstream form Trypanosoma brucei can be understood in terms of the kinetics of the glycolytic enzymes. *Journal of Biological Chemistry* **272:** 3207-3215

Barbirato F, Chedaille D, Bories A (1997) Propionic acid fermentation from glycerol: Comparison with conventional substrates. *Applied Microbiology and Biotechnology* **47**

Bates DL, Danson MJ, Hale G, Hooper EA, Perham RN (1977) Self-assembly and catalytic activity of pyruvate-dehydrogenase multienzyme complex of *Escherichia-coli*. *Nature* **268:** 313-316

Beard DA, Liang SC, Qian H (2002) Energy balance for analysis of complex metabolic networks. *Biophysical Journal* **83:** 79-86

Berg IA, Kockelkorn D, Buckel W, Fuchs G (2007) A 3-hydroxypropionate/4-hydroxybutyrate autotrophic carbon dioxide assimilation pathway in archaea. *Science* **318:** 1782-1786

Blankschien MD, Clomburg J, Gonzalez R (2010) Metabolic engineering of *Escherichia coli* for the production of succinate from glycerol. *Metabolic Engineering* **12**

Blattner FR, Plunkett G, Bloch CA, Perna NT, Burland V, Riley M, ColladoVides J, Glasner JD, Rode CK, Mayhew GF, Gregor J, Davis NW, Kirkpatrick HA, Goeden MA, Rose DJ, Mau B, Shao Y (1997) The complete genome sequence of *Escherichia coli* K-12. *Science* **277:** 1453-&

Booth IR. (2005) Chapter 3.4.3, Glycerol and methylglyoxal metabolism. In al. CIe (ed.), *EcoSal-Escherichia coli and Salmonella; cellular and molecular biology*. ASM Press, Washington, DC.

Bories A, Himmi E, Jauregui JJA, Pelayo-Ortiz C, Gonzales VA (2004) Glycerol fermentation with Propionibacteria and optimisation of the production of propionic acid. *Sciences Des Aliments* **24:** 121-135

Britton HG, Carreras J, Grisolia S (1972) MECHANISM OF YEAST PHOSPHOGLYCERATE MUTASE. *Biochemistry* **11:** 3008-&

Burgard AP, Pharkya P, Maranas CD (2003) OptKnock: A bilevel programming framework for identifying gene knockout strategies for microbial strain optimization. *Biotechnology and Bioengineering* **84**

Cain BD, Simoni RD (1989) Proton translocation by the F1F0-ATPase of *Escherichia-coli* mutagenic analysis of the alpha-subunit. *Journal of Biological Chemistry* **264:** 3292-3300

Charon MH, Volbeda A, Chabriere E, Pieulle L, Fontecilla-Camps JC (1999) Structure and electron transfer mechanism of pyruvate : ferredoxin oxidoreductase. *Current Opinion in Structural Biology* **9:** 663-669

Chassagnole C, Noisommit-Rizzi N, Schmid JW, Mauch K, Reuss M (2002) Dynamic modeling of the central carbon metabolism of *Escherichia coli*. *Biotechnology and Bioengineering* **79:** 53-73

Cintolesi A, Clomburg JM, Rigou V, Zygourakis K, Gonzalez R (2012) Quantitative analysis of the fermentative metabolism of glycerol in *Escherichia coli*. *Biotechnology and Bioengineering* **109**

Clark D, Cronan J. (2005) Chapter 3.4.4, Two-Carbon Compounds and Fatty Acids as Carbon Sources. In al. CIe (ed.), *EcoSal-Escherichia coli and Salmonella; cellular and molecular biology*. ASM Press, Washington, DC.

Clomburg JM, Gonzalez R (2010) Biofuel production in *Escherichia coli*: the role of metabolic engineering and synthetic biology. *Applied Microbiology and Biotechnology* **86:** 419-434

Clomburg JM, Gonzalez R (2011) Metabolic Engineering of *Escherichia coli* for the Production of 1,2-Propanediol From Glycerol. *Biotechnology and Bioengineering* **108**

Clomburg JM, Vick JE, Blankschien MD, Rodriguez-Moya M, Gonzalez R (2012) A Synthetic Biology Approach to Engineer a Functional Reversal of the beta-Oxidation Cycle. *Acs Synthetic Biology* **1**

Covert MW, Schilling CH, Palsson B (2001) Regulation of gene expression in flux balance models of metabolism. *Journal of Theoretical Biology* **213:** 73-88

Cronan J, Rock C (2008) Chapter 3.6.4: Biosynthesis of Membrane Lipids. In *Escherichia coli and Salmonella Cellular and Molecular Biology*, Cronan J (ed). Washington, DC: ASM Press.

Daniel R, Bobik TA, Gottschalk G (1998) Biochemistry of coenzyme B-12-dependent glycerol and diol dehydratases and organization of the encoding genes. *Fems Microbiology Reviews* **22:** 553-566

Dellomonaco C, Clomburg JM, Miller EN, Gonzalez R (2011) Engineered reversal of the beta-oxidation cycle for the synthesis of fuels and chemicals. *Nature* **476:** 355-U131

Dellomonaco C, Fava F, Gonzalez R (2010) The path to next generation biofuels: successes and challenges in the era of synthetic biology. *Microbial Cell Factories* **9**

Deng Y, Fong SS (2011) Metabolic engineering of Thermobifida fusca for direct aerobic bioconversion of untreated lignocellulosic biomass to 1-propanol. *Metabolic Engineering* **13**

Dharmadi Y, Murarka A, Gonzalez R (2006) Anaerobic fermentation of glycerol by *Escherichia coli*: A new platform for metabolic engineering. *Biotechnology and Bioengineering* **94:** 821-829

Dreger A, Kronfeld M, Ziller MJ, Supper J, Planatscher H, Magnus JB, Oldiges M, Kohlbacher O, Zell A (2009) Modeling metabolic networks in C. glutamicum: a comparison of rate laws in combination with various parameter optimization strategies. *Bmc Systems Biology* **3**

Duggleby RG (1994) Product inhibition of reversible enzyme-catalyzed reactions. *Biochimica Et Biophysica Acta-Protein Structure and Molecular Enzymology* **1209:** 238-240

Durnin G, Clomburg J, Yeates Z, Alvarez PJJ, Zygourakis K, Campbell P, Gonzalez R (2009) Understanding and Harnessing the Microaerobic Metabolism of Glycerol in *Escherichia coli*. *Biotechnology and Bioengineering* **103**

Durot M, Bourguignon PY, Schachter V (2009) Genome-scale models of bacterial metabolism: reconstruction and applications. *Fems Microbiology Reviews* **33:** 164-190

Edgar JR, Bell RM (1978) Biosynthesis in *Escherichia-coli* of sn-glycerol 3-phosphate, a precursor of phospholipid - purification and physical characterization of wild-type and feedback-resistant forms of biosynthetic sn-glycerol-3-phosphate dehydrogenase. *Journal of Biological Chemistry* **253**

Edwards JS, Palsson BO (2000) The *Escherichia coli* MG1655 *in silico* metabolic genotype: Its definition, characteristics, and capabilities. *Proceedings of the National Academy of Sciences of the United States of America* **97:** 5528-5533

Feist AM, Henry CS, Reed JL, Krummenacker M, Joyce AR, Karp PD, Broadbelt LJ, Hatzimanikatis V, Palsson BO (2007) A genome-scale metabolic reconstruction for *Escherichia coli* K-12 MG1655 that accounts for 1260 ORFs and thermodynamic information. *Molecular Systems Biology* **3**

Feist AM, Palsson BO (2008) The growing scope of applications of genome-scale metabolic reconstructions using *Escherichia coli*. *Nature Biotechnology* **26:** 659-667

Fell DA (1992) Metabolic control analysis - A survey of its theoretical and experimental development. *Biochemical Journal* **286:** 313-330

Fell DA (1998) Increasing the flux in metabolic pathways: A metabolic control analysis perspective. *Biotechnology and Bioengineering* **58:** 121-124

Fell DA, Sauro HM (1985) Metabolic control and its analysis - additional relationships between elasticities and control coefficients. *European Journal of Biochemistry* **148:** 555-561

Fifis T, Scopes RK (1978) Purification of 3-phosphoglycerate kinase from diverse sources by affinity elution chromatography. *Biochemical Journal* **175:** 311-319

Fischer CR, Klein-Marcuschamer D, Stephanopoulos G (2008) Selection and optimization of microbial hosts for biofuels production. *Metabolic Engineering* **10:** 295-304

Fjellstrom O, Johansson C, Rydstrom J (1997) Structural and catalytic properties of the expressed and purified NAD(H)- and NADP(H)-binding domains of proton-pumping transhydrogenase from *Escherichia coli*. *Biochemistry* **36**

Fong SS, Burgard AP, Herring CD, Knight EM, Blattner FR, Maranas CD, Palsson BO (2005) *In silico* design and adaptive evolution of *Escherichia coli* for production of lactic acid. *Biotechnology and Bioengineering* **91**

Garcia V. (2002) Sensitivity Analysis for ODEs and DAEs. Matlab.

Garcia-Alles LF, Siebolo C, Nyffeler TL, Flukiger-Bruhwiler K, Schneider P, Burgi HB, Baumann U, Erni B (2004) Phosphoenolpyruvate- and ATP-dependent dihydroxyacetone kinases: Covalent substrate-binding and kinetic mechanism. *Biochemistry* **43:** 13037-13045

Gombert AK, Nielsen J (2000) Mathematical modelling of metabolism. *Current Opinion in Biotechnology* **11:** 180-186

Gonzalez R, Murarka A, Dharmadi Y, Yazdani SS (2008) A new model for the anaerobic fermentation of glycerol in enteric bacteria: Trunk and auxiliary pathways in *Escherichia coli*. *Metabolic Engineering* **10:** 234-245

Grana X, Urena J, Ludevid D, Carreras J, Climent F (1989) Purification, characterization and immunological properties of 2,3-bisphosphoglycerate-independent phosphoglycerate mutase from maize (zea-mays) seeds. *European Journal of Biochemistry* **186:** 149-153

Gutknecht R, Beutler R, Garcia-Alles LF, Baumann U, Erni B (2001) The dihydroxyacetone kinase of *Escherichia coli* utilizes a phosphoprotein instead of ATP as phosphoryl donor. *Embo Journal* **20:** 2480-2486

Hatzimanikatis V, Bailey JE (1997) Effects of spatiotemporal variations on metabolic control: Approximate analysis using (log)linear kinetic models. *Biotechnology and Bioengineering* **54:** 91-104

Heijnen JJ (2005) Approximative kinetic formats used in metabolic network modeling. *Biotechnology and Bioengineering* **91:** 534-545

Heller KB, Lin ECC, Wilson TH (1980) Substrate-specificity and transport-properties of the glycerol facilitator of *Escherichia-coli*. *Journal of Bacteriology* **144:** 274-278

Hoefnagel MHN, Starrenburg MJC, Martens DE, Hugenholtz J, Kleerebezem M, Van Swam, II, Bongers R, Westerhoff HV, Snoep JL (2002) Metabolic engineering of lactic acid bacteria, the combined approach: kinetic modelling, metabolic control and experimental analysis. *Microbiology-Sgm* **148:** 1003-1013

Hoffmeister M, Piotrowski M, Nowitzki U, Martin W (2005) Mitochondrial trans-2-enoyl-CoA reductase of wax ester fermentation from Euglena gracilis defines a new family of enzymes involved in lipid synthesis. *Journal of Biological Chemistry* **280:** 4329-4338

Hofmeyr JHS, Kacser H, Vandermerwe KJ (1986) Metabolic control analysis of moiety-conserved cycles. *European Journal of Biochemistry* **155:** 631-641

Jain R, Yan Y (2011) Dehydratase mediated 1-propanol production in metabolically engineered *Escherichia coli*. *Microbial Cell Factories* **10**

Jensen KF, Dandanell G, Hove-Jensen B, Willemoes M. (2008) Chapter 3.6.2: Nucleotides, nucleosides and nucleobases. In Ingraham J (ed.), *Ecosal- Escherichia coli and Salmonella; Cellular and Molecular Biology*. ASM, Washington, DC.

Jo J-E, Raj SM, Rathnasingh C, Selvakumar E, Jung W-C, Park S (2008) Cloning, expression, and characterization of an aldehyde dehydrogenase from *Escherichia coli* K-12 that utilizes 3-Hydroxypropionaldehyde as a substrate. *Applied Microbiology and Biotechnology* **81:** 51-60

Kang YS, Durfee T, Glasner JD, Qiu Y, Frisch D, Winterberg KM, Blattner F (2004) Systematic mutagenesis of the *Escherichia coli* genome. *Journal of Bacteriology* **186:** 4921-4930

Karp PD, Keseler IM, Shearer A, Latendresse M, Krummenacker M, Paley SM, Paulsen I, Collado-Vides J, Gama-Castro S, Peralta-Gil M, Santos-Zavaleta A, Penaloza-Spinola MI, Bonavides-Martinez C, Ingraham J (2007) Multidimensional annotation of the *Escherichia coli* K-12 genome. *Nucleic Acids Research* **35:** 7577-7590

Kasimoglu E, Park SJ, Malek J, Tseng CP, Gunsalus RP (1996) Transcriptional regulation of the proton-translocating ATPase (atpIBEFHAGDC) operon of *Escherichia coli*: Control by cell growth rate. *Journal of Bacteriology* **178:** 5563-5567

Kauffman KJ, Prakash P, Edwards JS (2003) Advances in flux balance analysis. *Current Opinion in Biotechnology* **14:** 491-496

Keseler IM, Bonavides-Martinez C, Collado-Vides J, Gama-Castro S, Gunsalus RP, Johnson DA, Krummenacker M, Nolan LM, Paley S, Paulsen IT, Peralta-Gil M, Santos-Zavaleta A, Shearer AG, Karp PD (2009) EcoCyc: A comprehensive view of *Escherichia coli* biology. *Nucleic Acids Research* **37:** D464-D470

Keseler IM, Collado-Vides J, Santos-Zavaleta A, Peralta-Gil M, Gama-Castro S, Muniz-Rascado L, Bonavides-Martinez C, Paley S, Krummenacker M, Altman T, Kaipa P, Spaulding A, Pacheco J, Latendresse M, Fulcher C, Sarker M, Shearer AG, Mackie A, Paulsen I, Gunsalus RP et al. (2011) EcoCyc: a comprehensive database of *Escherichia coli* biology. *Nucleic Acids Research* **39:** D583-D590

Keseler IM, Mackie A, Peralta-Gil M, Santos-Zavaleta A, Gama-Castro S, Bonavides-Martinez C, Fulcher C, Huerta AM, Kothari A, Krummenacker M, Latendresse M, Muniz-Rascado L, Ong Q, Paley S, Schroeder I, Shearer AG, Subhraveti P, Travers M, Weerasinghe D, Weiss V et al. (2013) EcoCyc: fusing model organism databases with systems biology. *Nucleic Acids Research* **41:** D605-D612

Kleinhans FW (1998) Membrane permeability modeling: Kedem-Katchalsky vs a two-parameter formalism. *Cryobiology* **37:** 271-289

Klenk HP, Clayton RA, Tomb JF, White O, Nelson KE, Ketchum KA, Dodson RJ, Gwinn M, Hickey EK, Peterson JD, Richardson DL, Kerlavage AR, Graham DE, Kyrpides NC, Fleischmann RD, Quackenbush J, Lee NH, Sutton GG, Gill S, Kirkness EF et al. (1997) The complete genome sequence of the hyperthermophilic, sulphate-reducing archaeon Archaeoglobus fulgidus. *Nature* **390:** 364-&

Knappe J, Blaschkowski HP, Grobner P, Schmitt T (1974) Pyruvate formate-lyase of *Escherichia-coli* - acetyl-enzyme intermediate. *European Journal of Biochemistry* **50:** 253-263

Koebmann BJ, Westerhoff HV, Snoep JL, Nilsson D, Jensen PR (2002) The glycolytic flux in *Escherichia coli* is controlled by the demand for ATP. *Journal of Bacteriology* **184:** 3909-3916

Kornberg HL, Reeves RE (1972) Inducible phosphoenolpyruvate-dependent hexose phosphotransferase activities in *Escherichia-coli*. *Biochemical Journal* **128:** 1339-&

Lavoinne A, Marchand JC, Chedeville A, Matray F (1983) Kinetic-studies of the reaction-mechanism of rat-liver phosphoglycerate kinase in the direction of ADP utilization. *Biochimie* **65:** 211-220

Leland WP (2009) *Ethanol and biofuels : production, standards and potential*, New York: Nova Science Publishers.

Limsuwun K, Jones PG (2000) Spermidine acetyltransferase is required to prevent spermidine toxicity at low temperatures in *Escherichia coli*. *Journal of Bacteriology* **182:** 5373-5380

Lin ECC (1976) Glycerol dissimilation and its regulation in bacteria. *Annual Review of Microbiology* **30:** 535-578

Llaneras F, Pico J (2008) Stoichiometric modelling of cell metabolism. *Journal of Bioscience and Bioengineering* **105:** 1-11

Lu DY, Grayson P, Schulten K (2003) Glycerol conductance and physical asymmetry of the *Escherichia coli* glycerol facilitator GlpF. *Biophysical Journal* **85:** 2977-2987

Marcheschi RJ, Li H, Zhang K, Noey EL, Kim S, Chaubey A, Houk KN, Liao JC (2012) A synthetic recursive "+1" pathway for carbon chain elongation. *ACS chemical biology* **7:** 689-697

Matias PM, Pereira IAC, Soares CM, Carrondo MA (2005) Sulphate respiration from hydrogen in Desulfovibrio bacteria: a structural biology overview. *Progress in Biophysics & Molecular Biology* **89**

Mayer C, Boos W (2005) Chapter 3.4.1, Hexose/Pentose and Hexitol/Pentitol Metabolism. In *Eschirichia coli and Salmonella Cellular and Molecular Biology*, Bock A (ed). Washington, DC: ASM Press

Mazumdar S, Clomburg JM, Gonzalez R (2010) *Escherichia coli* Strains Engineered for Homofermentative Production of D-Lactic Acid from Glycerol. *Applied and Environmental Microbiology* **76**

Membrillo-Hernandez J, Echave P, Cabiscol E, Tamarit J, Ros J, Lin ECC (2000) Evolution of the adhE gene product of *Escherichia coli* from a functional reductase to a dehydrogenase - Genetic and biochemical studies of the mutant proteins. *Journal of Biological Chemistry* **275:** 33869-33875

Moisset P, Vaisman D, Cintolesi A, Urrutia J, Rapaport I, Andrews BA, Asenjo JA (2012) Continuous modeling of metabolic networks with gene regulation in yeast and *in vivo* determination of rate parameters. *Biotechnology and Bioengineering* **109**

Molnar M, Vas M (1993) Mg2+ affects the binding of ADP but not ATP to 3-phosphoglycerate kinase - correlation between equilibrium dialysis binding and enzyme-kinetic data. *Biochemical Journal* **293:** 595-599

Murarka A, Dharmadi Y, Yazdani SS, Gonzalez R (2008) Fermentative utilization of glycerol by *Escherichia coli* and its implications for the production of fuels and chemicals. *Applied and Environmental Microbiology* **74:** 1124-1135

Nakahigashi K, Toya Y, Ishii N, Soga T, Hasegawa M, Watanabe H, Takai Y, Honma M, Mori H, Tomita M (2009) Systematic phenome analysis of *Escherichia coli* multiple-knockout mutants reveals hidden reactions in central carbon metabolism. *Molecular Systems Biology* **5**

Neidhard.Fc, Bloch PL, Smith DF (1974) Culture medium for enterobacteria. *Journal of Bacteriology* **119:** 736-747

Ni TC, Savageau MA (1996) Model assessment and refinement using strategies from biochemical systems theory: Application to metabolism in human red blood cells. *Journal of Theoretical Biology* **179:** 329-368

Nielsen J (1997) Metabolic control analysis of biochemical pathways based on a thermokinetic description of reaction rates. *Biochemical Journal* **321:** 133-138

Orth JD, Conrad TM, Na J, Lerman JA, Nam H, Feist AM, Palsson BO (2011) A comprehensive genome-scale reconstruction of *Escherichia coli* metabolism-2011. *Molecular Systems Biology* **7**

Orth JD, Thiele I, Palsson BO (2010) What is flux balance analysis? *Nature Biotechnology* **28:** 245-248

Parkinson AR, Balling RJ (2002) The OptdesX design optimization software. *Structural and Multidisciplinary Optimization* **23:** 127-139

Pedersen A, Karlsson GB, Rydstrom J (2008) Proton-translocating transhydrogenase: an update of unsolved and controversial issues. *Journal of Bioenergetics and Biomembranes* **40**

Peralta-Yahya PP, Keasling JD (2010) Advanced biofuel production in microbes. *Biotechnology Journal* **5:** 147-162

Pettersson G (1990) What metabolite levels may be evolutionarily reached in the glycolytic pathway. *European Journal of Biochemistry* **194:** 141-146

Ramakrishna R, Ramkrishna D, Konopka AE (1996) Cybernetic modeling of growth in mixed, substitutable substrate environments: Preferential and simultaneous utilization. *Biotechnology and Bioengineering* **52:** 141-151

Ratledge C, Kristiansen B (2001) *Basic biotechnology*, 2nd edn. Cambridge [England] ; New York: Cambridge University Press.

Reed JL, Vo TD, Schilling CH, Palsson BO (2003) An expanded genome-scale model of *Escherichia coli* K-12 (iJR904 GSM/GPR). *Genome Biology* **4**

Reijnders L, Huijbregts MAJ (2009) *Biofuels for road transport : a seed to wheel perspective*, London: Springer.

Reitzer L. (2005) Chapter 3.4.7: Catabolism of Amino Acids and Related Compounds. In Bock A (ed.), *EcoSal-Escherichia coli and Salmonella: cellular and molecular biology*. ASM Press, Washington, DC.

Reizer J, Reizer A, Saier MH (1995) Novel phosphotransferase system genes revealed by bacterial genome analysis - A gene-cluster encoding a unique enzyme-i and the proteins of a fructose-like permease system. *Microbiology-Uk* **141:** 961-971

Richter O, Betz A, Giersch C (1975) Response of oscillating glycolysis to perturbations in NADH-NAD system - comparison between experiments and a computer model. *Biosystems* **7:** 137-146

Rizzi M, Baltes M, Theobald U, Reuss M (1997) *In vivo* analysis of metabolic dynamics in Saccharomyces cerevisiae .2. Mathematical model. *Biotechnology and Bioengineering* **55:** 592-608

Romeo T, Snoep J. (2005) Chapter 3.5.1, Glycolysis and Flux Control. In al. RCIe (ed.), *EcoSal-Escherichia coli and Salmonella; cellular and molecular biology*. ASM Press, Washington, DC.

Sauro HM (1994) Moiety-conserved cycles and metabolic control analysis - problems in sequestration and metabolic channeling. *Biosystems* **33:** 55-67

Sauro HM, Small JR, Fell DA (1987) Metabolic control and its analysis - extensions to the theory and matrix-method. *European Journal of Biochemistry* **165:** 215-221

Sawers G, Clark DP. (2004) Chapter 3.5.3, Fermentative pyruvate and scetyl-coenzyme A metabolism. In al RCIe (ed.), *EcoSal-Escherichia coli and Salmonella; cellular and molecular biology*. ASM Press, Washington, DC.

Schaub J, Reuss M (2008) *In Vivo* Dynamics of Glycolysis in *Escherichia coli* Shows Need for Growth-Rate Dependent Metabolome Analysis. *Biotechnology Progress* **24:** 1402-1407

Schellenberger J, Que R, Fleming RMT, Thiele I, Orth JD, Feist AM, Zielinski DC, Bordbar A, Lewis NE, Rahmanian S, Kang J, Hyduke DR, Palsson BO (2011) Quantitative prediction of cellular metabolism with constraint-based models: the COBRA Toolbox v2.0. *Nature Protocols* **6:** 1290-1307

Schirmer A, Rude MA, Li X, Popova E, del Cardayre SB (2010) Microbial Biosynthesis of Alkanes. *Science* **329:** 559-562

Schmidt PP, Travers F, Barman T (1995) Transient and equilibrium kinetic-studies on yeast 3-phosphoglycerate kinase - evidence that an intermediate containing 1,3-bisphosphoglycerate accumulates in the steady-state. *Biochemistry* **34:** 824-832

Schomburg I, Chang A, Placzek S, Sohngen C, Rother M, Lang M, Munaretto C, Ulas S, Stelzer M, Grote A, Scheer M, Schomburg D (2013) BRENDA in 2013: integrated reactions, kinetic data, enzyme function data, improved disease classification: new options and contents in BRENDA. *Nucleic acids research* **41**

Schurmann M, Sprenger GA (2001) Fructose-6-phosphate aldolase is a novel class I aldolase from *Escherichia coli* and is related to a novel group of bacterial transaldolases. *Journal of Biological Chemistry* **276:** 11055-11061

Segel IH (1975) *Enzyme kinetics : behavior and analysis of rapid equilibrium and steady state enzyme systems*, New York: Wiley.

Serres MH, Goswami S, Riley M (2004) GenProtEC: an updated and improved analysis of functions of *Escherichia coli* K-12 proteins. *Nucleic Acids Research* **32**

Shen CR, Liao JC (2008) Metabolic engineering of *Escherichia coli* for 1-butanol and 1-propanol production via the keto-acid pathways. *Metabolic Engineering* **10:** 312-320

Shen CR, Liao JC (2011) A synthetic iterative pathway for ketoacid elongation. *Methods in Enzymology, Vol 497: Synthetic Biology, Methods for Part/Device Characterization and Chassis Engineering, Pt A* **497:** 469-481

Shone CC, Fromm HJ (1981) Steady-state and pre-steady-state kinetics of coenzyme-a linked aldehyde dehydrogenase from *Escherichia-coli*. *Biochemistry* **20:** 7494-7501

Soetaert W, Vandamme EJ (2009) *Biofuels*, Chichester, U.K.: Wiley.

Spring TG, Wold F (1971) Purification and charactization of *Escherichia-coli* enolase. *Journal of Biological Chemistry* **246:** 6797-&

Steen EJ, Kang Y, Bokinsky G, Hu Z, Schirmer A, McClure A, del Cardayre SB, Keasling JD (2010) Microbial production of fatty-acid-derived fuels and chemicals from plant biomass. *Nature* **463:** 559-U182

Stephanopoulos G (2007) Challenges in engineering microbes for biofuels production. *Science* **315:** 801-804

Stephanopoulos G, Aristidou AA, Nielsen J (1998) *Metabolic engineering : principles and methodologies*, San Diego: Academic Press.

Steuer R, Gross T, Selbig J, Blasius B (2006) Structural kinetic modeling of metabolic networks. *Proceedings of the National Academy of Sciences of the United States of America* **103:** 11868-11873

Subedi KP, Kim I, Kim J, Min B, Park C (2008) Role of GldA in dihydroxyacetone and methylglyoxal metabolism of *Escherichia coli* K12. *Fems Microbiology Letters* **279:** 180-187

Sugio T, Mizunashi W, Inagaki K, Tano T (1987) Purification and some properties of sulfur - ferric ion oxidoreductase from thiobacillus-ferrooxidans. *Journal of Bacteriology* **169:** 4916-4922

Sun Y, Ye J, Mu X, Teng H, Feng E, Zeng A, Xiu Z (2012) Nonlinear Mathematical Simulation and Analysis of Dha Regulon for Glycerol Metabolism in Klebsiella pneumoniae. *Chinese Journal of Chemical Engineering* **20:** 958-970

Sun YQ, Qi WT, Teng H, Xiu ZL, Zeng AP (2008) Mathematical modeling of glycerol fermentation by Klebsiella pneumoniae: Concerning enzyme-catalytic reductive pathway and transport of glycerol and 1,3-propanediol across cell membrane. *Biochemical Engineering Journal* **38:** 22-32

Sundararaj S, Guo A, Habibi-Nazhad B, Rouani M, Stothard P, Ellison M, Wishart DS (2004) The CyberCell Database (CCDB): a comprehensive, self-updating, relational database to coordinate and facilitate *in silico* modeling of *Escherichia coli*. *Nucleic Acids Research* **32**

Tang X, Tan Y, Zhu H, Zhao K, Shen W (2009) Microbial Conversion of Glycerol to 1,3-Propanediol by an Engineered Strain of *Escherichia coli*. *Applied and Environmental Microbiology* **75**

Teusink B, Passarge J, Reijenga CA, Esgalhado E, van der Weijden CC, Schepper M, Walsh MC, Bakker BM, van Dam K, Westerhoff HV, Snoep JL (2000) Can yeast glycolysis be understood in terms of *in vitro* kinetics of the constituent enzymes? Testing biochemistry. *European Journal of Biochemistry* **267:** 5313-5329

Tholudur A, Ramirez WF, McMillan JD (1999) Mathematical modeling and optimization of cellulase protein production using Trichoderma reesei RL-P37. *Biotechnology and Bioengineering* **66:** 1-16

Torres NV, Voit EO (2002) *Pathway analysis and optimization in metabolic engineering*, Cambridge, U.K. ; New York, NY, USA: Cambridge University Press.

Truniger V, Boos W (1994) Mapping and cloning of glda, the structural gene of the *Escherichia-coli* glycerol dehydrogenase. *Journal of Bacteriology* **176:** 1796-1800

U.S. Department of Energy ISA. (2012) Biofuels Issues and Trends. In U.S. Energy Information Administration ISA (ed.). U.S. Department of Energy, Washington DC 20585, www.eia.gov.

Visser D, Heijnen JJ (2003) Dynamic simulation and metabolic re-design of a branched pathway using linlog kinetics. *Metabolic Engineering* **5:** 164-176

Voegele RT, Sweet GD, Boos W (1993) Glycerol kinase of *Escherichia-coli* is activated by interaction with the glycerol facilitator. *Journal of Bacteriology* **175:** 1087-1094

Yazdani SS, Gonzalez R (2007) Anaerobic fermentation of glycerol: a path to economic viability for the biofuels industry. *Current Opinion in Biotechnology* **18:** 213-219

Yazdani SS, Gonzalez R (2008) Engineering *Escherichia coli* for the efficient conversion of glycerol to ethanol and co-products. *Metabolic Engineering* **10:** 340-351

Zhang K, Sawaya MR, Eisenberg DS, Liao JC (2008) Expanding metabolism for biosynthesis of nonnatural alcohols. *Proceedings of the National Academy of Sciences of the United States of America* **105:** 20653-20658

Zhang X, Shanmugam KT, Ingram LO (2010) Fermentation of Glycerol to Succinate by Metabolically Engineered Strains of *Escherichia coli*. *Applied and Environmental Microbiology* **76:** 2397-2401

Zhu J, Shimizu K (2004) The effect of pfl gene knockout on the metabolism for optically pure D-lactate production by *Escherichia coli*. *Applied Microbiology and Biotechnology* **64:** 367-375

Zhu MM, Lawman PD, Cameron DC (2002) Improving 1,3-propanediol production from glycerol in a metabolically engineered *Escherichia coli* by reducing accumulation of sn-glycerol-3-phosphate. *Biotechnology Progress* **18:** 694-699

Zidansek A, Blinc R, Jeglic A, Kabashi S, Bekteshi S, Slaus I (2009) Climate changes, biofuels and the sustainable future. *International Journal of Hydrogen Energy* **34:** 6980-6995

Zomorrodi AR, Suthers PF, Ranganathan S, Maranas CD (2012) Mathematical optimization applications in metabolic networks. *Metabolic Engineering* **14:** 672-686

10 Appendix

10.1 Matrix system for FCC

The system of equations for the calculation of FCC in themodel for glycerol fermentation, as presented in Figure 28, is as follows:

$$M*C=R \quad (95)$$

$$M = \begin{bmatrix}
1 & 1 & 1 & 1 & 1 \\
\varepsilon_{GLYC}^{GlpF} & \varepsilon_{GLYC}^{glyDH} & 0 & 0 & 0 \\
0 & \varepsilon_{DHA}^{glyDH} & \varepsilon_{DHA}^{DHAPK} & 0 & 0 \\
0 & 0 & \varepsilon_{DHAP}^{DHAPK} & \varepsilon_{DHAP}^{TPI} - \varepsilon_{GAP}^{TPI} \cdot \frac{C_{DHAP}}{C_{GAP}} & -\varepsilon_{GAP}^{GAPDH} \cdot \frac{C_{DHAP}}{C_{GAP}} \\
0 & 0 & 0 & \varepsilon_{GAP}^{TPI} & \varepsilon_{GAP}^{GAPDH} - \varepsilon_{PGP}^{GAPDH} \cdot \frac{C_{GAP}}{C_{PGP}} \\
0 & 0 & 0 & 0 & \varepsilon_{PGP}^{GAPDH} \\
0 & 0 & 0 & 0 & 0 \\
0 & 0 & -\varepsilon_{PEP}^{DHAK} \cdot \frac{C_{2PG}}{C_{PEP}} & 0 & 0 \\
0 & 0 & 0 & 0 & 0 \\
0 & 0 & 0 & 0 & 0 \\
0 & 0 & 0 & 0 & 0
\end{bmatrix}$$

$$\begin{bmatrix}
1 & 1 & 1 & 1 & 1 & 1 \\
0 & 0 & 0 & 0 & 0 & 0 \\
0 & 0 & 0 & 0 & 0 & 0 \\
0 & 0 & 0 & 0 & 0 & 0 \\
-\varepsilon_{PGP}^{PGK} \cdot \frac{C_{GAP}}{C_{PGP}} & 0 & 0 & 0 & 0 & 0 \\
\varepsilon_{PGP}^{PGK} - \varepsilon_{3PG}^{PGK} \cdot \frac{C_{PGP}}{C_{3PG}} & -\varepsilon_{3PG}^{PGM} \cdot \frac{C_{PGP}}{C_{3PG}} & 0 & 0 & 0 & 0 \\
\varepsilon_{3PG}^{PGK} & \varepsilon_{3PG}^{PGM} - \varepsilon_{2PG}^{PGM} \cdot \frac{C_{3PG}}{C_{2PG}} & -\varepsilon_{2PG}^{ENO} \cdot \frac{C_{3PG}}{C_{2PG}} & 0 & 0 & 0 \\
0 & \varepsilon_{2PG}^{PGM} & \varepsilon_{2PG}^{ENO} - \varepsilon_{PEP}^{DHAK} \cdot \frac{C_{2PG}}{C_{PEP}} & 0 & 0 & 0 \\
0 & 0 & \varepsilon_{PYR}^{ENO} & \varepsilon_{PYR}^{PFL} & 0 & 0 \\
0 & 0 & 0 & \varepsilon_{ACCOA}^{PFL} & \varepsilon_{ACCOA}^{ALDH} & 0 \\
0 & 0 & 0 & 0 & \varepsilon_{ACALD}^{ALDH} & \varepsilon_{ACALD}^{ADH}
\end{bmatrix}$$

$$C = \begin{bmatrix} FCC^{GlpF} \\ FCC^{glyDH} \\ FCC^{DHAK} \\ FCC^{TPI} \\ FCC^{GAPDH} \\ FCC^{PGK} \\ FCC^{PGMA} \\ FCC^{ENO} \\ FCC^{PFL} \\ FCC^{ALDH} \\ FCC^{ADH} \end{bmatrix} \qquad R = \begin{bmatrix} 1 \\ 0 \\ 0 \\ 0 \\ 0 \\ 0 \\ 0 \\ 0 \\ 0 \\ 0 \\ 0 \end{bmatrix}$$

10.2 List of reactions modified in glyc-GEM

All the modifications were implemented in the matlab function AC_BiomassvsProduct_GlyceroliJO1366.m. This funtion calculates optimal solutions, solution spaces, and evaluate the different cases that were included for the production of lactate, succinate, 1,2-PDO, 1,3-PDO, propanol, propionic acid and butanol.

Table 25: List of modifications to the iJO1366 model in order to represent glycerol fermentation. The numbers within bracket correspond to the original value, previous to this modification. All reactions and metabolite abbreviations corresponds to those used in the iJO1366, with the exception of FBPA3 (originally FBA3), which was changes to avoid misleading with the abbreviation of flux balance analysis (FBA).

Reaction name	Reaction	Comments	Lower bound	Upper bound
EX_26dap-M(e)	26dap-M[e] <=>	no amino acids exchange	0	0 (1000)
EX_5mtr(e)	5mtr[e] <=>	no 5mtr exchange	0	0 (1000)
EX_ala-B(e)	ala-B[e] <=>	no amino acids exchange	0	0 (1000)
EX_ala-D(e)	ala-D[e] <=>	no amino acids exchange	0	0 (1000)
EX_ala-L(e)	ala-L[e] <=>	no amino acids exchange	0	0 (1000)

EX_asn-L(e)	asn-L[e] <=>	no amino acids exchange	0	0 (1000)
EX_asp-L(e)	asp-L[e] <=>	no amino acids exchange	0	0 (1000)
EX_co2(e)	co2[e] <=>	no amino acids exchange	0 (-1000)	1000
EX_cys-D(e)	cys-D[e] <=>	no amino acids exchange	0	0 (1000)
EX_cys-L(e)	cys-L[e] <=>	no amino acids exchange	0	0 (1000)
EX_fe2(e)	fe2[e] <=>	no Fe2+ exchange	-1000	0 (1000)
EX_frulys(e)	frulys[e] <=>	no amino acids exchange	0	0 (1000)
EX_glc(e)	glc-D[e] <=>	no glucose consumption	0 (-10)	1000
EX_gln-L(e)	gln-L[e] <=>	no amino acids exchange	0	0 (1000)
EX_glu-L(e)	glu-L[e] <=>	no amino acids exchange	0	0 (1000)
EX_gly(e)	gly[e] <=>	no amino acids exchange	0	0 (1000)
EX_glyc(e)	glyc[e] <=>	glycerol fermentation	-20	1000
EX_h2s(e)	h2s[e] <=>	no H2S exchange	0	0 (1000)
EX_his-L(e)	his-L[e] <=>	no amino acids exchange	0	0 (1000)
EX_hom-L(e)	hom-L[e] <=>	no amino acids exchange	0	0 (1000)
EX_hxa(e)	hxa[e] <=>	no hexanoate exchange	0	0 (1000)
EX_ile-L(e)	ile-L[e] <=>	no amino acids exchange	0	0 (1000)
EX_leu-L(e)	leu-L[e] <=>	no amino acids exchange	0	0 (1000)
EX_lys-L(e)	lys-L[e] <=>	no amino acids exchange	0	0 (1000)
EX_met-D(e)	met-D[e] <=>	no amino acids exchange	0	0 (1000)
EX_met-L(e)	met-L[e] <=>	no amino acids exchange	0	0 (1000)

EX_o2(e)	o2[e] <=>	no oxygen consumption	0 (-1000)	1000
EX_orn(e)	orn[e] <=>	no amino acids exchange	0	0 (1000)
EX_phe-L(e)	phe-L[e] <=>	no amino acids exchange	0	0 (1000)
EX_pro-L(e)	pro-L[e] <=>	no amino acids exchange	0	0 (1000)
EX_ser-D(e)	ser-D[e] <=>	no amino acids exchange	0	0 (1000)
EX_ser-L(e)	ser-L[e] <=>	no amino acids exchange	0	0 (1000)
EX_spmd(e)	spmd[e] <=>	no spirmidine production	0	0 (1000)
EX_thr-L(e)	thr-L[e] <=>	no amino acids exchange	0	0 (1000)
EX_trp-L(e)	trp-L[e] <=>	no amino acids exchange	0	0 (1000)
EX_tyr-L(e)	tyr-L[e] <=>	no amino acids exchange	0	0 (1000)
EX_val-L(e)	val-L[e] <=>	no amino acids exchange	0	0 (1000)
42A12BOOXpp	dopa[p] + h2o[p] + o2[p] -> 34dhpac[p] + h2o2[p] + nh4[p]	no amino acids degradation	0	0 (1000)
ADA	adn[c] + h[c] + h2o[c] -> ins[c] + nh4[c]	no nucleotides degradation	0	0 (1000)
ARGDC	arg-L[c] + h[c] -> agm[c] + co2[c]	no amino acids degradation	0	0 (1000)
ARGDCpp	arg-L[p] + h[p] -> agm[p] + co2[p]	no amino acids degradation	0	0 (1000)
ASPT	asp-L[c] -> fum[c] + nh4[c]	no amino acids degradation	0	0 (1000)
AST	arg-L[c] + succoa[c] -> coa[c] + h[c] + sucarg[c]	no amino acids degradation	0	0 (1000)
CYSDS	cys-L[c] + h2o[c] -> h2s[c] + nh4[c] + pyr[c]	no amino acids degradation	0	0 (1000)
CYTD	cytd[c] + h[c] + h2o[c] -> nh4[c] + uri[c]	no nucleotides degradation	0	0 (1000)
DAAD	ala-D[c] + fad[c] + h2o[c] -> fadh2[c] + nh4[c] + pyr[c]	no amino acids degradation	0	0 (1000)
DADA	dad-2[c] + h[c] + h2o[c] -> din[c] + nh4[c]	no nucleotides degradation	0	0 (1000)

DCYTD	dcyt[c] + h[c] + h2o[c] -> duri[c] + nh4[c]	no nucleotides degradation	0	0 (1000)
DRPA	2dr5p[c] -> acald[c] + g3p[c]	no nucleotides degradation	0	0 (1000)
DURIPP	duri[c] + pi[c] <=> 2dr1p[c] + ura[c]	no nucleotides degradation	0 (-1000)	0 (1000)
F6PA	f6p[c] <=> dha[c] + g3p[c]	Limit F6PA	-4(-1000)	1000
FBPA3	s17bp[c] <=> dhap[c] + e4p[c]	no FBPA3	0 (-1000)	0 (1000)
FHL	for[c] + h[c] -> co2[c] + h2[c]	Reverse FHL	-1000	1000
G3PD2	glyc3p[c] + nadp[c] <=> dhap[c] + h[c] + nadph[c]	G3PD2 irreversible	-1000	0 (1000)
GLUN	gln-L[c] + h2o[c] -> glu-L[c] + nh4[c]	no amino acids degradation	0	0 (1000)
GLYAT	accoa[c] + gly[c] <=> 2aobut[c] + coa[c]	no amino acids degradation	0 (-1000)	0 (1000)
OBTFL	2obut[c] + coa[c] -> for[c] + ppcoa[c]	no amino acids degradation	0	0 (1000)
P5CD	1pyr5c[c] + 2 h2o[c] + nad[c] -> glu-L[c] + h[c] + nadh[c]	no amino acids degradation	0	0 (1000)
PEAMNOpp	h2o[p] + o2[p] + peamn[p] -> h2o2[p] + nh4[p] + pacald[p]	no amino acids degradation	0	0 (1000)
PFK_3	atp[c] + s7p[c] -> adp[c] + h[c] + s17bp[c]	no PFK_3	0	0 (1000)
POR5	coa[c] + 2 flxso[c] + pyr[c] <=> accoa[c] + co2[c] + 2 flxr[c] + h[c]	no flavodoxins-dependent PYR synthase.	0 (-1000)	0 (1000)
PPAKr	adp[c] + ppap[c] <=> atp[c] + ppa[c]	no amino acids degradation	0 (-1000)	0 (1000)
PPM2	2dr1p[c] <=> 2dr5p[c]	no nucleotides degradation	0 (-1000)	0 (1000)
PROD2	fad[c] + pro-L[c] -> 1pyr5c[c] + fadh2[c] + h[c]	no amino acids degradation	0	0 (1000)
PUNP1	adn[c] + pi[c] <=> ade[c] + r1p[c]	no nucleotides degradation	0 (-1000)	0 (1000)
PUNP2	dad-2[c] + pi[c] <=> 2dr1p[c] + ade[c]	no nucleotides degradation	0 (-1000)	0 (1000)
PUNP3	gsn[c] + pi[c] <=> gua[c] + r1p[c]	no nucleotides degradation	0 (-1000)	0 (1000)
PUNP4	dgsn[c] + pi[c] <=> 2dr1p[c] + gua[c]	no nucleotides degradation	0 (-1000)	0 (1000)
PUNP5	ins[c] + pi[c] <=> hxan[c] + r1p[c]	no nucleotides degradation	0 (-1000)	0 (1000)

PUNP6	din[c] + pi[c] <=> 2dr1p[c] + hxan[c]	no nucleotides degradation	0 (-1000)	0 (1000)
PUNP7	pi[c] + xtsn[c] <=> r1p[c] + xan[c]	no nucleotides degradation	0 (-1000)	0 (1000)
PYNP2r	pi[c] + uri[c] <=> r1p[c] + ura[c]	no nucleotides degradation	0 (-1000)	0 (1000)
SADH	2 h[c] + 2 h2o[c] + sucarg[c] -> co2[c] + 2 nh4[c] + sucorn[c]	no amino acids degradation	0	0 (1000)
SERD_L	ser-L[c] -> nh4[c] + pyr[c]	no amino acids degradation	0	0 (1000)
SGDS	h2o[c] + sucglu[c] -> glu-L[c] + succ[c]	no amino acids degradation	0	0 (1000)
SGSAD	h2o[c] + nad[c] + sucgsa[c] -> 2 h[c] + nadh[c] + sucglu[c]	no amino acids degradation	0	0 (1000)
THRAi	thr-L[c] -> acald[c] + gly[c]	no amino acids degradation	0	0 (1000)
THRD	nad[c] + thr-L[c] -> 2aobut[c] + h[c] + nadh[c]	no amino acids degradation	0	0 (1000)
TMDPP	pi[c] + thymd[c] <=> 2dr1p[c] + thym[c]	no nucleotides degradation	0 (-1000)	0 (1000)
TRPAS2	h2o[c] + trp-L[c] <=> indole[c] + nh4[c] + pyr[c]	no amino acids degradation	0 (-1000)	0 (1000)
TYROXDApp	h2o[p] + o2[p] + tym[p] -> 4hoxpacd[p] + h2o2[p] + nh4[p]	no amino acids degradation	0	0 (1000)
Add_PntAB	nadh[c] + nadp[c] + h[p] <=> h[c] + nad[c] + nadph[c]	Add PntAB	0	1000

*** Numbers within bracket correspond to original lower and upper bound.**

10.3 List of reactions modified in lcp-GEM

I implemented all the modifications in the matlab function AC_BiomassvsProduct_GlucoseJO1366.m. This funtion simulates the reversal of the β-oxidation cycle, the FA biosynthesis pathway and the α-keto acid pathway. This function calculates optimal solutions and solution spaces. The following table represents the modifications that were done in addition to those made for the glyc-GEM.

The no flavodoxins-dependant acyl dehydrogenases were removed, as they have not been reported in *E. coli*. In contrast, these reactions have been associated with

ferredoxins; therefore, I added these reactions as reported previously for the functioning of the reversal of the β-oxidation cycle (Dellomonaco et al., 2011).

Table 26: List of additional modifications to the iJO1366 model in order to represent synthesis of long chain products. The numbers within bracket correspond to the original value, previous to this modification. All reactions and metabolite abbreviations corresponds to those used in the iJO1366.

Reaction name	Reaction	Comments	Lower bound	Upper bound
EX_cys-L(e)	cys-L[e] <=>	no amino acids	0	0 (1000)
EX_dca(e)	dca[e] <=>	no production of FAs	0	0 (1000)
EX_hdca(e)	hdca[e] <=>	no production of FAs	0	0 (1000)
EX_ocdca(e)	ocdca[e] <=>	no production of FAs	0	0 (1000)
EX_octa(e)	octa[e] <=>	no production of FAs	0	0 (1000)
EX_pyr(e)	pyr[e] <=>	no production of PYR	0	0 (1000)
EX_ttdca(e)	ttdca[e] <=>	no production of FAs	0	0 (1000)
ACCOAC	accoa[c] + atp[c] + hco3[c] -> adp[c] + h[c] + malcoa[c] + pi[c]	Prevent ficticious flux toward the FA biosynthesis pathway when analysis the reversed β-oxidation cycle	0	0.1 (1000)
ACOAD1f	btcoa[c] + fad[c] <=> b2coa[c] + fadh2[c]	no flavodoxins-dependant acyl dehydrogenase	0 (-1000)	0 (1000)
ACOAD2f	fad[c] + hxcoa[c] <=> fadh2[c] + hx2coa[c]	no flavodoxins-dependant acyl dehydrogenase	0 (-1000)	0 (1000)
ACOAD3f	fad[c] + occoa[c] <=> fadh2[c] + oc2coa[c]	no flavodoxins-dependant acyl dehydrogenase	0 (-1000)	0 (1000)
ACOAD4f	dcacoa[c] + fad[c] <=> dc2coa[c] + fadh2[c]	no flavodoxins-dependant acyl dehydrogenase	0 (-1000)	0 (1000)
ACOAD5f	ddcacoa[c] + fad[c] <=> dd2coa[c] + fadh2[c]	no flavodoxins-dependant acyl dehydrogenase	0 (-1000)	0 (1000)
ACOAD6f	fad[c] + tdcoa[c] <=> fadh2[c] + td2coa[c]	no flavodoxins-dependant acyl dehydrogenase	0 (-1000)	0 (1000)
ACOAD7f	fad[c] + pmtcoa[c] <=> fadh2[c] + hdd2coa[c]	no flavodoxins-dependant acyl dehydrogenase	0 (-1000)	0 (1000)

ACOAD8f	fad[c] + stcoa[c] <=> fadh2[c] + od2coa[c]	no flavodoxins-dependant acyl dehydrogenase	0 (-1000)	0 (1000)
FHL	for[c] + h[c] -> co2[c] + h2[c]	Keep original values	0	0
G3PD2	glyc3p[c] + nadp[c] <=> dhap[c] + h[c] + nadph[c]	Keep original values	-1000	1000
ACOAD1f_ferr	btcoa[c] + fd_oxi <=> b2coa[c] + h[c] + fd_red	New Reaction	-1000	0 (1000)
ACOAD2f_ferr	hxcoa[c] + fd_oxi <=> h[c] + hx2coa[c] + fd_red	New Reaction	-1000	0 (1000)
ACOAD3f_ferr	occoa[c] + fd_oxi <=> h[c] + oc2coa[c] + fd_red	New Reaction	-1000	0 (1000)
ACOAD4f_ferr	dcacoa[c] + fd_oxi <=> dc2coa[c] + h[c] + fd_red	New Reaction	-1000	0 (1000)
ACOAD5f_ferr	ddcacoa[c] + fd_oxi <=> dd2coa[c] + h[c] + fd_red	New Reaction	-1000	0 (1000)
ACOAD6f_ferr	tdcoa[c] + fd_oxi <=> h[c] + td2coa[c] + fd_red	New Reaction	-1000	0 (1000)
ACOAD7f_ferr	pmtcoa[c] + fd_oxi <=> h[c] + hdd2coa[c] + fd_red	New Reaction	-1000	0 (1000)
ACOAD8f_ferr	stcoa[c] + fd_oxi <=> h[c] + od2coa[c] + fd_red	New Reaction	-1000	0 (1000)
PFOR	coa[c] + pyr[c] + fd_oxi <=> accoa[c] + co2[c] + h[c] + fd_red	New Reaction	0	1000
P_butanal_ACP	butACP[c] + h[c] + nadh[c] <=> ACP[c] + nad[c] + butanal[c]	New Reaction	0	0
P_hexanal_ACP	h[c] + hexACP[c] + nadh[c] <=> ACP[c] + nad[c] + hexanal[c]	New Reaction	0	0
P_octanal_ACP	h[c] + nadh[c] + ocACP[c] <=> ACP[c] + nad[c] + octanal[c]	New Reaction	0	0
P_decanal_ACP	dcaACP[c] + h[c] + nadh[c] <=> ACP[c] + nad[c] + decanal[c]	New Reaction	0	0
P_dodecanal_ACP	ddcaACP[c] + h[c] + nadh[c] <=> ACP[c] + nad[c] + dodecanal[c]	New Reaction	0	0

P_tetradecanal_ACP	h[c] + myrsACP[c] + nadh[c] <=> ACP[c] + nad[c] + tetradecanal[c]	New Reaction	0	0
P_hexadecanal_ACP	h[c] + nadh[c] + palmACP[c] <=> ACP[c] + nad[c] + hexadecanal[c]	New Reaction	0	0
P_octadecanal_ACP	h[c] + nadh[c] + ocdcaACP[c] <=> ACP[c] + nad[c] + octadecanal[c]	New Reaction	0	0
P_butanal_CoA	btcoa[c] + h[c] + nadh[c] <=> coa[c] + nad[c] + butanal[c]	New Reaction	0	1000
P_hexanal_CoA	h[c] + hxcoa[c] + nadh[c] <=> coa[c] + nad[c] + hexanal[c]	New Reaction	0	1000
P_octanal_CoA	h[c] + nadh[c] + occoa[c] <=> coa[c] + nad[c] + octanal[c]	New Reaction	0	1000
P_decanal_CoA	dcacoa[c] + h[c] + nadh[c] <=> coa[c] + nad[c] + decanal[c]	New Reaction	0	1000
P_dodecanal_CoA	ddcacoa[c] + h[c] + nadh[c] <=> coa[c] + nad[c] + dodecanal[c]	New Reaction	0	1000
P_tetradecanal_CoA	h[c] + nadh[c] + tdcoa[c] <=> coa[c] + nad[c] + tetradecanal[c]	New Reaction	0	1000
P_hexadecanal_CoA	h[c] + nadh[c] + pmtcoa[c] <=> coa[c] + nad[c] + hexadecanal[c]	New Reaction	0	1000
P_octadecanal_CoA	h[c] + nadh[c] + stcoa[c] <=> coa[c] + nad[c] + octadecanal[c]	New Reaction	0	1000
P_propane	butanal[c] <=> propane[c] + co[c]	New Reaction	0	1000
P_pentane	hexanal[c] <=> co[c] + pentane[c]	New Reaction	0	1000
P_heptane	octanal[c] <=> co[c] + heptane[c]	New Reaction	0	1000
P_nonane	decanal[c] <=> co[c] + nonane[c]	New Reaction	0	1000
P_undecane	dodecanal[c] <=> co[c] + undecane[c]	New Reaction	0	1000
P_tridecane	tetradecanal[c] <=> co[c] + tridecane[c]	New Reaction	0	1000
P_pentadecane	hexadecanal[c] <=> co[c]+pentadecane[c]	New Reaction	0	1000

P_heptadecane	octadecanal[c] <=> co[c] + heptadecane[c]	New Reaction	0	1000
P_butanol	h[c] + nadh[c] + butanal[c] <=> nad[c] + butanol[c]	New Reaction	0	1000
P_hexanol	h[c] + nadh[c] + hexanal[c] <=> nad[c] + hexanol[c]	New Reaction	0	1000
P_octanol	h[c] + nadh[c] + octanal[c] <=> nad[c] + octanol[c]	New Reaction	0	1000
P_decanol	h[c] + nadh[c] + decanal[c] <=> nad[c] + decanol[c]	New Reaction	0	1000
P_dodecanol	h[c] + nadh[c] + dodecanal[c] <=> nad[c] + dodecanol[c]	New Reaction	0	1000
P_tetradecanol	h[c] + nadh[c] + tetradecanal[c] <=> nad[c] + tetradecanol[c]	New Reaction	0	1000
P_hexadecanol	h[c] + nadh[c] + hexadecanal[c] <=> nad[c] + hexadecanol[c]	New Reaction	0	1000
P_octadecanol	h[c] + nadh[c] + octadecanal[c] <=> nad[c] + octadecanol[c]	New Reaction	0	1000
P_but_CoA	btcoa[c] + h2o[c] <=> but[c] + coa[c] + h[c]	New Reaction	0	1000
P_but_ACP	butACP[c] + h2o[c] <=> ACP[c] + but[c] + h[c]	New Reaction	0	0
P_hxa_ACP	h2o[c] + hexACP[c] <=> ACP[c] + h[c] + hxa[c]	New Reaction	0	0
P_ocdca_ACP	h2o[c] + ocdcaACP[c] <=> ACP[c] + h[c] + ocdca[c]	New Reaction	0	0
P_octa_trans	octa[c] <=> octa[e]	New Reaction	0	1000
P_dca_trans	dca[c] <=> dca[e]	New Reaction	0	1000
P_ddca_trans	ddca[c] <=> ddca[e]	New Reaction	0	1000
P_ttdca_trans	ttdca[c] <=> ttdca[e]	New Reaction	0	1000
P_hdca_trans	hdca[c] <=> hdca[e]	New Reaction	0	1000
P_ocdca_trans_extra	ocdca[c] <=> ocdca[e]	New Reaction	0	1000
EX_butanol	butanol[c] <=>	New Reaction	0	1000
EX_hexanol	hexanol[c] <=>	New Reaction	0	0

EX_octanol	octanol[c] <=>	New Reaction	0	0
EX_decanol	decanol[c] <=>	New Reaction	0	0
EX_dodecanol	dodecanol[c] <=>	New Reaction	0	0
EX_tetradecanol	tetradecanol[c] <=>	New Reaction	0	0
EX_hexadecanol	hexadecanol[c] <=>	New Reaction	0	0
EX_octadecanol	octadecanol[c] <=>	New Reaction	0	0
EX_propane	propane[c] <=>	New Reaction	0	0
EX_pentane	pentane[c] <=>	New Reaction	0	0
EX_heptane	heptane[c] <=>	New Reaction	0	0
EX_nonane	nonane[c] <=>	New Reaction	0	0
EX_undecane	undecane[c] <=>	New Reaction	0	0
EX_tridecane	tridecane[c] <=>	New Reaction	0	0
EX_pentadecane	pentadecane[c] <=>	New Reaction	0	0
EX_heptadecane	heptadecane[c] <=>	New Reaction	0	0
EX_co	co[c] <=>	New Reaction	0	1000
P_leuA1	2obut[c] + accoa[c] + h2o[c] <=> coa[c] + 2ethylmalate '	New Reaction	0	1000
P_leuCD1	2ethylmalate <=> 3ethylmalate '	New Reaction	0	1000
P_3ethylmalate	nad[c] + 3ethylmalate <=> co2[c] + nadh[c] + 2ketovalerate	New Reaction	0	1000
P_2ketovalerate	2ketovalerate <=> co2[c] + butanal[c]	New Reaction	0	1000
P_leuA2	accoa[c] + h2o[c] + 2ketovalerate <=> coa[c] + 2propylmalate	New Reaction	0	1000
P_leuCD2	2propylmalate <=> 3propylmalate	New Reaction	0	1000
P_3propylmalate	nad[c] + 3propylmalate <=> co2[c] + nadh[c] + 2ketocaproate	New Reaction	0	1000
P_leuA3	accoa[c] + h2o[c] + 2ketocaproate <=> coa[c] + 2butylmalate	New Reaction	0	1000
P_leuCD3	2butylmalate <=> 3butylmalate	New Reaction	0	1000
P_3butylmalate	nad[c] + 3butylmalate <=> co2[c] + nadh[c] + 2ketoheptanoate	New Reaction	0	1000
P_2ketoheptanoate	2ketoheptanoate <=> co2[c] + hexanal[c]	New Reaction	0	1000

*** Numbers within bracket correspond to original lower and upper bound.**

10.4 Single gene deletion

The following genes were predicted to be essential to support cell growth under glycerol fermentative consitions. The analysis was done using the glyc-GEM.

Table 27: List of essential genes in glycerol fermentation.

genes	genes	genes	genes	genes	genes	genes	genes	genes	genes	genes
accA	bioB	dapA	fpr	hisA	ispU	metA	murE	pgk	pyrF	thiS
accB	bioC	dapB	gapA	hisB	kdsA	metB	murF	pheA	pyrG	thrB
accC	bioD	dapD	gldA	hisC	kdsB	metF	murG	plsC	ribA	thrC
accD	bioF	dapE	glmM	hisD	kdsC	metK	murI	plxH	ribB	thyA
acpP	bioH	dapF	glmS	hisF	leuA	mgsA	murJ	proC	ribC	tmk
acroD	cdsA	dfp	glmU	hisG	leuB	moaA	nadA	psd	ribD	tpiA
aldA	coaA	dxr	gltA	hisH	leuC	moaC	nadB	pssA	ribE	trpA
argA	coaD	dxs	gltX	hisI	leuD	moaD	nadC	purA	ribF	trpB
argB	coaE	eno	glyA	icd	lptA	moaE	nadD	purB	serA	trpC
argC	cyaY	fabB	gmk	ilvC	lptB	mobA	nadE	purC	serB	trpD
argD	cycA	fabD	guaA	ilvD	lptC	moeA	nadK	purD	serC	trpE
argE	cysC	fabG	hemA	ilvE	lptF	moeB	pabA	purE	thiC	tyrA
argG	cysD	fabH	hemB	iscS	lptG	mog	pabB	purF	thiD	ubiA
argH	cysE	fabI	hemC	ispA	lpxA	mraY	pabC	purH	thiE	ubiC
aroA	cysG	fabZ	hemD	ispB	lpxB	msbA	panB	purK	thiF	ubiD
aroB	cysH	folB	hemE	ispD	lpxC	mtn	panC	purL	thiG	ubiX
aroC	cysI	folC	hemG	ispE	lpxD	murA	panD	purM	thiH	waaA
asd	cysJ	folE	hemH	ispF	lpxK	murB	pdxA	pyrB	thiI	yrbG
aspC	cysN	folK	hemL	ispG	luxS	murC	pdxB	pyrC	thiL	zupT
bioA	cysQ	folP	hemN	ispH	lysA	murD	pdxJ	pyrE		

10.5 Diagrams of new models identified by the glyc-GEM with high predicted specific growth rates.

This section presents diagrams of the 16 new models identified using the glyc-GEM. Each of these models is predicted to enable glycerol fermentation in *E. coli* at higher specific growth rates than the optimal prediction for the wild type *E. coli*.

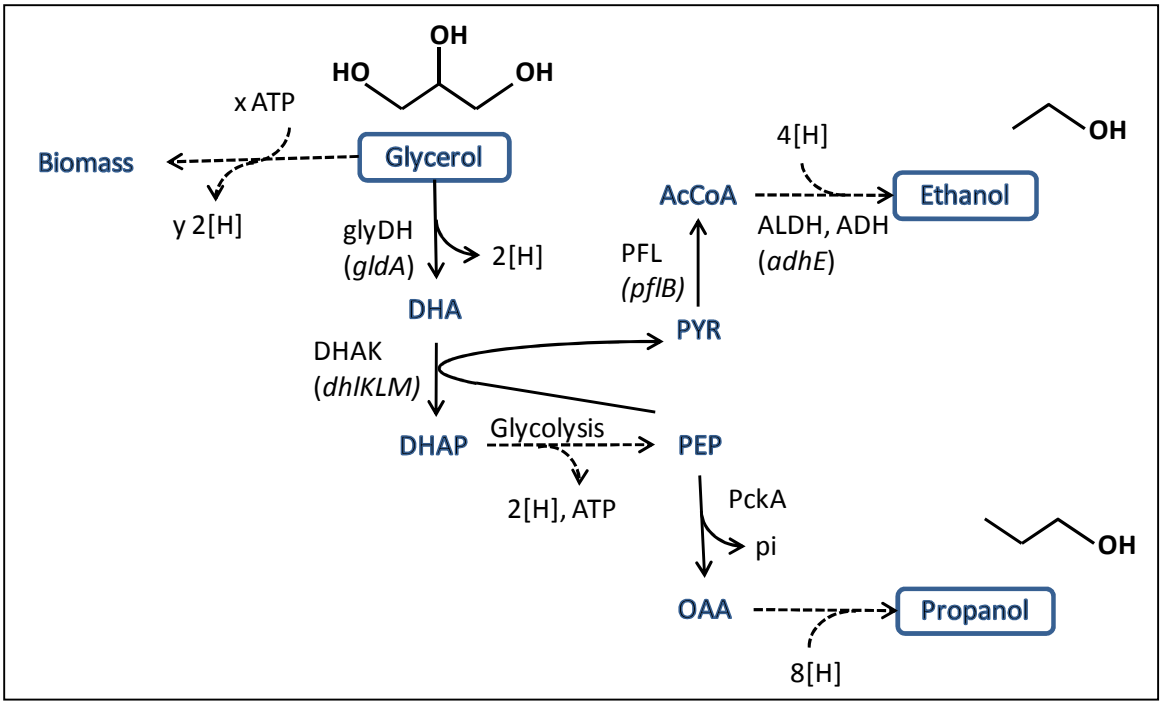

Figure 63: Model 1: Ethanol-Propanol. See Nomenclature for abbreviations (page 214).

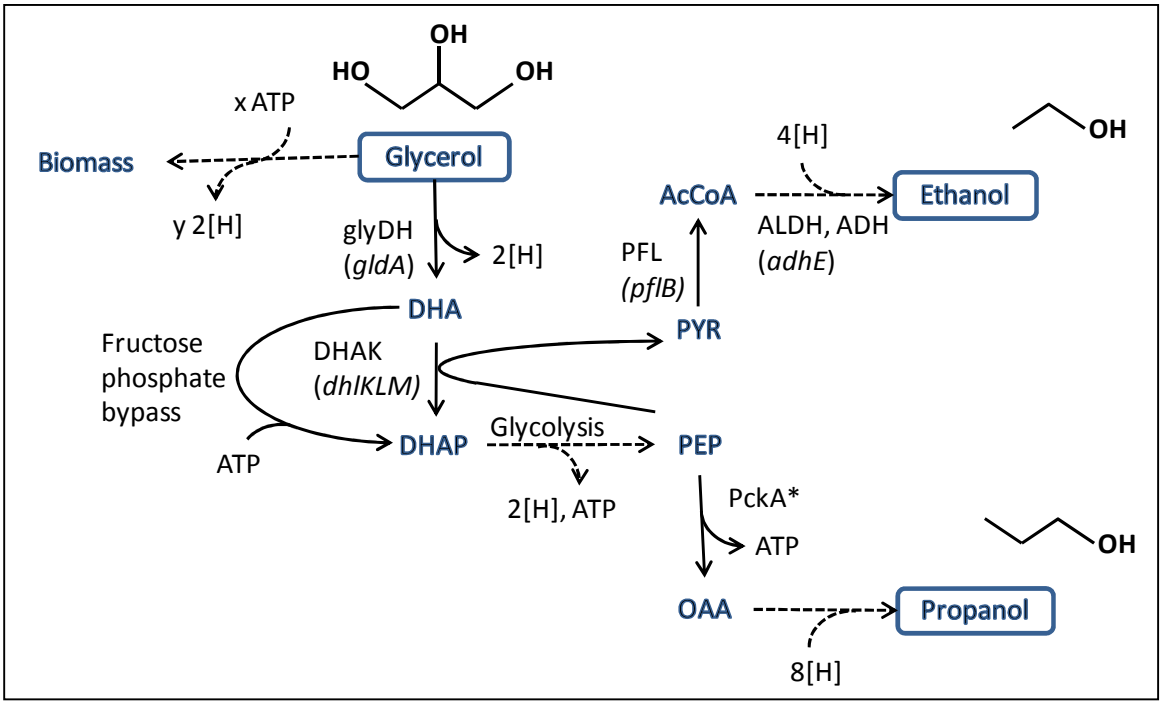

Figure 64: Model 2: Ethanol-Propanol (reversible PckA). See Nomenclature for abbreviations (page 214).

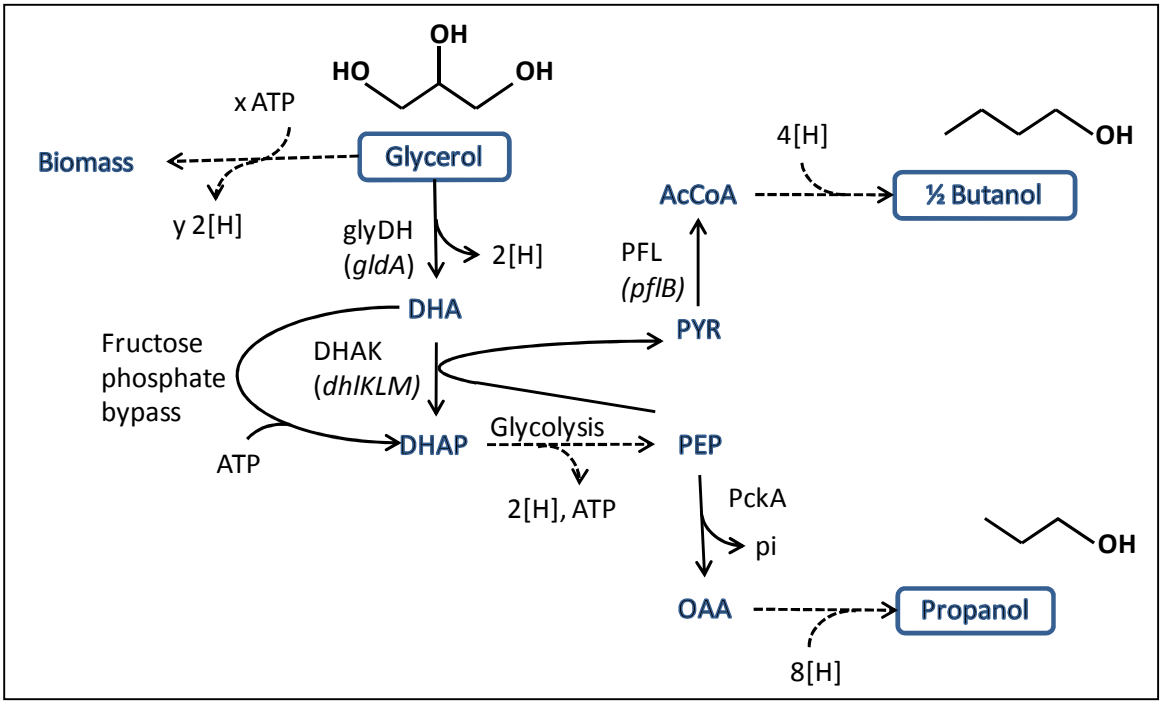

Figure 65: Model 3: Butanol-Propanol. See Nomenclature for abbreviations (page 214).

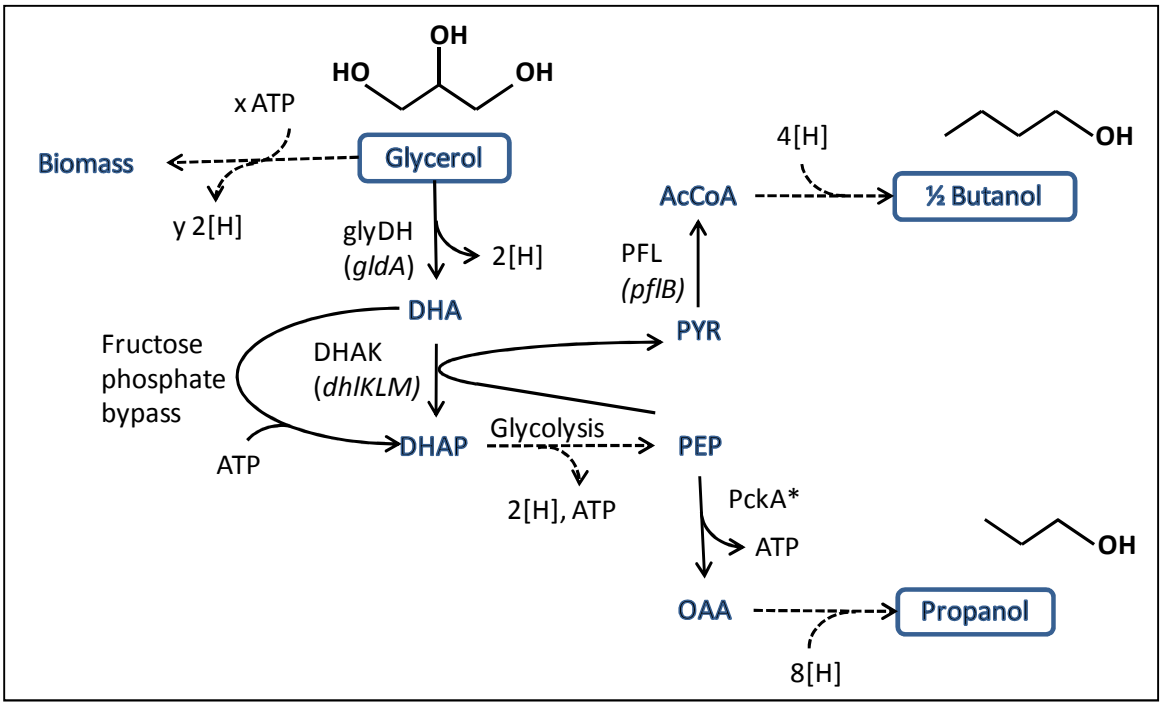

Figure 66: Model 4: Butanol-Propanol (reversible PckA). See Nomenclature for abbreviations (page 214).

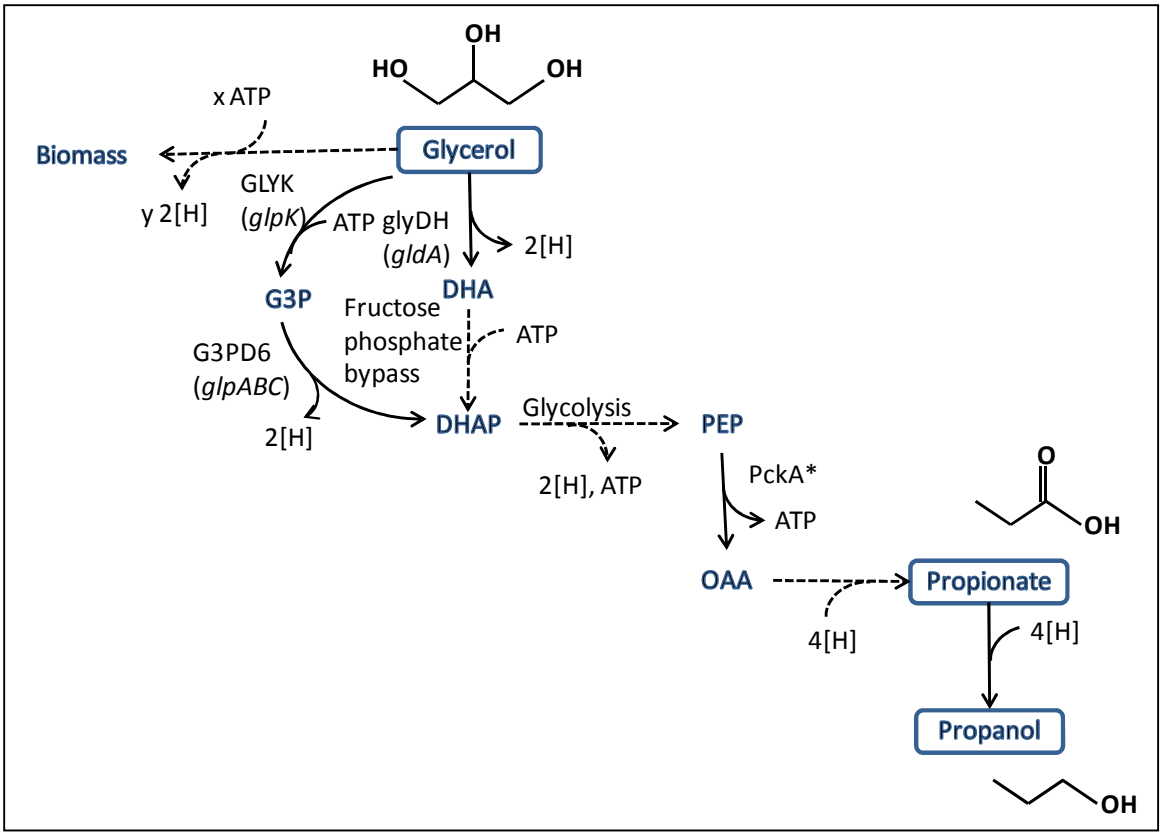

Figure 67: Model 5: Propanol-Propionate (reversible PckA). See Nomenclature for abbreviations (page 214).

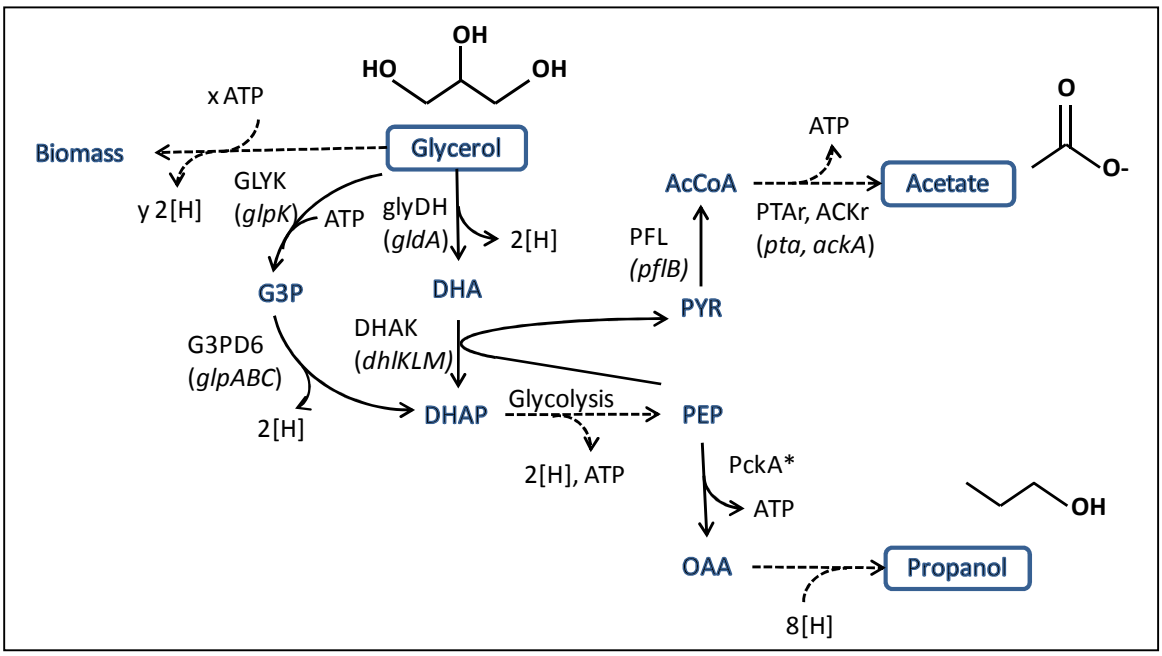

Figure 68: Model 6: Propanol-Acetate (reversible PckA). See Nomenclature for abbreviations (page 214).

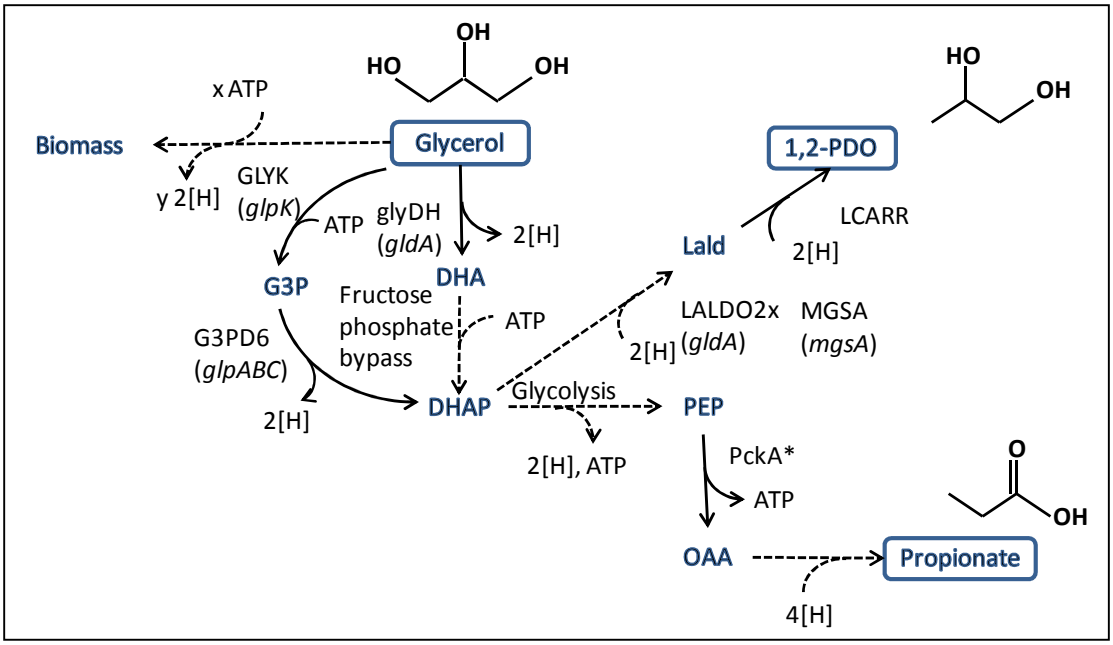

Figure 69: Model 7:Propionate (reversible PckA)-1,2PDO (MG to lald) See Nomenclature for abbreviations (page 214).

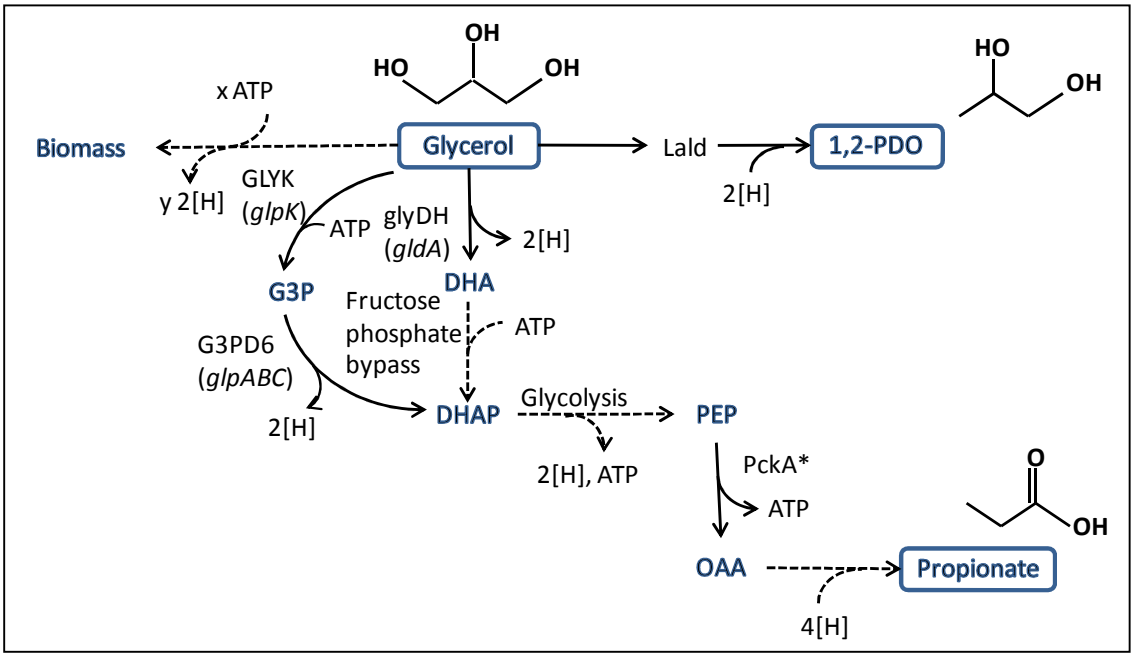

Figure 70: Model 8:Propionate (reversible PckA) – 1,2-PDO (glycerol to lald). See Nomenclature for abbreviations (page 214).

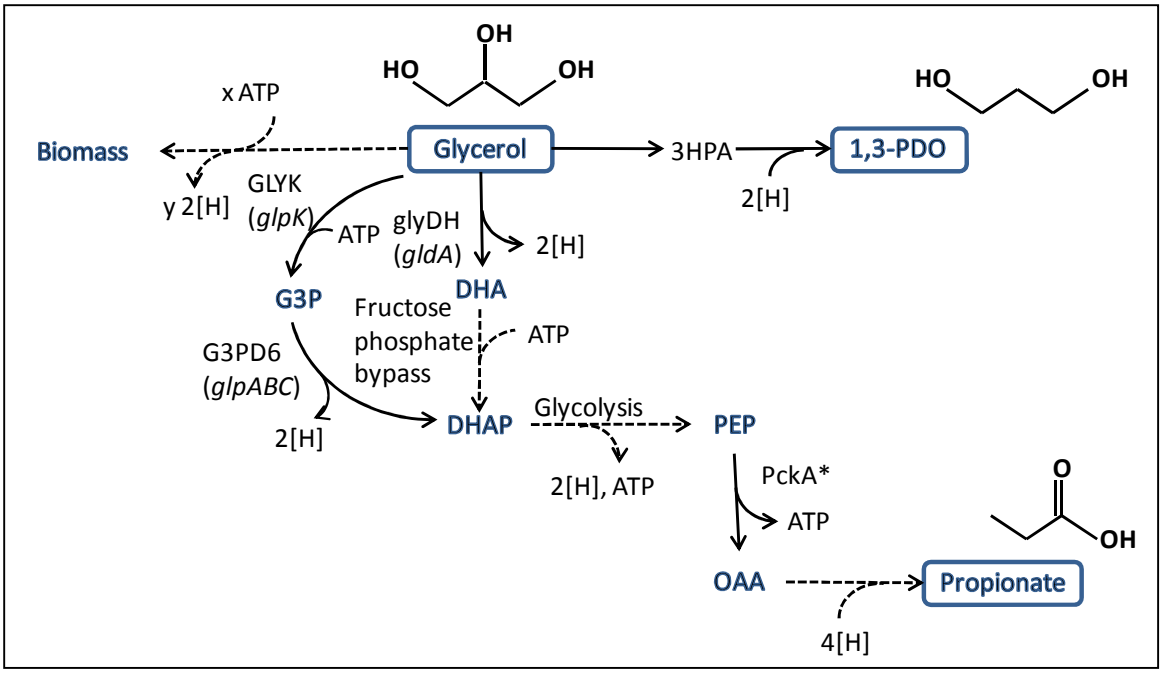

Figure 71: Model 9: Propionate (reversible PckA) – 1,3-PDO. See Nomenclature for abbreviations (page 214).

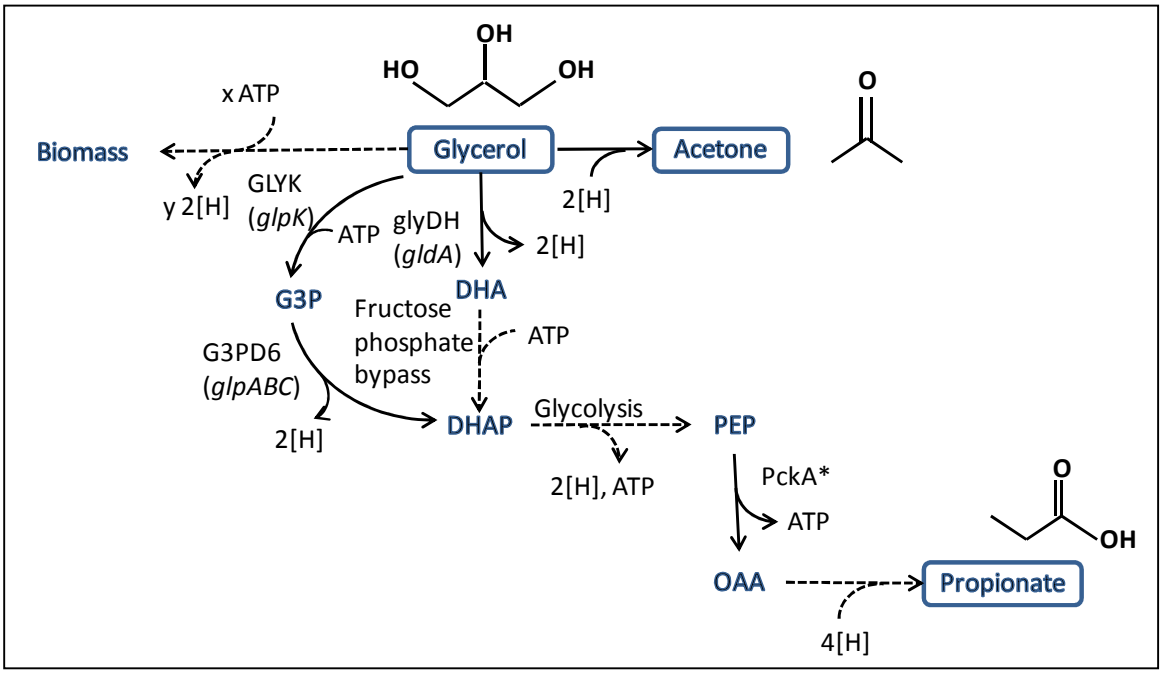

Figure 72: Model 10: Propionate (reversible PckA) – Acetone. See Nomenclature for abbreviations (page 214).

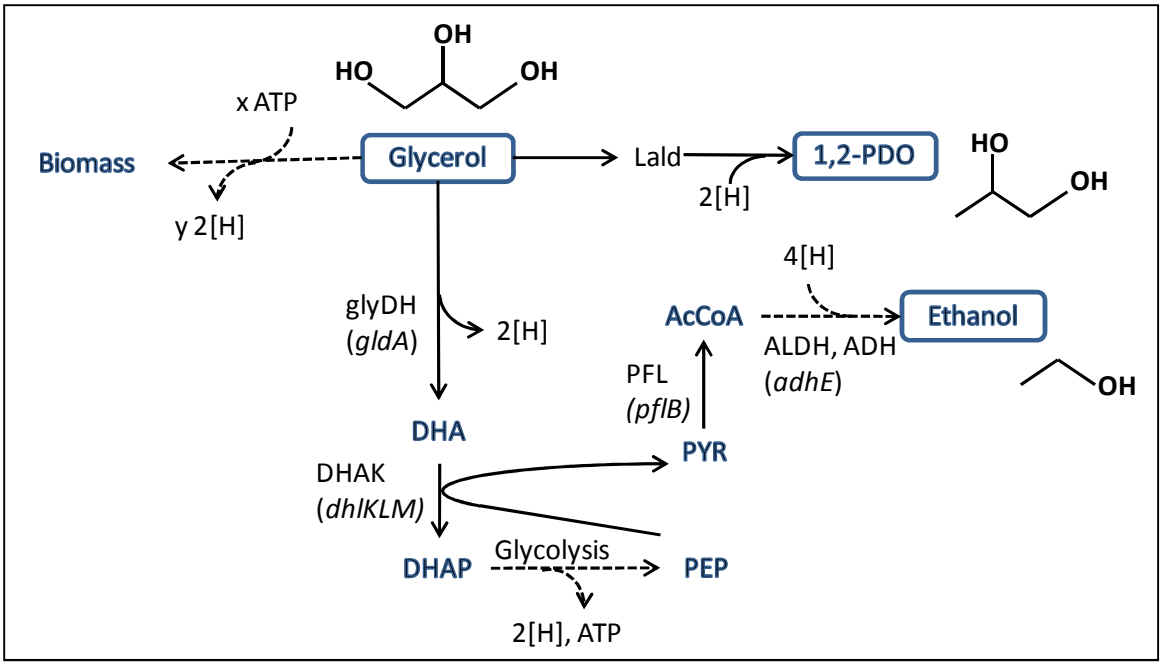

Figure 73: Model 11: Ethanol - 1,2-PDO (MG to lald). See Nomenclature for abbreviations (page 214).

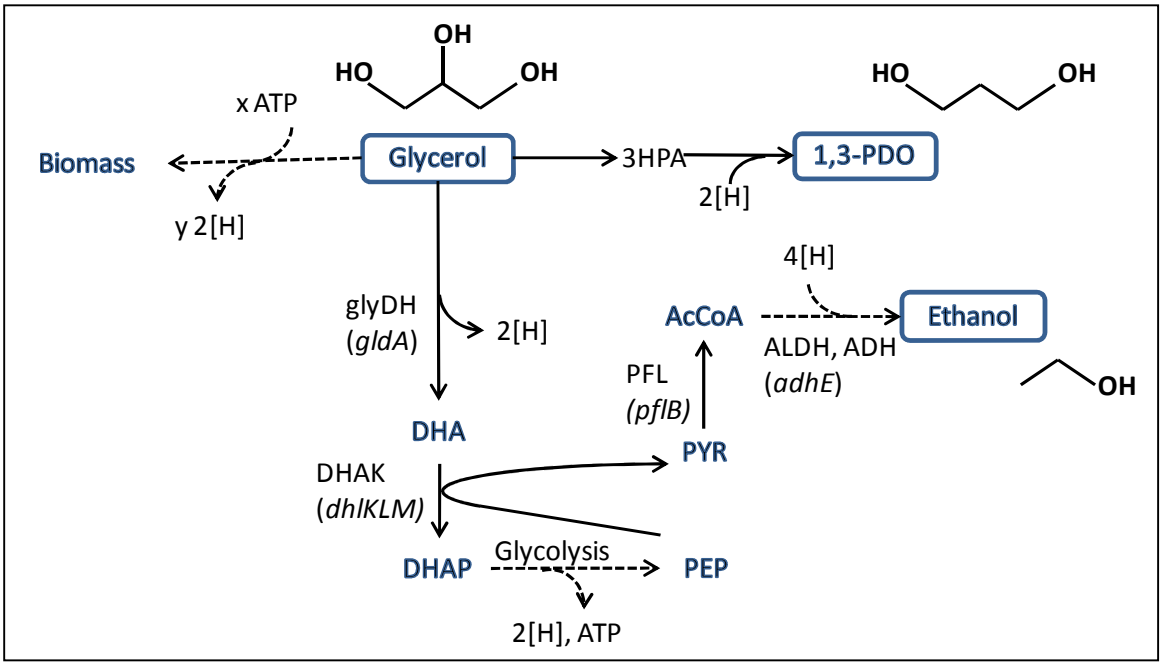

Figure 74: Model 12: Ethanol - 1,3-PDO. See Nomenclature for abbreviations (page 214).

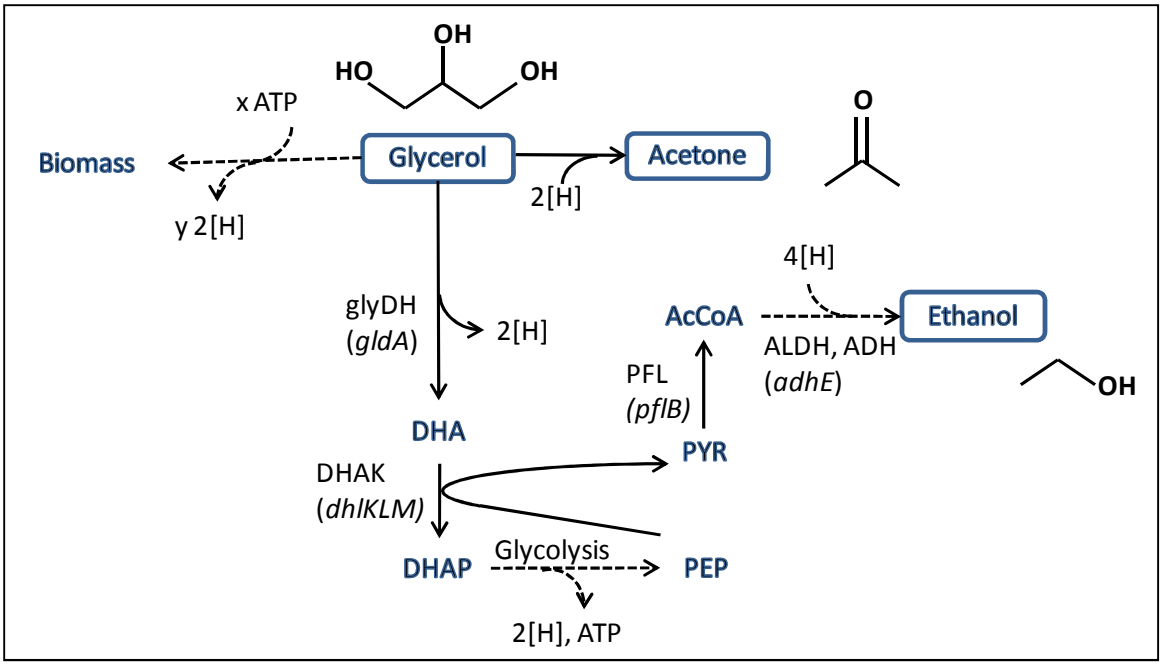

Figure 75: Model 13: Ethanol – Acetone. See Nomenclature for abbreviations (page 214).

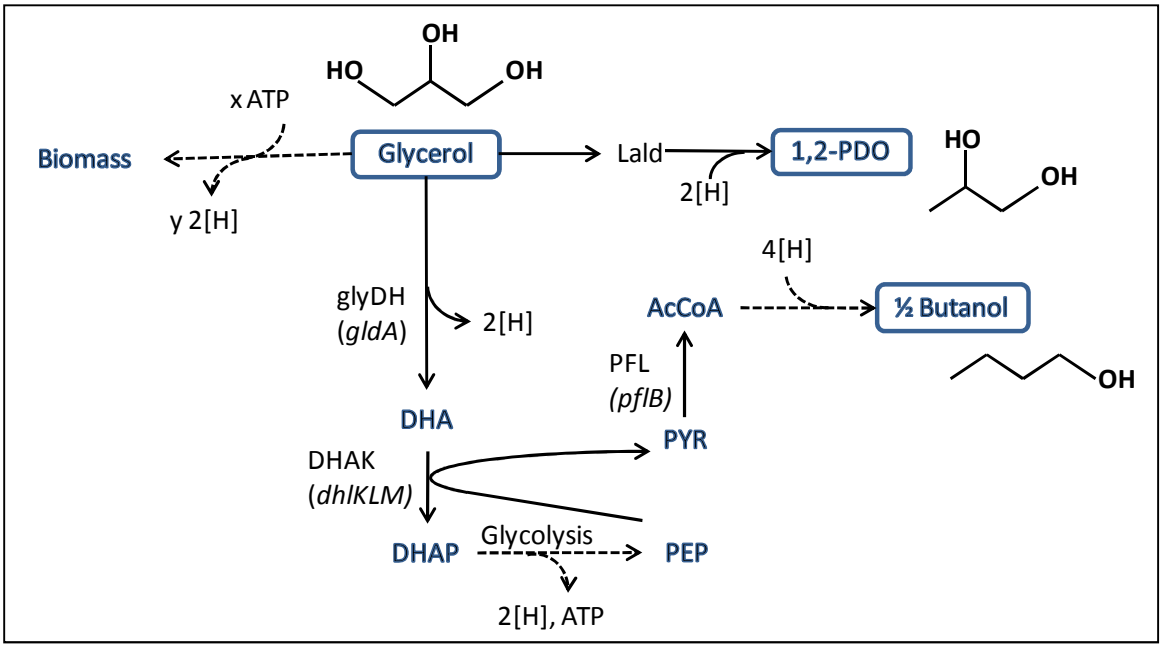

Figure 76: Model 14: Butanol - 1,2-PDO (MG to lald). See Nomenclature for abbreviations (page 214).

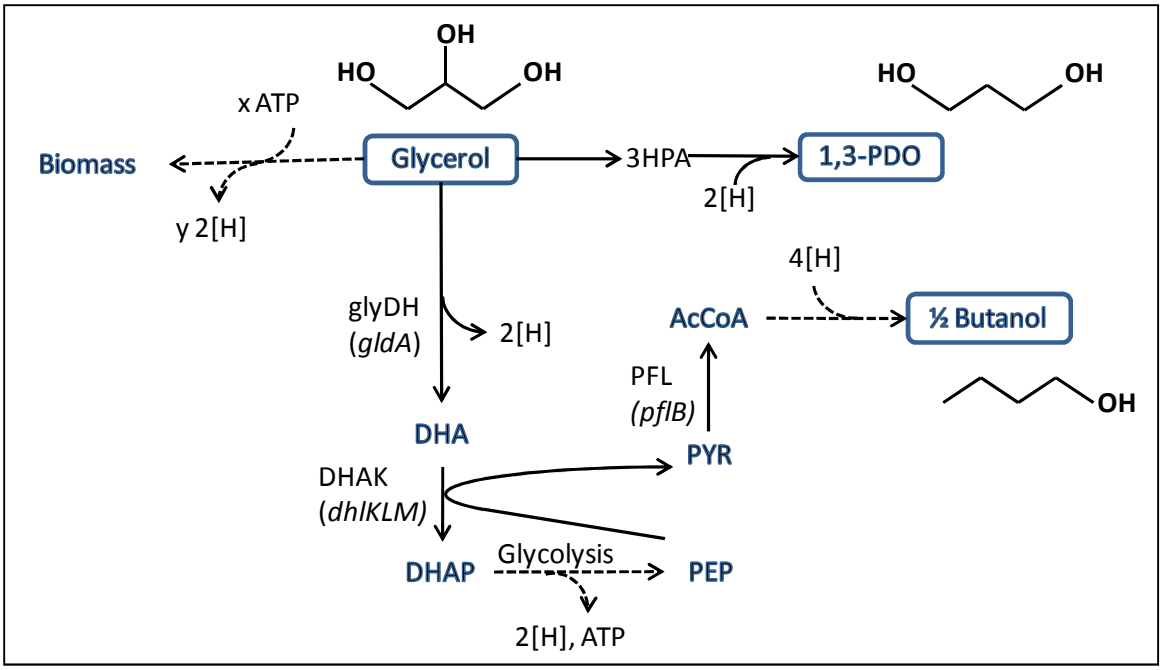

Figure 77: Model 15: Butanol - 1,3-PDO. See Nomenclature for abbreviations (page 214).

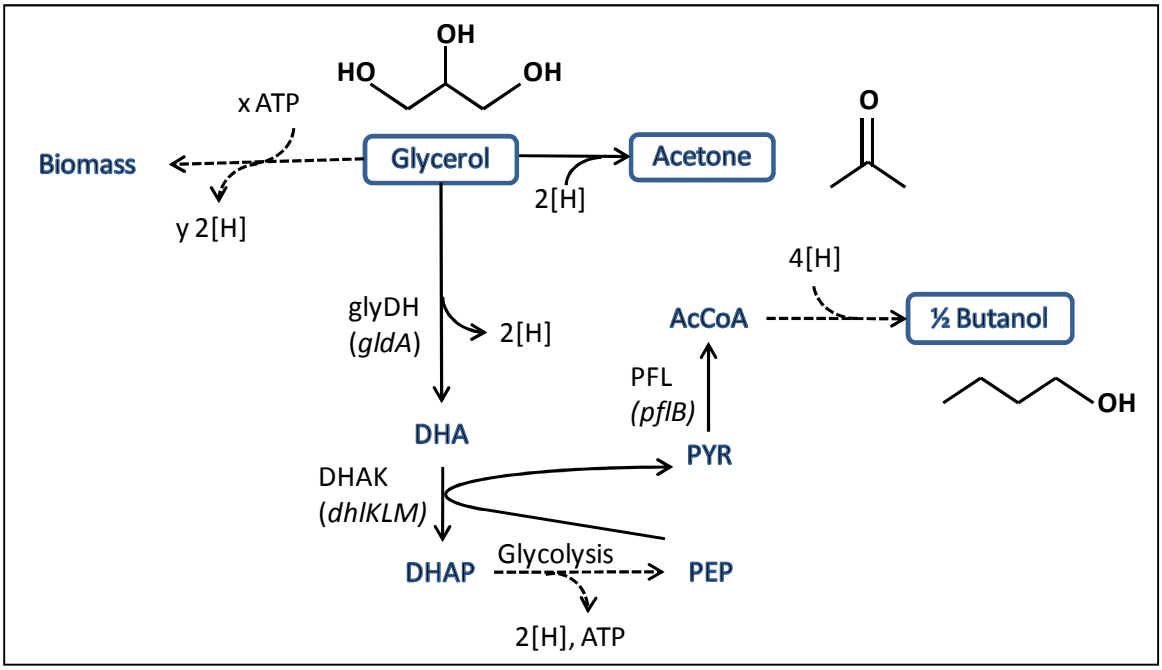

Figure 78: Model 16: Butanol - Acetone. See Nomenclature for abbreviations (page 214).

10.6 Detail of calculations from experimental data for glycerol metabolism toward the synthesis of desired products.

The production rates and specific growth rates were obtained, calculated or estimated from previous experimental studies. Below is explained each calculation.

1,2-PDO

Source: Clomburg and Gonzalez, 2011.

The paper reports a production rate of 5.6 g/l (73.6 mmol/l). The estimated average biomass concentration is 1.5 OD (read from Figure 5.A), which is equivalent to 0.51 gCDW/l (1OD = 0.34 gCDW/l). The total fermentation time is 72 hours (read from Figure 5.A). Thus, the average production rate is 73.6 mmol/l /0.51 gCDW/l / 72 h = 2.00 mmol/gCDW/h. The estimated specific growth rate is zero (stationary state after 12 hours of cultivation).

1,3-PDO

source: Tang et al., 2009.

The paper reports a production rate of 104.4 g/l (1372.1 mmol/l). The estimated average biomass concentration is 95 OD (read from Figure 4), which is equivalent to 32.3 gCDW/l (1OD = 0.34 gCDW/l). The total fermentation time is 30 hours. Thus, the average production rate is 1372.1 mmol/l /32.3 gCDW/l / 30 h = 1.42 mmol/gCDW/h. The average specific growth rate was calculated from Figure 4, from time 10 to 40 hours, which gave an average value of 0.014 h^{-1}, with a correlation coefficient R^2 = 0.62.

Although this number represents a poor correlation, it is still representative of the average specific growth rate.

Succinate - microaerobic

source: Blankschien et al., 2010.

The production rate was reported as 0.4 g/gCDW/h (3.45 mmol/gCDW/h). Specific growth rate was calculated using data from Figure 6, which gave a value of 0.038 h^{-1}, which a correlation coefficient R^2 = 0. 91 (good correlation).

Succinate - anaerobic

source: Zhang et al., 2010.

The production rate was estimated by using the reported production of succinate (102 mmol) in a total time of 6 days (144 hours), with an associated production of biomass of 0.5 gCDW/l. If I assume linearity in the production of biomass, and I use the average biomass concentration (0.25 gCDW/l), then the production rate is estimated as 102 mmol/0.25 gCDW/144 h = 2.8 mmol/gCDW/h.

Lactatic acid

Source: Mazumdar et al. 2010.

The production rate was reported as 1.25 g/gCDW/h (13.88 mmol/gCDW/h). Cell mass as a function of time was read from Figure 6.A, and I used data from 12 to 72 hours to calculate a specific growth rate equal to 0.048 h^{-1}, which a correlation coefficient R^2 = 0. 96 (good correlation).

10.7 Maximal theoretical yields for long chain products

Analysis of production of Alcohols using the reversal of the β-oxidation cycle

I did the general balance for the production of alcohols using the reversal of the β-oxidation. Figure 79 shows a simplified pathway for the maximal production rate. To achieve redox balance the conversion of PYR into AcCoA is split to go through the PFOR and the PDH. In the figure, 'n' is the flux of glucose, 'm' is the number of carbons in the product, and Alcohol_Cm is the product (example: Alcohols_C8 is octanol).

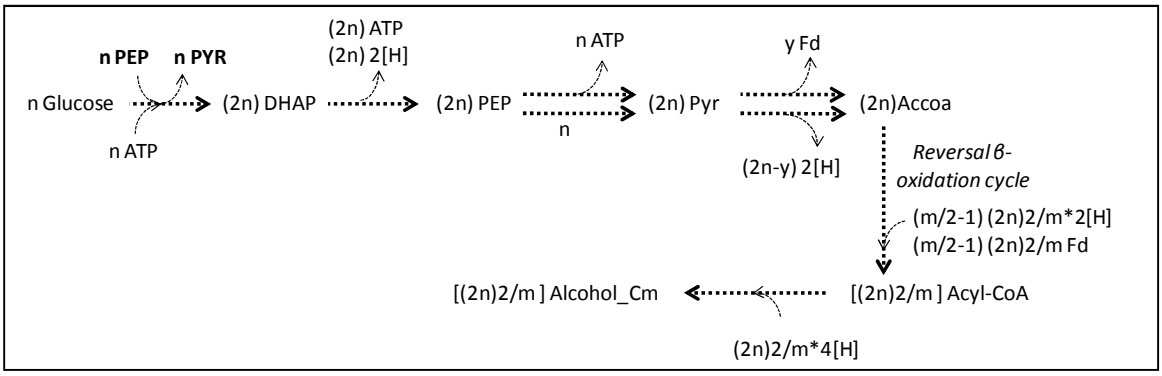

Figure 79: Simplified diagram for the production of alcohols using the reversal of the β-oxidation cycle. This diagram shows production and consumption of energy (ATP) and of reducing equivalents ([H] and fd). n: flux of glucose, m: number of carbon molecules in product, Alcohol_Cm: product (an alcohol with m carbon molecules). See Nomenclature for abbreviations (page 214).

The achieving of redox balance for optimal production of alcohols can be calculated as follows:

- $Flux\ per\ cycle: \frac{(2n)2}{m}$
- $\#\ of\ cycles: (\frac{m}{2} - 1)$
- $Glycosysis: (2n)2[H] + (2n)ATP$
- $Pyruvate\ node: (y)\ fd^{2-} + (2n - y)2[H]$
- $Reversed\ \beta - oxidation\ cycle: \frac{-(2n)2}{m}\ (\frac{m}{2} - 1)(2[H] + fd^{2-})$

- $Termination\ reactions$: $\frac{-(2n)2}{m}\ 4[H]$

The system is redox balance, and the solution to the system gives the following overall equation:

n Glucose→ ($^{4n}/_{m}$) Alcohol_Cm + 2n ATP

Analysis of production of alkanes using the reversal of the β-oxidation cycle

I did the general balance for the production of alkanes using the reversal of the β-oxidation. Figure 80 shows a simplified pathway for the maximal production rate. To achieve redox balance the conversion of PYR into AcCoA is split to go through the PFOR and the PFL. In the figure, 'n' is the flux of glucose, 'm' is the number of carbons in the product, and Alkane_Cm-1 is the product (example: Alkane_C7 is heptane). The number of cycles in the reversal β-oxidation cycle is (m/2-1).

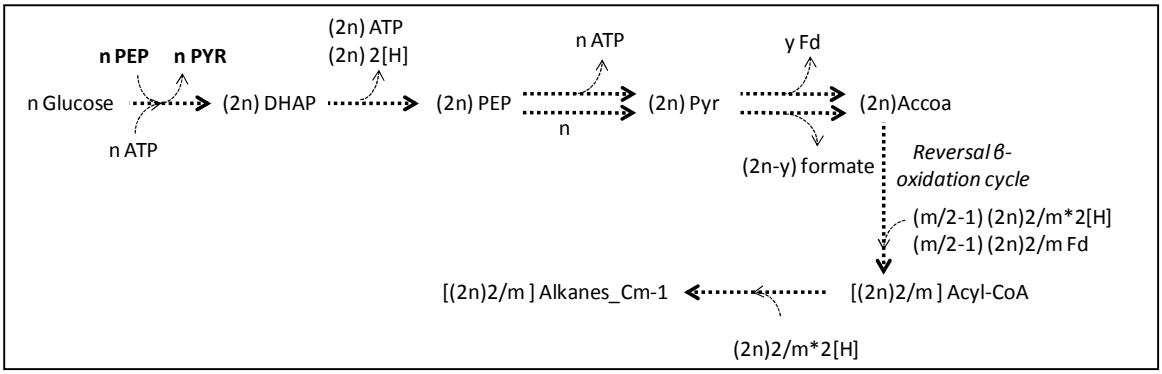

Figure 80: Simplified diagram for the production of alkanes using the reversal of the β-oxidation cycle. This diagram shows production and consumption of energy (ATP) and of reducing equivalents ([H] and Fd). n: flux of glucose, m: number of carbon molecules in product, Alkane_Cm-1: product (an alkane with m-1 carbon molecules). See Nomenclature for abbreviations (page 214).

The achieving of redox balance for optimal production of alkanes can be calculated as follows:

- $Flux\ per\ cycle$: $\frac{(2n)2}{m}$
- $\#\ of\ cycles$: $(\frac{m}{2}-1)$

- $Glycosysis: (2n)2[H] + (2n)ATP$
- $Pyruvate\ node: (y)\ fd^{2-} + (2n - y)formate$
- $Reversed\ \beta - oxidation\ cycle: \frac{-(2n)2}{m}\ (\frac{m}{2} - 1)(2[H] + fd^{2-})$
- $Termination\ reactions: \frac{-(2n)2}{m}\ 2[H]$

The system is redox balance, and the solution to the system gives the following overall equation:

n Glucose → (4n/m) Alkane_Cm-1 + 2n ATP + 4n/m formate.

Analysis of production of fatty acids using the reversal of the β-oxidation cycle

By performing FBA of the production of fatty acids using the reversal β-oxidation cycle, I found that the production of 1,2-PDO was required when I deleted other fermentation by-products. Figure 81 shows the overall flux distribution from glucose to a FA. In the figure, 'n' is the flux of glucose, 'm' is the number of carbons in the product, 'x' is the flux of production of 1,2-PDO and FA_Cm is the product (example: FA_C4 is butyric acid). The production of 1,2-PDO is required to achieve redox balance.

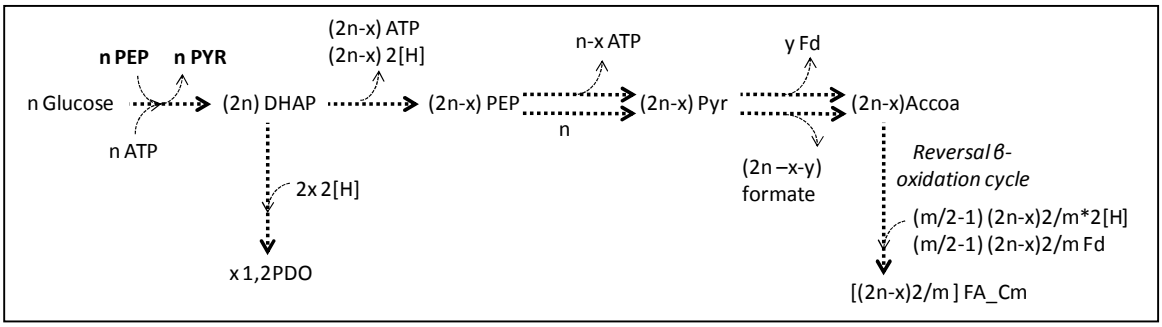

Figure 81: Simplified diagram for the production of FAs using the reversal of the β-oxidation cycle. This diagram shows production and consumption of energy (ATP) and of reducing equivalents ([H] and Fd). Production of 1,2-PDO is required for redox balance in this system. n: flux of glucose, m: number of carbon molecules in product, FA_Cm: product (a FA with m carbon molecules). See Nomenclature for abbreviations (page 214).

The achieving of redox balance for optimal production of FAs can be calculated as follows:

- $Flux\ per\ cycle: \frac{(2n-x)2}{m}$
- $\#\ of\ cycles: (\frac{m}{2} - 1)$
- $Glycosysis: (2n - x)2[H] + (2n - 2x)ATP$
- $Pyruvate\ node: (y)\ fd^{2-} + (2n - y - x)formate$
- $Reversed\ \beta - oxidation\ cycle: \frac{-(2n-x)2}{m}\ (\frac{m}{2} - 1)(2[H] + fd^{2-})$
- $1{,}2 - PDO\ production: 2x\ 2[H]$

The system is redox balance, and the solution to the system gives the following overall equation:

$$n\ Glucose = \frac{4n}{m+1} FA_{Cm} + 2n\left(\frac{m-1}{m+1}\right) ATP + \frac{2n}{m+1} 1{,}2PDO + \frac{4n}{m+1} formate$$

Analysis of production of butanol and hexanol using the α-keto acid pathway

The following diagrams show the production of butanol and hexanol using the α-keto acid pathway. Information to infer this diagram is based on published metabolic pathways (Marcheschi et al., 2012; Shen & Liao, 2008), and the fluxes were confirmed using the lcp-GEM.

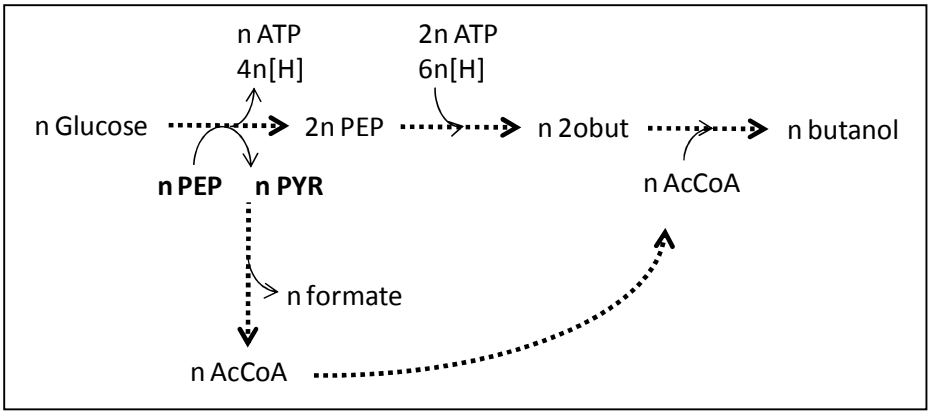

Figure 82: Simplified diagram for the production of butanol using the α-keto acid pathway. Emphasis is in the requirements of ATP and the achiving of redox balance. See Nomenclature for abbreviations (page 214).

The production of butanol results in the consumption of ATP and reducing equivalents, and thus other fermentative products are required. The overall equation that describes the production of butanol using this pathway is as follows:

n Glucose + 2n[H] + nATP → n butanol + n formate

The production of hexanol is represented in Figure 83:

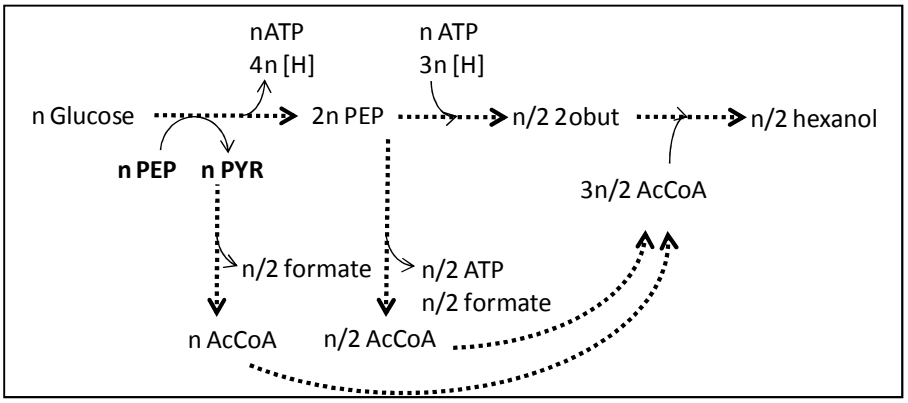

Figure 83: Simplified diagram for the production of hexanol using the α-keto acid pathway. Emphasis is in the requirements of ATP and the achiving of redox balance . See Nomenclature for abbreviations (page 214).

Hexanol production produces ATP and reducing equivalents. The overall equation that describes the production of hexanol using this pathway is as follows:

n Glucose → n/2 hexanol + n [H] + n/2 ATP + n formate

Analysis of production of Alcohols using the FA biosynthesis pathway

I did the overall balance for the production of alcohols using the FA biosynthesis pathway. Figure 84 shows a simplified pathway for the maximal production rate. In the figure, 'n' is the flux of glucose, 'm' is the number of carbons in the product, and Alcohol_Cm is the product (example: Alcohols_C8 is octanol).

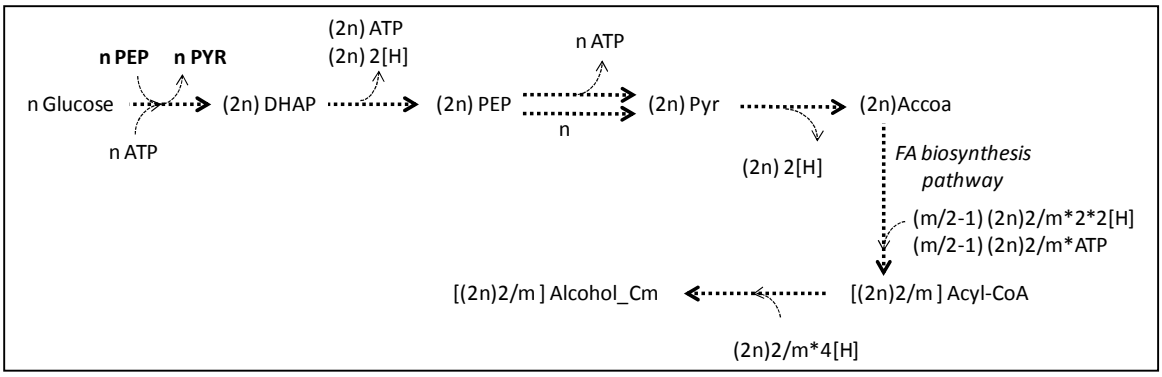

Figure 84: Simplified diagram for the production of alcohols using the FA biosynthesis pathway. This diagram shows production and consumption of energy (ATP) and of reducing equivalents ([H] and fd). n: flux of glucose, m: number of carbon molecules in product, Alcohol_Cm: product (an alcohol with m carbon molecules). See Nomenclature for abbreviations (page 214).

The achieving of redox balance for optimal production of alcohols can be calculated as follows:

- $Flux\ per\ cycle: \frac{(2n)2}{m}$
- $\#\ of\ cycles: (\frac{m}{2} - 1)$
- $Glycosysis: (2n)2[H] + (2n)ATP$
- $Pyruvate\ node: (2n)2[H]$
- $FA\ biosynthesis\ pathway: \frac{-(2n)2}{m}\left(\frac{m}{2} - 1\right)2(2[H]) - \frac{(4n)}{m}\left(\frac{m}{2} - 1\right)ATP$
- $Termination\ reactions: \frac{-(2n)2}{m}\ 4[H]$

The system is redox balance, and the solution to the system gives the following overall equation:

n Glucose→ ($^{4n}/_{m}$) Alcohol_Cm + ($^{4n}/_{m}$) ATP

Analysis of production of alkanes using the FA biosynthesis pathway

I did the overall balance for the production of alkanes using the FA biosynthesis pathway. Figure 85 shows a simplified pathway for the maximal production rate. In the figure, 'n' is the flux of glucose, 'm' is the number of carbons in the product, and Alkane_Cm-1 is the product (example: Alkane_C7 is heptane).

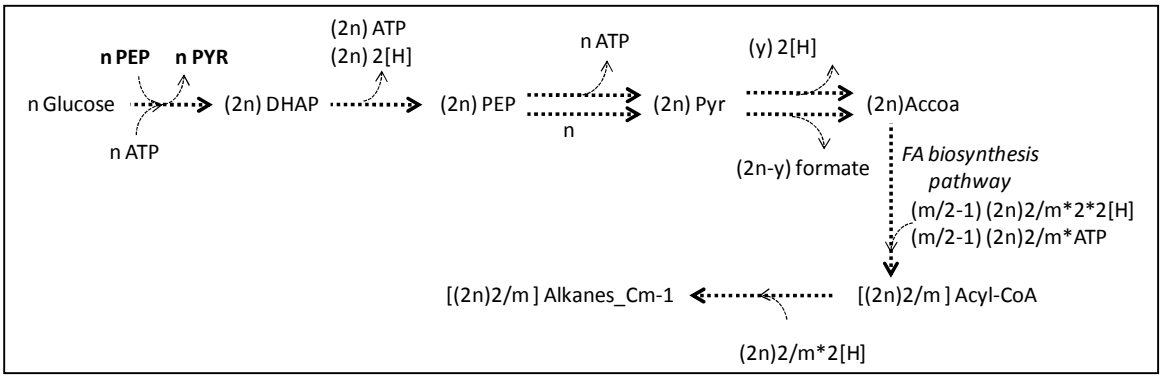

Figure 85: Simplified diagram for the production of alkanes using the FA biosynthesis pathway. This diagram shows production and consumption of energy (ATP) and of reducing equivalents ([H] and Fd). n: flux of glucose, m: number of carbon molecules in product, Alkane_Cm-1: product (an alkane with m-1 carbon molecules). See Nomenclature for abbreviations (page 214).

The achieving of redox balance for optimal production of alkanes can be calculated as follows:

- $Flux\ per\ cycle: \frac{(2n)2}{m}$
- $\#\ of\ cycles: (\frac{m}{2} - 1)$
- $Glycosysis: (2n)2[H] + (2n)ATP$
- $Pyruvate\ node: (y)2[H] + (2n - y)formate$
- $FA\ biosynthesis\ pathway: \frac{-(2n)2}{m}\left(\frac{m}{2} - 1\right)2(2[H]) - \frac{(4n)}{m}\left(\frac{m}{2} - 1\right)ATP$
- $Termination\ reactions: \frac{-(2n)2}{m}\ 2[H]$

The system is redox balance, and the solution to the system gives the following overall equation:

n Glucose → (4n/m) Alkane_Cm-1 + $(^{4n}/_{m})$ ATP + 4n/m formate.

Analysis of production of fatty acids using the FA biosynthesis pathway

Figure 86 shows the overall flux distribution to optimize production of FA from glucose. In the figure, 'n' is the flux of glucose, 'm' is the number of carbons in the product and FA_Cm is the product (example: FA_C4 is butyric acid).

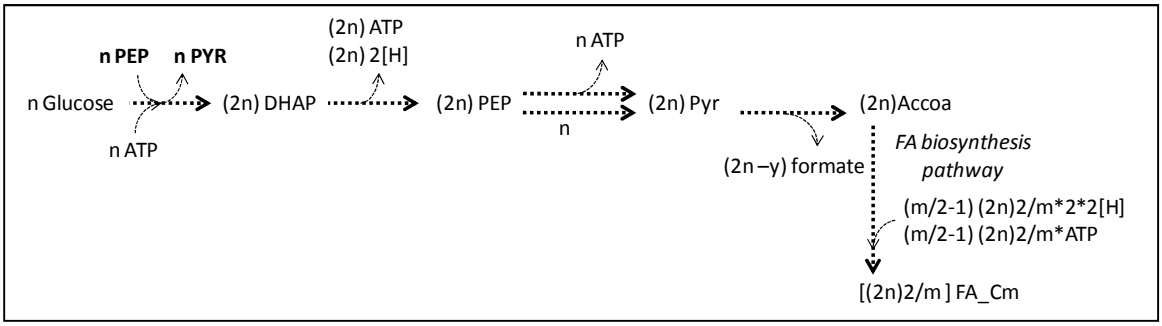

Figure 86: Simplified diagram for the production of FAs using the FA biosynthesis pathway. This diagram shows production and consumption of energy (ATP) and of reducing equivalents ([H] and Fd). Production of 1,2-PDO is required to achieve redox balance in this system. n: flux of glucose, m: number of carbon molecules in product, FA_Cm: product (a FA with m carbon molecules). See Nomenclature for abbreviations (page 214).

The achieving of redox balance for optimal production of FAs can be calculated as follows:

- $Flux\ per\ cycle: \frac{(2n)2}{m}$
- $\#\ of\ cycles: (\frac{m}{2} - 1)$
- $Glycosysis: (2n)2[H] + (2n)ATP$
- $Pyruvate\ node: (y)2[H] + (2n - y)formate$
- $FA\ biosynthesis\ pathway: \frac{-(4n)}{m}\left(\frac{m}{2} - 1\right)2(2[H]) - \frac{(4n)}{m}\left(\frac{m}{2} - 1\right)ATP$

The system is redox balance, and the solution to the system gives the following overall equation:

n Glucose → (4n/m) FA_Cm + (4n/m) ATP + 8n/m formate.

10.8 Calculation of titers

The titer can be calculating as follows:

$$Titer = \int_{t0=0}^{tf} specific\ production\ rate * Biomass\ (t)\ dt$$

The biomass can be calculated at any time as:

$$Biomass\ (t) = x_0 * e^{\mu t}$$

Then, assuming that x_0 = 1 gCDW/L, the titer can be calculated as

$$Titer = \frac{specific\ production\ rate}{\mu} * (e^{\mu t} - 1)$$

10.9 Matlab function for the kinetic model

```
KineticModelGlycerolFermentation_AngelaCintolesi
% Model developed by Angela CIntolesi, 2011
% Model developed by Angela Cintolesi as part of her Doctoral Research
% Chemical and Biomolecular Engineering, Rice University, March 2013
% Return a matrix Y with the optimal cell growth of each product

function F = Glycerol
global CcoA Cfdp Camp
CcoA=0.1; Cfdp=0.2; Camp=0;

global r2_max k2eq k2dha r3_max k3 d1 k4eq k5pgp k5gap k5nad k5nadh
k6pgp k63pg k6atp k7eq r10_maxr r11_maxf Kia r12_max k2gly r4_max
k4dhap k4gap r5_max k5eq r6_max k6eq k6adp r7_max k73pg k72pg r8_max
k8eq k82pg k8pep Cformate e10 r10_maxf k10_pyr k10_coa k10_form
k10_acetylcoa k11eq k11accoa k11acetal k11nad k11nadh k11coa k12eq
k12acet k12etoh km19 mu
d1=1;
k2gly=56;
k4eq=0.04;
r4_max=68.7;
k4dhap=2.8;
k4gap=0.3;
r5_max=921.6;
k5eq=0.67;
k5pgp=0.1;
k5gap=0.89;
k5nad=0.045;
k5nadh=0.02;
k6pgp=0.006;
k63pg=0.17;
k6atp=0.24;
r6_max=3021.77;
k6eq=1800;
k6adp=0.18;
r7_max=89.0497;
k73pg=0.2;
k72pg=0.369;
k7eq=0.1;
Kia=1;
r8_max=330.448;
k8eq=6.7;
k82pg=0.1;
k8pep=0.135;
r10_maxr=656;
Cformate = 0;
r10_maxf=0.46*r10_maxr/1.33;
k10_pyr=2.05;
k10_coa=0.0068;
k10_form=24.5;
k10_acetylcoa=0.051;
r11_maxf=2311;
k11eq =1;
k11accoa=0.007;
```

```
k11acetal=10;
k11nad=0.08;
k11nadh=0.025;
k11coa=0.008;
r12_max=2311;
k12eq=12354.9;
k12acet=5.4;
k12etoh=2.4;
r2_max=1.33;
k2eq = 22.4/17.2 * 0.3/56;
k2dha = 0.3;
r3_max=0.72;
k3=45/1000;
km19=159.2;
mu=0.04/3600;
tf=120*3600;
tglyc=[0; 12; 24; 36; 48; 60; 72; 84; 96; 108; 120]; %h
glyc=[11.07; 10.50; 9.69; 8.32; 6.43; 4.05; 2.80; 1.98; 1.43; 1.07;
0.87]*1000/92; %mM
EtOH=[0; 0.22; 0.59; 1.20; 2.01; 3.14; 3.61; 3.90; 4.10; 4.11;
4.24]*1000/46.07; %mM
biomass=[0.0545; 0.59; 0.69; 0.843; 1.04; 1.34; 1.32; 1.33; 1.32; 1.29;
1.29]*0.34; %OD
clear t Y
b0=0.48*0.34;
V=[glyc(1) 1 1 1 1 1 1 1 1 1 1 0 1 EtOH(1) 4.27 0.595 1.47 0.1 b0]; %
All values are in mM, except Biomass, in g/L
% Values of ATP, ADP, NAD, NADH were taken from JWS, model of
Chassagnole
[t Y]=ode23t(@model, [0 tf], V);

%%%%%%%%%%%%%%% Plot %%%%%%%%%%%%%%
B=[t Y];
xlswrite('MonodMetabolitesFinal', B)
figure (1)
plot (t/3600, Y(:,1)/1000, '--b'); % Value in Molar
hold on
plot (t/3600, Y(:,19)/2, '--g');
hold on
plot (t/3600, Y(:,14)/1000, '--r'); % Value in Molar
hold on
plot (tglyc, glyc/1000, '+b'); %MW of Glycerol is 92. Value is in Molar
hold on
plot (tglyc, biomass/2, '+g'); %conversion to g/l/2
hold on
plot (tglyc, EtOH/1000, '+r');% MW of Ethanol is 46.07. Value is in
Molar
xlabel ('time [h]');
ylabel('Glycerol [M], Biomass[g DW/L /2], EtOH [M]');
figure (2)
ylabel('Metabolite [mM]');
xlabel('Time [h]');
title ({'Glyc_in (--blue), DHA (--red), DHAP (--magenta), GAP (--
green), pgp (--blak), 3pg (--cyan)'; '2pg (-*blue), PEP (-*red), PYR (-
*magenta), AcCoA (-*green), Acetahdehyde (-*black)'})
hold on
plot (t/3600, Y(:,3), '--r');
```

```
hold on
plot (t/3600, Y(:,4), '--m');
hold on
plot (t/3600, Y(:,5), '--g');
hold on
plot (t/3600, Y(:,6), '--k');
hold on
plot (t/3600, Y(:,7), '--c');
hold on
plot (t/3600, Y(:,8), '--b*');
hold on
plot (t/3600, Y(:,9), '--r*');
hold on
plot (t/3600, Y(:,10), '--m*');
hold on
plot (t/3600, Y(:,11), '--g*');
hold on
plot (t/3600, Y(:,13), '--k*');

%% Elasticities and FCC
clear t Y
tf = 50*3600;
%V=[g0 1 1 1 1 1 1 1 1 1 0 1 0 4.27 0.595 1.47 0.1 x0]; % All values
are in mM, except Biomass, in g/L
%Values of ATP, ADP, NAD, NADH were taken from JWS, model of
Chassagnole
[t Y]=ode23t(@model, [0 tf], V);
Y(end,:)
Y12=V(1,12);
Y15=V(1,15);
Y16=V(1,16);
Y17=V(1,17);
Y18=V(1,18);
CcoA=0.1;
Cfdp=0.2;
Camp=0;

% Define parameters
Y1=sym('Y1');
Y2=sym('Y2');
Y3=sym('Y3');
Y4=sym('Y4');
Y5=sym('Y5');
Y6=sym('Y6');
Y7=sym('Y7');
Y8=sym('Y8');
Y9=sym('Y9');
Y10=sym('Y10');
Y11=sym('Y11');
Y13=sym('Y13');
Y14=sym('Y14');

% Jacobian
f=[d1*(Y1-Y2); r2_max/k2gly*(Y2-Y3/k2eq)/(1+Y2/k2gly+Y3/k2dha);
r3_max*(Y3/(k3+Y3)); r4_max*(Y4-Y5/k4eq)/(k4dhap*(1+Y5/k4gap)+Y4);
r5_max*(Y5*Y17-
```

```
Y6*Y18/k5eq)/((k5gap*(1+Y6/k5pgp)+Y5)*(k5nad*(1+Y18/k5nadh)+Y17));
r6_max*(Y6*Y16-
Y15*Y7/k6eq)/((k6adp*(1+Y15/k6atp)+Y16)*(k6pgp*(1+Y7/k63pg)+Y6));
r7_max*(Y7-Y8/k7eq)/(k73pg*(1+Y8/k72pg)+Y7); r8_max*(Y8-
Y9/k8eq)/(k82pg*(1+Y9/k8pep)+Y8);
r10_maxf*Y10*CcoA/(Y10*CcoA+k10_pyr*CcoA+k10_coa*Y10)-
(r10_maxf)*Cformate*Y11/(Y11*Cformate+k10_form*Y11+k10_acetylcoa*Cforma
te); r11_maxf*(Y11*Y18)/(Y18*k11accoa+Y11*(Y18+k11nadh*Y13/Kia))-
r11_maxf/k11eq*Y13*Y17*CcoA/(Kia*k11nad*CcoA+k11coa*Y13*Y17+k11nad*Y13*
CcoA+k11acetal*Y17*CcoA+Y13*Y17*CcoA); r12_max/k12acet*(Y13-
Y14/k12eq)/(1+Y13/k12acet+Y14/k12etoh)];
x=[Y2, Y3, Y4, Y5, Y6, Y7, Y8, Y9, Y10, Y11, Y13];
R=jacobian (f,x);
T = R';

% Data at 50 hrs
sf = subs(f, {Y1, Y2, Y3, Y4, Y5, Y6, Y7, Y8, Y9, Y10, Y11, Y13, Y14},
{Y(end,1), Y(end,2), Y(end,3), Y(end,4), Y(end,5), Y(end,6), Y(end,7),
Y(end,8), Y(end,9), Y(end,10), Y(end,11), Y(end,13), Y(end,14)});
sx=  subs(x, {Y1, Y2, Y3, Y4, Y5, Y6, Y7, Y8, Y9, Y10, Y11, Y13},
{Y(end,1), Y(end,2), Y(end,3), Y(end,4), Y(end,5), Y(end,6), Y(end,7),
Y(end,8), Y(end,9), Y(end,10), Y(end,11), Y(end,13)});
sT = subs(T, {Y1, Y2, Y3, Y4, Y5, Y6, Y7, Y8, Y9, Y10, Y11, Y13, Y14},
{Y(end,1), Y(end,2), Y(end,3), Y(end,4), Y(end,5), Y(end,6), Y(end,7),
Y(end,8), Y(end,9), Y(end,10), Y(end,11), Y(end,13), Y(end,14)});
xCycle=[Y(end,2) Y(end,3) Y(end,4) Y(end,5) Y(end,6) Y(end,7) Y(end,8)
Y(end,9) Y(end,10) Y(end,11) Y(end,13)]; % {Y2, Y3, Y4, Y5, Y6, Y7, Y8,
Y9, Y10, Y11, Y13}
E=zeros (11, 11);
for j=1:1:11
    for i=1:1:11
        E(i,j)=sx(i)/sf(j)*sT(i,j);
    end
end
E
M=zeros (11, 11);

for j=1:1:11
    M(1,j)=1;
end
M(2,1)=E(1,1);
M(2,2)=E(1,2);
M(3,2)=E(2,2);
M(3,3)=E(2,3);
M(9,8)=E(9,8);
M(9,9)=E(9,9);
M(10,9)=E(10,9);
M(10,10)=E(10,10);
M(11,10)=E(11,10);
M(11,11)=E(11,11);
for i=4:1:8
    M(i,i-1)=E(i-1,i-1);
    M(i,i)=E(i-1,i)-E(i,i)*xCycle(i-1)/xCycle(i);
    M(i,i+1)=-1*E(i,i+1)*xCycle(i-1)/xCycle(i);
end
M(8,3)=-1*E(8,3)*xCycle(7)/xCycle(8);
```

```
M(8,9)=0;
rank_of_M = rank(M)
pseudoI=-1*eye(11,11);
pseudoI(1,1)=1;
pseudoI(4,5)=xCycle(3)/xCycle(4);
pseudoI(5,6)=xCycle(4)/xCycle(5);
pseudoI(6,7)=xCycle(5)/xCycle(6);
pseudoI(7,8)=xCycle(6)/xCycle(7);
pseudoI(8,9)=xCycle(7)/xCycle(8);
CC=M\eye(11,11)*pseudoI;
display('FCC=');
CC(:,1)
xlswrite ('Monod_Elasticities', E)
xlswrite ('Monod_CC', CC)
function dY = model (t, Y)
dY(1) = -1*vglpf_F(Y(1), Y(2))*Y(19)*0.0022333;%Substrate. Conversion
of units using L-cells/g-DW cells = 0.0022333
dY(2) = 1*vglpf_F(Y(1), Y(2))-1*vglda_F(Y(2), Y(3))-vgrowth_F
(Y(1))*Y(2);
dY(3)= vglda_F(Y(2), Y(3))-vdhak_F(Y(3))-vgrowth_F (Y(1))*Y(3);
dY(4)= vdhak_F(Y(3))-vtpia_F(Y(4), Y(5))-vgrowth_F (Y(1))*Y(4);
dY(5)= vtpia_F(Y(4), Y(5))-vgapdh_F(Y(5), Y(6), Y(17), Y(18))-vgrowth_F
(Y(1))*Y(5);
dY(6)= vgapdh_F(Y(5), Y(6), Y(17), Y(18))-vpgk_F(Y(6), Y(7), Y(15),
Y(16))-vgrowth_F (Y(1))*Y(6);
dY(7)= vpgk_F(Y(6), Y(7), Y(15), Y(16))-vpgam_F(Y(7), Y(8))-vgrowth_F
(Y(1))*Y(7);
dY(8)= vpgam_F(Y(7), Y(8))-veno_F(Y(8), Y(9))-vgrowth_F (Y(1))*Y(8);
dY(9)= veno_F(Y(8), Y(9))-vdhak_F(Y(3))-vgrowth_F (Y(1))*Y(9);
dY(10)= -1*vpfl_F(Y(10), Y(11), Y(12))+vdhak_F(Y(3))-vgrowth_F
(Y(1))*Y(10);
dY(11)= vpfl_F(Y(10), Y(11), Y(12))-vadhe1_F(Y(11), Y(13), Y(17),
Y(18))-vgrowth_F (Y(1))*Y(11);
dY(12)= (vpfl_F(Y(10), Y(11), Y(12)))*Y(19)*0.0022333; %product
dY(13)= vadhe1_F(Y(11), Y(13), Y(17), Y(18))-vadhe2_F(Y(13), Y(14))-
vgrowth_F (Y(1))*Y(13);
dY(14)= (vadhe2_F(Y(13), Y(14)))*Y(19)*0.0022333; % Product
dY(15)=0;
dY(16)=0;
dY(17)= -1*vglda_F(Y(2), Y(3))-vgapdh_F(Y(5), Y(6), Y(17),
Y(18))+vadhe1_F(Y(11), Y(13), Y(17), Y(18))+vadhe2_F(Y(13), Y(14))-
vgrowth_F (Y(1))*Y(17);
dY(18)= vglda_F(Y(2), Y(3))+vgapdh_F(Y(5), Y(6), Y(17), Y(18))-
vadhe1_F(Y(11), Y(13), Y(17), Y(18))-vadhe2_F(Y(13), Y(14))-vgrowth_F
(Y(1))*Y(18);
dY(19)= vgrowth_F (Y(1))*Y(19);%Biomass
dY=dY';

function vglpf =vglpf_F(Y1, Y2)
global d1
vglpf = d1*(Y1-Y2);

function vglda =vglda_F(Y2, Y3)
global r2_max k2eq k2dha k2gly
vglda = r2_max/k2gly*(Y2-Y3/k2eq)/(1+Y2/k2gly+Y3/k2dha);
```

```
function vdhak =vdhak_F(Y3)
global r3_max k3
vdhak = r3_max*(Y3/(k3+Y3));

function vtpia =vtpia_F(Y4, Y5)
global k4eq r4_max k4dhap k4gap
vtpia = r4_max*(Y4-Y5/k4eq)/(k4dhap*(1+Y5/k4gap)+Y4);

function vgapdh =vgapdh_F(Y5, Y6, Y17, Y18)
global k5gap k5pgp k5nad k5nadh r5_max k5eq
vgapdh = r5_max*(Y5*Y17-
Y6*Y18/k5eq)/((k5gap*(1+Y6/k5pgp)+Y5)*(k5nad*(1+Y18/k5nadh)+Y17));

function vpgk =vpgk_F(Y6, Y7, Y15, Y16)
global k6pgp k63pg k6atp r6_max k6eq k6adp
vpgk = r6_max*(Y6*Y16-
Y15*Y7/k6eq)/((k6adp*(1+Y15/k6atp)+Y16)*(k6pgp*(1+Y7/k63pg)+Y6));

function vpgam =vpgam_F(Y7, Y8)
global k7eq r7_max k73pg k72pg
vpgam = r7_max*(Y7-Y8/k7eq)/(k73pg*(1+Y8/k72pg)+Y7);

function veno =veno_F(Y8, Y9)
global r8_max k8eq k82pg k8pep
veno = r8_max*(Y8-Y9/k8eq)/(k82pg*(1+Y9/k8pep)+Y8);

function vpfl =vpfl_F(Y10, Y11, Y12)
global CcoA r10_maxr Cformate r10_maxf k10_pyr k10_coa k10_form
k10_acetylcoa
vpfl = r10_maxf*Y10*CcoA/(Y10*CcoA+k10_pyr*CcoA+k10_coa*Y10)-
(r10_maxr)*Cformate*Y11/(Y11*Cformate+k10_form*Y11+k10_acetylcoa*Cforma
te);

function vadhe1 =vadhe1_F(Y11, Y13, Y17, Y18)
global CcoA r11_maxf Kia k11eq k11accoa k11acetal k11nad k11nadh k11coa
vadhe1 = r11_maxf*(Y11*Y18)/(Y18*k11accoa+Y11*(Y18+k11nadh*Y13/Kia))-
r11_maxf/k11eq*Y13*Y17*CcoA/(Kia*k11nad*CcoA+k11coa*Y13*Y17+k11nad*Y13*
CcoA+k11acetal*Y17*CcoA+Y13*Y17*CcoA);

function vadhe2 =vadhe2_F(Y13, Y14)
global r12_max k12eq k12acet k12etoh
vadhe2 = r12_max/k12acet*(Y13-Y14/k12eq)/(1+Y13/k12acet+Y14/k12etoh);

function vgrowth=vgrowth_F (Y1)
global km19 mu
vgrowth=mu*Y1/(km19+Y1);
```

10.10 Matlab function for glyc-GEM

AC_BiomassvsProduct_GlyceroliJO1366.m

```
% Glycerol fermentation in E. coli as a platform for the synthesis of
% desired products.
% Model developed by Angela Cntolesi as part of her Doctoral Research
```

```
% Chemical and Biomolecular Engineering, Rice University, March 2013
% Plot solution spaces
%% Use the updated model iJO1366 (2011)

clear all
global SizeModel
initCobraToolbox()
%changeCobraSolver('glpk');
%% Open model
model1=readCbModel('iJO1366');
biomassposition=8;
Biomass_name='Ec_biomass_iJO1366_core_53p95M';
modelname='iJO1366';
model1=changeRxnBounds(model1,{'EX_o2(e)', 'EX_glc(e)', 'EX_glyc(e)',
'EX_co2(e)','FHL'}, [0 0 -20 0 -1000], 'l');
% Reverse FHL
model1=changeRxnBounds(model1,'FHL', 1000, 'u');
% G3PD2 is irreversible
model1=changeRxnBounds(model1,'G3PD2', 0, 'u');
%no aa degradation
model1=changeRxnBounds(model1,{'DAAD', 'AST', 'SADH', 'SGSAD', 'SGDS',
'ARGDC', 'ARGDCpp', 'ASPT', 'GLUN', 'P5CD', 'PROD2', 'SERD_L', 'OBTFL',
'PPAKr', 'THRD', 'GLYAT', 'TYROXDApp', 'PEAMNOpp', 'TRPAS2',
'CYSDS','42A12BOOXpp', 'THRAi'}, [0 0 0 0 0 0 0 0 0 0 0 0 0 0 0 0 0 0 0 0
0 0 0], 'u');
model1=changeRxnBounds(model1,{'DAAD', 'AST', 'SADH', 'SGSAD', 'SGDS',
'ARGDC', 'ARGDCpp', 'ASPT', 'GLUN', 'P5CD', 'PROD2', 'SERD_L', 'OBTFL',
'PPAKr', 'THRD', 'GLYAT', 'TYROXDApp', 'PEAMNOpp', 'TRPAS2',
'CYSDS','42A12BOOXpp', 'THRAi'}, [0 0 0 0 0 0 0 0 0 0 0 0 0 0 0 0 0 0 0 0
0 0 0], 'l');
%no nucleotides degradation
model1=changeRxnBounds(model1,{'CYTD', 'DCYTD', 'DURIPP', 'TMDPP',
'PPM2', 'DRPA', 'ADA', 'DADA', 'PUNP1', 'PUNP4', 'PUNP2', 'PUNP3',
'PUNP5', 'PUNP6', 'PUNP7', 'PYNP2r'}, [0 0 0 0 0 0 0 0 0 0 0 0 0 0 0 0
0], 'u');
model1=changeRxnBounds(model1,{'CYTD', 'DCYTD', 'DURIPP', 'TMDPP',
'PPM2', 'DRPA', 'ADA', 'DADA', 'PUNP1', 'PUNP4', 'PUNP2', 'PUNP3',
'PUNP5', 'PUNP6', 'PUNP7', 'PYNP2r'}, [0 0 0 0 0 0 0 0 0 0 0 0 0 0 0 0
0], 'l');
% export aa (direct + non escential):
model1=changeRxnBounds(model1,{'EX_ala-B(e)', 'EX_ala-D(e)', 'EX_ala-
L(e)', 'EX_asn-L(e)', 'EX_asp-L(e)', 'EX_cys-D(e)', 'EX_cys-L(e)',
'EX_glu-L(e)', 'EX_gln-L(e)', 'EX_gly(e)', 'EX_his-L(e)', 'EX_ile-
L(e)', 'EX_leu-L(e)', 'EX_lys-L(e)', 'EX_met-D(e)', 'EX_met-L(e)',
'EX_phe-L(e)', 'EX_pro-L(e)', 'EX_ser-D(e)', 'EX_ser-L(e)','EX_thr-
L(e)', 'EX_trp-L(e)', 'EX_tyr-L(e)', 'EX_val-L(e)' }, [0 0 0 0 0 0 0 0
0 0 0 0 0 0 0 0 0 0 0 0 0 0 0 0 0 0 0 0 0 0 0 0 0 0 0 0 ], 'u');
model1= changeRxnBounds(model1,{'EX_26dap-M(e)','EX_frulys(e)','EX_hom-
L(e)', 'EX_orn(e)'}, [0 0 0 0 ], 'u');
%no Fe2+ export. no H2S export
model1=changeRxnBounds(model1,'EX_fe2(e)', 0, 'u');
model1=changeRxnBounds(model1,'EX_h2s(e)', 0, 'u');
%no POR5 export.
model1=changeRxnBounds(model1,'POR5', 0, 'l');
model1=changeRxnBounds(model1,'POR5', 0, 'u');
%no production of 5mtr and spmd, for redox purposes
model1=changeRxnBounds(model1,'EX_5mtr(e)', 0, 'u');
```

```
model1=changeRxnBounds(model1,'EX_spmd(e)', 0, 'u');
%Add PntAB
model1=addReaction(model1, 'Add_PntAB', {'nadh[c]', 'nadp[c]', 'h[p]',
'nad[c]', 'nadph[c]', 'h[c]'}, [-1 -1 -1 1 1 1], 1, 0, 1000);
% remove hxa as possible product
model1=changeRxnBounds(model1,'EX_hxa(e)', 0, 'l');
model1=changeRxnBounds(model1,'EX_hxa(e)', 0, 'u');
% restrict F6PA
model1=changeRxnBounds(model1,'F6PA', -4, 'l');
% no FBA3 and PFK_3
model1=changeRxnBounds(model1,'FBA3', 0, 'l');
model1=changeRxnBounds(model1,'FBA3', 0, 'u');
model1=changeRxnBounds(model1,'PFK_3', 0, 'l');
model1=changeRxnBounds(model1,'PFK_3', 0, 'u');

% Study of synthesis of additional products. Case (1) correspond to E.
coli
% wild tyle
display ('Add: (1)none; (2)13PDO(nadh); (3)acetone; (4)Propanol;
(5)PPCKr; (6)Propanol+PPCKr; (7)ATP-depend DhaK; (8)13PDO(nadph);
(9)PPCKr+ppa; ');
K=input ('(10)Butanol (revB-oxi); (11)Propanol(12pdo); (12)D-lac:
(13)Succ(add pyc,CO2), (14)Propanol(ppa), (15)Propanol(ppcoa), (16)
succ(PckA,CO2)');
switch K
    case 1
    case 2
        model1=addReaction(model1,'Add3HPA','glyc[c] -> 3HPA +
h2o[c]');
        model1=addReaction(model1,'Add13PDO','3HPA + h[c] + nadh[c] ->
13PDO[c] + nad[c]');
        model1=addReaction(model1,'EX_13PDO','13PDO[c] ->');
    case 3
        model1=addReaction(model1,'AddAcetone','glyc[c] + h[c] +
nadh[c] -> Acetone[c] + nad[c] + 2 h2o[c]');
        model1=addReaction(model1,'EX_Acetone','Acetone[c] ->');
    case 4
        model1=addReaction(model1,'AddPropionate','succ[c] -> ppa[c] +
co2[c]');
        model1=addReaction(model1,'AddPropanol','ppa[c] + 3 h[c] + 2
nadh[c] -> propanol[c] + 2 nad[c] + h2o[c]');
        model1=addReaction(model1,'EX_Propanol','propanol[c] ->');
    case 5
        model1=addReaction(model1,'PPCK_r','adp[c] + co2[c] + pep[c]
<=> atp[c] + oaa[c]');
        model1=changeRxnBounds(model1, 'PPCK', 0, 'u');
    case 6
        model1=addReaction(model1,'PPCK_r','adp[c] + co2[c] + pep[c]
<=> atp[c] + oaa[c]');
        model1=changeRxnBounds(model1, 'PPCK', 0, 'u');
        model1=addReaction(model1,'AddPropionate','succ[c] -> ppa[c] +
co2[c]');
        model1=addReaction(model1,'AddPropanol','ppa[c] + 3 h[c] + 2
nadh[c] -> propanol[c] + 2 nad[c] + h2o[c]');
        model1=addReaction(model1,'EX_Propanol','propanol[c] ->');
    case 7
```

```
        model1=addReaction(model1,'DhaKLM_Cfreundii','atp[c] + dha[c]
<=> adp[c] + dhap[c] + h[c]');

    case 8
        model1=addReaction(model1,'Add3HPA','glyc[c] -> 3HPA +
h2o[c]');
        model1=addReaction(model1,'Add13PDO','3HPA + h[c] + nadph[c] ->
13PDO[c] + nadp[c]');
        model1=addReaction(model1,'EX_13PDO','13PDO[c] ->');

    case 9
        model1=addReaction(model1,'AddTransport_ppa','ppa[c] + h[c] ->
ppa[p] + h[p]');
        model1=addReaction(model1,'PPCK_r','adp[c] + co2[c] + pep[c]
<=> atp[c] + oaa[c]');
        model1=changeRxnBounds(model1, 'PPCK', 0, 'u');
    case 10
        model1=addReaction(model1,'P_butanal_CoA',{'btcoa[c]',
'nadh[c]', 'h[c]', 'butanal[c]', 'nad[c]', 'coa[c]'},[-1 -1 -1 1 1
1],1,0,1000);
        model1=addReaction(model1,'P_butanol',{'butanal[c]', 'nadh[c]',
'h[c]', 'butanol[c]', 'nad[c]'},[-1 -1 -1 1 1],1,0,1000);
        model1=addReaction(model1,'EX_butanol',{'butanol[c]'},[-1],1,
0,1000);
        model1=changeRxnBounds(model1,'ACOAD1f', 0, 'l');
        model1=addReaction(model1,'ACOAD1f_nadh',{'btcoa[c]', 'nad[c]',
'b2coa[c]', 'nadh[c]', 'h[c]'},[-1 -1 1 1 1],1,-1000,0);
%    case 11
%        model1=addReaction(model1,'EX_cobamamide', 'cobamamide <=>');
%        model1=addReaction(model1,'Add_cobamamide_ppa', '12ppd-R[e] +
cobamamide -> h2o[c] + ppa[c]');
%        model1=addReaction(model1,'Add_propanal', 'ppa[c] + nadh[c] ?
propanol[c] + nad[c]');
%        model1=addReaction(model1,'EX_Propanol','propanol[c] ->');
    case 12
        model1=changeRxnBounds(model1,'EX_glyc(e)', -20, 'u');
        model1=changeRxnBounds(model1,'EX_o2(e)', -2, 'l');

    case 13
        model1=addReaction(model1,'pyc','atp[c] + pyr[c] + hco3[c] ->
adp[c] + pi[c] + oaa[c] + h[c]');
        model1=changeRxnBounds(model1,'EX_co2(e)', -1000, 'l');
        model1=changeRxnBounds(model1,'EX_o2(e)', -2, 'l');
        model1=changeRxnBounds(model1,'EX_glyc(e)', -20, 'u');

    case 14
        model1=addReaction(model1,'PPCK_r','adp[c] + co2[c] + pep[c]
<=> atp[c] + oaa[c]');
        model1=changeRxnBounds(model1, 'PPCK', 0, 'u');
        model1=addReaction(model1,'AddPropionate','succ[c] -> ppa[c] +
co2[c]');
        %model1=addReaction(model1,'AddPropanol','ppa[c] + 3 h[c] + 2
nadh[c] + atp[c] -> propanol[c] + 2 nad[c] + h2o[c] + amp[c] +
ppi[c]'); %Checl this reaction!
        model1=addReaction(model1,'AddPropanol','ppa[c] + 3 h[c] + 2
nadh[c] -> propanol[c] + 2 nad[c] + h2o[c]'); %Check this reaction!
```

```
        model1=addReaction(model1,'EX_Propanol','propanol[c] ->');

    case 15
        model1=addReaction(model1,'PPCK_r','adp[c] + co2[c] + pep[c]
<=> atp[c] + oaa[c]');
        model1=changeRxnBounds(model1, 'PPCK', 0, 'u');
        model1=addReaction(model1,'AddPropanal1','ppcoa[c] + h[c] +
nadh[c] -> propanal[c] + nad[c] + coa[c]');
        model1=addReaction(model1,'AddPropanal2','12ppd-R[c] ->
propanal[c] + h2o[c]');
        model1=addReaction(model1,'AddPropanol','propanal[c] + h[c] +
nadh[c] -> propanol[c] + nad[c]');

        model1=addReaction(model1,'EX_Propanol','propanol[c] ->');
    case 16
        model1=addReaction(model1,'PPCK_r','adp[c] + co2[c] + pep[c]
<=> atp[c] + oaa[c]');
        model1=changeRxnBounds(model1, 'PPCK', 0, 'u');
        model1=changeRxnBounds(model1,'EX_co2(e)', -1000, 'l');
end
A= size(model1.rxns);
SizeModel=(A(1));

%% Enter knockouts
I= input('List of reactions to delete: ');
%Example of inputs: {' '}, {'FBA', DHAPT'}
SizeI=size(I);
for p=1:1:SizeI(2)
    RxnDelete=I(p);
    model1=changeRxnBounds(model1, RxnDelete, 0, 'u');
    model1=changeRxnBounds(model1, RxnDelete, 0, 'l');
    if p==1
        KnockoutReaction=RxnDelete;
    else
        KnockoutReaction=strcat(KnockoutReaction,',',RxnDelete);
    end
end

%% Desired product
prompt = {'Desired product: '};
%Example of input: EX_etoh(e)
Product=inputdlg(prompt);
model1=changeRxnBounds(model1, Product, 1000, 'u');
A=(model1.rxns);
productposition=AC_findp_F(A,Product);
model1=changeObjective(model1, Biomass_name, 1);
solution=optimizeCbModel(model1);
%Maximal specific growth rate
maxbiomass =solution.f
if solution.stat ~= 1
    display ('The selected condition does not have any valid solution')
    return
end
%Production rate of desired product at maximal specific growth rate
Product_when_biomass_is_optimized=solution.x(productposition)
```

```
TitlePlot=strcat('Product versus Biomass, deletion of: ',
KnockoutReaction);
xlsTitle=strcat('Model_', modelname, '_', KnockoutReaction);
model1=changeObjective(model1, Product(1), 1);
solution=optimizeCbModel(model1);
%Maximal production rate
OptimeProduct=solution.x(productposition)
%Solution space. The matrix will be storage as "Y", and it can be
called
%from the main screen for further analysis
model1=changeObjective(model1, Biomass_name, 1);
Y=zeros(101,3);
for i=1:1:101
    biomass1=0.01*(i-1)*maxbiomass;
    model1=changeRxnBounds(model1, Biomass_name, biomass1, 'l');
    model1=changeRxnBounds(model1, Biomass_name, biomass1, 'u');
    [minF maxF]=fluxVariability(model1, 100,'max',{Product}, false,
true);
    Y(i,:)= [biomass1 minF maxF];

end

model1=changeObjective(model1, Biomass_name, 1);
model1=changeRxnBounds(model1, Biomass_name, 0, 'l');
model1=changeRxnBounds(model1, Biomass_name, 1000, 'u');
solution=optimizeCbModel(model1);

%% Plot SOlution space
figure(1)
set(0, 'DefaultTextInterpreter', 'none') %Change set of all plots Text-
Interpreter to none, as oppose to Text (default)
plot(Y(:,1), Y(:,2), '--b','LineWidth',2);
hold on
plot(Y(:,1), Y(:,3), '--b','LineWidth',2);
xlabel('Specific Growth Rate');
ylabel(strcat('Product: ', Product));
title(TitlePlot);
```

10.11 Matlab function to test multiple models for glycerol fermentation

```
AC_BiomassvsProduct_GlyceroliJO1366_ModelTesting_Thesis
% Glycerol fermentation in E. coli as a platform for the synthesis of
% desired products.
% Evaluation of multiple possible models
% Model developed by Angela CIntolesi as part of her Doctoral Research
% Chemical adn Biomolecular Engineering, Rice University, March 2013
% Return a matrix Y with the optimal cell growth of each product

%% Use the updated model iJO1366 (2011)
clear all
global SizeModel
initCobraToolbox()
%changeCobraSolver('glpk');
%% Evaluation of multiple models
```

```
Y=zeros(17,17);
FigNum=1;
for ll=1:1:15
    for mm=1:1:ll
P1=ll;
        P2=mm;

        clear strArray1
clear strArray2
model1=readCbModel('iJO1366');
biomassposition=8;
Biomass_name='Ec_biomass_iJO1366_core_53p95M';
modelname='iJO1366';
model1=changeRxnBounds(model1,{'EX_o2(e)', 'EX_glc(e)', 'EX_glyc(e)',
'EX_co2(e)','FHL'}, [0 0 -20 0 -1000], 'l');
%model1=changeRxnBounds(model1,'EX_glyc(e)', -20, 'u');
model1=changeRxnBounds(model1,'FHL', 1000, 'u');
model1=changeRxnBounds(model1,'G3PD2', 0, 'u');
%no aa degradation
model1=changeRxnBounds(model1,{'DAAD', 'AST', 'SADH', 'SGSAD', 'SGDS',
'ARGDC', 'ARGDCpp', 'ASPT', 'GLUN', 'P5CD', 'PROD2', 'SERD_L', 'OBTFL',
'PPAKr', 'THRD', 'GLYAT', 'TYROXDApp', 'PEAMNOpp', 'TRPAS2',
'CYSDS','42A12BOOXpp', 'THRAi'}, [0 0 0 0 0 0 0 0 0 0 0 0 0 0 0 0 0 0 0
0 0 0], 'u');
model1=changeRxnBounds(model1,{'DAAD', 'AST', 'SADH', 'SGSAD', 'SGDS',
'ARGDC', 'ARGDCpp', 'ASPT', 'GLUN', 'P5CD', 'PROD2', 'SERD_L', 'OBTFL',
'PPAKr', 'THRD', 'GLYAT', 'TYROXDApp', 'PEAMNOpp', 'TRPAS2',
'CYSDS','42A12BOOXpp', 'THRAi'}, [0 0 0 0 0 0 0 0 0 0 0 0 0 0 0 0 0 0 0
0 0 0], 'l');
%no nucleotides degradation
model1=changeRxnBounds(model1,{'CYTD', 'DCYTD', 'DURIPP', 'TMDPP',
'PPM2', 'DRPA', 'ADA', 'DADA', 'PUNP1', 'PUNP4', 'PUNP2', 'PUNP3',
'PUNP5', 'PUNP6', 'PUNP7', 'PYNP2r'}, [0 0 0 0 0 0 0 0 0 0 0 0 0 0 0
0], 'u');
model1=changeRxnBounds(model1,{'CYTD', 'DCYTD', 'DURIPP', 'TMDPP',
'PPM2', 'DRPA', 'ADA', 'DADA', 'PUNP1', 'PUNP4', 'PUNP2', 'PUNP3',
'PUNP5', 'PUNP6', 'PUNP7', 'PYNP2r'}, [0 0 0 0 0 0 0 0 0 0 0 0 0 0 0
0], 'l');
% export aa (direct + non escential):
model1=changeRxnBounds(model1,{'EX_ala-B(e)', 'EX_ala-D(e)', 'EX_ala-
L(e)', 'EX_asn-L(e)', 'EX_asp-L(e)', 'EX_cys-D(e)', 'EX_cys-L(e)',
'EX_glu-L(e)', 'EX_gln-L(e)', 'EX_gly(e)', 'EX_his-L(e)', 'EX_ile-
L(e)', 'EX_leu-L(e)', 'EX_lys-L(e)', 'EX_met-D(e)', 'EX_met-L(e)',
'EX_phe-L(e)', 'EX_pro-L(e)', 'EX_ser-D(e)', 'EX_ser-L(e)','EX_thr-
L(e)', 'EX_trp-L(e)', 'EX_tyr-L(e)', 'EX_val-L(e)' }, [0 0 0 0 0 0 0 0
0 0 0 0 0 0 0 0 0 0 0 0 0 0 0 0 ], 'u');
model1= changeRxnBounds(model1,{'EX_26dap-M(e)','EX_frulys(e)','EX_hom-
L(e)', 'EX_orn(e)'}, [0 0 0 0 ], 'u');
%no Fe2+ export. no H2S export
model1=changeRxnBounds(model1,'EX_fe2(e)', 0, 'u');
model1=changeRxnBounds(model1,'EX_h2s(e)', 0, 'u');
%no POR5 export.
model1=changeRxnBounds(model1,'POR5', 0, 'l');
model1=changeRxnBounds(model1,'POR5', 0, 'u');
%no production of 5mtr and spmd, for redox purposes
model1=changeRxnBounds(model1,'EX_5mtr(e)', 0, 'u');
model1=changeRxnBounds(model1,'EX_spmd(e)', 0, 'u');
```

```
%Add PntAB
model1=addReaction(model1, 'Add_PntAB', {'nadh[c]', 'nadp[c]', 'h[p]',
'nad[c]', 'nadph[c]', 'h[c]'}, [-1 -1 -1 1 1 1], 1, 0, 1000);
%other products
model1=changeRxnBounds(model1,'EX_hxa(e)', 0, 'l');
model1=changeRxnBounds(model1,'EX_hxa(e)', 0, 'u');
%F6PA
model1=changeRxnBounds(model1,'F6PA', -4, 'l');
%FBA3, PFK_3
model1=changeRxnBounds(model1,'FBA3', 0, 'l');
model1=changeRxnBounds(model1,'FBA3', 0, 'u');
model1=changeRxnBounds(model1,'PFK_3', 0, 'l');
model1=changeRxnBounds(model1,'PFK_3', 0, 'u');

%% Remove natural Products (except succinate, which is essential in
small amounts)
model1=changeRxnBounds(model1,'EX_etoh(e)', 0, 'b');
model1=changeRxnBounds(model1,'EX_ac(e)', 0, 'b');
model1=changeRxnBounds(model1,'EX_lac-D(e)', 0, 'b');
model1=changeRxnBounds(model1,'EX_12ppd-R(e)', 0, 'b');
model1=changeRxnBounds(model1,'EX_12ppd-S(e)', 0, 'b');
model1=changeRxnBounds(model1,'EX_succ(e)', 2, 'u');
model1=changeRxnBounds(model1,'EX_acald(e)', 0, 'b');
model1=changeRxnBounds(model1,'EX_pyr(e)', 0, 'b');

model1=changeRxnBounds(model1,'EX_4abut(e)', 0, 'b');
model1=changeRxnBounds(model1,'EX_lipa_cold(e)', 0, 'b');
model1=changeRxnBounds(model1,'EX_lipa(e)', 0, 'b');
model1=changeRxnBounds(model1,'EX_lipoate(e)', 0, 'b');
model1=changeRxnBounds(model1,'EX_enlipa(e)', 0, 'b');
model1=changeRxnBounds(model1,'EX_akg(e)', 0, 'b');
model1=changeRxnBounds(model1,'EX_acser(e)', 0, 'b');
model1=changeRxnBounds(model1,'EX_pyr(e)', 0, 'b');
model1=changeRxnBounds(model1,'EX_pyr(e)', 0, 'b');
model1=changeRxnBounds(model1,'EX_pyr(e)', 0, 'b');

%% Chose Product 1
%display('Chose product 1:etoh, 2:Propanol, 3:Propanol(PckA), 4:Butoh,
5:Propionate, 6:Propionate(pckA), 7:lactate, 8:Succ');
%P1=input('9:succ(PckA), 10:12PDO(LAL), 11:12PDO(AC), 12:12PDO(Glyc),
13:13PDO, 14:Acetate, 15:Acetone, 16:Acald, 17:pyr ');

switch P1
    case 1
        model1=changeRxnBounds(model1,'EX_etoh(e)', 1000, 'u');
        strArray1(1) = java.lang.String('EX_etoh(e)');
    case 2

        model1=addReaction(model1,'AddPropanal1','ppcoa[c] + h[c] +
nadh[c] -> propanal[c] + nad[c] + coa[c]');
        model1=addReaction(model1,'AddPropanal2','12ppd-R[c] ->
propanal[c] + h2o[c]');
        model1=addReaction(model1,'AddPropanol','propanal[c] + h[c] +
nadh[c] -> propanol[c] + nad[c]');
        model1=addReaction(model1,'EX_Propanol','propanol[c] ->');
        strArray1(1) = java.lang.String('EX_Propanol');
```

```
    case 3
        model1=addReaction(model1,'PPCK_r','adp[c] + co2[c] + pep[c]
<=> atp[c] + oaa[c]');
        model1=changeRxnBounds(model1, 'PPCK', 0, 'u');
        model1=addReaction(model1,'AddPropanal1','ppcoa[c] + h[c] +
nadh[c] -> propanal[c] + nad[c] + coa[c]');
        model1=addReaction(model1,'AddPropanal2','12ppd-R[c] ->
propanal[c] + h2o[c]');
        model1=addReaction(model1,'AddPropanol','propanal[c] + h[c] +
nadh[c] -> propanol[c] + nad[c]');
        model1=addReaction(model1,'EX_Propanol','propanol[c] ->');
        strArray1(1) = java.lang.String('EX_Propanol');
    case 4
        model1=addReaction(model1,'P_butanal_CoA',{'btcoa[c]',
'nadh[c]', 'h[c]', 'butanal[c]', 'nad[c]', 'coa[c]'},[-1 -1 -1 1 1
1],1,0,1000);
        model1=addReaction(model1,'P_butanol',{'butanal[c]', 'nadh[c]',
'h[c]', 'butanol[c]', 'nad[c]'},[-1 -1 -1 1 1],1,0,1000);
        model1=addReaction(model1,'EX_butanol',{'butanol[c]'},[-1],1,
0,1000);
        model1=changeRxnBounds(model1,'ACOAD1f', 0, 'l');
        model1=addReaction(model1,'ACOAD1f_nadh',{'btcoa[c]', 'nad[c]',
'b2coa[c]', 'nadh[c]', 'h[c]'},[-1 -1 1 1 1],1,-1000,0);
        strArray1(1) = java.lang.String('EX_butanol');
    case 5
        model1=addReaction(model1,'TransPropionate','ppa[c] + h[c] ->
ppa[p] + h[p]');
        strArray1(1) = java.lang.String('EX_ppa(e)');
    case 6
        model1=addReaction(model1,'TransPropionate','ppa[c] + h[c] ->
ppa[p] + h[p]');
        model1=addReaction(model1,'PPCK_r','adp[c] + co2[c] + pep[c]
<=> atp[c] + oaa[c]');
        model1=changeRxnBounds(model1, 'PPCK', 0, 'u');

        strArray1(1) = java.lang.String('EX_ppa(e)');
    case 7
        model1=changeRxnBounds(model1,'EX_lac-D(e)', 1000, 'u');
        strArray1(1) = java.lang.String('EX_lac-D(e)');
    case 8
        model1=changeRxnBounds(model1,'EX_succ(e)', 1000, 'u');
         model1=changeRxnBounds(model1,'EX_co2(e)', -1000, 'l');
        strArray1(1) = java.lang.String('EX_succ(e)');
    case 9
        model1=changeRxnBounds(model1,'EX_succ(e)', 1000, 'u');
        model1=addReaction(model1,'PPCK_r','adp[c] + co2[c] + pep[c]
<=> atp[c] + oaa[c]');
        model1=changeRxnBounds(model1, 'PPCK', 0, 'u');
         model1=changeRxnBounds(model1,'EX_co2(e)', -1000, 'l');
        strArray1(1) = java.lang.String('EX_succ(e)');
    case 10
        model1=changeRxnBounds(model1,'EX_12ppd-R(e)', 1000, 'u');
        model1=changeRxnBounds(model1,'ALR2', 0, 'b');
        strArray1(1) = java.lang.String('EX_12ppd-R(e)');
    case 11
        model1=changeRxnBounds(model1,'EX_12ppd-R(e)', 1000, 'u');
        model1=changeRxnBounds(model1,'LALDO2x', 0, 'b');
```

```
        strArray1(1) = java.lang.String('EX_12ppd-R(e)');
    case 12
        model1=changeRxnBounds(model1,'EX_12ppd-R(e)', 1000, 'u');
        model1=addReaction(model1,'AddGlyctoLald','glyc[c] + h[c] ->
lald-D[c] + h2o[c]');
        strArray1(1) = java.lang.String('EX_12ppd-R(e)');
    case 13
        model1=addReaction(model1,'Add13PDO','glyc[c] + h[c] + nadph[c]
-> 13PDO[c] + nadp[c] + h2o[c]');
        model1=addReaction(model1,'EX_13PDO','13PDO[c] ->');
        strArray1(1) = java.lang.String('EX_13PDO');
    case 14
        model1=changeRxnBounds(model1,'EX_ac(e)', 1000, 'u');
        strArray1(1) = java.lang.String('EX_ac(e)');
    case 15
        model1=addReaction(model1,'AddAcetone','h[c] + nadh[c] +
glyc[c] -> acetone[c] + nad[c] + 2 h2o[c]');
        model1=addReaction(model1,'EX_Acetone','acetone[c] ->');
        strArray1(1) = java.lang.String('EX_Acetone');
    case 16
        model1=changeRxnBounds(model1,'EX_acald(e)', 1000, 'u');
        strArray1(1) = java.lang.String('EX_acald(e)');
    case 17
        model1=changeRxnBounds(model1,'EX_pyr(e)', 1000, 'u');
        strArray1(1) = java.lang.String('EX_pyr(e)');

end
Product1=cell(strArray1(1));

%% Chose Product 2
%display('Chose product 1:etoh, 2:Propanol, 3:Propanol(PckA), 4:Butoh,
5:Propionate, 6:Propionate(pckA), 7:lactate, 8:Succ');
%P2=input('9:succ(PckA), 10:12PDO(LAL), 11:12PDO(AC), 12:12PDO(Glyc),
13:13PDO, 14:Acetate, 15:Acetone ');

switch P2
    case 1
        model1=changeRxnBounds(model1,'EX_etoh(e)', 1000, 'u');
        strArray2(1) = java.lang.String('EX_etoh(e)');
    case 2
        model1=addReaction(model1,'AddPropanal1','ppcoa[c] + h[c] +
nadh[c] -> propanal[c] + nad[c] + coa[c]');
        model1=addReaction(model1,'AddPropanal2','12ppd-R[c] ->
propanal[c] + h2o[c]');
        model1=addReaction(model1,'AddPropanol','propanal[c] + h[c] +
nadh[c] -> propanol[c] + nad[c]');
        model1=addReaction(model1,'EX_Propanol','propanol[c] ->');
        strArray2(1) = java.lang.String('EX_Propanol');
    case 3
        model1=addReaction(model1,'PPCK_r','adp[c] + co2[c] + pep[c]
<=> atp[c] + oaa[c]');
        model1=changeRxnBounds(model1, 'PPCK', 0, 'u');
        model1=addReaction(model1,'AddPropanal1','ppcoa[c] + h[c] +
nadh[c] -> propanal[c] + nad[c] + coa[c]');
        model1=addReaction(model1,'AddPropanal2','12ppd-R[c] ->
propanal[c] + h2o[c]');
```

```
        model1=addReaction(model1,'AddPropanol','propanal[c] + h[c] +
nadh[c] -> propanol[c] + nad[c]');
        model1=addReaction(model1,'EX_Propanol','propanol[c] ->');
        strArray2(1) = java.lang.String('EX_Propanol');
    case 4
        model1=addReaction(model1,'P_butanal_CoA',{'btcoa[c]',
'nadh[c]', 'h[c]', 'butanal[c]', 'nad[c]', 'coa[c]'},[-1 -1 -1 1 1
1],1,0,1000);
        model1=addReaction(model1,'P_butanol',{'butanal[c]', 'nadh[c]',
'h[c]', 'butanol[c]', 'nad[c]'},[-1 -1 -1 1 1],1,0,1000);
        model1=addReaction(model1,'EX_butanol',{'butanol[c]'},[-1],1,
0,1000);
        model1=changeRxnBounds(model1,'ACOAD1f', 0, 'l');
        model1=addReaction(model1,'ACOAD1f_nadh',{'btcoa[c]', 'nad[c]',
'b2coa[c]', 'nadh[c]', 'h[c]'},[-1 -1 1 1 1],1,-1000,0);
        strArray2(1) = java.lang.String('EX_butanol');
    case 5
        model1=addReaction(model1,'TransPropionate','ppa[c] + h[c] ->
ppa[p] + h[p]');
        strArray2(1) = java.lang.String('EX_ppa(e)');
    case 6
        model1=addReaction(model1,'TransPropionate','ppa[c] + h[c] ->
ppa[p] + h[p]');
        model1=addReaction(model1,'PPCK_r','adp[c] + co2[c] + pep[c]
<=> atp[c] + oaa[c]');
        model1=changeRxnBounds(model1, 'PPCK', 0, 'u');

        strArray2(1) = java.lang.String('EX_ppa(e)');
    case 7
        model1=changeRxnBounds(model1,'EX_lac-D(e)', 1000, 'u');
        strArray2(1) = java.lang.String('EX_lac-D(e)');
    case 8
        model1=changeRxnBounds(model1,'EX_succ(e)', 1000, 'u');
         model1=changeRxnBounds(model1,'EX_co2(e)', -1000, 'l');
        strArray2(1) = java.lang.String('EX_succ(e)');
    case 9
        model1=changeRxnBounds(model1,'EX_succ(e)', 1000, 'u');
        model1=addReaction(model1,'PPCK_r','adp[c] + co2[c] + pep[c]
<=> atp[c] + oaa[c]');
        model1=changeRxnBounds(model1, 'PPCK', 0, 'u');
         model1=changeRxnBounds(model1,'EX_co2(e)', -1000, 'l');
        strArray2(1) = java.lang.String('EX_succ(e)');
    case 10
        model1=changeRxnBounds(model1,'EX_12ppd-R(e)', 1000, 'u');
        model1=changeRxnBounds(model1,'ALR2', 0, 'b');
        strArray2(1) = java.lang.String('EX_12ppd-R(e)');
    case 11
        model1=changeRxnBounds(model1,'EX_12ppd-R(e)', 1000, 'u');
        model1=changeRxnBounds(model1,'LALDO2x', 0, 'b');
        strArray2(1) = java.lang.String('EX_12ppd-R(e)');
    case 12
        model1=changeRxnBounds(model1,'EX_12ppd-R(e)', 1000, 'u');
        model1=addReaction(model1,'AddGlyctoLald','glyc[c] + h[c] ->
lald-D[c] + h2o[c]');
        strArray2(1) = java.lang.String('EX_12ppd-R(e)');
    case 13
```

```
        model1=addReaction(model1,'Add13PDO','glyc[c] + h[c] + nadph[c]
-> 13PDO[c] + nadp[c] + h2o[c]');
        model1=addReaction(model1,'EX_13PDO','13PDO[c] ->');
        strArray2(1) = java.lang.String('EX_13PDO');
    case 14
        model1=changeRxnBounds(model1,'EX_ac(e)', 1000, 'u');
        strArray2(1) = java.lang.String('EX_ac(e)');
    case 15
        model1=addReaction(model1,'AddAcetone','h[c] + nadh[c] +
glyc[c] -> acetone[c] + nad[c] + 2 h2o[c]');
        model1=addReaction(model1,'EX_Acetone','acetone[c] ->');
        strArray2(1) = java.lang.String('EX_Acetone');
    case 16
        model1=changeRxnBounds(model1,'EX_acald(e)', 1000, 'u');
        strArray2(1) = java.lang.String('EX_acald(e)');
    case 17
        model1=changeRxnBounds(model1,'EX_pyr(e)', 1000, 'u');
        strArray2(1) = java.lang.String('EX_pyr(e)');

end
Product2=cell(strArray2(1));

A= size(model1.rxns);
SizeModel=(A(1));

%% Optimal solution
solution=optimizeCbModel(model1);
if solution.stat == 1
    Y(ll,mm)=solution.f;
end
    end
end

Y
```

10.12 Matlab function for lcp-GEM

```
AC_BiomassvsProduct_GlucoseiJO1366
% Production of long chain productsin E. coli.
% Evaluation of the reversal B-oxidation cycle, FA biosynthesis
pathway,and the alpha-keto acids.
% Model developed by Angela Cintolesi as part of her Doctoral Research
% Chemical and Biomolecular Engineering, Rice University, March 2013
% Return a matrix Y with the optimal cell growth of each product

%% Use the updated model iJO1366 (2011)
clear all
global SizeModel
initCobraToolbox()
%changeCobraSolver('glpk');
%% Open model
```

```
K=input ('Choose pathway: (1)Reverse B-oxd; (2)FA biosynthesis;
(3)alpha ketoacids for butanol and hexanol: ');
        model1=readCbModel('iJO1366');
        biomassposition=8;
        Biomass_name='Ec_biomass_iJO1366_core_53p95M';
        modelname='iJO1366';
        %no aa degradation
        model1=changeRxnBounds(model1,{'DAAD', 'AST', 'SADH', 'SGSAD',
'SGDS', 'ARGDC', 'ARGDCpp', 'ASPT', 'GLUN', 'P5CD', 'PROD2', 'SERD_L',
'OBTFL', 'PPAKr', 'THRD', 'GLYAT', 'TYROXDApp', 'PEAMNOpp', 'TRPAS2',
'CYSDS','42A12BOOXpp', 'THRAi'}, [0 0 0 0 0 0 0 0 0 0 0 0 0 0 0 0 0 0 0
0 0 0], 'u');
        model1=changeRxnBounds(model1,{'DAAD', 'AST', 'SADH', 'SGSAD',
'SGDS', 'ARGDC', 'ARGDCpp', 'ASPT', 'GLUN', 'P5CD', 'PROD2', 'SERD_L',
'OBTFL', 'PPAKr', 'THRD', 'GLYAT', 'TYROXDApp', 'PEAMNOpp', 'TRPAS2',
'CYSDS','42A12BOOXpp', 'THRAi'}, [0 0 0 0 0 0 0 0 0 0 0 0 0 0 0 0 0 0 0
0 0 0], 'l');
        %no nucleotides degradation
        model1=changeRxnBounds(model1,{'CYTD', 'DCYTD', 'DURIPP',
'TMDPP', 'PPM2', 'DRPA', 'ADA', 'DADA', 'PUNP1', 'PUNP4', 'PUNP2',
'PUNP3', 'PUNP5', 'PUNP6', 'PUNP7', 'PYNP2r'}, [0 0 0 0 0 0 0 0 0 0 0 0
0 0 0 0], 'u');
        model1=changeRxnBounds(model1,{'CYTD', 'DCYTD', 'DURIPP',
'TMDPP', 'PPM2', 'DRPA', 'ADA', 'DADA', 'PUNP1', 'PUNP4', 'PUNP2',
'PUNP3', 'PUNP5', 'PUNP6', 'PUNP7', 'PYNP2r'}, [0 0 0 0 0 0 0 0 0 0 0 0
0 0 0 0], 'l');
        % export aa (direct + non escential):
        model1=changeRxnBounds(model1,{'EX_ala-B(e)', 'EX_ala-D(e)',
'EX_ala-L(e)', 'EX_asn-L(e)', 'EX_asp-L(e)', 'EX_cys-D(e)', 'EX_cys-
L(e)', 'EX_glu-L(e)', 'EX_gln-L(e)', 'EX_gly(e)', 'EX_his-L(e)',
'EX_ile-L(e)', 'EX_leu-L(e)', 'EX_lys-L(e)', 'EX_met-D(e)', 'EX_met-
L(e)', 'EX_phe-L(e)', 'EX_pro-L(e)', 'EX_ser-D(e)', 'EX_ser-
L(e)','EX_thr-L(e)', 'EX_trp-L(e)', 'EX_tyr-L(e)', 'EX_val-L(e)' }, [0
0 0 0 0 0 0 0 0 0 0 0 0 0 0 0 0 0 0 0 0 0 0 0 0 0 0 0 0 0 0 0 0 0 0 ], 'u');
        model1= changeRxnBounds(model1,{'EX_26dap-
M(e)','EX_frulys(e)','EX_hom-L(e)', 'EX_orn(e)'}, [0 0 0 0 ], 'u');
        %no Fe2+ export. no H2S export
        model1=changeRxnBounds(model1,'EX_fe2(e)', 0, 'u');
        model1=changeRxnBounds(model1,'EX_h2s(e)', 0, 'u');
        %no POR5 export.
        model1=changeRxnBounds(model1,'POR5', 0, 'l');
        model1=changeRxnBounds(model1,'POR5', 0, 'u');
        %Add PntAB
        model1=addReaction(model1, 'Add_PntAB', {'nadh[c]', 'nadp[c]',
'h[p]', 'nad[c]', 'nadph[c]', 'h[c]'}, [-1 -1 -1 1 1 1], 1, 0, 1000);
        %FBA3, PFK_3
        model1=changeRxnBounds(model1,'FBA3', 0, 'l');
        model1=changeRxnBounds(model1,'FBA3', 0, 'u');
        model1=changeRxnBounds(model1,'PFK_3', 0, 'l');
        model1=changeRxnBounds(model1,'PFK_3', 0, 'u');
        %no production of 5mtr and spmd, for redox purposes
        model1=changeRxnBounds(model1,'EX_5mtr(e)', 0, 'u');
        model1=changeRxnBounds(model1,'EX_spmd(e)', 0, 'u');

%% Modify model according to specific scenarios
switch K
```

```
    case 1 % Detailed reverse B-oxidation. Production of alcohols,
alkanes and FA (from acyl-coa)

        model1=changeRxnBounds(model1,'EX_o2(e)', 0, 'l');
        model1=changeRxnBounds(model1,'EX_glc(e)', -15, 'l');
        %Delete by-products
        model1=changeRxnBounds(model1,'EX_pyr(e)', 0, 'u');
        model1=changeRxnBounds(model1,'EX_acald(e)', 0, 'u');
        model1=changeRxnBounds(model1,'EX_hxa(e)', 0, 'u');
        %restrict fA biosynthesis. ACCOC
        model1=changeRxnBounds(model1,'ACCOAC', 0.1, 'u');
        %ACOAD1f are inactive in this case.
        model1=changeRxnBounds(model1,'ACOAD1f', 0, 'l');
        model1=changeRxnBounds(model1,'ACOAD1f', 0, 'u');
        model1=changeRxnBounds(model1,'ACOAD2f', 0, 'l');
        model1=changeRxnBounds(model1,'ACOAD2f', 0, 'u');
        model1=changeRxnBounds(model1,'ACOAD3f', 0, 'l');
        model1=changeRxnBounds(model1,'ACOAD3f', 0, 'u');
        model1=changeRxnBounds(model1,'ACOAD4f', 0, 'l');
        model1=changeRxnBounds(model1,'ACOAD4f', 0, 'u');
        model1=changeRxnBounds(model1,'ACOAD5f', 0, 'l');
        model1=changeRxnBounds(model1,'ACOAD5f', 0, 'u');
        model1=changeRxnBounds(model1,'ACOAD6f', 0, 'l');
        model1=changeRxnBounds(model1,'ACOAD6f', 0, 'u');
        model1=changeRxnBounds(model1,'ACOAD7f', 0, 'l');
        model1=changeRxnBounds(model1,'ACOAD7f', 0, 'u');
        model1=changeRxnBounds(model1,'ACOAD8f', 0, 'l');
        model1=changeRxnBounds(model1,'ACOAD8f', 0, 'u');

        % Ferredoxins / Reversal B-oxidation cycle
        model1=addReaction(model1,'ACOAD1f_ferr',{'btcoa[c]', 'fd_oxi',
'b2coa[c]', 'fd_red', 'h[c]'},[-1 -1 1 1 1],1,-1000,0);
        model1=addReaction(model1,'ACOAD2f_ferr',{'fd_oxi', 'hxcoa[c]',
'hx2coa[c]', 'fd_red', 'h[c]'},[-1 -1 1 1 1],1,-1000,0);
        model1=addReaction(model1,'ACOAD3f_ferr',{'fd_oxi', 'occoa[c]',
'oc2coa[c]', 'fd_red', 'h[c]'},[-1 -1 1 1 1],1,-1000,0);
        model1=addReaction(model1,'ACOAD4f_ferr',{'dcacoa[c]',
'fd_oxi', 'dc2coa[c]', 'fd_red', 'h[c]'},[-1 -1 1 1 1],1,-1000,0);
        model1=addReaction(model1,'ACOAD5f_ferr',{'ddcacoa[c]',
'fd_oxi', 'dd2coa[c]', 'fd_red', 'h[c]'},[-1 -1 1 1 1],1,-1000,0);
        model1=addReaction(model1,'ACOAD6f_ferr',{'fd_oxi', 'tdcoa[c]',
'td2coa[c]', 'fd_red', 'h[c]'},[-1 -1 1 1 1],1,-1000,0);
        model1=addReaction(model1,'ACOAD7f_ferr',{'fd_oxi',
'pmtcoa[c]', 'hdd2coa[c]', 'fd_red', 'h[c]'},[-1 -1 1 1 1],1,-1000,0);
        model1=addReaction(model1,'ACOAD8f_ferr',{'fd_oxi', 'stcoa[c]',
'od2coa[c]', 'fd_red', 'h[c]'},[-1 -1 1 1 1],1,-1000,0);
        model1=addReaction(model1,'PFOR',{'coa[c]', 'fd_oxi', 'pyr[c]',
'accoa[c]', 'co2[c]', 'fd_red', 'h[c]'},[-1 -1 -1 1 1 1 1],1,0,1000);

        %acyl-ACP --> aldehyde (butanal, hexanal, octanal, ...) %set
al.l to
        %zero
        model1=addReaction(model1,'P_butanal_ACP',{'butACP[c]',
'nadh[c]', 'h[c]', 'butanal[c]', 'nad[c]', 'ACP[c]'},[-1 -1 -1 1 1
1],1,0,0);
```

```
        model1=addReaction(model1,'P_hexanal_ACP',{'hexACP[c]',
'nadh[c]', 'h[c]', 'hexanal[c]', 'nad[c]', 'ACP[c]'},[-1 -1 -1 1 1
1],1,0,0);
        model1=addReaction(model1,'P_octanal_ACP',{'ocACP[c]',
'nadh[c]', 'h[c]', 'octanal[c]', 'nad[c]', 'ACP[c]'},[-1 -1 -1 1 1
1],1,0,0);
        model1=addReaction(model1,'P_decanal_ACP',{'dcaACP[c]',
'nadh[c]', 'h[c]', 'decanal[c]', 'nad[c]', 'ACP[c]'},[-1 -1 -1 1 1
1],1,0,0);
        model1=addReaction(model1,'P_dodecanal_ACP',{'ddcaACP[c]',
'nadh[c]', 'h[c]', 'dodecanal[c]', 'nad[c]', 'ACP[c]'},[-1 -1 -1 1 1
1],1,0,0);
        model1=addReaction(model1,'P_tetradecanal_ACP',{'myrsACP[c]',
'nadh[c]', 'h[c]', 'tetradecanal[c]', 'nad[c]', 'ACP[c]'},[-1 -1 -1 1 1
1],1,0,0); %myristoyl-ACP
        model1=addReaction(model1,'P_hexadecanal_ACP',{'palmACP[c]',
'nadh[c]', 'h[c]', 'hexadecanal[c]', 'nad[c]', 'ACP[c]'},[-1 -1 -1 1 1
1],1,0,0);
        model1=addReaction(model1,'P_octadecanal_ACP',{'ocdcaACP[c]',
'nadh[c]', 'h[c]', 'octadecanal[c]', 'nad[c]', 'ACP[c]'},[-1 -1 -1 1 1
1],1,0,0);

        %Reduction of acyl-coa / acyl-CoA --> aldehyde (butanal,
hexanal, octanal, ...)
        model1=addReaction(model1,'P_butanal_CoA',{'btcoa[c]',
'nadh[c]', 'h[c]', 'butanal[c]', 'nad[c]', 'coa[c]'},[-1 -1 -1 1 1
1],1,0,1000);
        model1=addReaction(model1,'P_hexanal_CoA',{'hxcoa[c]',
'nadh[c]', 'h[c]', 'hexanal[c]', 'nad[c]', 'coa[c]'},[-1 -1 -1 1 1
1],1,0,1000);
        model1=addReaction(model1,'P_octanal_CoA',{'occoa[c]',
'nadh[c]', 'h[c]', 'octanal[c]', 'nad[c]', 'coa[c]'},[-1 -1 -1 1 1
1],1,0,1000);
        model1=addReaction(model1,'P_decanal_CoA',{'dcacoa[c]',
'nadh[c]', 'h[c]', 'decanal[c]', 'nad[c]', 'coa[c]'},[-1 -1 -1 1 1
1],1,0,1000);
        model1=addReaction(model1,'P_dodecanal_CoA',{'ddcacoa[c]',
'nadh[c]', 'h[c]', 'dodecanal[c]', 'nad[c]', 'coa[c]'},[-1 -1 -1 1 1
1],1,0,1000);
        model1=addReaction(model1,'P_tetradecanal_CoA',{'tdcoa[c]',
'nadh[c]', 'h[c]', 'tetradecanal[c]', 'nad[c]', 'coa[c]'},[-1 -1 -1 1 1
1],1,0,1000);
        model1=addReaction(model1,'P_hexadecanal_CoA',{'pmtcoa[c]',
'nadh[c]', 'h[c]', 'hexadecanal[c]', 'nad[c]', 'coa[c]'},[-1 -1 -1 1 1
1],1,0,1000);
        model1=addReaction(model1,'P_octadecanal_CoA',{'stcoa[c]',
'nadh[c]', 'h[c]', 'octadecanal[c]', 'nad[c]', 'coa[c]'},[-1 -1 -1 1 1
1],1,0,1000);

        %Aldehyde decarboxilation / Production of alkanes
        model1=addReaction(model1,'P_propane',{'butanal[c]',
'propane[c]', 'co[c]'},[-1 1 1],1,0,1000);
        model1=addReaction(model1,'P_pentane',{'hexanal[c]',
'pentane[c]','co[c]'},[-1 1 1],1,0,1000);
        model1=addReaction(model1,'P_heptane',{'octanal[c]',
'heptane[c]','co[c]'},[-1 1 1],1,0,1000);
```

```
        model1=addReaction(model1,'P_nonane',{'decanal[c]',
'nonane[c]','co[c]'},[-1 1 1],1,0,1000);
        model1=addReaction(model1,'P_undecane',{'dodecanal[c]',
'undecane[c]', 'co[c]'},[-1 1 1],1,0,1000);
        model1=addReaction(model1,'P_tridecane',{'tetradecanal[c]',
'tridecane[c]','co[c]'},[-1 1 1],1,0,1000);
        model1=addReaction(model1,'P_pentadecane',{'hexadecanal[c]',
'pentadecane[c]', 'co[c]'},[-1 1 1],1,0,1000);
        model1=addReaction(model1,'P_heptadecane',{'octadecanal[c]',
'heptadecane[c]','co[c]'},[-1 1 1],1,0,1000);

        %Alcohol production
        model1=addReaction(model1,'P_butanol',{'butanal[c]', 'nadh[c]',
'h[c]', 'butanol[c]', 'nad[c]'},[-1 -1 -1 1 1],1,0,1000);
        model1=addReaction(model1,'P_hexanol',{'hexanal[c]', 'nadh[c]',
'h[c]', 'hexanol[c]', 'nad[c]'},[-1 -1 -1 1 1],1,0,1000);
        model1=addReaction(model1,'P_octanol',{'octanal[c]', 'nadh[c]',
'h[c]', 'octanol[c]', 'nad[c]'},[-1 -1 -1 1 1],1,0,1000);
        model1=addReaction(model1,'P_decanol',{'decanal[c]', 'nadh[c]',
'h[c]', 'decanol[c]', 'nad[c]'},[-1 -1 -1 1 1],1,0,1000);
        model1=addReaction(model1,'P_dodecanol',{'dodecanal[c]',
'nadh[c]', 'h[c]', 'dodecanol[c]', 'nad[c]'},[-1 -1 -1 1 1],1,0,1000);
        model1=addReaction(model1,'P_tetradecanol',{'tetradecanal[c]',
'nadh[c]', 'h[c]', 'tetradecanol[c]', 'nad[c]'},[-1 -1 -1 1
1],1,0,1000);
        model1=addReaction(model1,'P_hexadecanol',{'hexadecanal[c]',
'nadh[c]', 'h[c]', 'hexadecanol[c]', 'nad[c]'},[-1 -1 -1 1
1],1,0,1000);
        model1=addReaction(model1,'P_octadecanol',{'octadecanal[c]',
'nadh[c]', 'h[c]', 'octadecanol[c]', 'nad[c]'},[-1 -1 -1 1
1],1,0,1000);

        %acyl-coa --> fatty acids
        model1=addReaction(model1,'P_but_CoA',{'btcoa[c]', 'h2o[c]',
'h[c]', 'but[c]', 'coa[c]'},[-1 -1 1 1 1],1,0,1000);
        %The rest of these reactions are already in the model:
FACOAE60-180

        %acyl-ACP --> fatty acids
        model1=addReaction(model1,'P_but_ACP',{'butACP[c]', 'h2o[c]',
'h[c]', 'but[c]', 'ACP[c]'},[-1 -1 1 1 1],1,0,0);
        model1=addReaction(model1,'P_hxa_ACP',{'hexACP[c]', 'h2o[c]',
'h[c]', 'hxa[c]', 'ACP[c]'},[-1 -1 1 1 1],1,0,0);
        %Other reactions are already in the model (ex: FA80ACPHi)
        model1=addReaction(model1,'P_ocdca_ACP',{'ocdcaACP[c]',
'h2o[c]', 'h[c]', 'ocdca[c]', 'ACP[c]'},[-1 -1 1 1 1],1,0,0);

        %transport reactions to export fatty acids. All for [c] to [e]
        %Simplified process from [c] to [p], and from [p] to [e].
        %because the model did not have the proper transport accross
membrane from [p] to [e]
        model1=addReaction(model1,'P_octa_trans',{'octa[c]', 'octa[e]',
'h[c]', 'h[p]'},[-1 1 -1 1],1,0,1000);
        model1=addReaction(model1,'P_dca_trans',{'dca[c]', 'dca[e]',
'h[c]', 'h[p]'},[-1 1 -1 1],1,0,1000);
```

```
        model1=addReaction(model1,'P_ddca_trans',{'ddca[c]', 'ddca[e]',
'h[c]', 'h[p]'},[-1 1 -1 1],1,0,1000);
        model1=addReaction(model1,'P_ttdca_trans',{'ttdca[c]',
'ttdca[e]', 'h[c]', 'h[p]'},[-1 1 -1 1],1,0,1000);
        model1=addReaction(model1,'P_hdca_trans',{'hdca[c]', 'hdca[e]',
'h[c]', 'h[p]'},[-1 1 -1 1],1,0,1000);
        model1=addReaction(model1,'P_ocdca_trans_extra',{'ocdca[c]',
'ocdca[e]', 'h[c]', 'h[p]'},[-1 1 -1 1],1,0,1000);

        %Set export of existing products to zero
        model1=changeRxnBounds(model1,'EX_but(e)', 0, 'u');
        model1=changeRxnBounds(model1,'EX_hxa(e)', 0, 'u');
        model1=changeRxnBounds(model1,'EX_octa(e)', 0, 'u');
        model1=changeRxnBounds(model1,'EX_dca(e)', 0, 'u');
        model1=changeRxnBounds(model1,'EX_ddca(e)', 0, 'u');
        model1=changeRxnBounds(model1,'EX_ttdca(e)', 0, 'u');
        model1=changeRxnBounds(model1,'EX_hdca(e)', 0, 'u');
        model1=changeRxnBounds(model1,'EX_ocdca(e)', 0, 'u');

        % Set export of new products to zero
        model1=addReaction(model1,'EX_butanol',{'butanol[c]'},[-1],1,
0,0);
        model1=addReaction(model1,'EX_hexanol',{'hexanol[c]'},[-1],1,
0,0);
        model1=addReaction(model1,'EX_octanol',{'octanol[c]'},[-1
],1,0,0);
        model1=addReaction(model1,'EX_decanol',{'decanol[c]'},[-1],1,
0,0);
        model1=addReaction(model1,'EX_dodecanol',{'dodecanol[c]'},[-1
],1,0,0);

model1=addReaction(model1,'EX_tetradecanol',{'tetradecanol[c]'},[-1],1,
0,0);

model1=addReaction(model1,'EX_hexadecanol',{'hexadecanol[c]'},[-1
],1,0,0);

model1=addReaction(model1,'EX_octadecanol',{'octadecanol[c]'},[-1],1,
0,0);

        model1=addReaction(model1,'EX_propane',{'propane[c]'},[-1],1,
0,0);
        model1=addReaction(model1,'EX_pentane',{'pentane[c]'},[-1],1,
0,0);
        model1=addReaction(model1,'EX_heptane',{'heptane[c]'},[-1
],1,0,0);
        model1=addReaction(model1,'EX_nonane',{'nonane[c]'},[-1],1,
0,0);
        model1=addReaction(model1,'EX_undecane',{'undecane[c]'},[-1
],1,0,0);
        model1=addReaction(model1,'EX_tridecane',{'tridecane[c]'},[-
1],1, 0,0);

model1=addReaction(model1,'EX_pentadecane',{'pentadecane[c]'},[-1
],1,0,0);
```

```
model1=addReaction(model1,'EX_heptadecane',{'heptadecane[c]'},[-1],1,
0,0);

        model1=addReaction(model1,'EX_co',{'co[c]'},[-1 ],1,0,1000);

    case 2 % (NO reverse B-oxidation). Production of alcohols, alkanes
and FA (from acyl-ACP)
        model1=changeRxnBounds(model1,'EX_o2(e)', 0, 'l');
        model1=changeRxnBounds(model1,'EX_glc(e)', -15, 'l');
        %Delete by-products
        model1=changeRxnBounds(model1,'EX_pyr(e)', 0, 'u');
        model1=changeRxnBounds(model1,'EX_acald(e)', 0, 'u');
        model1=changeRxnBounds(model1,'EX_hxa(e)', 0, 'u');
        %ACOAD1f are inactive in this case.
        model1=changeRxnBounds(model1,'ACOAD1f', 0, 'l');
        model1=changeRxnBounds(model1,'ACOAD1f', 0, 'u');
        model1=changeRxnBounds(model1,'ACOAD2f', 0, 'l');
        model1=changeRxnBounds(model1,'ACOAD2f', 0, 'u');
        model1=changeRxnBounds(model1,'ACOAD3f', 0, 'l');
        model1=changeRxnBounds(model1,'ACOAD3f', 0, 'u');
        model1=changeRxnBounds(model1,'ACOAD4f', 0, 'l');
        model1=changeRxnBounds(model1,'ACOAD4f', 0, 'u');
        model1=changeRxnBounds(model1,'ACOAD5f', 0, 'l');
        model1=changeRxnBounds(model1,'ACOAD5f', 0, 'u');
        model1=changeRxnBounds(model1,'ACOAD6f', 0, 'l');
        model1=changeRxnBounds(model1,'ACOAD6f', 0, 'u');
        model1=changeRxnBounds(model1,'ACOAD7f', 0, 'l');
        model1=changeRxnBounds(model1,'ACOAD7f', 0, 'u');
        model1=changeRxnBounds(model1,'ACOAD8f', 0, 'l');
        model1=changeRxnBounds(model1,'ACOAD8f', 0, 'u');

        % Ferredoxins / Reversal B-oxidation cycle / inactive in this
case
        model1=addReaction(model1,'ACOAD1f_ferr',{'btcoa[c]', 'fd_oxi',
'b2coa[c]', 'fd_red', 'h[c]'},[-1 -1 1 1 1],1,0,0);
        model1=addReaction(model1,'ACOAD2f_ferr',{'fd_oxi', 'hxcoa[c]',
'hx2coa[c]', 'fd_red', 'h[c]'},[-1 -1 1 1 1],1,0,0);
        model1=addReaction(model1,'ACOAD3f_ferr',{'fd_oxi', 'occoa[c]',
'oc2coa[c]', 'fd_red', 'h[c]'},[-1 -1 1 1 1],1,0,0);
        model1=addReaction(model1,'ACOAD4f_ferr',{'dcacoa[c]',
'fd_oxi', 'dc2coa[c]', 'fd_red', 'h[c]'},[-1 -1 1 1 1],1,0,0);
        model1=addReaction(model1,'ACOAD5f_ferr',{'ddcacoa[c]',
'fd_oxi', 'dd2coa[c]', 'fd_red', 'h[c]'},[-1 -1 1 1 1],1,0,0);
        model1=addReaction(model1,'ACOAD6f_ferr',{'fd_oxi', 'tdcoa[c]',
'td2coa[c]', 'fd_red', 'h[c]'},[-1 -1 1 1 1],1,0,0);
        model1=addReaction(model1,'ACOAD7f_ferr',{'fd_oxi',
'pmtcoa[c]', 'hdd2coa[c]', 'fd_red', 'h[c]'},[-1 -1 1 1 1],1,0,0);
        model1=addReaction(model1,'ACOAD8f_ferr',{'fd_oxi', 'stcoa[c]',
'od2coa[c]', 'fd_red', 'h[c]'},[-1 -1 1 1 1],1,0,0);
        model1=addReaction(model1,'PFOR',{'coa[c]', 'fd_oxi', 'pyr[c]',
'accoa[c]', 'co2[c]', 'fd_red', 'h[c]'},[-1 -1 -1 1 1 1 1],1,0,0);

        %acyl-ACP --> aldehyde (butanal, hexanal, octanal, ...) %set
al.l to
        %zero
```

```
        model1=addReaction(model1,'P_butanal_ACP',{'butACP[c]',
'nadh[c]', 'h[c]', 'butanal[c]', 'nad[c]', 'ACP[c]'},[-1 -1 -1 1 1
1],1,0,1000);
        model1=addReaction(model1,'P_hexanal_ACP',{'hexACP[c]',
'nadh[c]', 'h[c]', 'hexanal[c]', 'nad[c]', 'ACP[c]'},[-1 -1 -1 1 1
1],1,0,1000);
        model1=addReaction(model1,'P_octanal_ACP',{'ocACP[c]',
'nadh[c]', 'h[c]', 'octanal[c]', 'nad[c]', 'ACP[c]'},[-1 -1 -1 1 1
1],1,0,1000);
        model1=addReaction(model1,'P_decanal_ACP',{'dcaACP[c]',
'nadh[c]', 'h[c]', 'decanal[c]', 'nad[c]', 'ACP[c]'},[-1 -1 -1 1 1
1],1,0,1000);
        model1=addReaction(model1,'P_dodecanal_ACP',{'ddcaACP[c]',
'nadh[c]', 'h[c]', 'dodecanal[c]', 'nad[c]', 'ACP[c]'},[-1 -1 -1 1 1
1],1,0,1000);
        model1=addReaction(model1,'P_tetradecanal_ACP',{'myrsACP[c]',
'nadh[c]', 'h[c]', 'tetradecanal[c]', 'nad[c]', 'ACP[c]'},[-1 -1 -1 1 1
1],1,0,1000); %myristoyl-ACP
        model1=addReaction(model1,'P_hexadecanal_ACP',{'palmACP[c]',
'nadh[c]', 'h[c]', 'hexadecanal[c]', 'nad[c]', 'ACP[c]'},[-1 -1 -1 1 1
1],1,0,1000);
        model1=addReaction(model1,'P_octadecanal_ACP',{'ocdcaACP[c]',
'nadh[c]', 'h[c]', 'octadecanal[c]', 'nad[c]', 'ACP[c]'},[-1 -1 -1 1 1
1],1,0,1000);

        %Reduction of acyl-coa / acyl-CoA --> aldehyde (butanal,
hexanal, octanal, ...)
        model1=addReaction(model1,'P_butanal_CoA',{'btcoa[c]',
'nadh[c]', 'h[c]', 'butanal[c]', 'nad[c]', 'coa[c]'},[-1 -1 -1 1 1
1],1,0,0);
        model1=addReaction(model1,'P_hexanal_CoA',{'hxcoa[c]',
'nadh[c]', 'h[c]', 'hexanal[c]', 'nad[c]', 'coa[c]'},[-1 -1 -1 1 1
1],1,0,0);
        model1=addReaction(model1,'P_octanal_CoA',{'occoa[c]',
'nadh[c]', 'h[c]', 'octanal[c]', 'nad[c]', 'coa[c]'},[-1 -1 -1 1 1
1],1,0,0);
        model1=addReaction(model1,'P_decanal_CoA',{'dcacoa[c]',
'nadh[c]', 'h[c]', 'decanal[c]', 'nad[c]', 'coa[c]'},[-1 -1 -1 1 1
1],1,0,0);
        model1=addReaction(model1,'P_dodecanal_CoA',{'ddcacoa[c]',
'nadh[c]', 'h[c]', 'dodecanal[c]', 'nad[c]', 'coa[c]'},[-1 -1 -1 1 1
1],1,0,0);
        model1=addReaction(model1,'P_tetradecanal_CoA',{'tdcoa[c]',
'nadh[c]', 'h[c]', 'tetradecanal[c]', 'nad[c]', 'coa[c]'},[-1 -1 -1 1 1
1],1,0,0);
        model1=addReaction(model1,'P_hexadecanal_CoA',{'pmtcoa[c]',
'nadh[c]', 'h[c]', 'hexadecanal[c]', 'nad[c]', 'coa[c]'},[-1 -1 -1 1 1
1],1,0,0);
        model1=addReaction(model1,'P_octadecanal_CoA',{'stcoa[c]',
'nadh[c]', 'h[c]', 'octadecanal[c]', 'nad[c]', 'coa[c]'},[-1 -1 -1 1 1
1],1,0,0);

        %Aldehyde decarboxilation / Production of alkanes
        model1=addReaction(model1,'P_propane',{'butanal[c]',
'propane[c]', 'co[c]'},[-1 1 1],1,0,1000);
```

```
        model1=addReaction(model1,'P_pentane',{'hexanal[c]',
'pentane[c]','co[c]'},[-1 1 1],1,0,1000);
        model1=addReaction(model1,'P_heptane',{'octanal[c]',
'heptane[c]','co[c]'},[-1 1 1],1,0,1000);
        model1=addReaction(model1,'P_nonane',{'decanal[c]',
'nonane[c]','co[c]'},[-1 1 1],1,0,1000);
        model1=addReaction(model1,'P_undecane',{'dodecanal[c]',
'undecane[c]', 'co[c]'},[-1 1 1],1,0,1000);
        model1=addReaction(model1,'P_tridecane',{'tetradecanal[c]',
'tridecane[c]','co[c]'},[-1 1 1],1,0,1000);
        model1=addReaction(model1,'P_pentadecane',{'hexadecanal[c]',
'pentadecane[c]', 'co[c]'},[-1 1 1],1,0,1000);
        model1=addReaction(model1,'P_heptadecane',{'octadecanal[c]',
'heptadecane[c]','co[c]'},[-1 1 1],1,0,1000);

        %Alcohol production
        model1=addReaction(model1,'P_butanol',{'butanal[c]', 'nadh[c]',
'h[c]', 'butanol[c]', 'nad[c]'},[-1 -1 -1 1 1],1,0,1000);
        model1=addReaction(model1,'P_hexanol',{'hexanal[c]', 'nadh[c]',
'h[c]', 'hexanol[c]', 'nad[c]'},[-1 -1 -1 1 1],1,0,1000);
        model1=addReaction(model1,'P_octanol',{'octanal[c]', 'nadh[c]',
'h[c]', 'octanol[c]', 'nad[c]'},[-1 -1 -1 1 1],1,0,1000);
        model1=addReaction(model1,'P_decanol',{'decanal[c]', 'nadh[c]',
'h[c]', 'decanol[c]', 'nad[c]'},[-1 -1 -1 1 1],1,0,1000);
        model1=addReaction(model1,'P_dodecanol',{'dodecanal[c]',
'nadh[c]', 'h[c]', 'dodecanol[c]', 'nad[c]'},[-1 -1 -1 1 1],1,0,1000);
        model1=addReaction(model1,'P_tetradecanol',{'tetradecanal[c]',
'nadh[c]', 'h[c]', 'tetradecanol[c]', 'nad[c]'},[-1 -1 -1 1
1],1,0,1000);
        model1=addReaction(model1,'P_hexadecanol',{'hexadecanal[c]',
'nadh[c]', 'h[c]', 'hexadecanol[c]', 'nad[c]'},[-1 -1 -1 1
1],1,0,1000);
        model1=addReaction(model1,'P_octadecanol',{'octadecanal[c]',
'nadh[c]', 'h[c]', 'octadecanol[c]', 'nad[c]'},[-1 -1 -1 1
1],1,0,1000);

        %acyl-coa --> fatty acids
        model1=addReaction(model1,'P_but_CoA',{'btcoa[c]', 'h2o[c]',
'h[c]', 'but[c]', 'coa[c]'},[-1 -1 1 1 1],1,0,1000);
        %The rest are already in the model: FACOAE60-180

        %acyl-ACP --> fatty acids
        model1=addReaction(model1,'P_but_ACP',{'butACP[c]', 'h2o[c]',
'h[c]', 'but[c]', 'ACP[c]'},[-1 -1 1 1 1],1,0,1000);
        model1=addReaction(model1,'P_hxa_ACP',{'hexACP[c]', 'h2o[c]',
'h[c]', 'hxa[c]', 'ACP[c]'},[-1 -1 1 1 1],1,0,1000);
        %Other reactions are already in the model (ex: FA80ACPHi)
        model1=addReaction(model1,'P_ocdca_ACP',{'ocdcaACP[c]',
'h2o[c]', 'h[c]', 'ocdca[c]', 'ACP[c]'},[-1 -1 1 1 1],1,0,1000);

        %transport reactions to export fatty acids. All for [c] to [e]
        %because the model did not have the proper transport accross
membrane form [p] to [e]
        model1=addReaction(model1,'P_octa_trans',{'octa[c]', 'octa[e]',
'h[c]', 'h[p]'},[-1 1 -1 1],1,0,1000);
```

```
        model1=addReaction(model1,'P_dca_trans',{'dca[c]', 'dca[e]',
'h[c]', 'h[p]'},[-1 1 -1 1],1,0,1000);
        model1=addReaction(model1,'P_ddca_trans',{'ddca[c]', 'ddca[e]',
'h[c]', 'h[p]'},[-1 1 -1 1],1,0,1000);
        model1=addReaction(model1,'P_ttdca_trans',{'ttdca[c]',
'ttdca[e]', 'h[c]', 'h[p]'},[-1 1 -1 1],1,0,1000);
        model1=addReaction(model1,'P_hdca_trans',{'hdca[c]', 'hdca[e]',
'h[c]', 'h[p]'},[-1 1 -1 1],1,0,1000);
        model1=addReaction(model1,'P_ocdca_trans_extra',{'ocdca[c]',
'ocdca[e]', 'h[c]', 'h[p]'},[-1 1 -1 1],1,0,1000);

        %Export of existing products to zero
        model1=changeRxnBounds(model1,'EX_but(e)', 0, 'u');
        model1=changeRxnBounds(model1,'EX_hxa(e)', 0, 'u');
        model1=changeRxnBounds(model1,'EX_octa(e)', 0, 'u');
        model1=changeRxnBounds(model1,'EX_dca(e)', 0, 'u');
        model1=changeRxnBounds(model1,'EX_ddca(e)', 0, 'u');
        model1=changeRxnBounds(model1,'EX_ttdca(e)', 0, 'u');
        model1=changeRxnBounds(model1,'EX_hdca(e)', 0, 'u');
        model1=changeRxnBounds(model1,'EX_ocdca(e)', 0, 'u');

        % Export of new products to zero
        model1=addReaction(model1,'EX_butanol',{'butanol[c]'},[-1],1,
0,0);
        model1=addReaction(model1,'EX_hexanol',{'hexanol[c]'},[-1],1,
0,0);
        model1=addReaction(model1,'EX_octanol',{'octanol[c]'},[-1
],1,0,0);
        model1=addReaction(model1,'EX_decanol',{'decanol[c]'},[-1],1,
0,0);
        model1=addReaction(model1,'EX_dodecanol',{'dodecanol[c]'},[-1
],1,0,0);

model1=addReaction(model1,'EX_tetradecanol',{'tetradecanol[c]'},[-1],1,
0,0);

model1=addReaction(model1,'EX_hexadecanol',{'hexadecanol[c]'},[-1
],1,0,0);

model1=addReaction(model1,'EX_octadecanol',{'octadecanol[c]'},[-1],1,
0,0);

        model1=addReaction(model1,'EX_propane',{'propane[c]'},[-1],1,
0,0);
        model1=addReaction(model1,'EX_pentane',{'pentane[c]'},[-1],1,
0,0);
        model1=addReaction(model1,'EX_heptane',{'heptane[c]'},[-1
],1,0,0);
        model1=addReaction(model1,'EX_nonane',{'nonane[c]'},[-1],1,
0,0);
        model1=addReaction(model1,'EX_undecane',{'undecane[c]'},[-1
],1,0,0);
        model1=addReaction(model1,'EX_tridecane',{'tridecane[c]'},[-
1],1, 0,0);
```

```
model1=addReaction(model1,'EX_pentadecane',{'pentadecane[c]'},[-1
],1,0,0);

model1=addReaction(model1,'EX_heptadecane',{'heptadecane[c]'},[-1],1,
0,0);

        model1=addReaction(model1,'EX_co',{'co[c]'},[-1 ],1,0,1000);


    case 3 % (NO reverse B-oxidation). Production of butanol and
hexanol suing alpha elongation pathway

        model1=changeRxnBounds(model1,'EX_o2(e)', 0, 'l');
        model1=changeRxnBounds(model1,'EX_glc(e)', -15, 'l');
        %Delete by-products
        model1=changeRxnBounds(model1,'EX_pyr(e)', 0, 'u');
        model1=changeRxnBounds(model1,'EX_acald(e)', 0, 'u');
        model1=changeRxnBounds(model1,'EX_hxa(e)', 0, 'u');

        %ACOAD1f are inactive in this case.
        model1=changeRxnBounds(model1,'ACOAD1f', 0, 'l');
        model1=changeRxnBounds(model1,'ACOAD1f', 0, 'u');
        model1=changeRxnBounds(model1,'ACOAD2f', 0, 'l');
        model1=changeRxnBounds(model1,'ACOAD2f', 0, 'u');
        model1=changeRxnBounds(model1,'ACOAD3f', 0, 'l');
        model1=changeRxnBounds(model1,'ACOAD3f', 0, 'u');
        model1=changeRxnBounds(model1,'ACOAD4f', 0, 'l');
        model1=changeRxnBounds(model1,'ACOAD4f', 0, 'u');
        model1=changeRxnBounds(model1,'ACOAD5f', 0, 'l');
        model1=changeRxnBounds(model1,'ACOAD5f', 0, 'u');
        model1=changeRxnBounds(model1,'ACOAD6f', 0, 'l');
        model1=changeRxnBounds(model1,'ACOAD6f', 0, 'u');
        model1=changeRxnBounds(model1,'ACOAD7f', 0, 'l');
        model1=changeRxnBounds(model1,'ACOAD7f', 0, 'u');
        model1=changeRxnBounds(model1,'ACOAD8f', 0, 'l');
        model1=changeRxnBounds(model1,'ACOAD8f', 0, 'u');

        % Ferredoxins / Reversal B-oxidation cycle / inactive in this
case
        model1=addReaction(model1,'ACOAD1f_ferr',{'btcoa[c]', 'fd_oxi',
'b2coa[c]', 'fd_red', 'h[c]'},[-1 -1 1 1 1],1,0,0);
        model1=addReaction(model1,'ACOAD2f_ferr',{'fd_oxi', 'hxcoa[c]',
'hx2coa[c]', 'fd_red', 'h[c]'},[-1 -1 1 1 1],1,0,0);
        model1=addReaction(model1,'ACOAD3f_ferr',{'fd_oxi', 'occoa[c]',
'oc2coa[c]', 'fd_red', 'h[c]'},[-1 -1 1 1 1],1,0,0);
        model1=addReaction(model1,'ACOAD4f_ferr',{'dcacoa[c]',
'fd_oxi', 'dc2coa[c]', 'fd_red', 'h[c]'},[-1 -1 1 1 1],1,0,0);
        model1=addReaction(model1,'ACOAD5f_ferr',{'ddcacoa[c]',
'fd_oxi', 'dd2coa[c]', 'fd_red', 'h[c]'},[-1 -1 1 1 1],1,0,0);
        model1=addReaction(model1,'ACOAD6f_ferr',{'fd_oxi', 'tdcoa[c]',
'td2coa[c]', 'fd_red', 'h[c]'},[-1 -1 1 1 1],1,0,0);
        model1=addReaction(model1,'ACOAD7f_ferr',{'fd_oxi',
'pmtcoa[c]', 'hdd2coa[c]', 'fd_red', 'h[c]'},[-1 -1 1 1 1],1,0,0);
        model1=addReaction(model1,'ACOAD8f_ferr',{'fd_oxi', 'stcoa[c]',
'od2coa[c]', 'fd_red', 'h[c]'},[-1 -1 1 1 1],1,0,0);
```

```
        model1=addReaction(model1,'PFOR',{'coa[c]', 'fd_oxi', 'pyr[c]',
'accoa[c]', 'co2[c]', 'fd_red', 'h[c]'},[-1 -1 -1 1 1 1 1],1,0,0);

        %acyl-ACP --> aldehyde (butanal, hexanal, octanal, ...) %set
al.l to
        %zero
        model1=addReaction(model1,'P_butanal_ACP',{'butACP[c]',
'nadh[c]', 'h[c]', 'butanal[c]', 'nad[c]', 'ACP[c]'},[-1 -1 -1 1 1
1],1,0,0);
        model1=addReaction(model1,'P_hexanal_ACP',{'hexACP[c]',
'nadh[c]', 'h[c]', 'hexanal[c]', 'nad[c]', 'ACP[c]'},[-1 -1 -1 1 1
1],1,0,0);
        model1=addReaction(model1,'P_octanal_ACP',{'ocACP[c]',
'nadh[c]', 'h[c]', 'octanal[c]', 'nad[c]', 'ACP[c]'},[-1 -1 -1 1 1
1],1,0,0);
        model1=addReaction(model1,'P_decanal_ACP',{'dcaACP[c]',
'nadh[c]', 'h[c]', 'decanal[c]', 'nad[c]', 'ACP[c]'},[-1 -1 -1 1 1
1],1,0,0);
        model1=addReaction(model1,'P_dodecanal_ACP',{'ddcaACP[c]',
'nadh[c]', 'h[c]', 'dodecanal[c]', 'nad[c]', 'ACP[c]'},[-1 -1 -1 1 1
1],1,0,0);
        model1=addReaction(model1,'P_tetradecanal_ACP',{'myrsACP[c]',
'nadh[c]', 'h[c]', 'tetradecanal[c]', 'nad[c]', 'ACP[c]'},[-1 -1 -1 1 1
1],1,0,0); %myristoyl-ACP
        model1=addReaction(model1,'P_hexadecanal_ACP',{'palmACP[c]',
'nadh[c]', 'h[c]', 'hexadecanal[c]', 'nad[c]', 'ACP[c]'},[-1 -1 -1 1 1
1],1,0,0);
        model1=addReaction(model1,'P_octadecanal_ACP',{'ocdcaACP[c]',
'nadh[c]', 'h[c]', 'octadecanal[c]', 'nad[c]', 'ACP[c]'},[-1 -1 -1 1 1
1],1,0,0);

        %Reduction of acyl-coa / acyl-CoA --> aldehyde (butanal,
hexanal, octanal, ...)
        model1=addReaction(model1,'P_butanal_CoA',{'btcoa[c]',
'nadh[c]', 'h[c]', 'butanal[c]', 'nad[c]', 'coa[c]'},[-1 -1 -1 1 1
1],1,0,0);
        model1=addReaction(model1,'P_hexanal_CoA',{'hxcoa[c]',
'nadh[c]', 'h[c]', 'hexanal[c]', 'nad[c]', 'coa[c]'},[-1 -1 -1 1 1
1],1,0,0);
        model1=addReaction(model1,'P_octanal_CoA',{'occoa[c]',
'nadh[c]', 'h[c]', 'octanal[c]', 'nad[c]', 'coa[c]'},[-1 -1 -1 1 1
1],1,0,0);
        model1=addReaction(model1,'P_decanal_CoA',{'dcacoa[c]',
'nadh[c]', 'h[c]', 'decanal[c]', 'nad[c]', 'coa[c]'},[-1 -1 -1 1 1
1],1,0,0);
        model1=addReaction(model1,'P_dodecanal_CoA',{'ddcacoa[c]',
'nadh[c]', 'h[c]', 'dodecanal[c]', 'nad[c]', 'coa[c]'},[-1 -1 -1 1 1
1],1,0,0);
        model1=addReaction(model1,'P_tetradecanal_CoA',{'tdcoa[c]',
'nadh[c]', 'h[c]', 'tetradecanal[c]', 'nad[c]', 'coa[c]'},[-1 -1 -1 1 1
1],1,0,0);
        model1=addReaction(model1,'P_hexadecanal_CoA',{'pmtcoa[c]',
'nadh[c]', 'h[c]', 'hexadecanal[c]', 'nad[c]', 'coa[c]'},[-1 -1 -1 1 1
1],1,0,0);
```

```
        model1=addReaction(model1,'P_octadecanal_CoA',{'stcoa[c]',
'nadh[c]', 'h[c]', 'octadecanal[c]', 'nad[c]', 'coa[c]'},[-1 -1 -1 1 1
1],1,0,0);

        %Aldehyde decarboxilation / Production of alkanes
        model1=addReaction(model1,'P_propane',{'butanal[c]',
'propane[c]', 'co[c]'},[-1 1 1],1,0,0);
        model1=addReaction(model1,'P_pentane',{'hexanal[c]',
'pentane[c]','co[c]'},[-1 1 1],1,0,0);
        model1=addReaction(model1,'P_heptane',{'octanal[c]',
'heptane[c]','co[c]'},[-1 1 1],1,0,0);
        model1=addReaction(model1,'P_nonane',{'decanal[c]',
'nonane[c]','co[c]'},[-1 1 1],1,0,0);
        model1=addReaction(model1,'P_undecane',{'dodecanal[c]',
'undecane[c]', 'co[c]'},[-1 1 1],1,0,0);
        model1=addReaction(model1,'P_tridecane',{'tetradecanal[c]',
'tridecane[c]','co[c]'},[-1 1 1],1,0,0);
        model1=addReaction(model1,'P_pentadecane',{'hexadecanal[c]',
'pentadecane[c]', 'co[c]'},[-1 1 1],1,0,0);
        model1=addReaction(model1,'P_heptadecane',{'octadecanal[c]',
'heptadecane[c]','co[c]'},[-1 1 1],1,0,0);

        %Alcohol production
        model1=addReaction(model1,'P_butanol',{'butanal[c]', 'nadh[c]',
'h[c]', 'butanol[c]', 'nad[c]'},[-1 -1 -1 1 1],1,0,1000);
        model1=addReaction(model1,'P_hexanol',{'hexanal[c]', 'nadh[c]',
'h[c]', 'hexanol[c]', 'nad[c]'},[-1 -1 -1 1 1],1,0,1000);
        model1=addReaction(model1,'P_octanol',{'octanal[c]', 'nadh[c]',
'h[c]', 'octanol[c]', 'nad[c]'},[-1 -1 -1 1 1],1,0,0);
        model1=addReaction(model1,'P_decanol',{'decanal[c]', 'nadh[c]',
'h[c]', 'decanol[c]', 'nad[c]'},[-1 -1 -1 1 1],1,0,0);
        model1=addReaction(model1,'P_dodecanol',{'dodecanal[c]',
'nadh[c]', 'h[c]', 'dodecanol[c]', 'nad[c]'},[-1 -1 -1 1 1],1,0,0);
        model1=addReaction(model1,'P_tetradecanol',{'tetradecanal[c]',
'nadh[c]', 'h[c]', 'tetradecanol[c]', 'nad[c]'},[-1 -1 -1 1 1],1,0,0);
        model1=addReaction(model1,'P_hexadecanol',{'hexadecanal[c]',
'nadh[c]', 'h[c]', 'hexadecanol[c]', 'nad[c]'},[-1 -1 -1 1 1],1,0,0);
        model1=addReaction(model1,'P_octadecanol',{'octadecanal[c]',
'nadh[c]', 'h[c]', 'octadecanol[c]', 'nad[c]'},[-1 -1 -1 1 1],1,0,0);


        %acyl-coa --> fatty acids
        model1=addReaction(model1,'P_but_CoA',{'btcoa[c]', 'h2o[c]',
'h[c]', 'but[c]', 'coa[c]'},[-1 -1 1 1 1],1,0,0);
        %The rest are already in the model: FACOAE60-180

        %acyl-ACP --> fatty acids
        model1=addReaction(model1,'P_but_ACP',{'butACP[c]', 'h2o[c]',
'h[c]', 'but[c]', 'ACP[c]'},[-1 -1 1 1 1],1,0,0);
        model1=addReaction(model1,'P_hxa_ACP',{'hexACP[c]', 'h2o[c]',
'h[c]', 'hxa[c]', 'ACP[c]'},[-1 -1 1 1 1],1,0,0);
        %Other reactions are already in the model (ex: FA80ACPHi)
        model1=addReaction(model1,'P_ocdca_ACP',{'ocdcaACP[c]',
'h2o[c]', 'h[c]', 'ocdca[c]', 'ACP[c]'},[-1 -1 1 1 1],1,0,0);

        %transport reactions to export fatty acids. All for [c] to [e]
```

```
        %because the model did not have the proper transport accross
membrane form [p] to [e]
        model1=addReaction(model1,'P_octa_trans',{'octa[c]', 'octa[e]',
'h[c]', 'h[p]'},[-1 1 -1 1],1,0,0);
        model1=addReaction(model1,'P_dca_trans',{'dca[c]', 'dca[e]',
'h[c]', 'h[p]'},[-1 1 -1 1],1,0,0);
        model1=addReaction(model1,'P_ddca_trans',{'ddca[c]', 'ddca[e]',
'h[c]', 'h[p]'},[-1 1 -1 1],1,0,0);
        model1=addReaction(model1,'P_ttdca_trans',{'ttdca[c]',
'ttdca[e]', 'h[c]', 'h[p]'},[-1 1 -1 1],1,0,0);
        model1=addReaction(model1,'P_hdca_trans',{'hdca[c]', 'hdca[e]',
'h[c]', 'h[p]'},[-1 1 -1 1],1,0,0);
        model1=addReaction(model1,'P_ocdca_trans_extra',{'ocdca[c]',
'ocdca[e]', 'h[c]', 'h[p]'},[-1 1 -1 1],1,0,0);

        %Export of existing products to zero
        model1=changeRxnBounds(model1,'EX_but(e)', 0, 'u');
        model1=changeRxnBounds(model1,'EX_hxa(e)', 0, 'u');
        model1=changeRxnBounds(model1,'EX_octa(e)', 0, 'u');
        model1=changeRxnBounds(model1,'EX_dca(e)', 0, 'u');
        model1=changeRxnBounds(model1,'EX_ddca(e)', 0, 'u');
        model1=changeRxnBounds(model1,'EX_ttdca(e)', 0, 'u');
        model1=changeRxnBounds(model1,'EX_hdca(e)', 0, 'u');
        model1=changeRxnBounds(model1,'EX_ocdca(e)', 0, 'u');

        % Export of new products to zero
        model1=addReaction(model1,'EX_butanol',{'butanol[c]'},[-1],1,
0,0);
        model1=addReaction(model1,'EX_hexanol',{'hexanol[c]'},[-1],1,
0,0);
        model1=addReaction(model1,'EX_octanol',{'octanol[c]'},[-1
],1,0,0);
        model1=addReaction(model1,'EX_decanol',{'decanol[c]'},[-1],1,
0,0);
        model1=addReaction(model1,'EX_dodecanol',{'dodecanol[c]'},[-1
],1,0,0);

model1=addReaction(model1,'EX_tetradecanol',{'tetradecanol[c]'},[-1],1,
0,0);

model1=addReaction(model1,'EX_hexadecanol',{'hexadecanol[c]'},[-1
],1,0,0);

model1=addReaction(model1,'EX_octadecanol',{'octadecanol[c]'},[-1],1,
0,0);

        model1=addReaction(model1,'EX_propane',{'propane[c]'},[-1],1,
0,0);
        model1=addReaction(model1,'EX_pentane',{'pentane[c]'},[-1],1,
0,0);
        model1=addReaction(model1,'EX_heptane',{'heptane[c]'},[-1
],1,0,0);
        model1=addReaction(model1,'EX_nonane',{'nonane[c]'},[-1],1,
0,0);
        model1=addReaction(model1,'EX_undecane',{'undecane[c]'},[-1
],1,0,0);
```

```
        model1=addReaction(model1,'EX_tridecane',{'tridecane[c]'},[-
1],1, 0,0);

model1=addReaction(model1,'EX_pentadecane',{'pentadecane[c]'},[-1
],1,0,0);

model1=addReaction(model1,'EX_heptadecane',{'heptadecane[c]'},[-1],1,
0,0);

        model1=addReaction(model1,'EX_co',{'co[c]'},[-1 ],1,0,1000);

        %add reactions fo butanol and hexanol, using alpha-ketoacid
        %elongation
        model1=addReaction(model1,'P_leuA1',{'2obut[c]', 'accoa[c]',
'h2o[c]', '2ethylmalate', 'coa[c]'},[-1 -1 -1 1 1],1,0,1000);
        model1=addReaction(model1,'P_leuCD1',{'2ethylmalate',
'3ethylmalate'},[-1 1],1,0,1000);
        model1=addReaction(model1,'P_3ethylmalate',{'3ethylmalate',
'nad[c]', '2ketovalerate', 'nadh[c]', 'co2[c]'},[-1 -1 1 1
1],1,0,1000);
        model1=addReaction(model1,'P_2ketovalerate',{'2ketovalerate',
'butanal[c]', 'co2[c]'},[-1 1 1],1,0,1000);

        model1=addReaction(model1,'P_leuA2',{'2ketovalerate',
'accoa[c]', 'h2o[c]', '2propylmalate', 'coa[c]'},[-1 -1 -1 1
1],1,0,1000);
        model1=addReaction(model1,'P_leuCD2',{'2propylmalate',
'3propylmalate'},[-1 1],1,0,1000);
        model1=addReaction(model1,'P_3propylmalate',{'3propylmalate',
'nad[c]', '2ketocaproate', 'nadh[c]', 'co2[c]'},[-1 -1 1 1
1],1,0,1000);
 %       model1=addReaction(model1,'P_2ketocaproate',{'2ketocaproate',
'pentanal[c]', 'co2[c]'},[-1 1 1],1,0,1000);

        model1=addReaction(model1,'P_leuA3',{'2ketocaproate',
'accoa[c]', 'h2o[c]', '2butylmalate', 'coa[c]'},[-1 -1 -1 1
1],1,0,1000);
        model1=addReaction(model1,'P_leuCD3',{'2butylmalate',
'3butylmalate'},[-1 1],1,0,1000);
        model1=addReaction(model1,'P_3butylmalate',{'3butylmalate',
'nad[c]', '2ketoheptanoate', 'nadh[c]', 'co2[c]'},[-1 -1 1 1
1],1,0,1000);

model1=addReaction(model1,'P_2ketoheptanoate',{'2ketoheptanoate',
'hexanal[c]', 'co2[c]'},[-1 1 1],1,0,1000);

end

A= size(model1.rxns);
SizeModel=(A(1));
%% Enter knockouts
I= input('List of reactions to delete: ');

SizeI=size(I);
for p=1:1:SizeI(2)
```

```
    RxnDelete=I(p);
    model1=changeRxnBounds(model1, RxnDelete, 0, 'u');
    model1=changeRxnBounds(model1, RxnDelete, 0, 'l');
    if p==1
        KnockoutReaction=RxnDelete;
    else
        KnockoutReaction=strcat(KnockoutReaction,',',RxnDelete);
    end
end


%% Desired product
prompt = {'Desired product: '};
Product=inputdlg(prompt);
model1=changeRxnBounds(model1, Product, 1000, 'u');
A=(model1.rxns);
productposition=AC_findp_F(A,Product);

model1=changeObjective(model1, Biomass_name, 1);
solution=optimizeCbModel(model1);
maxbiomass =solution.f
if solution.stat ~= 1
    display ('The selected condition does not have any valid solution')
    return
end
Product_when_biomass_is_optimized=solution.x(productposition)
TitlePlot=strcat('Product versus Biomass, deletion of: ',
KnockoutReaction);
xlsTitle=strcat('Model_', modelname, '_', KnockoutReaction);
model1=changeObjective(model1, Biomass_name, -1);
solution=optimizeCbModel(model1);
minbiomass=solution.f;
product2=solution.x(productposition);
model1=changeObjective(model1, Product(1), 1);
solution=optimizeCbModel(model1);
OptimeProduct=solution.x(productposition)
Y=zeros(101,3);
%Y=zeros(101,7);
for i=1:1:101
    model1=changeRxnBounds(model1, Biomass_name, 0.01*(i-1)*maxbiomass,
'l');
    % min
    model1=changeObjective(model1, Product(1), 1);
    maxsolution=optimizeCbModel(model1);
    maxproduct=maxsolution.f;
    biomass1=maxsolution.x(biomassposition);
    %[maxminF maxmaxF]=fluxVariability(model1, 100,'max',{'ATPS4rpp'},
false, true);
    %max
    model1=changeObjective(model1, Product(1), -1);
    minsolution=optimizeCbModel(model1);
    minproduct=minsolution.x(productposition);
    %[minminF minmaxF]=fluxVariability(model1, 100,'max',{'ATPS4rpp'},
false, true);
```

```
    %Y(i,:)= [biomass1 minproduct maxproduct maxminF maxmaxF minminF
minmaxF];
    Y(i,:)= [biomass1 minproduct maxproduct];

end

model1=changeObjective(model1, Biomass_name, 1);
model1=changeRxnBounds(model1, Biomass_name, 0, 'l');
solution=optimizeCbModel(model1);
%% Plot
figure(1)
set(0, 'DefaultTextInterpreter', 'none') %Change set of all plots Text-
Interpreter to none, as oppose to Text (default)
plot(Y(:,1), Y(:,2), '--g*');
hold on
plot(Y(:,1), Y(:,3), '--r*');
xlabel('Biomass');
ylabel(strcat('Product: ', Product));
title(TitlePlot);
h=area(Y(:,1),Y(:,3));
set(h(1),'FaceColor',[1 1 0.5])
j=area(Y(:,1),Y(:,2));
set(j(1),'FaceColor',[1 1 1])
```

10.13 Matlab function for the synthesis of products derived from intermediate metabolites of the reversal β-oxidation cycle

I added the following code to the function lcp-GEM (presented in section 10.12)

```
   AC_BiomassvsProduct_GlucoseiJO1366_DiversificationProducts
%%
% Termination Diversification 1: from B-ketoacyl-coa to substituted FA,
alcohols and alkanes

% Reduction of B-ketoaldehyde / B-ketoacyl-CoA --> B-ketoaldehyde (B-
keto-butanal, B-keto-hexanal, B-keto-octanal, ...)
        model1=addReaction(model1,'P_B-ketobutanal_CoA',{'aacoa[c]',
'nadh[c]', 'h[c]', 'B-ketobutanal[c]', 'nad[c]', 'coa[c]'},[-1 -1 -1 1
1 1],1,0,1000);
        model1=addReaction(model1,'P_B-ketohexanal_CoA',{'3ohcoa[c]',
'nadh[c]', 'h[c]', 'B-ketohexanal[c]', 'nad[c]', 'coa[c]'},[-1 -1 -1 1
1 1],1,0,1000);
        model1=addReaction(model1,'P_B-ketooctanal_CoA',{'3oocoa[c]',
'nadh[c]', 'h[c]', 'B-ketooctanal[c]', 'nad[c]', 'coa[c]'},[-1 -1 -1 1
1 1],1,0,1000);
        model1=addReaction(model1,'P_B-ketodecanal_CoA',{'3odcoa[c]',
'nadh[c]', 'h[c]', 'B-ketodecanal[c]', 'nad[c]', 'coa[c]'},[-1 -1 -1 1
1 1],1,0,1000);
        model1=addReaction(model1,'P_B-
ketododecanal_CoA',{'3oddcoa[c]', 'nadh[c]', 'h[c]', 'B-
ketododecanal[c]', 'nad[c]', 'coa[c]'},[-1 -1 -1 1 1 1],1,0,1000);
```

```
        model1=addReaction(model1,'P_B-
ketotetradecanal_CoA',{'3otdcoa[c]', 'nadh[c]', 'h[c]', 'B-
ketotetradecanal[c]', 'nad[c]', 'coa[c]'},[-1 -1 -1 1 1 1],1,0,1000);
        model1=addReaction(model1,'P_B-
ketohexadecanal_CoA',{'3ohdcoa[c]', 'nadh[c]', 'h[c]', 'B-
ketohexadecanal[c]', 'nad[c]', 'coa[c]'},[-1 -1 -1 1 1 1],1,0,1000);
        model1=addReaction(model1,'P_B-
ketooctadecanal_CoA',{'3oodcoa[c]', 'nadh[c]', 'h[c]', 'B-
ketooctadecanal[c]', 'nad[c]', 'coa[c]'},[-1 -1 -1 1 1 1],1,0,1000);

        %B-ketoaldehyde decarboxilation / Production of B-ketoalkanes
        model1=addReaction(model1,'P_acetone',{'B-ketobutanal[c]',
'acetone[c]', 'co[c]'},[-1 1 1],1,0,1000);
        model1=addReaction(model1,'P_2pentanone',{'B-ketohexanal[c]',
'2pentanone[c]','co[c]'},[-1 1 1],1,0,1000);
        model1=addReaction(model1,'P_2heptanone',{'B-ketooctanal[c]',
'2heptanone[c]','co[c]'},[-1 1 1],1,0,1000);
        model1=addReaction(model1,'P_2nonanone',{'B-ketodecanal[c]',
'2nonanone[c]','co[c]'},[-1 1 1],1,0,1000);
        model1=addReaction(model1,'P_2undecanone',{'B-
ketododecanal[c]', '2undecanone[c]', 'co[c]'},[-1 1 1],1,0,1000);
        model1=addReaction(model1,'P_2tridecanone',{'B-
ketotetradecanal[c]', '2tridecanone[c]','co[c]'},[-1 1 1],1,0,1000);
        model1=addReaction(model1,'P_2pentadecanone',{'B-
ketohexadecanal[c]', '2pentadecanone[c]', 'co[c]'},[-1 1 1],1,0,1000);
        model1=addReaction(model1,'P_2heptadecanone',{'B-
ketooctadecanal[c]', '2heptadecanone[c]','co[c]'},[-1 1 1],1,0,1000);

        %B-ketoalcohol production
        model1=addReaction(model1,'P_B-ketobutanol',{'B-
ketobutanal[c]', 'nadh[c]', 'h[c]', 'B-ketobutanol[c]', 'nad[c]'},[-1 -
1 -1 1 1],1,0,1000);
        model1=addReaction(model1,'P_B-ketohexanol',{'B-
ketohexanal[c]', 'nadh[c]', 'h[c]', 'B-ketohexanol[c]', 'nad[c]'},[-1 -
1 -1 1 1],1,0,1000);
        model1=addReaction(model1,'P_B-ketooctanol',{'B-
ketooctanal[c]', 'nadh[c]', 'h[c]', 'B-ketooctanol[c]', 'nad[c]'},[-1 -
1 -1 1 1],1,0,1000);
        model1=addReaction(model1,'P_B-ketodecanol',{'B-
ketodecanal[c]', 'nadh[c]', 'h[c]', 'B-ketodecanol[c]', 'nad[c]'},[-1 -
1 -1 1 1],1,0,1000);
        model1=addReaction(model1,'P_B-ketododecanol',{'B-
ketododecanal[c]', 'nadh[c]', 'h[c]', 'B-ketododecanol[c]',
'nad[c]'},[-1 -1 -1 1 1],1,0,1000);
        model1=addReaction(model1,'P_B-ketotetradecanol',{'B-
ketotetradecanal[c]', 'nadh[c]', 'h[c]', 'B-ketotetradecanol[c]',
'nad[c]'},[-1 -1 -1 1 1],1,0,1000);
        model1=addReaction(model1,'P_B-ketohexadecanol',{'B-
ketohexadecanal[c]', 'nadh[c]', 'h[c]', 'B-ketohexadecanol[c]',
'nad[c]'},[-1 -1 -1 1 1],1,0,1000);
        model1=addReaction(model1,'P_B-ketooctadecanol',{'B-
ketooctadecanal[c]', 'nadh[c]', 'h[c]', 'B-ketooctadecanol[c]',
'nad[c]'},[-1 -1 -1 1 1],1,0,1000);

        %acyl-coa --> fatty acids
```

```
        model1=addReaction(model1,'P_B-ketobut_CoA',{'aacoa[c]',
'h2o[c]', 'h[c]', 'B-ketobut[c]', 'coa[c]'},[-1 -1 1 1 1],1,0,1000);
        model1=addReaction(model1,'P_B-ketohxa_CoA',{'3ohcoa[c]',
'h2o[c]', 'h[c]', 'B-ketohxa[c]', 'coa[c]'},[-1 -1 1 1 1],1,0,1000);
        model1=addReaction(model1,'P_B-ketoocta_CoA',{'3oocoa[c]',
'h2o[c]', 'h[c]', 'B-ketoocta[c]', 'coa[c]'},[-1 -1 1 1 1],1,0,1000);
        model1=addReaction(model1,'P_B-ketodca_CoA',{'3odcoa[c]',
'h2o[c]', 'h[c]', 'B-ketodca[c]', 'coa[c]'},[-1 -1 1 1 1],1,0,1000);
        model1=addReaction(model1,'P_B-ketoddca_CoA',{'3oddcoa[c]',
'h2o[c]', 'h[c]', 'B-ketoddca[c]', 'coa[c]'},[-1 -1 1 1 1],1,0,1000);
        model1=addReaction(model1,'P_B-ketottdca_CoA',{'3otdcoa[c]',
'h2o[c]', 'h[c]', 'B-ketottdca[c]', 'coa[c]'},[-1 -1 1 1 1],1,0,1000);
        model1=addReaction(model1,'P_B-ketohdca_CoA',{'3ohdcoa[c]',
'h2o[c]', 'h[c]', 'B-ketohdca[c]', 'coa[c]'},[-1 -1 1 1 1],1,0,1000);
        model1=addReaction(model1,'P_B-ketoocdca_CoA',{'3oodcoa[c]',
'h2o[c]', 'h[c]', 'B-ketoocdca[c]', 'coa[c]'},[-1 -1 1 1 1],1,0,1000);


        %transport reactions to export fatty acids. All for [c] to [e]
        %because the model did not have the proper transport accross
membrane form [p] to [e]
        model1=addReaction(model1,'P_B-ketobut_trans',{'B-ketobut[c]',
'B-ketobut[e]', 'h[c]', 'h[p]'},[-1 1 -1 1],1,0,1000);
        model1=addReaction(model1,'P_B-ketohxa_trans',{'B-ketohxa[c]',
'B-ketohxa[e]', 'h[c]', 'h[p]'},[-1 1 -1 1],1,0,1000);
        model1=addReaction(model1,'P_B-ketoocta_trans',{'B-
ketoocta[c]', 'B-ketoocta[e]', 'h[c]', 'h[p]'},[-1 1 -1 1],1,0,1000);
        model1=addReaction(model1,'P_B-ketodca_trans',{'B-ketodca[c]',
'B-ketodca[e]', 'h[c]', 'h[p]'},[-1 1 -1 1],1,0,1000);
        model1=addReaction(model1,'P_B-ketoddca_trans',{'B-
ketoddca[c]', 'B-ketoddca[e]', 'h[c]', 'h[p]'},[-1 1 -1 1],1,0,1000);
        model1=addReaction(model1,'P_B-ketottdca_trans',{'B-
ketottdca[c]', 'B-ketottdca[e]', 'h[c]', 'h[p]'},[-1 1 -1 1],1,0,1000);
        model1=addReaction(model1,'P_B-ketohdca_trans',{'B-
ketohdca[c]', 'B-ketohdca[e]', 'h[c]', 'h[p]'},[-1 1 -1 1],1,0,1000);
        model1=addReaction(model1,'P_B-ketoocdca_trans_extra',{'B-
ketoocdca[c]', 'B-ketoocdca[e]', 'h[c]', 'h[p]'},[-1 1 -1 1],1,0,1000);

        % Export of new products to zero
        model1=addReaction(model1,'EX_B-ketobut', {'B-ketobut[e]'}, [-
1],1, 0,0);
        model1=addReaction(model1,'EX_B-ketohxa',{'B-ketohxa[e]'}, [-
1],1, 0,0);
        model1=addReaction(model1,'EX_B-ketoocta',{'B-ketoocta[e]'}, [-
1],1, 0,0);
        model1=addReaction(model1,'EX_B-ketodca',{'B-ketodca[e]'}, [-
1],1, 0,0);
        model1=addReaction(model1,'EX_B-ketoddca',{'B-ketoddca[e]'}, [-
1],1, 0,0);
        model1=addReaction(model1,'EX_B-ketottdca',{'B-ketottdca[e]'},
[-1],1, 0,0);
        model1=addReaction(model1,'EX_B-ketohdca',{'B-ketohdca[e]'}, [-
1],1, 0,0);
        model1=addReaction(model1,'EX_B-ketoocdca',{'B-ketoocdca[e]'},
[-1],1, 0,0);
```

```
        model1=addReaction(model1,'EX_B-ketobutanol',{'B-
ketobutanol[c]'},[-1],1, 0,0);
        model1=addReaction(model1,'EX_B-ketohexanol',{'B-
ketohexanol[c]'},[-1],1, 0,0);
        model1=addReaction(model1,'EX_B-ketooctanol',{'B-
ketooctanol[c]'},[-1 ],1,0,0);
        model1=addReaction(model1,'EX_B-ketodecanol',{'B-
ketodecanol[c]'},[-1],1, 0,0);
        model1=addReaction(model1,'EX_B-ketododecanol',{'B-
ketododecanol[c]'},[-1 ],1,0,0);
        model1=addReaction(model1,'EX_B-ketotetradecanol',{'B-
ketotetradecanol[c]'},[-1],1, 0,0);
        model1=addReaction(model1,'EX_B-ketohexadecanol',{'B-
ketohexadecanol[c]'},[-1 ],1,0,0);
        model1=addReaction(model1,'EX_B-ketooctadecanol',{'B-
ketooctadecanol[c]'},[-1],1, 0,0);

        model1=addReaction(model1,'EX_acetone',{'acetone[c]'},[-1],1,
0,0);
        model1=addReaction(model1,'EX_2pentanone',{'2pentanone[c]'},[-
1],1, 0,0);
        model1=addReaction(model1,'EX_2heptanone',{'2heptanone[c]'},[-1
],1,0,0);
        model1=addReaction(model1,'EX_2nonanone',{'2nonanone[c]'},[-
1],1, 0,0);

model1=addReaction(model1,'EX_2undecanone',{'2undecanone[c]'},[-1
],1,0,0);

model1=addReaction(model1,'EX_2tridecanone',{'2tridecanone[c]'},[-1],1,
0,0);

model1=addReaction(model1,'EX_2pentadecanone',{'2pentadecanone[c]'},[-1
],1,0,0);

model1=addReaction(model1,'EX_2heptadecanone',{'2heptadecanone[c]'},[-
1],1, 0,0);

        %%
        % Termination Diversification 2: from Trans-B-hydroacyl-coa to
substituted FA, alcohols and alkanes

        % Reduction of Trans-B-hydroacyl-coa / Trans-B-hydroacyl-CoA --
> Trans-B-hydroaldehyde (Trans-B-hydro-butanal, Trans-B-hydro-hexanal,
Trans-B-hydro-octanal, ...)
        model1=addReaction(model1,'P_B-hydroxybutanal',{'3hbcoa[c]',
'nadh[c]', 'h[c]', 'B-hydroxybutanal[c]', 'nad[c]', 'coa[c]'},[-1 -1 -1
1 1 1],1,0,1000);
        model1=addReaction(model1,'P_B-hydroxyhexanal',{'3hhcoa[c]',
'nadh[c]', 'h[c]', 'B-hydroxyhexanal[c]', 'nad[c]', 'coa[c]'},[-1 -1 -1
1 1 1],1,0,1000);
        model1=addReaction(model1,'P_B-hydroxyoctanal',{'3hocoa[c]',
'nadh[c]', 'h[c]', 'B-hydroxyoctanal[c]', 'nad[c]', 'coa[c]'},[-1 -1 -1
1 1 1],1,0,1000);
```

```
        model1=addReaction(model1,'P_B-hydroxydecanal',{'3hdcoa[c]',
'nadh[c]', 'h[c]', 'B-hydroxydecanal[c]', 'nad[c]', 'coa[c]'},[-1 -1 -1
1 1 1],1,0,1000);
        model1=addReaction(model1,'P_B-hydroxydodecanal',{'3hddcoa[c]',
'nadh[c]', 'h[c]', 'B-hydroxydodecanal[c]', 'nad[c]', 'coa[c]'},[-1 -1
-1 1 1 1],1,0,1000);
        model1=addReaction(model1,'P_B-
hydroxytetradecanal',{'3htdcoa[c]', 'nadh[c]', 'h[c]', 'B-
hydroxytetradecanal[c]', 'nad[c]', 'coa[c]'},[-1 -1 -1 1 1
1],1,0,1000);
        model1=addReaction(model1,'P_B-
hydroxyhexadecanal',{'3hhdcoa[c]', 'nadh[c]', 'h[c]', 'B-
hydroxyhexadecanal[c]', 'nad[c]', 'coa[c]'},[-1 -1 -1 1 1 1],1,0,1000);
        model1=addReaction(model1,'P_B-
hydroxyoctadecanal',{'3hodcoa[c]', 'nadh[c]', 'h[c]', 'B-
hydroxyoctadecanal[c]', 'nad[c]', 'coa[c]'},[-1 -1 -1 1 1 1],1,0,1000);

        %Trans-B-hydroaldehyde decarboxilation / Production of alcohols
        model1=addReaction(model1,'P_3propanol',{'B-hydroxybutanal[c]',
'3propanol[c]', 'co[c]'},[-1 1 1],1,0,1000);
        model1=addReaction(model1,'P_3pentanol',{'B-hydroxyhexanal[c]',
'3pentanol[c]','co[c]'},[-1 1 1],1,0,1000);
        model1=addReaction(model1,'P_3heptanol',{'B-hydroxyoctanal[c]',
'3heptanol[c]','co[c]'},[-1 1 1],1,0,1000);
        model1=addReaction(model1,'P_3nonanol',{'B-hydroxydecanal[c]',
'3nonanol[c]','co[c]'},[-1 1 1],1,0,1000);
        model1=addReaction(model1,'P_3undecanol',{'B-
hydroxydodecanal[c]', '3undecanol[c]', 'co[c]'},[-1 1 1],1,0,1000);
        model1=addReaction(model1,'P_3tridecanol',{'B-
hydroxytetradecanal[c]', '3tridecanol[c]','co[c]'},[-1 1 1],1,0,1000);
        model1=addReaction(model1,'P_3pentadecanol',{'B-
hydroxyhexadecanal[c]', '3pentadecanol[c]', 'co[c]'},[-1 1
1],1,0,1000);
        model1=addReaction(model1,'P_3heptadecanol',{'B-
hydroxyoctadecanal[c]', '3heptadecanol[c]','co[c]'},[-1 1 1],1,0,1000);

        %Trans-B-hydroalcohol production
        model1=addReaction(model1,'P_13butanediol',{'B-
hydroxybutanal[c]', 'nadh[c]', 'h[c]', '13butanediol[c]', 'nad[c]'},[-1
-1 -1 1 1],1,0,1000);
        model1=addReaction(model1,'P_13hexanediol',{'B-
hydroxyhexanal[c]', 'nadh[c]', 'h[c]', '13hexanediol[c]', 'nad[c]'},[-1
-1 -1 1 1],1,0,1000);
        model1=addReaction(model1,'P_13octanediol',{'B-
hydroxyoctanal[c]', 'nadh[c]', 'h[c]', '13octanediol[c]', 'nad[c]'},[-1
-1 -1 1 1],1,0,1000);
        model1=addReaction(model1,'P_13decanediol',{'B-
hydroxydecanal[c]', 'nadh[c]', 'h[c]', '13decanediol[c]', 'nad[c]'},[-1
-1 -1 1 1],1,0,1000);
        model1=addReaction(model1,'P_13dodecanediol',{'B-
hydroxydodecanal[c]', 'nadh[c]', 'h[c]', '13dodecanediol[c]',
'nad[c]'},[-1 -1 -1 1 1],1,0,1000);
        model1=addReaction(model1,'P_13tetradecanediol',{'B-
hydroxytetradecanal[c]', 'nadh[c]', 'h[c]', '13tetradecanediol[c]',
'nad[c]'},[-1 -1 -1 1 1],1,0,1000);
```

```
        model1=addReaction(model1,'P_13hexadecanediol',{'B-
hydroxyhexadecanal[c]', 'nadh[c]', 'h[c]', '13hexadecanediol[c]',
'nad[c]'},[-1 -1 -1 1 1],1,0,1000);
        model1=addReaction(model1,'P_13octadecanediol',{'B-
hydroxyoctadecanal[c]', 'nadh[c]', 'h[c]', '13octadecanediol[c]',
'nad[c]'},[-1 -1 -1 1 1],1,0,1000);

        %Trans-B-hydroxyacyl-coa --> B-hydroxyacids
        model1=addReaction(model1,'P_B-hydroxybut',{'3hbcoa[c]',
'h2o[c]', 'h[c]', 'B-hydroxybut[c]', 'coa[c]'},[-1 -1 1 1 1],1,0,1000);
        model1=addReaction(model1,'P_B-hydroxyhxa',{'3hhcoa[c]',
'h2o[c]', 'h[c]', 'B-hydroxyhxa[c]', 'coa[c]'},[-1 -1 1 1 1],1,0,1000);
        model1=addReaction(model1,'P_B-hydroxyocta',{'3hocoa[c]',
'h2o[c]', 'h[c]', 'B-hydroxyocta[c]', 'coa[c]'},[-1 -1 1 1
1],1,0,1000);
        model1=addReaction(model1,'P_B-hydroxydca',{'3hdcoa[c]',
'h2o[c]', 'h[c]', 'B-hydroxydca[c]', 'coa[c]'},[-1 -1 1 1 1],1,0,1000);
        model1=addReaction(model1,'P_B-hydroxyddca',{'3hddcoa[c]',
'h2o[c]', 'h[c]', 'B-hydroxyddca[c]', 'coa[c]'},[-1 -1 1 1
1],1,0,1000);
        model1=addReaction(model1,'P_B-hydroxyttdca',{'3htdcoa[c]',
'h2o[c]', 'h[c]', 'B-hydroxyttdca[c]', 'coa[c]'},[-1 -1 1 1
1],1,0,1000);
        model1=addReaction(model1,'P_B-hydroxyhdca',{'3hhdcoa[c]',
'h2o[c]', 'h[c]', 'B-hydroxyhdca[c]', 'coa[c]'},[-1 -1 1 1
1],1,0,1000);
        model1=addReaction(model1,'P_B-hydroxyocdca',{'3hodcoa[c]',
'h2o[c]', 'h[c]', 'B-hydroxyocdca[c]', 'coa[c]'},[-1 -1 1 1
1],1,0,1000);

        %transport reactions to export fatty acids. All for [c] to [e]
        %because the model did not have the proper transport accross
membrane form [p] to [e]
        model1=addReaction(model1,'P_B-hydroxybut_trans',{'B-
hydroxybut[c]', 'B-hydroxybut[e]', 'h[c]', 'h[p]'},[-1 1 -1
1],1,0,1000);
        model1=addReaction(model1,'P_B-hydroxyhxa_trans',{'B-
hydroxyhxa[c]', 'B-hydroxyhxa[e]', 'h[c]', 'h[p]'},[-1 1 -1
1],1,0,1000);
        model1=addReaction(model1,'P_B-hydroxyocta_trans',{'B-
hydroxyocta[c]', 'B-hydroxyocta[e]', 'h[c]', 'h[p]'},[-1 1 -1
1],1,0,1000);
        model1=addReaction(model1,'P_B-hydroxydca_trans',{'B-
hydroxydca[c]', 'B-hydroxydca[e]', 'h[c]', 'h[p]'},[-1 1 -1
1],1,0,1000);
        model1=addReaction(model1,'P_B-hydroxyddca_trans',{'B-
hydroxyddca[c]', 'B-hydroxyddca[e]', 'h[c]', 'h[p]'},[-1 1 -1
1],1,0,1000);
        model1=addReaction(model1,'P_B-hydroxyttdca_trans',{'B-
hydroxyttdca[c]', 'B-hydroxyttdca[e]', 'h[c]', 'h[p]'},[-1 1 -1
1],1,0,1000);
        model1=addReaction(model1,'P_B-hydroxyhdca_trans',{'B-
hydroxyhdca[c]', 'B-hydroxyhdca[e]', 'h[c]', 'h[p]'},[-1 1 -1
1],1,0,1000);
```

```
        model1=addReaction(model1,'P_B-hydroxyocdca_trans_extra',{'B-
hydroxyocdca[c]', 'B-hydroxyocdca[e]', 'h[c]', 'h[p]'},[-1 1 -1
1],1,0,1000);

        % Export of new products to zero
        model1=addReaction(model1,'EX_B-hydroxybut', {'B-
hydroxybut[e]'}, [-1],1, 0,0);
        model1=addReaction(model1,'EX_B-hydroxyhxa',{'B-
hydroxyhxa[e]'}, [-1],1, 0,0);
        model1=addReaction(model1,'EX_B-hydroxyocta',{'B-
hydroxyocta[e]'}, [-1],1, 0,0);
        model1=addReaction(model1,'EX_B-hydroxydca',{'B-
hydroxydca[e]'}, [-1],1, 0,0);
        model1=addReaction(model1,'EX_B-hydroxyddca',{'B-
hydroxyddca[e]'}, [-1],1, 0,0);
        model1=addReaction(model1,'EX_B-hydroxyttdca',{'B-
hydroxyttdca[e]'}, [-1],1, 0,0);
        model1=addReaction(model1,'EX_B-hydroxyhdca',{'B-
hydroxyhdca[e]'}, [-1],1, 0,0);
        model1=addReaction(model1,'EX_B-hydroxyocdca',{'B-
hydroxyocdca[e]'}, [-1],1, 0,0);


model1=addReaction(model1,'EX_13butanediol',{'13butanediol[c]'},[-1],1,
0,0);

model1=addReaction(model1,'EX_13hexanediol',{'13hexanediol[c]'},[-1],1,
0,0);

model1=addReaction(model1,'EX_13octanediol',{'13octanediol[c]'},[-1
],1,0,0);

model1=addReaction(model1,'EX_13decanediol',{'13decanediol[c]'},[-1],1,
0,0);

model1=addReaction(model1,'EX_13dodecanediol',{'13dodecanediol[c]'},[-1
],1,0,0);

model1=addReaction(model1,'EX_13tetradecanediol',{'13tetradecanediol[c]
'},[-1],1, 0,0);

model1=addReaction(model1,'EX_13hexadecanediol',{'13hexadecanediol[c]'}
,[-1 ],1,0,0);

model1=addReaction(model1,'EX_13octadecanediol',{'13octadecanediol[c]'}
,[-1],1, 0,0);

        model1=addReaction(model1,'EX_3propanol',{'3propanol[c]'},[-
1],1, 0,0);
        model1=addReaction(model1,'EX_3pentanol',{'3pentanol[c]'},[-
1],1, 0,0);
        model1=addReaction(model1,'EX_3heptanol',{'3heptanol[c]'},[-1
],1,0,0);
        model1=addReaction(model1,'EX_3nonanol',{'3nonanol[c]'},[-1],1,
0,0);
```

```
        model1=addReaction(model1,'EX_3undecanol',{'3undecanol[c]'},[-1
],1,0,0);

model1=addReaction(model1,'EX_3tridecanol',{'3tridecanol[c]'},[-1],1,
0,0);

model1=addReaction(model1,'EX_3pentadecanol',{'3pentadecanol[c]'},[-1
],1,0,0);

model1=addReaction(model1,'EX_3heptadecanol',{'3heptadecanol[c]'},[-
1],1, 0,0);

        %%
        % Termination Diversification 3: from trans-enoyl-coa to
substituted FA, alcohols and alkanes

        % Reduction of trans-enoyl / trans-enoyl-CoA --> trans-
enoaldehyde
        model1=addReaction(model1,'P_Trans-d2-eno-butanal',{'b2coa[c]',
'nadh[c]', 'h[c]', 'Trans-d2-eno-butanal[c]', 'nad[c]', 'coa[c]'},[-1 -
1 -1 1 1 1],1,0,1000);
        model1=addReaction(model1,'P_Trans-d2-eno-
hexanal',{'hx2coa[c]', 'nadh[c]', 'h[c]', 'Trans-d2-eno-hexanal[c]',
'nad[c]', 'coa[c]'},[-1 -1 -1 1 1 1],1,0,1000);
        model1=addReaction(model1,'P_Trans-d2-eno-
octanal',{'oc2coa[c]', 'nadh[c]', 'h[c]', 'Trans-d2-eno-octanal[c]',
'nad[c]', 'coa[c]'},[-1 -1 -1 1 1 1],1,0,1000);
        model1=addReaction(model1,'P_Trans-d2-eno-
decanal',{'dc2coa[c]', 'nadh[c]', 'h[c]', 'Trans-d2-eno-decanal[c]',
'nad[c]', 'coa[c]'},[-1 -1 -1 1 1 1],1,0,1000);
        model1=addReaction(model1,'P_Trans-d2-eno-
dodecanal',{'dd2coa[c]', 'nadh[c]', 'h[c]', 'Trans-d2-eno-
dodecanal[c]', 'nad[c]', 'coa[c]'},[-1 -1 -1 1 1 1],1,0,1000);
        model1=addReaction(model1,'P_Trans-d2-eno-
tetradecanal',{'td2coa[c]', 'nadh[c]', 'h[c]', 'Trans-d2-eno-
tetradecanal[c]', 'nad[c]', 'coa[c]'},[-1 -1 -1 1 1 1],1,0,1000);
        model1=addReaction(model1,'P_Trans-d2-eno-
hexadecanal',{'hdd2coa[c]', 'nadh[c]', 'h[c]', 'Trans-d2-eno-
hexadecanal[c]', 'nad[c]', 'coa[c]'},[-1 -1 -1 1 1 1],1,0,1000);
        model1=addReaction(model1,'P_Trans-d2-eno-
octadecanal',{'od2coa[c]', 'nadh[c]', 'h[c]', 'Trans-d2-eno-
octadecanal[c]', 'nad[c]', 'coa[c]'},[-1 -1 -1 1 1 1],1,0,1000);

        %B-ketoaldehyde decarboxilation / Production of eno-alkanes
        model1=addReaction(model1,'P_propene',{'Trans-d2-eno-
butanal[c]', 'propene[c]', 'co[c]'},[-1 1 1],1,0,1000);
        model1=addReaction(model1,'P_pentene',{'Trans-d2-eno-
hexanal[c]', 'pentene[c]','co[c]'},[-1 1 1],1,0,1000);
        model1=addReaction(model1,'P_heptene',{'Trans-d2-eno-
octanal[c]', 'heptene[c]','co[c]'},[-1 1 1],1,0,1000);
        model1=addReaction(model1,'P_nonene',{'Trans-d2-eno-
decanal[c]', 'nonene[c]','co[c]'},[-1 1 1],1,0,1000);
        model1=addReaction(model1,'P_undecene',{'Trans-d2-eno-
dodecanal[c]', 'undecene[c]', 'co[c]'},[-1 1 1],1,0,1000);
        model1=addReaction(model1,'P_tridecene',{'Trans-d2-eno-
tetradecanal[c]', 'tridecene[c]','co[c]'},[-1 1 1],1,0,1000);
```

```
        model1=addReaction(model1,'P_pentadecene',{'Trans-d2-eno-
hexadecanal[c]', 'pentadecene[c]', 'co[c]'},[-1 1 1],1,0,1000);
        model1=addReaction(model1,'P_heptadecene',{'Trans-d2-eno-
octadecanal[c]', 'heptadecene[c]','co[c]'},[-1 1 1],1,0,1000);

        %Trans-d2-alcohol production
        model1=addReaction(model1,'P_Trans-d2-fatty-butanol',{'Trans-
d2-eno-butanal[c]', 'nadh[c]', 'h[c]', 'Trans-d2-fatty-butanol[c]',
'nad[c]'},[-1 -1 -1 1 1],1,0,1000);
        model1=addReaction(model1,'P_Trans-d2-fatty-hexanol',{'Trans-
d2-eno-hexanal[c]', 'nadh[c]', 'h[c]', 'Trans-d2-fatty-hexanol[c]',
'nad[c]'},[-1 -1 -1 1 1],1,0,1000);
        model1=addReaction(model1,'P_Trans-d2-fatty-octanol',{'Trans-
d2-eno-octanal[c]', 'nadh[c]', 'h[c]', 'Trans-d2-fatty-octanol[c]',
'nad[c]'},[-1 -1 -1 1 1],1,0,1000);
        model1=addReaction(model1,'P_Trans-d2-fatty-decanol',{'Trans-
d2-eno-decanal[c]', 'nadh[c]', 'h[c]', 'Trans-d2-fatty-decanol[c]',
'nad[c]'},[-1 -1 -1 1 1],1,0,1000);
        model1=addReaction(model1,'P_Trans-d2-fatty-dodecanol',{'Trans-
d2-eno-dodecanal[c]', 'nadh[c]', 'h[c]', 'Trans-d2-fatty-dodecanol[c]',
'nad[c]'},[-1 -1 -1 1 1],1,0,1000);
        model1=addReaction(model1,'P_Trans-d2-fatty-
tetradecanol',{'Trans-d2-eno-tetradecanal[c]', 'nadh[c]', 'h[c]',
'Trans-d2-fatty-tetradecanol[c]', 'nad[c]'},[-1 -1 -1 1 1],1,0,1000);
        model1=addReaction(model1,'P_Trans-d2-fatty-
hexadecanol',{'Trans-d2-eno-hexadecanal[c]', 'nadh[c]', 'h[c]', 'Trans-
d2-fatty-hexadecanol[c]', 'nad[c]'},[-1 -1 -1 1 1],1,0,1000);
        model1=addReaction(model1,'P_Trans-d2-fatty-
octadecanol',{'Trans-d2-eno-octadecanal[c]', 'nadh[c]', 'h[c]', 'Trans-
d2-fatty-octadecanol[c]', 'nad[c]'},[-1 -1 -1 1 1],1,0,1000);

        %Trans-d2-enoyl-coa --> Trans-d2-fatty acids
        model1=addReaction(model1,'P_Trans-d2-but_CoA',{'b2coa[c]',
'h2o[c]', 'h[c]', 'Trans-d2-but[c]', 'coa[c]'},[-1 -1 1 1 1],1,0,1000);
        model1=addReaction(model1,'P_Trans-d2-hxa_CoA',{'hx2coa[c]',
'h2o[c]', 'h[c]', 'Trans-d2-hxa[c]', 'coa[c]'},[-1 -1 1 1 1],1,0,1000);
        model1=addReaction(model1,'P_Trans-d2-octa_CoA',{'oc2coa[c]',
'h2o[c]', 'h[c]', 'Trans-d2-octa[c]', 'coa[c]'},[-1 -1 1 1
1],1,0,1000);
        model1=addReaction(model1,'P_Trans-d2-dca_CoA',{'dc2coa[c]',
'h2o[c]', 'h[c]', 'Trans-d2-dca[c]', 'coa[c]'},[-1 -1 1 1 1],1,0,1000);
        model1=addReaction(model1,'P_Trans-d2-ddca_CoA',{'dd2coa[c]',
'h2o[c]', 'h[c]', 'Trans-d2-ddca[c]', 'coa[c]'},[-1 -1 1 1
1],1,0,1000);
        model1=addReaction(model1,'P_Trans-d2-ttdca_CoA',{'td2coa[c]',
'h2o[c]', 'h[c]', 'Trans-d2-ttdca[c]', 'coa[c]'},[-1 -1 1 1
1],1,0,1000);
        model1=addReaction(model1,'P_Trans-d2-hdca_CoA',{'hdd2coa[c]',
'h2o[c]', 'h[c]', 'Trans-d2-hdca[c]', 'coa[c]'},[-1 -1 1 1
1],1,0,1000);
        model1=addReaction(model1,'P_Trans-d2-ocdca_CoA',{'od2coa[c]',
'h2o[c]', 'h[c]', 'Trans-d2-ocdca[c]', 'coa[c]'},[-1 -1 1 1
1],1,0,1000);

        %transport reactions to export fatty acids. All for [c] to [e]
```

```
        %because the model did not have the proper transport accross
membrane form [p] to [e]
        model1=addReaction(model1,'P_Trans-d2-but_trans',{'Trans-d2-
but[c]', 'Trans-d2-but[e]', 'h[c]', 'h[p]'},[-1 1 -1 1],1,0,1000);
        model1=addReaction(model1,'P_Trans-d2-hxa_trans',{'Trans-d2-
hxa[c]', 'Trans-d2-hxa[e]', 'h[c]', 'h[p]'},[-1 1 -1 1],1,0,1000);
        model1=addReaction(model1,'P_Trans-d2-octa_trans',{'Trans-d2-
octa[c]', 'Trans-d2-octa[e]', 'h[c]', 'h[p]'},[-1 1 -1 1],1,0,1000);
        model1=addReaction(model1,'P_Trans-d2-dca_trans',{'Trans-d2-
dca[c]', 'Trans-d2-dca[e]', 'h[c]', 'h[p]'},[-1 1 -1 1],1,0,1000);
        model1=addReaction(model1,'P_Trans-d2-ddca_trans',{'Trans-d2-
ddca[c]', 'Trans-d2-ddca[e]', 'h[c]', 'h[p]'},[-1 1 -1 1],1,0,1000);
        model1=addReaction(model1,'P_Trans-d2-ttdca_trans',{'Trans-d2-
ttdca[c]', 'Trans-d2-ttdca[e]', 'h[c]', 'h[p]'},[-1 1 -1 1],1,0,1000);
        model1=addReaction(model1,'P_Trans-d2-hdca_trans',{'Trans-d2-
hdca[c]', 'Trans-d2-hdca[e]', 'h[c]', 'h[p]'},[-1 1 -1 1],1,0,1000);
        model1=addReaction(model1,'P_Trans-d2-
ocdca_trans_extra',{'Trans-d2-ocdca[c]', 'Trans-d2-ocdca[e]', 'h[c]',
'h[p]'},[-1 1 -1 1],1,0,1000);

        % Export of new products to zero
        model1=addReaction(model1,'EX_Trans-d2-but', {'Trans-d2-
but[e]'}, [-1],1, 0,0);
        model1=addReaction(model1,'EX_Trans-d2-hxa',{'Trans-d2-
hxa[e]'}, [-1],1, 0,0);
        model1=addReaction(model1,'EX_Trans-d2-octa',{'Trans-d2-
octa[e]'}, [-1],1, 0,0);
        model1=addReaction(model1,'EX_Trans-d2-dca',{'Trans-d2-
dca[e]'}, [-1],1, 0,0);
        model1=addReaction(model1,'EX_Trans-d2-ddca',{'Trans-d2-
ddca[e]'}, [-1],1, 0,0);
        model1=addReaction(model1,'EX_Trans-d2-ttdca',{'Trans-d2-
ttdca[e]'}, [-1],1, 0,0);
        model1=addReaction(model1,'EX_Trans-d2-hdca',{'Trans-d2-
hdca[e]'}, [-1],1, 0,0);
        model1=addReaction(model1,'EX_Trans-d2-ocdca',{'Trans-d2-
ocdca[e]'}, [-1],1, 0,0);

        model1=addReaction(model1,'EX_Trans-d2-fatty-butanol',{'Trans-
d2-fatty-butanol[c]'},[-1],1, 0,0);
        model1=addReaction(model1,'EX_Trans-d2-fatty-hexanol',{'Trans-
d2-fatty-hexanol[c]'},[-1],1, 0,0);
        model1=addReaction(model1,'EX_Trans-d2-fatty-octanol',{'Trans-
d2-fatty-octanol[c]'},[-1 ],1,0,0);
        model1=addReaction(model1,'EX_Trans-d2-fatty-decanol',{'Trans-
d2-fatty-decanol[c]'},[-1],1, 0,0);
        model1=addReaction(model1,'EX_Trans-d2-fatty-
dodecanol',{'Trans-d2-fatty-dodecanol[c]'},[-1 ],1,0,0);
        model1=addReaction(model1,'EX_Trans-d2-fatty-
tetradecanol',{'Trans-d2-fatty-tetradecanol[c]'},[-1],1, 0,0);
        model1=addReaction(model1,'EX_Trans-d2-fatty-
hexadecanol',{'Trans-d2-fatty-hexadecanol[c]'},[-1 ],1,0,0);
        model1=addReaction(model1,'EX_Trans-d2-fatty-
octadecanol',{'Trans-d2-fatty-octadecanol[c]'},[-1],1, 0,0);
```

```
        model1=addReaction(model1,'EX_propene',{'propene[c]'},[-1],1,
0,0);
        model1=addReaction(model1,'EX_pentene',{'pentene[c]'},[-1],1,
0,0);
        model1=addReaction(model1,'EX_heptene',{'heptene[c]'},[-1
],1,0,0);
        model1=addReaction(model1,'EX_nonene',{'nonene[c]'},[-1],1,
0,0);
        model1=addReaction(model1,'EX_undecene',{'undecene[c]'},[-1
],1,0,0);
        model1=addReaction(model1,'EX_tridecene',{'tridecene[c]'},[-
1],1, 0,0);

model1=addReaction(model1,'EX_pentadecene',{'pentadecene[c]'},[-1
],1,0,0);

model1=addReaction(model1,'EX_heptadecene',{'heptadecene[c]'},[-1],1,
0,0);

A= size(model1.rxns);
SizeModel=(A(1));
```

10.14 Matlab function for the use of hydroxylated primers for the synthesis of carboxyacids and diols using reversal β-oxidation cycle

AC_BioamssvsProduct_HydroxilatedPrimer6

```
% Production of diols and carboxiacids in E. coli using hydroxylated
primers.
% Reversal B-oxidation cycle.
% Model developed by Angela Cintolesi as part of her Doctoral Research
% Chemical and Biomolecular Engineering, Rice University, March 2013
% Return a matrix Y with the optimal cell growth of each product

global SizeModel
initCobraToolbox()
changeCobraSolver('glpk');
%% Open model
        model1=readCbModel('iJO1366');
        biomassposition=8;
        Biomass_name='Ec_biomass_iJO1366_core_53p95M';
        modelname='iJO1366';
        %no aa degradation
        model1=changeRxnBounds(model1,{'DAAD', 'AST', 'SADH', 'SGSAD',
'SGDS', 'ARGDC', 'ARGDCpp', 'ASPT', 'GLUN', 'P5CD', 'PROD2', 'SERD_L',
'OBTFL', 'PPAKr', 'THRD', 'GLYAT', 'TYROXDApp', 'PEAMNOpp', 'TRPAS2',
'CYSDS','42A12BOOXpp', 'THRAi'}, [0 0 0 0 0 0 0 0 0 0 0 0 0 0 0 0 0 0 0
0 0 0], 'u');
        model1=changeRxnBounds(model1,{'DAAD', 'AST', 'SADH', 'SGSAD',
'SGDS', 'ARGDC', 'ARGDCpp', 'ASPT', 'GLUN', 'P5CD', 'PROD2', 'SERD_L',
'OBTFL', 'PPAKr', 'THRD', 'GLYAT', 'TYROXDApp', 'PEAMNOpp', 'TRPAS2',
```

```
'CYSDS','42A12BOOXpp', 'THRAi'}, [0 0 0 0 0 0 0 0 0 0 0 0 0 0 0 0 0 0 0 0
0 0 0], 'l');
        %no nucleotides degradation
        model1=changeRxnBounds(model1,{'CYTD', 'DCYTD', 'DURIPP',
'TMDPP', 'PPM2', 'DRPA', 'ADA', 'DADA', 'PUNP1', 'PUNP4', 'PUNP2',
'PUNP3', 'PUNP5', 'PUNP6', 'PUNP7', 'PYNP2r'}, [0 0 0 0 0 0 0 0 0 0 0 0
0 0 0 0], 'u');
        model1=changeRxnBounds(model1,{'CYTD', 'DCYTD', 'DURIPP',
'TMDPP', 'PPM2', 'DRPA', 'ADA', 'DADA', 'PUNP1', 'PUNP4', 'PUNP2',
'PUNP3', 'PUNP5', 'PUNP6', 'PUNP7', 'PYNP2r'}, [0 0 0 0 0 0 0 0 0 0 0 0
0 0 0 0], 'l');
        % export aa (direct + non escential):
        model1=changeRxnBounds(model1,{'EX_ala-B(e)', 'EX_ala-D(e)',
'EX_ala-L(e)', 'EX_asn-L(e)', 'EX_asp-L(e)', 'EX_cys-D(e)', 'EX_cys-
L(e)', 'EX_glu-L(e)', 'EX_gln-L(e)', 'EX_gly(e)', 'EX_his-L(e)',
'EX_ile-L(e)', 'EX_leu-L(e)', 'EX_lys-L(e)', 'EX_met-D(e)', 'EX_met-
L(e)', 'EX_phe-L(e)', 'EX_pro-L(e)', 'EX_ser-D(e)', 'EX_ser-
L(e)','EX_thr-L(e)', 'EX_trp-L(e)', 'EX_tyr-L(e)', 'EX_val-L(e)' }, [0
0 0 0 0 0 0 0 0 0 0 0 0 0 0 0 0 0 0 0 0 0 0 0 0 0 0 ], 'u');
        model1= changeRxnBounds(model1,{'EX_26dap-
M(e)','EX_frulys(e)','EX_hom-L(e)', 'EX_orn(e)'}, [0 0 0 0 ], 'u');
        %no Fe2+ export. no H2S export
        model1=changeRxnBounds(model1,'EX_fe2(e)', 0, 'u');
        model1=changeRxnBounds(model1,'EX_h2s(e)', 0, 'u');
        %no POR5 export.
        model1=changeRxnBounds(model1,'POR5', 0, 'l');
        model1=changeRxnBounds(model1,'POR5', 0, 'u');
        %Add PntAB
        model1=addReaction(model1, 'Add_PntAB', {'nadh[c]', 'nadp[c]',
'h[p]', 'nad[c]', 'nadph[c]', 'h[c]'}, [-1 -1 -1 1 1 1], 1, 0, 1000);

        model1=changeRxnBounds(model1,'EX_o2(e)', 0, 'l');
        model1=changeRxnBounds(model1,'EX_glc(e)', -15, 'l');
        %Delete by-products
        model1=changeRxnBounds(model1,'EX_pyr(e)', 0, 'u');
        model1=changeRxnBounds(model1,'EX_acald(e)', 0, 'u');
        model1=changeRxnBounds(model1,'EX_hxa(e)', 0, 'u');
        %FBA3, PFK_3
        model1=changeRxnBounds(model1,'FBA3', 0, 'l');
        model1=changeRxnBounds(model1,'FBA3', 0, 'u');
        model1=changeRxnBounds(model1,'PFK_3', 0, 'l');
        model1=changeRxnBounds(model1,'PFK_3', 0, 'u');
        %no production of 5mtr and spmd, for redox purposes
        model1=changeRxnBounds(model1,'EX_5mtr(e)', 0, 'u');
        model1=changeRxnBounds(model1,'EX_spmd(e)', 0, 'u');
        %ACOAD1f are inactive in this case.
        model1=changeRxnBounds(model1,'ACOAD1f', 0, 'l');
        model1=changeRxnBounds(model1,'ACOAD1f', 0, 'u');
        model1=changeRxnBounds(model1,'ACOAD2f', 0, 'l');
        model1=changeRxnBounds(model1,'ACOAD2f', 0, 'u');
        model1=changeRxnBounds(model1,'ACOAD3f', 0, 'l');
        model1=changeRxnBounds(model1,'ACOAD3f', 0, 'u');
        model1=changeRxnBounds(model1,'ACOAD4f', 0, 'l');
        model1=changeRxnBounds(model1,'ACOAD4f', 0, 'u');
        model1=changeRxnBounds(model1,'ACOAD5f', 0, 'l');
        model1=changeRxnBounds(model1,'ACOAD5f', 0, 'u');
        model1=changeRxnBounds(model1,'ACOAD6f', 0, 'l');
```

```
        model1=changeRxnBounds(model1,'ACOAD6f', 0, 'u');
        model1=changeRxnBounds(model1,'ACOAD7f', 0, 'l');
        model1=changeRxnBounds(model1,'ACOAD7f', 0, 'u');
        model1=changeRxnBounds(model1,'ACOAD8f', 0, 'l');
        model1=changeRxnBounds(model1,'ACOAD8f', 0, 'u');


model1=addReaction(model1,'PFOR',{'coa[c]', 'fd_oxi', 'pyr[c]',
'accoa[c]', 'co2[c]', 'fd_red', 'h[c]'},[-1 -1 -1 1 1 1 1],1,0,1000);
%% Production of Diols, hydroxylated acids, and bi-acids
%Export acids
model1=addReaction(model1,'EX_hydroxyacetate',{ 'hydroxyacetate[e]'},[-
1],1, 0,0);
model1=addReaction(model1,'EX_hydroxypropionate',{
'hydroxypropionate[e]'},[-1],1, 0,0);
model1=addReaction(model1,'EX_hydroxybutyrate',{ 'ghb[e]'},[-1],1,
0,0); % already in the model, as gamma-hydroxybutyrycacid (ghb)
%Transport
model1=addReaction(model1,'TR_hydroxyacetate','hydroxyacetate[e] + h[p]
-> hydroxyacetate[c] + h[c]');
model1=addReaction(model1,'TR_hydroxypropionate','hydroxypropionate[e]
+ h[p] -> hydroxypropionate[c] + h[c]');% This is as r8: 3-
hydroxypropionate
model1=addReaction(model1,'TR_hydroxybutyrate','ghb[e] + h[p] -> ghb[c]
+ h[c]'); %ghb[c] is gamma-hydroxybutyrycacid
%activation:
model1=addReaction(model1,'P_hydroxyacetylCoA','hydroxyacetate[c] +
atp[c] + coa[c] -> hydroxyacetyl-CoA + amp[c] + ppi[c]');
model1=addReaction(model1,'P_3hydroxypropionylCoA','hydroxypropionate[c
] + atp[c] + coa[c] -> 3-hydroxypropionyl-CoA + amp[c] + ppi[c]');
model1=addReaction(model1,'P_4hydroxybutyrylCoA','ghb[c] + atp[c] +
coa[c] -> 4hydroxybutyryl-CoA + amp[c] + ppi[c]');
%initiation
model1=addReaction(model1,'P_4hydroxyacetoacetylCoA',{ 'hydroxyacetyl-
CoA', 'accoa[c]', '4-hydroxy-acetoacetyl-CoA', 'coa[c]'},[-1 -1 1 1],1,
0,1000);
model1=addReaction(model1,'P_5hyxdroxypentanoylCoA',{'3-
hydroxypropionyl-CoA', 'accoa[c]', '5-hydroxy-3-Oxopentanoyl-CoA',
'coa[c]'},[-1 -1 1 1],1, 0,1000);
model1=addReaction(model1,'P_6hyxdroxyhexanoylCoA',{'4hydroxybutyryl-
CoA', 'accoa[c]', '6-hydroxy-3-Oxohexanoyl-CoA', 'coa[c]'},[-1 -1 1
1],1, 0,1000);
%
%Export acids
model1=addReaction(model1,'EX_oxalate',{ 'oxa[e]'},[-1],1, 0,0);
%oxa[c] is part of the model. I add it as source
model1=addReaction(model1,'EX_malonate',{ 'malonate[e]'},[-1],1, 0,0);
%Transport
model1=addReaction(model1,'TR_oxalate','oxa[e] + h[p] -> oxa[c] +
h[c]');%oxa[c] is part of the model.
model1=addReaction(model1,'TR_malonate','malonate[e] + h[p] ->
malonate[c] + h[c]');
% Transport of succ is already part of the model, and it uses 2 protons

%activation
```

```
model1=addReaction(model1,'P_oxalylCoA','oxa[c] + atp[c] + coa[c] ->
oxalcoa[c] + amp[c] + ppi[c]');%oxalyl-CoA already in the model
model1=addReaction(model1,'P_malonylCoA','malonate[c] + atp[c] + coa[c]
-> malcoa[c] + amp[c] + ppi[c]');%malonyl-coa = malcoa
model1=addReaction(model1,'P_succinylCoA','succ[c] + atp[c] + coa[c] ->
succoa[c] + amp[c] + ppi[c]');% Already in the model (succinyl-
coa=succoa). There is a close reaction in the model, that only uses one
P group.

%initiation
model1=addReaction(model1,'P_3oxosuccinylCoA',{ 'oxalcoa[c]',
'accoa[c]', '3oxosuccinyl-CoA', 'coa[c]'},[-1 -1 1 1],1, 0,1000);
model1=addReaction(model1,'P_3oxoglutarylCoA',{'malcoa[c]', 'accoa[c]',
'3oxoglutaryl-CoA', 'coa[c]'},[-1 -1 1 1],1, 0,1000);
model1=addReaction(model1,'P_3oxoadipylCoA',{'succoa[c]', 'accoa[c]',
'oxadpcoa[c]', 'coa[c]'},[-1 -1 1 1],1, 0,1000);%3oxoadipyl-CoA =
oxadpcoa[c] already in model
%----------------------
%Primers 1, 2, and 3: 4-hydroxyacetoacetyl-coa, 5-hydroxy3oxopentanoyl-
coa,
%and 6hydroxy3oxohexanoyl-coa
%3-hydroxyacyl-CoA dehydrogenase (Adapted from HACDxi in B-oxidation
cycle):
model1=addReaction(model1,'PA_1', {'4-hydroxy-acetoacetyl-CoA',
'nadh[c]', 'h[c]', '3,4-dihydroxybutanoyl-CoA', 'nad[c]'},[-1 -1 -1 1
1],1, 0,1000);
model1=addReaction(model1,'PA_2', {'5-hydroxy-3-Oxopentanoyl-CoA',
'nadh[c]', 'h[c]', '3,5-dihydroxypentanoyl-CoA', 'nad[c]'},[-1 -1 -1 1
1],1, 0,1000);
model1=addReaction(model1,'PA_3', {'6-hydroxy-3-Oxohexanoyl-CoA',
'nadh[c]', 'h[c]', '3,6-dihydroxyhexanoyl-CoA', 'nad[c]'},[-1 -1 -1 1
1],1, 0,1000);
model1=addReaction(model1,'PA_4', {'7-hydroxy-3-Oxoheptanoyl-CoA',
'nadh[c]', 'h[c]', '3,7-dihydroxyheptanoyl-CoA', 'nad[c]'},[-1 -1 -1 1
1],1, 0,1000);
model1=addReaction(model1,'PA_5', {'8-hydroxy-3-Oxooctanoyl-CoA',
'nadh[c]', 'h[c]', '3,8-dihydroxyoctanoyl-CoA', 'nad[c]'},[-1 -1 -1 1
1],1, 0,1000);
model1=addReaction(model1,'PA_6', {'9-hydroxy-3-Oxononanoyl-CoA',
'nadh[c]', 'h[c]', '3,9-dihydroxynonanoyl-CoA', 'nad[c]'},[-1 -1 -1 1
1],1, 0,1000);
model1=addReaction(model1,'PA_7', {'10-hydroxy-3-Oxodecanoyl-CoA',
'nadh[c]', 'h[c]', '3,10-dihydroxydecanoyl-CoA', 'nad[c]'},[-1 -1 -1 1
1],1, 0,1000);
model1=addReaction(model1,'PA_8', {'11-hydroxy-3-Oxoundecanoyl-CoA',
'nadh[c]', 'h[c]', '3,11-dihydroxyundecanoyl-CoA', 'nad[c]'},[-1 -1 -1
1 1],1, 0,1000);
model1=addReaction(model1,'PA_9', {'12-hydroxy-3-Oxododecanoyl-CoA',
'nadh[c]', 'h[c]', '3,12-dihydroxydodecanoyl-CoA', 'nad[c]'},[-1 -1 -1
1 1],1, 0,1000);
model1=addReaction(model1,'PA_10', {'13-hydroxy-3-Oxotridecanoyl-CoA',
'nadh[c]', 'h[c]', '3,13-dihydroxytridecanoyl-CoA', 'nad[c]'},[-1 -1 -1
1 1],1, 0,1000);
model1=addReaction(model1,'PA_11', {'14-hydroxy-3-Oxotetradecanoyl-
CoA', 'nadh[c]', 'h[c]', '3,14-dihydroxytetradecanoyl-CoA',
'nad[c]'},[-1 -1 -1 1 1],1, 0,1000);
```

```
model1=addReaction(model1,'PA_12', {'15-hydroxy-3-Oxopentadecanoyl-
CoA', 'nadh[c]', 'h[c]', '3,15-dihydroxypentadecanoyl-CoA',
'nad[c]'},[-1 -1 -1 1 1],1, 0,1000);
model1=addReaction(model1,'PA_13', {'16-hydroxy-3-Oxohexadecanoyl-CoA',
'nadh[c]', 'h[c]', '3,16-dihydroxyhexadecanoyl-CoA', 'nad[c]'},[-1 -1 -
1 1 1],1, 0,1000);
model1=addReaction(model1,'PA_14', {'17-hydroxy-3-Oxoheptadecanoyl-
CoA', 'nadh[c]', 'h[c]', '3,17-dihydroxyheptadecanoyl-CoA',
'nad[c]'},[-1 -1 -1 1 1],1, 0,1000);
model1=addReaction(model1,'PA_15', {'18-hydroxy-3-Oxooctadecanoyl-CoA',
'nadh[c]', 'h[c]', '3,18-dihydroxyoctadecanoyl-CoA', 'nad[c]'},[-1 -1 -
1 1 1],1, 0,1000);
%3-hydroxyacyl-CoA dehydratase (Adapted from ECOAHx in B-oxidation
cycle):
model1=addReaction(model1,'PB_1', {'3,4-dihydroxybutanoyl-CoA', '4-
hydroxy-crotonyl-CoA', 'h2o[c]'},[-1 1 1],1, 0,1000);
model1=addReaction(model1,'PB_2', {'3,5-dihydroxypentanoyl-CoA', '5-
hydroxy-trans-pen-2-enoyl-CoA', 'h2o[c]'},[-1 1 1],1, 0,1000);
model1=addReaction(model1,'PB_3', {'3,6-dihydroxyhexanoyl-CoA', '6-
hydroxy-trans-hex-2-enoyl-CoA', 'h2o[c]'},[-1 1 1],1, 0,1000);
model1=addReaction(model1,'PB_4', {'3,7-dihydroxyheptanoyl-CoA', '7-
hydroxy-trans-hep-2-enoyl-CoA', 'h2o[c]'},[-1 1 1],1, 0,1000);
model1=addReaction(model1,'PB_5', {'3,8-dihydroxyoctanoyl-CoA', '8-
hydroxy-trans-oct-2-enoyl-CoA', 'h2o[c]'},[-1 1 1],1, 0,1000);
model1=addReaction(model1,'PB_6', {'3,9-dihydroxynonanoyl-CoA', '9-
hydroxy-trans-non-2-enoyl-CoA', 'h2o[c]'},[-1 1 1],1, 0,1000);
model1=addReaction(model1,'PB_7', {'3,10-dihydroxydecanoyl-CoA', '10-
hydroxy-trans-dec-2-enoyl-CoA', 'h2o[c]'},[-1 1 1],1, 0,1000);
model1=addReaction(model1,'PB_8', {'3,11-dihydroxyundecanoyl-CoA', '11-
hydroxy-trans-undec-2-enoyl-CoA', 'h2o[c]'},[-1 1 1],1, 0,1000);
model1=addReaction(model1,'PB_9', {'3,12-dihydroxydodecanoyl-CoA', '12-
hydroxy-trans-dodec-2-enoyl-CoA', 'h2o[c]'},[-1 1 1],1, 0,1000);
model1=addReaction(model1,'PB_10', {'3,13-dihydroxytridecanoyl-CoA',
'13-hydroxy-trans-tridec-2-enoyl-CoA', 'h2o[c]'},[-1 1 1],1, 0,1000);
model1=addReaction(model1,'PB_11', {'3,14-dihydroxytetradecanoyl-CoA',
'14-hydroxy-trans-tetradec-2-enoyl-CoA', 'h2o[c]'},[-1 1 1],1, 0,1000);
model1=addReaction(model1,'PB_12', {'3,15-dihydroxypentadecanoyl-CoA',
'15-hydroxy-trans-pentadec-2-enoyl-CoA', 'h2o[c]'},[-1 1 1],1, 0,1000);
model1=addReaction(model1,'PB_13', {'3,16-dihydroxyhexadecanoyl-CoA',
'16-hydroxy-trans-hexadec-2-enoyl-CoA', 'h2o[c]'},[-1 1 1],1, 0,1000);
model1=addReaction(model1,'PB_14', {'3,17-dihydroxyheptadecanoyl-CoA',
'17-hydroxy-trans-heptadec-2-enoyl-CoA', 'h2o[c]'},[-1 1 1],1, 0,1000);
model1=addReaction(model1,'PB_15', {'3,18-dihydroxyoctadecanoyl-CoA',
'18-hydroxy-trans-octadec-2-enoyl-CoA', 'h2o[c]'},[-1 1 1],1, 0,1000);
%acyl-CoA dehydrogenase (Adapted from ACOADxf_ferr in reversal B-
oxidation cycle)
model1=addReaction(model1,'PC_1', {'4-hydroxy-crotonyl-CoA', 'fd_red',
'h[c]', '4hydroxybutyryl-CoA', 'fd_oxi'},[-1 -1 -1 1 1],1, 0,1000);
model1=addReaction(model1,'PC_2', {'5-hydroxy-trans-pen-2-enoyl-CoA',
'fd_red', 'h[c]', '5-hydroxy-pentanoyl-coa', 'fd_oxi'},[-1 -1 -1 1
1],1, 0,1000);
model1=addReaction(model1,'PC_3', {'6-hydroxy-trans-hex-2-enoyl-CoA',
'fd_red', 'h[c]', '6-hydroxy-hexanoyl-coa', 'fd_oxi'},[-1 -1 -1 1 1],1,
0,1000);
model1=addReaction(model1,'PC_4', {'7-hydroxy-trans-hep-2-enoyl-CoA',
'fd_red', 'h[c]', '7-hydroxy-heptanoyl-coa', 'fd_oxi'},[-1 -1 -1 1
1],1, 0,1000);
```

```
model1=addReaction(model1,'PC_5', {'8-hydroxy-trans-oct-2-enoyl-CoA',
'fd_red', 'h[c]', '8-hydroxy-octanoyl-coa', 'fd_oxi'},[-1 -1 -1 1 1],1,
0,1000);
model1=addReaction(model1,'PC_6', {'9-hydroxy-trans-non-2-enoyl-CoA',
'fd_red', 'h[c]', '9-hydroxy-nonanoyl-coa', 'fd_oxi'},[-1 -1 -1 1 1],1,
0,1000);
model1=addReaction(model1,'PC_7', {'10-hydroxy-trans-dec-2-enoyl-CoA',
'fd_red', 'h[c]', '10-hydroxy-decanoyl-coa', 'fd_oxi'},[-1 -1 -1 1
1],1, 0,1000);
model1=addReaction(model1,'PC_8', {'11-hydroxy-trans-undec-2-enoyl-
CoA', 'fd_red', 'h[c]', '11-hydroxy-undecanoyl-coa', 'fd_oxi'},[-1 -1 -
1 1 1],1, 0,1000);
model1=addReaction(model1,'PC_9', {'12-hydroxy-trans-dodec-2-enoyl-
CoA', 'fd_red', 'h[c]', '12-hydroxy-dodecanoyl-coa', 'fd_oxi'},[-1 -1 -
1 1 1],1, 0,1000);
model1=addReaction(model1,'PC_10', {'13-hydroxy-trans-tridec-2-enoyl-
CoA', 'fd_red', 'h[c]', '13-hydroxy-tridecanoyl-coa', 'fd_oxi'},[-1 -1
-1 1 1],1, 0,1000);
model1=addReaction(model1,'PC_11', {'14-hydroxy-trans-tetradec-2-enoyl-
CoA', 'fd_red', 'h[c]', '14-hydroxy-tetradecanoyl-coa', 'fd_oxi'},[-1 -
1 -1 1 1],1, 0,1000);
model1=addReaction(model1,'PC_12', {'15-hydroxy-trans-pentadec-2-enoyl-
CoA', 'fd_red', 'h[c]', '15-hydroxy-pentadecanoyl-coa', 'fd_oxi'},[-1 -
1 -1 1 1],1, 0,1000);
model1=addReaction(model1,'PC_13', {'16-hydroxy-trans-hexadec-2-enoyl-
CoA', 'fd_red', 'h[c]', '16-hydroxy-palmitoyl-coa', 'fd_oxi'},[-1 -1 -1
1 1],1, 0,1000);
model1=addReaction(model1,'PC_14', {'17-hydroxy-trans-heptadec-2-enoyl-
CoA', 'fd_red', 'h[c]', '17-hydroxy-heptadecanoyl-coa', 'fd_oxi'},[-1 -
1 -1 1 1],1, 0,1000);
model1=addReaction(model1,'PC_15', {'18-hydroxy-trans-octadec-2-enoyl-
CoA', 'fd_red', 'h[c]', '18-hydroxy-stearoyl-coa', 'fd_oxi'},[-1 -1 -1
1 1],1, 0,1000);
%3-ketoacyl-CoA thiolase (Adapted from KATx in reversal B-oxidation
cycle)
model1=addReaction(model1,'PD_1', {'4hydroxybutyryl-CoA', 'accoa[c]',
'6-hydroxy-3-Oxohexanoyl-CoA', 'coa[c]'},[-1 -1 1 1],1, 0,1000);
model1=addReaction(model1,'PD_2', {'5-hydroxy-pentanoyl-coa',
'accoa[c]', '7-hydroxy-3-Oxoheptanoyl-CoA', 'coa[c]'},[-1 -1 1 1],1,
0,1000);
model1=addReaction(model1,'PD_3', {'6-hydroxy-hexanoyl-coa',
'accoa[c]', '8-hydroxy-3-Oxooctanoyl-CoA', 'coa[c]'},[-1 -1 1 1],1,
0,1000);
model1=addReaction(model1,'PD_4', {'7-hydroxy-heptanoyl-coa',
'accoa[c]', '9-hydroxy-3-Oxononanoyl-CoA', 'coa[c]'},[-1 -1 1 1],1,
0,1000);
model1=addReaction(model1,'PD_5', {'8-hydroxy-octanoyl-coa',
'accoa[c]', '10-hydroxy-3-Oxodecanoyl-CoA', 'coa[c]'},[-1 -1 1 1],1,
0,1000);
model1=addReaction(model1,'PD_6', {'9-hydroxy-nonanoyl-coa',
'accoa[c]', '11-hydroxy-3-Oxoundecanoyl-CoA', 'coa[c]'},[-1 -1 1 1],1,
0,1000);
model1=addReaction(model1,'PD_7', {'10-hydroxy-decanoyl-coa',
'accoa[c]', '12-hydroxy-3-Oxododecanoyl-CoA', 'coa[c]'},[-1 -1 1 1],1,
0,1000);
```

```
model1=addReaction(model1,'PD_8', {'11-hydroxy-undecanoyl-coa',
'accoa[c]', '13-hydroxy-3-Oxotridecanoyl-CoA', 'coa[c]'},[-1 -1 1 1],1,
0,1000);
model1=addReaction(model1,'PD_9', {'12-hydroxy-dodecanoyl-coa',
'accoa[c]', '14-hydroxy-3-Oxotetradecanoyl-CoA', 'coa[c]'},[-1 -1 1
1],1, 0,1000);
model1=addReaction(model1,'PD_10', {'13-hydroxy-tridecanoyl-coa',
'accoa[c]', '15-hydroxy-3-Oxopentadecanoyl-CoA', 'coa[c]'},[-1 -1 1
1],1, 0,1000);
model1=addReaction(model1,'PD_11', {'14-hydroxy-tetradecanoyl-coa',
'accoa[c]', '16-hydroxy-3-Oxohexadecanoyl-CoA', 'coa[c]'},[-1 -1 1
1],1, 0,1000);
model1=addReaction(model1,'PD_12', {'15-hydroxy-pentadecanoyl-coa',
'accoa[c]', '17-hydroxy-3-Oxoheptadecanoyl-CoA', 'coa[c]'},[-1 -1 1
1],1, 0,1000);
model1=addReaction(model1,'PD_13', {'16-hydroxy-palmitoyl-coa',
'accoa[c]', '18-hydroxy-3-Oxooctadecanoyl-CoA', 'coa[c]'},[-1 -1 1
1],1, 0,1000);
%Termination I (Alcohol). Reduction of acyl-CoA
model1=addReaction(model1,'PE_1', {'4hydroxybutyryl-CoA', 'nadh[c]',
'h[c]', '4-hydroxy-butyraldehyde', 'nad[c]', 'coa[c]'},[-1 -1 -1 1 1
1],1, 0,1000);
model1=addReaction(model1,'PE_2', {'5-hydroxy-pentanoyl-coa',
'nadh[c]', 'h[c]', '5-hydroxy-pentanaldehyde', 'nad[c]', 'coa[c]'},[-1
-1 -1 1 1 1],1, 0,1000);
model1=addReaction(model1,'PE_3', {'6-hydroxy-hexanoyl-coa', 'nadh[c]',
'h[c]', '6-hydroxy-hexanaldehyde', 'nad[c]', 'coa[c]'},[-1 -1 -1 1 1
1],1, 0,1000);
model1=addReaction(model1,'PE_4', {'7-hydroxy-heptanoyl-coa',
'nadh[c]', 'h[c]', '7-hydroxy-heptanaldehyde', 'nad[c]', 'coa[c]'},[-1
-1 -1 1 1 1],1, 0,1000);
model1=addReaction(model1,'PE_5', {'8-hydroxy-octanoyl-coa', 'nadh[c]',
'h[c]', '8-hydroxy-octanaldehyde', 'nad[c]', 'coa[c]'},[-1 -1 -1 1 1
1],1, 0,1000);
model1=addReaction(model1,'PE_6', {'9-hydroxy-nonanoyl-coa', 'nadh[c]',
'h[c]', '9-hydroxy-nonaldehyde', 'nad[c]', 'coa[c]'},[-1 -1 -1 1 1
1],1, 0,1000);
model1=addReaction(model1,'PE_7', {'10-hydroxy-decanoyl-coa',
'nadh[c]', 'h[c]', '10-hydroxy-decanaldehyde', 'nad[c]', 'coa[c]'},[-1
-1 -1 1 1 1],1, 0,1000);
model1=addReaction(model1,'PE_8', {'11-hydroxy-undecanoyl-coa',
'nadh[c]', 'h[c]', '11-hydroxy-undecanaldehyde', 'nad[c]', 'coa[c]'},[-
1 -1 -1 1 1 1],1, 0,1000);
model1=addReaction(model1,'PE_9', {'12-hydroxy-dodecanoyl-coa',
'nadh[c]', 'h[c]', '12-hydroxy-dodecanaldehyde', 'nad[c]', 'coa[c]'},[-
1 -1 -1 1 1 1],1, 0,1000);
model1=addReaction(model1,'PE_10', {'13-hydroxy-tridecanoyl-coa',
'nadh[c]', 'h[c]', '13-hydroxy-tridecanaldehyde', 'nad[c]',
'coa[c]'},[-1 -1 -1 1 1 1],1, 0,1000);
model1=addReaction(model1,'PE_11', {'14-hydroxy-tetradecanoyl-coa',
'nadh[c]', 'h[c]', '14-hydroxy-tetradecanaldehyde', 'nad[c]',
'coa[c]'},[-1 -1 -1 1 1 1],1, 0,1000);
model1=addReaction(model1,'PE_12', {'15-hydroxy-pentadecanoyl-coa',
'nadh[c]', 'h[c]', '15-hydroxy-pentadecanaldehyde', 'nad[c]',
'coa[c]'},[-1 -1 -1 1 1 1],1, 0,1000);
```

```
model1=addReaction(model1,'PE_13', {'16-hydroxy-palmitoyl-coa',
'nadh[c]', 'h[c]', '16-hydroxy-hexadecanaldehyde', 'nad[c]',
'coa[c]'},[-1 -1 -1 1 1 1],1, 0,1000);
model1=addReaction(model1,'PE_14', {'17-hydroxy-heptadecanoyl-coa',
'nadh[c]', 'h[c]', '17-hydroxy-heptadecanaldehyde', 'nad[c]',
'coa[c]'},[-1 -1 -1 1 1 1],1, 0,1000);
model1=addReaction(model1,'PE_15', {'18-hydroxy-stearoyl-coa',
'nadh[c]', 'h[c]', '18-hydroxy-octadecanaldehyde', 'nad[c]',
'coa[c]'},[-1 -1 -1 1 1 1],1, 0,1000);
%Termination I (Alcohol). Reduction of aldehyde
model1=addReaction(model1,'PF_1', {'4-hydroxy-butyraldehyde',
'nadh[c]', 'h[c]', '1,4 butanediol', 'nad[c]'},[-1 -1 -1 1 1],1,
0,1000);
model1=addReaction(model1,'PF_2', {'5-hydroxy-pentanaldehyde',
'nadh[c]', 'h[c]', '1,5 pentanediol', 'nad[c]'},[-1 -1 -1 1 1],1,
0,1000);
model1=addReaction(model1,'PF_3', {'6-hydroxy-hexanaldehyde',
'nadh[c]', 'h[c]', '1,6 hexanediol', 'nad[c]'},[-1 -1 -1 1 1],1,
0,1000);
model1=addReaction(model1,'PF_4', {'7-hydroxy-heptanaldehyde',
'nadh[c]', 'h[c]', '1,7 heptanediol', 'nad[c]'},[-1 -1 -1 1 1],1,
0,1000);
model1=addReaction(model1,'PF_5', {'8-hydroxy-octanaldehyde',
'nadh[c]', 'h[c]', '1,8 octanediol', 'nad[c]'},[-1 -1 -1 1 1],1,
0,1000);
model1=addReaction(model1,'PF_6', {'9-hydroxy-nonaldehyde', 'nadh[c]',
'h[c]', '1,9 nonanediol', 'nad[c]'},[-1 -1 -1 1 1],1, 0,1000);
model1=addReaction(model1,'PF_7', {'10-hydroxy-decanaldehyde',
'nadh[c]', 'h[c]', '1,10 decanediol', 'nad[c]'},[-1 -1 -1 1 1],1,
0,1000);
model1=addReaction(model1,'PF_8', {'11-hydroxy-undecanaldehyde',
'nadh[c]', 'h[c]', '1,11 undecanediol', 'nad[c]'},[-1 -1 -1 1 1],1,
0,1000);
model1=addReaction(model1,'PF_9', {'12-hydroxy-dodecanaldehyde',
'nadh[c]', 'h[c]', '1,12 dodecanediol', 'nad[c]'},[-1 -1 -1 1 1],1,
0,1000);
model1=addReaction(model1,'PF_10', {'13-hydroxy-tridecanaldehyde',
'nadh[c]', 'h[c]', '1,13 tridecanediol', 'nad[c]'},[-1 -1 -1 1 1],1,
0,1000);
model1=addReaction(model1,'PF_11', {'14-hydroxy-tetradecanaldehyde',
'nadh[c]', 'h[c]', '1,14 tetradecanediol', 'nad[c]'},[-1 -1 -1 1 1],1,
0,1000);
model1=addReaction(model1,'PF_12', {'15-hydroxy-pentadecanaldehyde',
'nadh[c]', 'h[c]', '1,15 pentadecanediol', 'nad[c]'},[-1 -1 -1 1 1],1,
0,1000);
model1=addReaction(model1,'PF_13', {'16-hydroxy-hexadecanaldehyde',
'nadh[c]', 'h[c]', '1,16 hexadecanediol', 'nad[c]'},[-1 -1 -1 1 1],1,
0,1000);
model1=addReaction(model1,'PF_14', {'17-hydroxy-heptadecanaldehyde',
'nadh[c]', 'h[c]', '1,17 heptadecanediol', 'nad[c]'},[-1 -1 -1 1 1],1,
0,1000);
model1=addReaction(model1,'PF_15', {'18-hydroxy-octadecanaldehyde',
'nadh[c]', 'h[c]', '1,18 octadecanediol', 'nad[c]'},[-1 -1 -1 1 1],1,
0,1000);
%Export (Diols)
model1=addReaction(model1,'EX_butanediol', {'1,4 butanediol'},[-1],1,
0,0);
```

```
model1=addReaction(model1,'EX_pentanediol', {'1,5 pentanediol'},[-1],1,
0,0);
model1=addReaction(model1,'EX_hexanediol', {'1,6 hexanediol'},[-1],1,
0,0);
model1=addReaction(model1,'EX_heptanediol', {'1,7 heptanediol'},[-1],1,
0,0);
model1=addReaction(model1,'EX_octanediol', {'1,8 octanediol'},[-1],1,
0,0);
model1=addReaction(model1,'EX_nonanediol', {'1,9 nonanediol'},[-1],1,
0,0);
model1=addReaction(model1,'EX_decanediol', {'1,10 decanediol'},[-1],1,
0,0);
model1=addReaction(model1,'EX_undecanediol', {'1,11 undecanediol'},[-
1],1, 0,0);
model1=addReaction(model1,'EX_dodecanediol', {'1,12 dodecanediol'},[-
1],1, 0,0);
model1=addReaction(model1,'EX_tridecanediol', {'1,13 tridecanediol'},[-
1],1, 0,0);
model1=addReaction(model1,'EX_tetradecanediol', {'1,14
tetradecanediol'},[-1],1, 0,0);
model1=addReaction(model1,'EX_pentadecanediol', {'1,15
pentadecanediol'},[-1],1, 0,0);
model1=addReaction(model1,'EX_hexadecanediol', {'1,16
hexadecanediol'},[-1],1, 0,0);
model1=addReaction(model1,'EX_heptadecanediol', {'1,17
heptadecanediol'},[-1],1, 0,0);
model1=addReaction(model1,'EX_octadecanediol', {'1,18
octadecanediol'},[-1],1, 0,0);
%Termination II (Acid).
model1=addReaction(model1,'PG_1', {'4hydroxybutyryl-CoA', 'h2o[c]',
'4hydroxybutanoicacid' 'coa[c]'},[-1 -1 1 1],1, 0,1000);
model1=addReaction(model1,'PG_2', {'5-hydroxy-pentanoyl-coa', 'h2o[c]',
'5hydroxypentanoicacid', 'coa[c]'},[-1 -1 1 1],1, 0,1000);
model1=addReaction(model1,'PG_3', {'6-hydroxy-hexanoyl-coa', 'h2o[c]',
'6hydroxyhexanoicacid', 'coa[c]'},[-1 -1 1 1],1, 0,1000);
model1=addReaction(model1,'PG_4', {'7-hydroxy-heptanoyl-coa', 'h2o[c]',
'7hydroxyheptanoicacid', 'coa[c]'},[-1 -1 1 1],1, 0,1000);
model1=addReaction(model1,'PG_5', {'8-hydroxy-octanoyl-coa', 'h2o[c]',
'8hydroxyoctanoicacid', 'coa[c]'},[-1 -1 1 1],1, 0,1000);
model1=addReaction(model1,'PG_6', {'9-hydroxy-nonanoyl-coa', 'h2o[c]',
'9hydroxynonanoicacid', 'coa[c]'},[-1 -1 1 1],1, 0,1000);
model1=addReaction(model1,'PG_7', {'10-hydroxy-decanoyl-coa', 'h2o[c]',
'10hydroxydecanoicacid', 'coa[c]'},[-1 -1 1 1],1, 0,1000);
model1=addReaction(model1,'PG_8', {'11-hydroxy-undecanoyl-coa',
'h2o[c]', '11hydroxyundecanoicacid', 'coa[c]'},[-1 -1 1 1],1, 0,1000);
model1=addReaction(model1,'PG_9', {'12-hydroxy-dodecanoyl-coa',
'h2o[c]', '12hydroxydodecanoicacid', 'coa[c]'},[-1 -1 1 1],1, 0,1000);
model1=addReaction(model1,'PG_10', {'13-hydroxy-tridecanoyl-coa',
'h2o[c]', '13hydroxytridecanoicacid', 'coa[c]'},[-1 -1 1 1],1, 0,1000);
model1=addReaction(model1,'PG_11', {'14-hydroxy-tetradecanoyl-coa',
'h2o[c]', '14hydroxytetradecanoicacid', 'coa[c]'},[-1 -1 1 1],1,
0,1000);
model1=addReaction(model1,'PG_12', {'15-hydroxy-pentadecanoyl-coa',
'h2o[c]', '15hydroxypentadecanoicacid', 'coa[c]'},[-1 -1 1 1],1,
0,1000);
```

```
model1=addReaction(model1,'PG_13', {'16-hydroxy-palmitoyl-coa',
'h2o[c]', '16hydroxyhexadecanoicacid', 'coa[c]'},[-1 -1 1 1],1,
0,1000);
model1=addReaction(model1,'PG_14', {'17-hydroxy-heptadecanoyl-coa',
'h2o[c]', '17hydroxyheptadecanoicacid', 'coa[c]'},[-1 -1 1 1],1,
0,1000);
model1=addReaction(model1,'PG_15', {'18-hydroxy-stearoyl-coa',
'h2o[c]', '18hydroxyoctadecanoicacid', 'coa[c]'},[-1 -1 1 1],1,
0,1000);
%Export (hydroxyacids)
model1=addReaction(model1,'EX_4hydroxybutanoicacid',
{'4hydroxybutanoicacid'},[-1],1, 0,0);
model1=addReaction(model1,'EX_5hydroxypentanoicacid',
{'5hydroxypentanoicacid'},[-1],1, 0,0);
model1=addReaction(model1,'EX_6hydroxyhexanoicacid',
{'6hydroxyhexanoicacid'},[-1],1, 0,0);
model1=addReaction(model1,'EX_7hydroxyheptanoicacid',
{'7hydroxyheptanoicacid'},[-1],1, 0,0);
model1=addReaction(model1,'EX_8hydroxyoctanoicacid',
{'8hydroxyoctanoicacid'},[-1],1, 0,0);
model1=addReaction(model1,'EX_9hydroxynonanoicacid',
{'9hydroxynonanoicacid'},[-1],1, 0,0);
model1=addReaction(model1,'EX_10hydroxydecanoicacid',
{'10hydroxydecanoicacid'},[-1],1, 0,0);
model1=addReaction(model1,'EX_11hydroxyundecanoicacid',
{'11hydroxyundecanoicacid'},[-1],1, 0,0);
model1=addReaction(model1,'EX_12hydroxydodecanoicacid',
{'12hydroxydodecanoicacid'},[-1],1, 0,0);
model1=addReaction(model1,'EX_13hydroxytridecanoicacid',
{'13hydroxytridecanoicacid'},[-1],1, 0,0);
model1=addReaction(model1,'EX_14hydroxytetradecanoicacid',
{'14hydroxytetradecanoicacid'},[-1],1, 0,0);
model1=addReaction(model1,'EX_15hydroxypentadecanoicacid',
{'15hydroxypentadecanoicacid'},[-1],1, 0,0);
model1=addReaction(model1,'EX_16hydroxyhexadecanoicacid',
{'16hydroxyhexadecanoicacid'},[-1],1, 0,0);
model1=addReaction(model1,'EX_17hydroxyheptadecanoicacid',
{'17hydroxyheptadecanoicacid'},[-1],1, 0,0);
model1=addReaction(model1,'EX_18hydroxyoctadecanoicacid',
{'18hydroxyoctadecanoicacid'},[-1],1, 0,0);
%% Primer 4 and 6. This section uses generic names for intermediate
metabolites for simplification.
%oxalate   ->-> 3-oxosuccinyl-coa(Adapted from HACDxi in B-oxidation
cycle)/
%succinate ->-> oxadpcoa[c](Adapted from HACDxi in B-oxidation cycle):
model1=addReaction(model1,'PH_1', {'3oxosuccinyl-CoA', 'nadh[c]',
'h[c]', '3oxosuccinyl-CoA_HACDxi', 'nad[c]'},[-1 -1 -1 1 1],1, 0,1000);
model1=addReaction(model1,'PH_2', {'oxadpcoa[c]', 'nadh[c]', 'h[c]',
'oxadpcoa_HACDxi', 'nad[c]'},[-1 -1 -1 1 1],1, 0,1000);
model1=addReaction(model1,'PH_3', {'5carboxypentanoyl-CoA_KATx',
'nadh[c]', 'h[c]', '5carboxypentanoyl-CoA_HACDxi', 'nad[c]'},[-1 -1 -1
1 1],1, 0,1000);
model1=addReaction(model1,'PH_4', {'7carboxyheptanoyl-CoA_KATx',
'nadh[c]', 'h[c]', '7carboxyheptanoyl-CoA_HACDxi', 'nad[c]'},[-1 -1 -1
1 1],1, 0,1000);
```

```
model1=addReaction(model1,'PH_5', {'9carboxynonanoyl-CoA_KATx',
'nadh[c]', 'h[c]', '9carboxynonanoyl-CoA_HACDxi', 'nad[c]'},[-1 -1 -1 1
1],1, 0,1000);
model1=addReaction(model1,'PH_6', {'11carboxyundecanoyl-CoA_KATx',
'nadh[c]', 'h[c]', '11carboxyundecanoyl-CoA_HACDxi', 'nad[c]'},[-1 -1 -
1 1 1],1, 0,1000);
model1=addReaction(model1,'PH_7', {'13carboxytridecanoyl-CoA_KATx',
'nadh[c]', 'h[c]', '13carboxytridecanoyl-CoA_HACDxi', 'nad[c]'},[-1 -1
-1 1 1],1, 0,1000);
model1=addReaction(model1,'PH_8', {'15carboxypentadecanoyl-CoA_KATx',
'nadh[c]', 'h[c]', '15carboxypentadecanoyl-CoA_HACDxi', 'nad[c]'},[-1 -
1 -1 1 1],1, 0,1000);
%3-hydroxyacyl-CoA dehydratase (Adapted from ECOAHx in B-oxidation
cycle). Use generic names adding the name of the enzyme that is
modifying
%the molecule:
model1=addReaction(model1,'PI_1', {'3oxosuccinyl-CoA_HACDxi',
'3oxosuccinyl-CoA_ECOAHi', 'h2o[c]'},[-1 1 1],1, 0,1000);
model1=addReaction(model1,'PI_2', {'oxadpcoa_HACDxi',
'oxadpcoa_ECOAHi', 'h2o[c]'},[-1 1 1],1, 0,1000);
model1=addReaction(model1,'PI_3', {'5carboxypentanoyl-CoA_HACDxi',
'5carboxypentanoyl-CoA_ECOAHi', 'h2o[c]'},[-1 1 1],1, 0,1000);
model1=addReaction(model1,'PI_4', {'7carboxyheptanoyl-CoA_HACDxi',
'7carboxyheptanoyl-CoA_ECOAHi', 'h2o[c]'},[-1 1 1],1, 0,1000);
model1=addReaction(model1,'PI_5', {'9carboxynonanoyl-CoA_HACDxi',
'9carboxynonanoyl-CoA_ECOAHi', 'h2o[c]'},[-1 1 1],1, 0,1000);
model1=addReaction(model1,'PI_6', {'11carboxyundecanoyl-CoA_HACDxi',
'11carboxyundecanoyl-CoA_ECOAHi', 'h2o[c]'},[-1 1 1],1, 0,1000);
model1=addReaction(model1,'PI_7', {'13carboxytridecanoyl-CoA_HACDxi',
'13carboxytridecanoyl-CoA_ECOAHi', 'h2o[c]'},[-1 1 1],1, 0,1000);
model1=addReaction(model1,'PI_8', {'15carboxypentadecanoyl-CoA_HACDxi',
'15carboxypentadecanoyl-CoA_ECOAHi', 'h2o[c]'},[-1 1 1],1, 0,1000);

%acyl-CoA dehydrogenase (Adapted from ACOADxf_ferr in reversal B-
oxidation
%cycle). Use generic names adding the name of the enzyme that is
modifying
%the molecule
model1=addReaction(model1,'PJ_1', {'3oxosuccinyl-CoA_ECOAHi', 'fd_red',
'h[c]', 'succoa[c]', 'fd_oxi'},[-1 -1 -1 1 1],1, 0,1000);
model1=addReaction(model1,'PJ_2', {'oxadpcoa_ECOAHi', 'fd_red', 'h[c]',
'5carboxypentanoyl-CoA', 'fd_oxi'},[-1 -1 -1 1 1],1, 0,1000);
model1=addReaction(model1,'PJ_3', {'5carboxypentanoyl-CoA_ECOAHi',
'fd_red', 'h[c]', '7carboxyheptanoyl-CoA', 'fd_oxi'},[-1 -1 -1 1 1],1,
0,1000);
model1=addReaction(model1,'PJ_4', {'7carboxyheptanoyl-CoA_ECOAHi',
'fd_red', 'h[c]', '9carboxynonanoyl-CoA', 'fd_oxi'},[-1 -1 -1 1 1],1,
0,1000);
model1=addReaction(model1,'PJ_5', {'9carboxynonanoyl-CoA_ECOAHi',
'fd_red', 'h[c]', '11carboxyundecanoyl-CoA', 'fd_oxi'},[-1 -1 -1 1
1],1, 0,1000);
model1=addReaction(model1,'PJ_6', {'11carboxyundecanoyl-CoA_ECOAHi',
'fd_red', 'h[c]', '13carboxytridecanoyl-CoA', 'fd_oxi'},[-1 -1 -1 1
1],1, 0,1000);
model1=addReaction(model1,'PJ_7', {'13carboxytridecanoyl-CoA_ECOAHi',
'fd_red', 'h[c]', '15carboxypentadecanoyl-CoA', 'fd_oxi'},[-1 -1 -1 1
1],1, 0,1000);
```

```
model1=addReaction(model1,'PJ_8', {'15carboxypentadecanoyl-CoA_ECOAHi',
'fd_red', 'h[c]', '17carboxyheptadecanoyl-CoA', 'fd_oxi'},[-1 -1 -1 1
1],1, 0,1000);

%3-ketoacyl-CoA thiolase (Adapted from KATx in reversal B-oxidation
cycle).
%Use generic names adding the name of the enzyme that is modifying
%the molecule
model1=addReaction(model1,'PK_1', {'succoa[c]', 'accoa[c]',
'3carboxypropanoyl-CoA_KATx', 'coa[c]'},[-1 -1 1 1],1, 0,1000);
model1=addReaction(model1,'PK_2', {'5carboxypentanoyl-CoA', 'accoa[c]',
'5carboxypentanoyl-CoA_KATx', 'coa[c]'},[-1 -1 1 1],1, 0,1000);
model1=addReaction(model1,'PK_3', {'7carboxyheptanoyl-CoA', 'accoa[c]',
'7carboxyheptanoyl-CoA_KATx', 'coa[c]'},[-1 -1 1 1],1, 0,1000);
model1=addReaction(model1,'PK_4', {'9carboxynonanoyl-CoA', 'accoa[c]',
'9carboxynonanoyl-CoA_KATx', 'coa[c]'},[-1 -1 1 1],1, 0,1000);
model1=addReaction(model1,'PK_5', {'11carboxyundecanoyl-CoA',
'accoa[c]', '11carboxyundecanoyl-CoA_KATx', 'coa[c]'},[-1 -1 1 1],1,
0,1000);
model1=addReaction(model1,'PK_6', {'13carboxytridecanoyl-CoA',
'accoa[c]', '13carboxytridecanoyl-CoA_KATx', 'coa[c]'},[-1 -1 1 1],1,
0,1000);
model1=addReaction(model1,'PK_7', {'15carboxypentadecanoyl-CoA',
'accoa[c]', '15carboxypentadecanoyl-CoA_KATx', 'coa[c]'},[-1 -1 1 1],1,
0,1000);
model1=addReaction(model1,'PK_8', {'17carboxyheptadecanoyl-CoA',
'accoa[c]', '17carboxyheptadecanoyl-CoA_KATx', 'coa[c]'},[-1 -1 1 1],1,
0,1000);
%Termination I (Alcohol). Reduction of acyl-CoA
model1=addReaction(model1,'PL_1', {'succoa[c]', 'nadh[c]', 'h[c]',
'4oxobutanoicacid', 'nad[c]', 'coa[c]'},[-1 -1 -1 1 1 1],1, 0,1000);
model1=addReaction(model1,'PL_2', {'5carboxypentanoyl-CoA', 'nadh[c]',
'h[c]', '6oxohexanoicacid', 'nad[c]', 'coa[c]'},[-1 -1 -1 1 1 1],1,
0,1000);
model1=addReaction(model1,'PL_3', {'7carboxyheptanoyl-CoA', 'nadh[c]',
'h[c]', '8oxooctanoicacid', 'nad[c]', 'coa[c]'},[-1 -1 -1 1 1 1],1,
0,1000);
model1=addReaction(model1,'PL_4', {'9carboxynonanoyl-CoA', 'nadh[c]',
'h[c]', '10oxodecanoicacid', 'nad[c]', 'coa[c]'},[-1 -1 -1 1 1 1],1,
0,1000);
model1=addReaction(model1,'PL_5', {'11carboxyundecanoyl-CoA',
'nadh[c]', 'h[c]', '12oxododecanoicacid', 'nad[c]', 'coa[c]'},[-1 -1 -1
1 1 1],1, 0,1000);
model1=addReaction(model1,'PL_6', {'13carboxytridecanoyl-CoA',
'nadh[c]', 'h[c]', '14oxotetradecanoicacid', 'nad[c]', 'coa[c]'},[-1 -1
-1 1 1 1],1, 0,1000);
model1=addReaction(model1,'PL_7', {'15carboxypentadecanoyl-CoA',
'nadh[c]', 'h[c]', '16oxohexadecanoicacid', 'nad[c]', 'coa[c]'},[-1 -1
-1 1 1 1],1, 0,1000);
model1=addReaction(model1,'PL_8', {'17carboxyheptadecanoyl-CoA',
'nadh[c]', 'h[c]', '18oxooctadecanoicacid', 'nad[c]', 'coa[c]'},[-1 -1
-1 1 1 1],1, 0,1000);
%Termination I (Alcohol). Reduction of aldehyde
model1=addReaction(model1,'PM_1', {'4oxobutanoicacid', 'nadh[c]',
'h[c]', '4hydroxybutanoicacid', 'nad[c]'},[-1 -1 -1 1 1],1, 0,1000);
model1=addReaction(model1,'PM_2', {'6oxohexanoicacid', 'nadh[c]',
'h[c]', '6hydroxyhexanoicacid', 'nad[c]'},[-1 -1 -1 1 1],1, 0,1000);
```

```
model1=addReaction(model1,'PM_3', {'8oxooctanoicacid', 'nadh[c]',
'h[c]', '8hydroxyoctanoicacid', 'nad[c]'},[-1 -1 -1 1 1],1, 0,1000);
model1=addReaction(model1,'PM_4', {'10oxodecanoicacid', 'nadh[c]',
'h[c]', '10hydroxydecanoicacid', 'nad[c]'},[-1 -1 -1 1 1],1, 0,1000);
model1=addReaction(model1,'PM_5', {'12oxododecanoicacid', 'nadh[c]',
'h[c]', '12hydroxydodecanoicacid', 'nad[c]'},[-1 -1 -1 1 1],1, 0,1000);
model1=addReaction(model1,'PM_6', {'14oxotetradecanoicacid', 'nadh[c]',
'h[c]', '14hydroxytetradecanoicacid', 'nad[c]'},[-1 -1 -1 1 1],1,
0,1000);
model1=addReaction(model1,'PM_7', {'16oxohexadecanoicacid', 'nadh[c]',
'h[c]', '16hydroxyhexadecanoicacid', 'nad[c]'},[-1 -1 -1 1 1],1,
0,1000);
model1=addReaction(model1,'PM_8', {'18oxooctadecanoicacid', 'nadh[c]',
'h[c]', '18hydroxyoctadecanoicacid', 'nad[c]'},[-1 -1 -1 1 1],1,
0,1000);
%Export Hydroxyacids --> already in the model
%Termination II (Acid).
model1=addReaction(model1,'PN_1', {'succoa[c]', 'h2o[c]',
'3carboxypropanoate', 'h[c]', 'coa[c]'},[-1 -1 1 1 1],1, 0,1000);
model1=addReaction(model1,'PN_2', {'5carboxypentanoyl-CoA', 'h2o[c]',
'5carboxypentanoate', 'h[c]', 'coa[c]'},[-1 -1 1 1 1],1, 0,1000);
model1=addReaction(model1,'PN_3', {'7carboxyheptanoyl-CoA', 'h2o[c]',
'7carboxyheptanoate', 'h[c]', 'coa[c]'},[-1 -1 1 1 1],1, 0,1000);
model1=addReaction(model1,'PN_4', {'9carboxynonanoyl-CoA', 'h2o[c]',
'9carboxynonanoate', 'h[c]', 'coa[c]'},[-1 -1 1 1 1],1, 0,1000);
model1=addReaction(model1,'PN_5', {'11carboxyundecanoyl-CoA', 'h2o[c]',
'11carboxyundecanoate', 'h[c]', 'coa[c]'},[-1 -1 1 1 1],1, 0,1000);
model1=addReaction(model1,'PN_6', {'13carboxytridecanoyl-CoA',
'h2o[c]', '13carboxytridecanoate', 'h[c]', 'coa[c]'},[-1 -1 1 1 1],1,
0,1000);
model1=addReaction(model1,'PN_7', {'15carboxypentadecanoyl-CoA',
'h2o[c]', '15carboxypentadecanoate', 'h[c]', 'coa[c]'},[-1 -1 1 1 1],1,
0,1000);
model1=addReaction(model1,'PN_8', {'17carboxyheptadecanoyl-CoA',
'h2o[c]', '17carboxyheptadecanoate', 'h[c]', 'coa[c]'},[-1 -1 1 1 1],1,
0,1000);
%Export Reactions (hydroxylated acid)
model1=addReaction(model1,'EX_3carboxypropanoate',
{'3carboxypropanoate'},[-1 ],1, 0,0);
model1=addReaction(model1,'EX_5carboxypentanoate',
{'5carboxypentanoate'},[-1 ],1, 0,0);
model1=addReaction(model1,'EX_7carboxyheptanoate',
{'7carboxyheptanoate'},[-1 ],1, 0,0);
model1=addReaction(model1,'EX_9carboxynonanoate',
{'9carboxynonanoate'},[-1 ],1, 0,0);
model1=addReaction(model1,'EX_11carboxyundecanoate',
{'11carboxyundecanoate'},[-1 ],1, 0,0);
model1=addReaction(model1,'EX_13carboxytridecanoate',
{'13carboxytridecanoate'},[-1 ],1, 0,0);
model1=addReaction(model1,'EX_15carboxypentadecanoate',
{'15carboxypentadecanoate'},[-1 ],1, 0,0);
model1=addReaction(model1,'EX_17carboxyheptadecanoate',
{'17carboxyheptadecanoate'},[-1 ],1, 0,0);
%% Primer 5: Malonate/3-oxoglutaryl-coa(Adapted from HACDxi in B-
oxidation cycle):
model1=addReaction(model1,'PHH_1', {'3oxoglutaryl-CoA', 'nadh[c]',
'h[c]', '3oxoglutaryl-CoA_HACDxi', 'nad[c]'},[-1 -1 -1 1 1],1, 0,1000);
```

```
model1=addReaction(model1,'PHH_2', {'4carboxybutanoyl-CoA_KATx',
'nadh[c]', 'h[c]', '4carboxybutanoyl-CoA_HACDxi', 'nad[c]'},[-1 -1 -1 1
1],1, 0,1000);
model1=addReaction(model1,'PHH_3', {'6carboxyhexanoyl-CoA_KATx',
'nadh[c]', 'h[c]', '6carboxyhexanoyl-CoA_HACDxi', 'nad[c]'},[-1 -1 -1 1
1],1, 0,1000);
model1=addReaction(model1,'PHH_4', {'8carboxyoctanoyl-CoA_KATx',
'nadh[c]', 'h[c]', '8carboxyoctanoyl-CoA_HACDxi', 'nad[c]'},[-1 -1 -1 1
1],1, 0,1000);
model1=addReaction(model1,'PHH_5', {'10carboxydecanoyl-CoA_KATx',
'nadh[c]', 'h[c]', '10carboxydecanoyl-CoA_HACDxi', 'nad[c]'},[-1 -1 -1
1 1],1, 0,1000);
model1=addReaction(model1,'PHH_6', {'12carboxydodecanoyl-CoA_KATx',
'nadh[c]', 'h[c]', '12carboxydodecanoyl-CoA_HACDxi', 'nad[c]'},[-1 -1 -
1 1 1],1, 0,1000);
model1=addReaction(model1,'PHH_7', {'14carboxytetradecanoyl-CoA_KATx',
'nadh[c]', 'h[c]', '14carboxytetradecanoyl-CoA_HACDxi', 'nad[c]'},[-1 -
1 -1 1 1],1, 0,1000);
model1=addReaction(model1,'PHH_8', {'16carboxyhexadecanoyl-CoA_KATx',
'nadh[c]', 'h[c]', '16carboxyhexadecanoyl-CoA_HACDxi', 'nad[c]'},[-1 -1
-1 1 1],1, 0,1000);
%3-hydroxyacyl-CoA dehydratase (Adapted from ECOAHx in B-oxidation
cycle). Use generic names adding the name of the enzyme that is
modifying
%the molecule:
model1=addReaction(model1,'PII_1', {'3oxoglutaryl-CoA_HACDxi',
'3oxoglutaryl-CoA_ECOAHi', 'h2o[c]'},[-1 1 1],1, 0,1000);
model1=addReaction(model1,'PII_2', {'4carboxybutanoyl-CoA_HACDxi',
'4carboxybutanoyl-CoA_ECOAHi', 'h2o[c]'},[-1 1 1],1, 0,1000);
model1=addReaction(model1,'PII_3', {'6carboxyhexanoyl-CoA_HACDxi',
'6carboxyhexanoyl-CoA_ECOAHi', 'h2o[c]'},[-1 1 1],1, 0,1000);
model1=addReaction(model1,'PII_4', {'8carboxyoctanoyl-CoA_HACDxi',
'8carboxyoctanoyl-CoA_ECOAHi', 'h2o[c]'},[-1 1 1],1, 0,1000);
model1=addReaction(model1,'PII_5', {'10carboxydecanoyl-CoA_HACDxi',
'10carboxydecanoyl-CoA_ECOAHi', 'h2o[c]'},[-1 1 1],1, 0,1000);
model1=addReaction(model1,'PII_6', {'12carboxydodecanoyl-CoA_HACDxi',
'12carboxydodecanoyl-CoA_ECOAHi', 'h2o[c]'},[-1 1 1],1, 0,1000);
model1=addReaction(model1,'PII_7', {'14carboxytetradecanoyl-
CoA_HACDxi', '14carboxytetradecanoyl-CoA_ECOAHi', 'h2o[c]'},[-1 1 1],1,
0,1000);
model1=addReaction(model1,'PII_8', {'16carboxyhexadecanoyl-CoA_HACDxi',
'16carboxyhexadecanoyl-CoA_ECOAHi', 'h2o[c]'},[-1 1 1],1, 0,1000);
%acyl-CoA dehydrogenase (Adapted from ACOADxf_ferr in reversal B-
oxidation
%cycle). Use generic names adding the name of the enzyme that is
modifying
%the molecule
model1=addReaction(model1,'PJJ_1', {'3oxoglutaryl-CoA_ECOAHi',
'fd_red', 'h[c]', '4carboxybutanoyl-CoA', 'fd_oxi'},[-1 -1 -1 1 1],1,
0,1000);
model1=addReaction(model1,'PJJ_2', {'4carboxybutanoyl-CoA_ECOAHi',
'fd_red', 'h[c]', '6carboxyhexanoyl-CoA', 'fd_oxi'},[-1 -1 -1 1 1],1,
0,1000);
model1=addReaction(model1,'PJJ_3', {'6carboxyhexanoyl-CoA_ECOAHi',
'fd_red', 'h[c]', '8carboxyoctanoyl-CoA', 'fd_oxi'},[-1 -1 -1 1 1],1,
0,1000);
```

```
model1=addReaction(model1,'PJJ_4', {'8carboxyoctanoyl-CoA_ECOAHi',
'fd_red', 'h[c]', '10carboxydecanoyl-CoA', 'fd_oxi'},[-1 -1 -1 1 1],1,
0,1000);
model1=addReaction(model1,'PJJ_5', {'10carboxydecanoyl-CoA_ECOAHi',
'fd_red', 'h[c]', '12carboxydodecanoyl-CoA', 'fd_oxi'},[-1 -1 -1 1
1],1, 0,1000);
model1=addReaction(model1,'PJJ_6', {'12carboxydodecanoyl-CoA_ECOAHi',
'fd_red', 'h[c]', '14carboxytetradecanoyl-CoA', 'fd_oxi'},[-1 -1 -1 1
1],1, 0,1000);
model1=addReaction(model1,'PJJ_7', {'14carboxytetradecanoyl-
CoA_ECOAHi', 'fd_red', 'h[c]', '16carboxyhexadecanoyl-CoA',
'fd_oxi'},[-1 -1 -1 1 1],1, 0,1000);
model1=addReaction(model1,'PJJ_8', {'16carboxyhexadecanoyl_ECOAHi',
'fd_red', 'h[c]', '18carboxyoctadecanoyl-CoA', 'fd_oxi'},[-1 -1 -1 1
1],1, 0,1000);
%3-ketoacyl-CoA thiolase (Adapted from KATx in reversal B-oxidation
cycle).
%Use generic names adding the name of the enzyme that is modifying
%the molecule
model1=addReaction(model1,'PKK_1', {'4carboxybutanoyl-CoA', 'accoa[c]',
'4carboxybutanoyl-CoA_KATx', 'coa[c]'},[-1 -1 1 1],1, 0,1000);
model1=addReaction(model1,'PKK_2', {'6carboxyhexanoyl-CoA', 'accoa[c]',
'6carboxyhexanoyl-CoA_KATx', 'coa[c]'},[-1 -1 1 1],1, 0,1000);
model1=addReaction(model1,'PKK_3', {'8carboxyoctanoyl-CoA', 'accoa[c]',
'8carboxyoctanoyl-CoA_KATx', 'coa[c]'},[-1 -1 1 1],1, 0,1000);
model1=addReaction(model1,'PKK_4', {'10carboxydecanoyl-CoA',
'accoa[c]', '10carboxydecanoyl-CoA_KATx', 'coa[c]'},[-1 -1 1 1],1,
0,1000);
model1=addReaction(model1,'PKK_5', {'12carboxydodecanoyl-CoA',
'accoa[c]', '12carboxydodecanoyl-CoA_KATx', 'coa[c]'},[-1 -1 1 1],1,
0,1000);
model1=addReaction(model1,'PKK_6', {'14carboxytetradecanoyl-CoA',
'accoa[c]', '14carboxytetradecanoyl-CoA_KATx', 'coa[c]'},[-1 -1 1 1],1,
0,1000);
model1=addReaction(model1,'PKK_7', {'16carboxyhexadecanoyl-CoA',
'accoa[c]', '16carboxyhexadecanoyl-CoA_KATx', 'coa[c]'},[-1 -1 1 1],1,
0,1000);
%Termination I (Alcohol). Reduction of acyl-CoA
model1=addReaction(model1,'PLL_1', {'4carboxybutanoyl-CoA', 'nadh[c]',
'h[c]', '5oxopentanoicacid', 'nad[c]', 'coa[c]'},[-1 -1 -1 1 1 1],1,
0,1000);
model1=addReaction(model1,'PLL_2', {'6carboxyhexanoyl-CoA', 'nadh[c]',
'h[c]', '7oxoheptanoicacid', 'nad[c]', 'coa[c]'},[-1 -1 -1 1 1 1],1,
0,1000);
model1=addReaction(model1,'PLL_3', {'8carboxyoctanoyl-CoA', 'nadh[c]',
'h[c]', '9oxononanoicacid', 'nad[c]', 'coa[c]'},[-1 -1 -1 1 1 1],1,
0,1000);
model1=addReaction(model1,'PLL_4', {'10carboxydecanoyl-CoA', 'nadh[c]',
'h[c]', '11oxoundecanoicacid', 'nad[c]', 'coa[c]'},[-1 -1 -1 1 1 1],1,
0,1000);
model1=addReaction(model1,'PLL_5', {'12carboxydodecanoyl-CoA',
'nadh[c]', 'h[c]', '13oxotridecanoicacid', 'nad[c]', 'coa[c]'},[-1 -1 -
1 1 1 1],1, 0,1000);
model1=addReaction(model1,'PLL_6', {'14carboxytetradecanoyl-CoA',
'nadh[c]', 'h[c]', '15oxopentadecanoicacid', 'nad[c]', 'coa[c]'},[-1 -1
-1 1 1 1],1, 0,1000);
```

```
model1=addReaction(model1,'PLL_7', {'16carboxyhexadecanoyl-CoA',
'nadh[c]', 'h[c]', '17oxoheptadecanoicacid', 'nad[c]', 'coa[c]'},[-1 -1
-1 1 1 1],1, 0,1000);
%Termination I (Alcohol). Reduction of aldehyde
model1=addReaction(model1,'PMM_1', {'5oxopentanoicacid', 'nadh[c]',
'h[c]', '5hydroxypentanoicacid', 'nad[c]'},[-1 -1 -1 1 1],1, 0,1000);
model1=addReaction(model1,'PMM_2', {'7oxoheptanoicacid', 'nadh[c]',
'h[c]', '7hydroxyheptanoicacid', 'nad[c]'},[-1 -1 -1 1 1],1, 0,1000);
model1=addReaction(model1,'PMM_3', {'9oxononanoicacid', 'nadh[c]',
'h[c]', '9hydroxynonanoicacid', 'nad[c]'},[-1 -1 -1 1 1],1, 0,1000);
model1=addReaction(model1,'PMM_4', {'11oxoundecanoicacid', 'nadh[c]',
'h[c]', '11hydroxyundecanoicacid', 'nad[c]'},[-1 -1 -1 1 1],1, 0,1000);
model1=addReaction(model1,'PMM_5', {'13oxotridecanoicacid', 'nadh[c]',
'h[c]', '13hydroxytridecanoicacid', 'nad[c]'},[-1 -1 -1 1 1],1,
0,1000);
model1=addReaction(model1,'PMM_6', {'15oxopentadecanoicacid',
'nadh[c]', 'h[c]', '15hydroxypentadecanoicacid', 'nad[c]'},[-1 -1 -1 1
1],1, 0,1000);
model1=addReaction(model1,'PMM_7', {'17oxoheptadecanoicacid',
'nadh[c]', 'h[c]', '17hydroxyheptadecanoicacid', 'nad[c]'},[-1 -1 -1 1
1],1, 0,1000);
%Export hydroxyacids --> Already in the model
%Termination II (Acid).
model1=addReaction(model1,'PNN_1', {'4carboxybutanoyl-CoA', 'h2o[c]',
'4carboxybutanoate', 'h[c]', 'coa[c]'},[-1 -1 1 1 1],1, 0,1000);
model1=addReaction(model1,'PNN_2', {'6carboxyhexanoyl-CoA', 'h2o[c]',
'6carboxyhexanoate', 'h[c]', 'coa[c]'},[-1 -1 1 1 1],1, 0,1000);
model1=addReaction(model1,'PNN_3', {'8carboxyoctanoyl-CoA', 'h2o[c]',
'8carboxyoctanoate', 'h[c]', 'coa[c]'},[-1 -1 1 1 1],1, 0,1000);
model1=addReaction(model1,'PNN_4', {'10carboxydecanoyl-CoA', 'h2o[c]',
'10carboxydecanoate', 'h[c]', 'coa[c]'},[-1 -1 1 1 1],1, 0,1000);
model1=addReaction(model1,'PNN_5', {'12carboxydodecanoyl-CoA',
'h2o[c]', '12carboxydodecanoate', 'h[c]', 'coa[c]'},[-1 -1 1 1 1],1,
0,1000);
model1=addReaction(model1,'PNN_6', {'14carboxytetradecanoyl-CoA',
'h2o[c]', '14carboxytetradecanoate', 'h[c]', 'coa[c]'},[-1 -1 1 1 1],1,
0,1000);
model1=addReaction(model1,'PNN_7', {'16carboxyhexadecanoyl-CoA',
'h2o[c]', '16carboxyhexadecanoate', 'h[c]', 'coa[c]'},[-1 -1 1 1 1],1,
0,1000);
%Export Reactions (hydroxylated acid)
model1=addReaction(model1,'EX_4carboxybutanoate',
{'4carboxybutanoate'},[-1 ],1, 0,0);
model1=addReaction(model1,'EX_6carboxyhexanoate',
{'6carboxyhexanoate'},[-1 ],1, 0,0);
model1=addReaction(model1,'EX_8carboxyoctanoate',
{'8carboxyoctanoate'},[-1 ],1, 0,0);
model1=addReaction(model1,'EX_10carboxydecanoate',
{'10carboxydecanoate'},[-1 ],1, 0,0);
model1=addReaction(model1,'EX_12carboxydodecanoate',
{'12carboxydodecanoate'},[-1 ],1, 0,0);
model1=addReaction(model1,'EX_14carboxytetradecanoate',
{'14carboxytetradecanoate'},[-1 ],1, 0,0);
model1=addReaction(model1,'EX_16carboxyhexadecanoate',
{'16carboxyhexadecanoate'},[-1 ],1, 0,0);
model1=addReaction(model1,'EX_18carboxyoctadecanoate',
{'18carboxyoctadecanoate'},[-1 ],1, 0,0);
```

```
%% Add reactions to produce missing internal primers
%(Fig 4, reaction 12)
model1=addReaction(model1,'P_Fig4_r12', {'malcoa[c]', 'nadph[c]',
'h[c]', 'Malonate-semialdehyde', 'coa[c]', 'nadp[c]'},[-1 -1 -1 1 1
1],1, 0,1000);
%(Fig 4, reaction 13)
model1=addReaction(model1,'P_Fig4_r_13', {'Malonate-semialdehyde',
'nadph[c]', 'h[c]', '3-hydroxypropionate', 'nadp[c]'},[-1 -1 -1 1 1],1,
0,1000);
%(Fig 4, reaction 8)
model1=addReaction(model1,'P_Fig4_r_8', {'3-hydroxypropionate',
'coa[c]', 'atp[c]', '3-hydroxypropionyl-CoA', 'ppi[c]', 'amp[c]'},[-1 -
1 -1 1 1 1],1, 0,1000);
%(Fig 4, reaction 6)
model1=addReaction(model1,'P_Fig4_r_6', {'glyc[c]', '3-
hydroxypropionaldehyde', 'h2o[c]'},[-1 1 1],1, 0,1000);
%(Fig 4, reaction 7)
model1=addReaction(model1,'P_Fig4_r_7', {'3-hydroxypropionaldehyde',
'nad[c]', 'h2o[c]', '3-hydroxypropionate', 'nadh[c]', 'h[c]'},[-1 -1 -1
1 1 2 ],1, 0,1000);
% Ferredoxins / Reversal B-oxidation cycle / inactive in this case
       model1=addReaction(model1,'ACOAD1f_ferr',{'btcoa[c]', 'fd_oxi',
'b2coa[c]', 'fd_red', 'h[c]'},[-1 -1 1 1 1],1,0,0);
       model1=addReaction(model1,'ACOAD2f_ferr',{'fd_oxi', 'hxcoa[c]',
'hx2coa[c]', 'fd_red', 'h[c]'},[-1 -1 1 1 1],1,0,0);
       model1=addReaction(model1,'ACOAD3f_ferr',{'fd_oxi', 'occoa[c]',
'oc2coa[c]', 'fd_red', 'h[c]'},[-1 -1 1 1 1],1,0,0);
       model1=addReaction(model1,'ACOAD4f_ferr',{'dcacoa[c]',
'fd_oxi', 'dc2coa[c]', 'fd_red', 'h[c]'},[-1 -1 1 1 1],1,0,0);
       model1=addReaction(model1,'ACOAD5f_ferr',{'ddcacoa[c]',
'fd_oxi', 'dd2coa[c]', 'fd_red', 'h[c]'},[-1 -1 1 1 1],1,0,0);
       model1=addReaction(model1,'ACOAD6f_ferr',{'fd_oxi', 'tdcoa[c]',
'td2coa[c]', 'fd_red', 'h[c]'},[-1 -1 1 1 1],1,0,0);
       model1=addReaction(model1,'ACOAD7f_ferr',{'fd_oxi',
'pmtcoa[c]', 'hdd2coa[c]', 'fd_red', 'h[c]'},[-1 -1 1 1 1],1,0,0);
       model1=addReaction(model1,'ACOAD8f_ferr',{'fd_oxi', 'stcoa[c]',
'od2coa[c]', 'fd_red', 'h[c]'},[-1 -1 1 1 1],1,0,0);
       model1=addReaction(model1,'PFOR',{'coa[c]', 'fd_oxi', 'pyr[c]',
'accoa[c]', 'co2[c]', 'fd_red', 'h[c]'},[-1 -1 -1 1 1 1 1],1,0,0);

%%
A= size(model1.rxns);
SizeModel=(A(1));
%% Enter knockouts
I= input('List of reactions to delete: ');

SizeI=size(I);
for p=1:1:SizeI(2)
    RxnDelete=I(p);
    model1=changeRxnBounds(model1, RxnDelete, 0, 'u');
    model1=changeRxnBounds(model1, RxnDelete, 0, 'l');
    if p==1
        KnockoutReaction=RxnDelete;
    else
        KnockoutReaction=strcat(KnockoutReaction,',',RxnDelete);
```

```
    end
end


%% Desired primer and product
prompt = {'Desired primer: '};
Primer=inputdlg(prompt);
model1=changeRxnBounds(model1, Primer, -15, 'l');
prompt = {'Desired product: '};
Product=inputdlg(prompt);
model1=changeRxnBounds(model1, Product, 1000, 'u');
A=(model1.rxns);
productposition=AC_findp_F(A,Product);
model1=changeObjective(model1, Biomass_name, 1);
solution=optimizeCbModel(model1);
maxbiomass =solution.f
if solution.stat ~= 1
    display ('The selected condition does not have any valid solution')
    return
end
Product_when_biomass_is_optimized=solution.x(productposition)
TitlePlot=strcat('Product versus Biomass, deletion of: ',
KnockoutReaction);
xlsTitle=strcat('Model_', modelname, '_', KnockoutReaction);
model1=changeObjective(model1, Biomass_name, -1);
solution=optimizeCbModel(model1);
minbiomass=solution.f;
product2=solution.x(productposition);
model1=changeObjective(model1, Product(1), 1);
solution=optimizeCbModel(model1);
OptimeProduct=solution.x(productposition)
Y=zeros(101,3);
%Y=zeros(101,7);
for i=1:1:101
    model1=changeRxnBounds(model1, Biomass_name, 0.01*(i-1)*maxbiomass,
'l');
    % min
    model1=changeObjective(model1, Product(1), 1);
    maxsolution=optimizeCbModel(model1);
    maxproduct=maxsolution.f;
    biomass1=maxsolution.x(biomassposition);
    model1=changeObjective(model1, Product(1), -1);
    minsolution=optimizeCbModel(model1);
    minproduct=minsolution.x(productposition);
    Y(i,:)= [biomass1 minproduct maxproduct];

end

model1=changeObjective(model1, Biomass_name, 1);
model1=changeRxnBounds(model1, Biomass_name, 0, 'l');
solution=optimizeCbModel(model1);
%% Plot
figure(1)
set(0, 'DefaultTextInterpreter', 'none') %Change set of all plots Text-
Interpreter to none, as oppose to Text (default)
plot(Y(:,1), Y(:,2), '--g*');
```

```
hold on
plot(Y(:,1), Y(:,3), '--r*');
xlabel('Biomass');
ylabel(strcat('Product: ', Product));
title(TitlePlot);
h=area(Y(:,1),Y(:,3));
set(h(1),'FaceColor',[1 1 0.5])
j=area(Y(:,1),Y(:,2));
set(j(1),'FaceColor',[1 1 1])
```